Durham E-Theses

Antenna Subtraction for NNLO Calculations at the LHC

CURRIE, JAMES,RICHARD

Antenna Subtraction for NNLO Calculations at the LHC

James Currie

A Thesis Presented for the Degree of

Doctor of Philosophy

Institute for Particle Physics Phenomenology

Department of Physics

University of Durham

England

September 2012

Antenna Subtraction for NNLO Calculations at the LHC

James Currie

Submitted for the degree of Doctor of Philosophy

September 2012

Abstract

In this thesis the task of computing higher order corrections to QCD scattering processes for the LHC is considered, specifically Next-to Leading Order (NLO) and Next-toNext-to Leading Order (NNLO) perturbative QCD corrections. The infrared (IR) divergent behaviour of the cross section is isolated using the antenna subtraction formalism. This method has previously been used at NNLO in the calculation of jet production in the context of e^+e^- annihilation and for the leading colour contribution to dijet production via pure gluon scattering. The research presented in this thesis extends the formalism to include scattering processes involving quarks with initial-state partons. General formulae, including sub-leading colour contributions, are presented for the isolation and cancellation of IR and singularities when calculating the production of colourless final-states at the LHC at NLO and NNLO accuracy. The leading colour NNLO correction to the sub-process $q\bar{q} \to gg$ is calculated and numerical results are presented to demonstrate the convergence of the physical cross section and the subtraction terms in the various unresolved limits. The calculations are organised with the aid of convenient quantities, referred to as *integrated antenna strings*. Using these quantities, the full calculation displays a clear and predictive structure, in particular at the double virtual level where the structures presented are new.

Declaration

The work in this thesis is based on research carried out at the Institute for Particle Physics Phenomenology, Department of Physics, University of Durham, England. No part of this thesis has been submitted elsewhere for any other degree or qualification. Unless otherwise stated, all original work is my own in collaboration with my supervisor Professor Nigel Glover. The contents of chapter five is based upon research done in collaboration with Professor Nigel Glover and Steven Wells.

Acknowledgements

Contents

List of Figures

List of Tables

Preface

In December 1947 George Dixon Rochester and Clifford Charles Butler reported evidence for the observation of two previously unseen unstable particles in cloud chamber experiments at Manchester University [8]. The key feature of these new *strange* particles was that their decay rates into the then known particles (pions, muons and neutrinos) were observed to be several orders of magnitude slower than the rates for typical hadronic reactions. Upon further investigation the strange particles appeared to be produced in pairs at particle colliders at a rate which was large with respect to their decay rate. These unexpected "V" particles[1], later termed the Kaons, and their properties led Gell-Mann and Nishijima to postulate an entirely new quantum number of hadronic matter, *strangeness* [9] [10]. The utility of this new quantum number was that it would be conserved in the strong interaction but not in the weak interaction. As such, strange particles can be produced with a large cross section by strong interactions so long as they are produced in multiples which conserve strangeness; yet as a single strange particle is unable to decay via the strange conserving strong interaction they are forced to decay much more slowly through the weak interaction.

Following the discovery of the Kaons, many more short lived resonances were found, some possessing strangeness and others not. In an attempt to understand the crowded spectrum of hadronic particles Gell-Mann [11], in parallel with Ne'eman [12], proposed a classification scheme based upon representations of the Lie algebra of the group SU(3). This model successfully predicted the mass and quantum num-

---

[1]So called due to the distinctive V-shaped track left in the cloud chamber by the $K^0 \to \pi^+ \pi^-$ and $K^+ \to \mu^+ \nu_\mu$ decays, see Fig.1
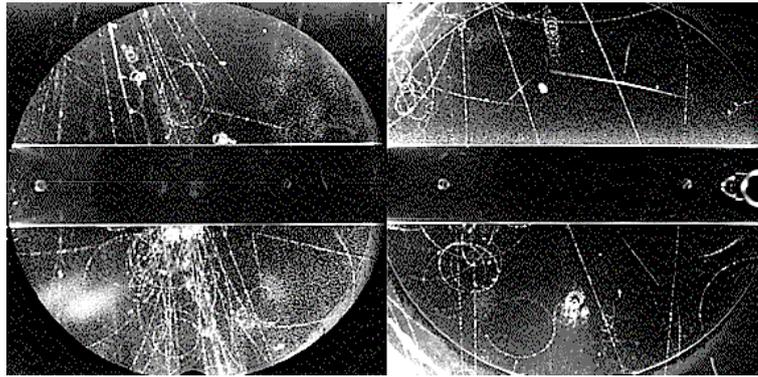
Figure 1: Rochester and Butler's photographic plates presented as evidence for new unstable particles. *Left*: Below the central bar on the right is the distinctive V shaped track explained as a decay of a neutral unstable particle into a pair of lighter charged particles, now understood as the decay $K^0 \to \pi^+\pi^-$. *Right*: Entering from the top right edge is the unstable charged particle which then decays to a lighter charged particle and a neutral particle leaving a kink in the track, now understood to be a $K^+ \to \mu^+\nu_\mu$ decay.

bers of the Ω^- hyperon which was found at the Brookhaven National Laboratory two years later [13]. The global SU(3) flavour symmetry model subsequently found physical justification in the quark model of Gell-Mann and Zweig [14] [15], in which the old quantum numbers of isospin and strangeness became flavour quantum numbers of the constituent "up", "down" and "strange" quarks. Given that the strong interaction is assumed to be flavour blind and all three quarks are roughly mass degenerate, an approximate global SU(3) flavour symmetry holds with each quark in the fundamental representation of the group's algebra. The shift in emphasis from properties of hadrons to the properties of *partons* was an elegant solution to the problem of classifying hadron multiplets but the baryon spectrum was yet to reveal its most revolutionary secret.

The quark model was an insightful way to generate the patterns of observed quantum numbers in hadronic matter but one property of baryons posed a problem. As fermions the baryons obey the quantum mechanical spin-statistics theorem stating that odd integer spin quantum states have antisymmetric total wave functions, given as the product of their flavour, spin and space states, under the exchange of

any two constituent particles. Looking in particular at the spin $\frac{3}{2}$ decuplet a few states cannot satisfy this antisymmetric wavefunction requirement within the basic quark model, for example the Δ^{++} and Ω^- baryons. Within the quark model these baryons have quark content (uuu) and (sss) respectively with all quark spins aligned to generate a total $\frac{3}{2}$ spin. When considering ground state s-wave spatial wavefunctions we are forced to conclude that the total wavefunction for these baryons is symmetric under the exchange of any two quarks, in contradiction to the spin-statistics theorem.

When confronted by a contradiction with observation, theory rarely emerges unscathed. In the case of the baryon quantum numbers the theory had two directions in which it could bend: At a fundamental level the spin-statistics theorem may not apply to quarks, which at that point were not generally considered elements of physical reality any more than a useful picture for calculation. Alternatively the theoretical framework could be extended to accommodate the observed results just as Gell-mann had proposed strangeness to accommodate Rochester and Butler's "V" particles almost twenty years earlier. Following the latter line of enquiry a new quantum number, *colour*, was proposed first as a global charge [16], and a year later as the charge associated with a local gauge symmetry described by the Lie algebra of the group SU(3) as an additional degree of freedom inherent to the quarks [17]. The assumption that physical states are formed from colour singlet combinations of coloured quarks severely restricts the possible hadronic spectrum of physical states. The colour singlet assumption implies that hadronic matter falls into one of two overall colour structures dictated by the possible ways to build a colour singlet from coloured quarks and anti-quarks, in the fundamental and conjugate fundamental representations respectively,

$$\epsilon_{ijk} q^i q^j q^k \quad , \quad q_i \bar{q}^i$$

which classify the hadrons into fermionic baryons and bosonic mesons. It is clear that the baryon spectrum when considered as a colour singlet is totally anti-symmetric in its colour indices by virtue of being proportional to the three dimensional Levi-Civita symbol and so the colour degree of freedom has the additional effect of anti-symmetrizing the baryonic total wavefunctions.

The colour degree of freedom may have been motivated as an ad hoc extension to the theory of hadron spectroscopy but its implications were far reaching and far beyond the remit of explaining baryon quantum numbers. Unlike the approximate flavour SU(3) symmetry resulting from the introduction of strangeness, the colour degree of freedom implies an exact local gauge symmetry whose dynamics are calculable through a gauge quantum field theory, Quantum Chromo Dymanics (QCD).

The examination of this theory in the years since its foundation has provided a wealth of understanding about the physical world we observe, not only justifying the assumptions which led to its postulation but revealing fascinating and unexpected structures reflected in the behaviour of matter over a vast range of energy scales. The frontier of discovery is currently being rolled back by the Large Hadron Collider (LHC) at CERN. A deep understanding of QCD lies at the heart of this research programme: from providing an accurate description of the hadronic initial-state, the dominant partonic hard scattering cross-section and its evolution to the observed hadronic final-state, through to the possibility of producing new coloured "V" particles, today in the form of squarks, gluinos, colour sextet diquarks, fourth generation quarks etc. It is clear that our understanding of the physical world at the teraelectronvolt (TeV) scale, as probed by the LHC, is irreducibly correlated with the depth of our understanding of QCD.

> "...Alice started to her feet, for it flashed across her mind that she had never before seen a rabbit with either a waistcoat-pocket, or a watch to take out of it, and burning with curiosity, she ran across the field after it, and fortunately was just in time to see it pop down a large rabbit-hole under the hedge. In another moment down went Alice after it, never once considering how in the world she was to get out again."
>
> (*Alice's Adventures in Wonderland*, Chapter 1, Lewis Caroll)

September 24, 2012

Chapter 1

QCD in the Collider Environment

In this chapter the underlying theory relevant to this thesis is presented. QCD is introduced at the level of the Lagrangian density from which a perturbative description of strong dynamics can be derived. The parton model is introduced in the context of hadronic collisions relevant for LHC era calculations and is refined by considering the effect of QCD corrections within the model. The self-consistency of perturbative QCD calculations is considered which in turn motivates the renormalization procedure and collinear factorization, necessary to perform higher order calculations. By invoking renormalization and collinear factorization we are naturally driven to consider the dependence of our calculations on unphysical scales introduced at intermediate stages of the calculation, and the consequences of this dependence for the self-consistency of the perturbative description. With the theory properly defined such that reliable calculations can be performed, some consideration is given to which calculations are actually desirable for LHC era phenomenology and the need for higher order calculations will be motivated. The technical difficulties of higher order calculations are presented and those solutions suitable to higher order calculations are discussed, with particular emphasis on the antenna subtraction method for isolating infrared singularities.

1.1 QCD and the Naïve Parton Model

1.1.1 Fundamentals of QCD

Within the framework of quantum field theory (QFT) individual theories may be specified by their Lagrangian density [18], (from this point referred to simply as the Lagrangian), defined as the integrand of the space-time integral defining the action functional,

$$S[\{\phi_\kappa\}] \;=\; i \int \mathrm{d}^4 x \; \mathcal{L}(\{\phi_\kappa(x)\}; \{\partial\phi_\kappa(x)\}), \qquad (1.1)$$

where $\{\phi_\kappa\}$ denotes the set of fields present in the Lagrangian. In the case of QCD the relevant fields are the spinor quark and anti-quark fields, $\boldsymbol{\psi}(x) = \psi_{\alpha,i}(x)$, $\bar{\boldsymbol{\psi}}(x) = \bar{\psi}_{\dot\alpha,i}(x)$, the vector gluon fields, $\boldsymbol{A}_\mu(x) = A_\mu^a(x)$ and the anti-commuting scalar ghost fields, $\boldsymbol{\eta}(x) = \eta^a(x)$, $\bar{\boldsymbol{\eta}}(x) = \bar{\eta}^a(x)$; where the indices α, μ denote the space-time spinor and Lorentz indices and the labels i, a denote the internal symmetry colour indices for the fundamental and adjoint representations of the symmetry group's Lie algebra respectively.

Two *a priori* assumptions about the QFT describing the strong force dramatically constrain the form of the QCD Lagrangian: the theory derived from the Lagrangian should be renormalizable and have a classical action which is invariant under local gauge transformations belonging to the Lie algebra of the symmetry group SU(3). The first requirement is discussed more comprehensively in section 1.2. For the purposes of defining the Lagrangian this requirement amounts to ensuring all operators in the Lagrangian have a mass dimension at most equal to the number of space-time dimensions, taken to be four in standard QCD; this statement is equivalent to requiring all coupling and mass parameters in the local Lagrangian have non-negative mass dimension. The second consideration concerns the gauge invariance of the classical action which amounts to a space-time dependent redefinition of the quark fields, $\boldsymbol{\psi}(x)$, under linear transformations, $\boldsymbol{U}(x)$, belonging to the Lie algebra of the symmetry group SU(3).

The classical action is characterised by the classical Lagrangian which may be

written as [19],

$$\mathcal{L}_{\text{classical}} \;\; = \;\; -\frac{1}{2}\text{Tr}\big[(\boldsymbol{t}\cdot\boldsymbol{F}_{\mu\nu})^2\big] + \sum_f \bar{\psi}^f(i\slashed{D} - m_f\boldsymbol{I})\psi^f, \qquad (1.2)$$

where f denotes the flavours of quarks in the matter sector of the theory and m_f their masses, which for the purposes of this thesis are set to zero for the active quark flavours. The field strength tensor and covariant derivative are defined respectively as,

$$\boldsymbol{F}_{\mu\nu} \;\; = \;\; \big(\partial_\mu\boldsymbol{A}_\nu - \partial_\nu\boldsymbol{A}_\mu - g\boldsymbol{A}_\mu \wedge \boldsymbol{A}_\nu\big), \qquad (1.3)$$

$$\slashed{D} \;\; = \;\; \gamma^\mu \cdot \big(\partial_\mu\boldsymbol{I} + ig\boldsymbol{t}\cdot\boldsymbol{A}_\mu\big), \qquad (1.4)$$

where g is the QCD coupling constant which determines the overall strength of interactions, γ^μ represents a matrix in spin-space belonging to a Clifford algebra with its spinor indices suppressed and $\boldsymbol{t} = t_{ij}^a$ are the generators of the fundamental representation of the Lie algebra for the group SU(3). Written in terms of components $\big[\boldsymbol{A}_\mu \wedge \boldsymbol{A}_\nu\big]_a = f_{abc}A_\mu^b A_\nu^c$ and f_{abc} are the structure constants for the group SU(3) defined by, $[t_a, t_b] = if_{abc}t^c$. Under a local gauge transformation the quark fields and, by definition, the covariant derivative transform in the same way, whereas the anti-quark fields transform in the opposite fashion appropriate to the conjugate fundamental representation,

$$\psi(x) \;\; \rightarrow \;\; \boldsymbol{U}(x)\psi(x), \qquad (1.5)$$

$$\bar{\psi}(x) \;\; \rightarrow \;\; \bar{\psi}(x)\boldsymbol{U}^{-1}(x), \qquad (1.6)$$

$$\boldsymbol{D}_\mu\psi(x) \;\; \rightarrow \;\; \boldsymbol{U}(x)\boldsymbol{D}_\mu\psi(x). \qquad (1.7)$$

This implies the transformation of the gluon field,

$$\boldsymbol{t}\cdot\boldsymbol{A}_\mu(x) \;\; \rightarrow \;\; \boldsymbol{U}(x)\Big(\boldsymbol{t}\cdot\boldsymbol{A}_\mu(x) + \frac{i}{g}\boldsymbol{U}^{-1}(x)\partial_\mu\boldsymbol{U}(x)\Big)\boldsymbol{U}^{-1}(x) \qquad (1.8)$$

The gluon field strength can be defined in terms of the covariant derivatives, whose transformation properties are displayed in (1.7), via the relation $[\boldsymbol{D}_\mu, \boldsymbol{D}_\nu] = ig\boldsymbol{t}\cdot\boldsymbol{F}_{\mu\nu}$ and so the gluon field strength's transformation properties are given by,

$$\boldsymbol{t}\cdot\boldsymbol{F}_{\mu\nu} \rightarrow \boldsymbol{U}(x)\boldsymbol{t}\cdot\boldsymbol{F}_{\mu\nu}\boldsymbol{U}^{-1}(x). \qquad (1.9)$$

The transformation properties listed in equations (1.5)-(1.7) and (1.9) are sufficient to demonstrate the local gauge invariance of the classical Lagrangian as formulated in (1.2), satisfying the second requirement on the QCD Lagrangian.

The classical QCD Lagrangian is fixed uniquely by the requirements of renormalizability and local gauge invariance[1], however to properly quantize the theory the classical notion of gauge invariance is superseded by the principle of gauge independence. In order to achieve this, the gauge invariance of the full QCD Lagrangian is broken by the addition of a term which fixes the gauge, $\mathcal{L}_{\text{g.f}}$. The gauge-fixing term is not uniquely prescribed *a priori*; each class of gauges can generally be fixed using a 1-parameter family of gauge-fixing terms, characterised by the gauge parameter λ, per class of gauge-fixing terms characterised by a functional of the gauge field $\mathcal{G}[\boldsymbol{A}_\mu(x)]$. The gauge-fixing term breaks classical gauge invariance using a term specified by a choice of λ, however gauge independence requires that calculated observables are independent of the choice of λ made when fixing the gauge.

The general form for the gauge-fixing term in a non-Abelian gauge theory's Lagrangian is written in terms of the gauge-fixing functional and the gauge parameter,

$$\mathcal{L}_{\text{g.f}} = -\frac{1}{\lambda}\text{Tr}\big[\mathcal{G}[\boldsymbol{A}_\mu(x)]^2\big]. \tag{1.10}$$

A commonly used class of gauge-fixing terms defines the class of covariant gauges, for which $\mathcal{G}[\boldsymbol{A}_\mu(x)] = \partial_\mu \boldsymbol{t} \cdot \boldsymbol{A}^\mu$. For this class of gauges the gauge-fixing term in the Lagrangian is given by,

$$\mathcal{L}_{\text{g.f}} = -\frac{1}{\lambda}\text{Tr}\big[(\partial_\mu \boldsymbol{t} \cdot \boldsymbol{A}^\mu)^2\big] \tag{1.11}$$

with the gauge parameter λ defining individual gauges, e.g., $\lambda = 1$ defines the Feynman gauge and $\lambda = 0$ the Landau gauge. In non-Abelian gauge theories such as QCD the gauge-fixing terms are not sufficient to properly define the gauge field in the class of covariant gauges. The gauge field's self-interaction through three and

---

[1]The intriguing exception to this statement is the so-called "θ-term", $\mathcal{L}_\theta = \frac{\theta g^2}{16\pi^2}\text{Tr}\big[\boldsymbol{t} \cdot \boldsymbol{F} \wedge \boldsymbol{t} \cdot \boldsymbol{F}\big]$. The effects of this term are not visible in perturbative calculations but for non-zero θ non-perturbative effects may induce CP violating contributions to observables; such effects are not observed and it remains an open problem for the Standard Model to explain their absence.

four gluon vertices requires that the unphysical longitudinal degree of freedom is removed through the inclusion of ghost fields to the Lagrangian. The complex scalar ghost fields are Grassmann valued fields which are introduced to the Lagrangian via the term,

$$\mathcal{L}_{\text{ghost}} \quad = \quad \partial_\mu \bar{\boldsymbol{\eta}} \cdot \boldsymbol{D}^\mu \cdot \boldsymbol{\eta} \qquad (1.12)$$

which couple to the gauge field through the covariant derivative. This term can be rewritten in the form,

$$\mathcal{L}_{\text{ghost}} \quad = \quad \partial_\mu \bar{\boldsymbol{\eta}} \cdot \partial^\mu \boldsymbol{\eta} + g\boldsymbol{A}_\mu \cdot \left(\partial^\mu \bar{\boldsymbol{\eta}} \wedge \boldsymbol{\eta} \right) \qquad (1.13)$$

where the non-Abelian nature of the coupling is evident in the presence of the exterior product, $\left[\partial^\mu \bar{\boldsymbol{\eta}} \wedge \boldsymbol{\eta} \right]_a = f_{abc} \partial^\mu \bar{\eta}^b \eta^c$. In the case of an Abelian theory such as QED $f_{abc} = 0$ and the ghost fields do not couple to the gauge field, admitting only kinetic terms; this allows the ghost fields to be integrated out of the functional integral without affecting the dynamics of the theory.

An alternative to the covariant gauges is the class of axial gauges where in addition to the gauge parameter an arbitrary space-time vector, n_μ, is used to define the gauge-fixing functional such that,

$$\mathcal{L}_{\text{g.f}} \quad = \quad -\frac{1}{\lambda} \text{Tr}\left[(n_\mu \boldsymbol{t} \cdot \boldsymbol{A}^\mu)^2 \right]. \qquad (1.14)$$

Once a theory is gauge fixed, whether in covariant or non-covariant axial gauges, the observable predictions of the theory are independent of the gauge choice so no gauge choice is in principle preferred. However practical concerns when performing a calculation can inform a convenient gauge choice. The practical advantage of axial gauges is the absence of the need for ghost fields, with the trade-off that the gluon propagator may be more complicated than in some covariant gauges. A commonly used axial gauge is the light-cone gauge where the reference vector is restricted to the light-cone, $n_\mu n^\mu = 0$, in addition to specifying the gauge parameter $\lambda = 0$.

With the full QCD Lagrangian properly defined it is possible to read off the Feynman diagrams from the Lagrangian and derive the associated Feynman rules.

1.1.2 Colour ordering and colour sums

The physical matrix elements are functions of several variables, primarily the external momenta $\{p_i\}$, the colours of the external states $\{c_i\}$ and their helicities $\{\lambda_i\}$. Accordingly the matrix element may be considered as a vector in a Hilbert space spanned by colour and helicity eigenvectors. The basis in colour and helicity space for n-parton scattering is given by a set of basis vectors [20],

$$|\boldsymbol{c}, \boldsymbol{\lambda}\rangle \;=\; |c_1, \ldots, c_n\rangle \otimes |\lambda_1, \ldots, \lambda_n\rangle \tag{1.15}$$

such that the matrix element is the projection of a vector in the Hilbert space into this basis of colour and helicity states,

$$\boldsymbol{\mathcal{M}}_n^{\{c_i\},\{\lambda_i\}}(\{p_i\}) \;=\; \langle \boldsymbol{c}, \boldsymbol{\lambda} | \boldsymbol{\mathcal{M}} \rangle. \tag{1.16}$$

When summed over all helicity and colour states the square of the matrix element is given by,

$$\begin{aligned} |\boldsymbol{\mathcal{M}}_n|^2(\{p_i\}) \;&=\; \sum_{\{c_i\},\{\lambda_i\}} \langle \boldsymbol{\mathcal{M}} | \boldsymbol{c}, \boldsymbol{\lambda} \rangle \langle \boldsymbol{c}, \boldsymbol{\lambda} | \boldsymbol{\mathcal{M}} \rangle \\ &=\; \langle \boldsymbol{\mathcal{M}} | \boldsymbol{\mathcal{M}} \rangle. \end{aligned} \tag{1.17}$$

It is often illuminating to consider the decomposition of the matrix element into its various colour structures. In such a decomposition the individual terms are factorized into a product of a function containing all the colour information for a given colour structure and a function which describes all kinematic behaviour belonging to that structure, known as the partial amplitude. Labelling the various colour structures for a given scattering process Λ_j, the matrix element may be decomposed into those colour structures accordingly,

$$\boldsymbol{\mathcal{M}}_n^{\{c_i\},\{\lambda_i\}}(\{p_i\}) \;=\; \sum_j \mathcal{F}_{\Lambda_j}(\{c_i\}) \, \mathcal{M}_n^{\{\lambda_i\}}(\{p_i\}, \Lambda_j) \tag{1.18}$$

where $\mathcal{F}_{\Lambda_j}$ denotes the function containing all colour dependence of the matrix element within the colour structure Λ_j and $\mathcal{M}_n^{\{\lambda_i\}}(\{p_i\}, \Lambda_j)$ is the partial amplitude belonging to that colour structure. The details of the decomposition depend on the partonic content of the scattering amplitude: the number of external states, the

types of particles, the loop order of the matrix element, etc [21–23]. Squaring (1.18) and summing over colours and helicities yields,

$$|\mathcal{M}_n|^2(\{p_i\}) = \sum_{j,k} \sum_{\{c_i\}} \mathcal{F}^\dagger_{\Lambda_j}(\{c_i\})\mathcal{F}_{\Lambda_k}(\{c_i\}) \sum_{\{\lambda_i\}} \mathcal{M}_n^{\{\lambda_i\}\dagger}(\{p_i\},\Lambda_j)\mathcal{M}_n^{\{\lambda_i\}}(\{p_i\},\Lambda_k).$$
(1.19)

In the special case where $\Lambda_j = \Lambda_k$ in the sum over colour structures, the squared partial amplitude is defined to be,

$$M_n^{\{\lambda_i\}}(\{p_i\},\Lambda_j) = \mathcal{M}_n^{\{\lambda_i\}\dagger}(\{p_i\},\Lambda_j)\mathcal{M}_n^{\{\lambda_i\}}(\{p_i\},\Lambda_j),$$
(1.20)

which may be kept in the helicity basis or summed over helicity to give the helicity-summed squared partial amplitude,

$$M_n(\{p_i\},\Lambda_j) = \sum_{\{\lambda_i\}} M_n^{\{\lambda_i\}}(\{p_i\},\Lambda_j).$$
(1.21)

The traditional method for calculating matrix elements in perturbation theory is via the evaluation of Feynman diagrams. In order to decompose the matrix element, calculated as the sum of Feynman diagrams, into colour-ordered partial amplitudes the Feynman diagrams themselves must be similarly factorized into a colour dependent function and a colour-stripped Feynman amplitude containing all kinematic dependence. Each propagator and vertex defined by the Feynman rules [19] is associated with a colour factor, e.g., the quark-gluon vertex carries the colour factor t_{ij}^a, which is a matrix in the fundamental representation of the Lie algebra of SU(3). As the colour information for each element of a Feynman diagram is simply an overall factor the colour dependence of an entire Feynman diagram trivially factors out, being the product of the colour factors for each propagator and vertex.

$$\mathcal{D}(\{p_i\},\{c_i\}) = \mathcal{C}(\{c_i\})\,\mathcal{D}(\{p_i\}).$$
(1.22)

Here $\mathcal{C}$ contains the explicit dependence of the Feynman amplitude on the colours of the external particles but also an implicit dependence on the colours of the internal virtual particles whose colour degrees of freedom must be summed over. In order to perform the sum over internal colours a number of identities are utilized, the first of which allows the structure functions of SU(3)'s Lie algebra (and thus the three-

(a) $\mathcal{D}_1$ (b) $\mathcal{D}_2$ (c) $\mathcal{D}_3$
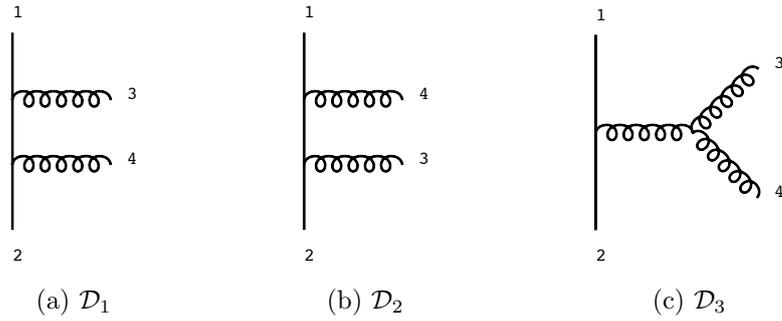
Figure 1.1: The Feynman diagrams contributing to two-quark two-gluon scattering at tree level.

and four-gluon vertices) to be rewritten in terms of generators in the fundamental representation,

$$f_{abc} = -2i\mathrm{Tr}([t_a, t_b]t_c). \tag{1.23}$$

The second identity allows generators with identical adjoint colour indices to be summed over and written in terms of Kronecker delta functions carrying only fundamental indices, named the Fierz rearrangement,

$$t_{ij}^a t_{kl}^a = \frac{1}{2}\left[\delta_{il}\delta_{kj} - \frac{1}{N}\delta_{ij}\delta_{kl}\right]. \tag{1.24}$$

Using these identities all structure constants may be eliminated from $\mathcal{C}$ in favour of generators in the fundamental representation and all internal colour degrees of freedom, by definition the colour factors with repeated adjoint indices at the amplitude level, may be summed over. The effect of summing over the internal colour degrees of freedom is to decompose the Feynman amplitude into the basis of colour-ordered partial amplitudes previously introduced in (1.18). This can be understood by noticing that the only colour dependence retained by the Feynman amplitude is that of the colour of the external states which is used to define the colour basis of the Hilbert space.

To demonstrate how Feynman amplitudes are decomposed into their various colour structures consider the tree level contribution to two-quark two-gluon scattering process. The Feynman diagrams for this process are displayed in figure 1.1 and the colour structure of their corresponding amplitudes in (1.25),

$$\mathcal{D}_1 = (t^a t^b)_{ij}\, \mathcal{D}_1,$$

$$\boldsymbol{\mathcal{D}}_2 = (t^b t^a)_{ij}\, \mathcal{D}_2,$$

$$\boldsymbol{\mathcal{D}}_3 = it^c_{ij} f^{cab}\, \mathcal{D}_3, \tag{1.25}$$

where i, j denote the colour indices of the quarks labelled 1 and 2 respectively and a, b the external gluons 3 and 4 respectively. The Feynman amplitude with the three gluon vertex contains internal colour degrees of freedom which are summed over using the identities (1.23) and (1.24), thus decomposing the Feynman amplitude into the colour structures of the other amplitudes whose colour factors depend only on external colour degrees of freedom,

$$\boldsymbol{\mathcal{D}}_3 = \left[(t^a t^b)_{ij} - (t^b t^a)_{ij} \right] \mathcal{D}_3 \tag{1.26}$$

The amplitude can therefore be decomposed into its colour structures according to (1.18),

$$\boldsymbol{\mathcal{M}}^0_4 = (t^a t^b)_{ij}\, \mathcal{M}^0_4(1_q, 3_g, 4_g, 2_{\bar{q}}) + (t^b t^a)_{ij}\, \mathcal{M}^0_4(1_q, 4_g, 3_g, 2_{\bar{q}}), \tag{1.27}$$

where the three Feynman amplitudes are decomposed into the two colour structures to form the colour-ordered partial amplitudes,

$$\mathcal{M}^0_4(1_q, 3_g, 4_g, 2_{\bar{q}}) = \mathcal{D}_1 + \mathcal{D}_3,$$

$$\mathcal{M}^0_4(1_q, 4_g, 3_g, 2_{\bar{q}}) = \mathcal{D}_2 - \mathcal{D}_3 \tag{1.28}$$

As stated in (1.19), the remaining colour belonging to the external particles is summed over when forming the square of the colour function $\mathcal{C}$. The Fierz identity can once again be used to express the sums over adjoint colour indices in terms of Kronecker delta functions. In the example of two-quark two-gluon scattering considered above, the square of the colour functions belonging to each colour structure summed over colours yields,

$$|\boldsymbol{\mathcal{M}}^0_4|^2 = N(N^2 - 1)\left[\sum_{\{i,j\}\in\{3,4\}} M^0_4(1_q, i_g, j_g, 2_{\bar{q}}) - \frac{1}{N^2}\, \widetilde{M}^0_4, (1_q, 3_g, 4_g, 2_{\bar{q}}) \right], \tag{1.29}$$

where the subleading colour contribution $\widetilde{M}^0_4 = |\widetilde{\mathcal{M}}^0_4|^2$ and the subleading colour amplitude is the sum of partial amplitudes,

$$\widetilde{\mathcal{M}}^0_4(1_q, 3_g, 4_g, 2_{\bar{q}}) = \mathcal{M}^0_4(1_q, 3_g, 4_g, 2_{\bar{q}}) + \mathcal{M}^0_4(1_q, 4_g, 3_g, 2_{\bar{q}}). \tag{1.30}$$

The subleading colour amplitude behaves as if one or two of the gluons were charged under a U(1) rather than SU(3) symmetry, sometimes referred to as an Abelian gluon. The Abelian nature of the amplitude can be seen explicitly by noticing that according to (1.28) the non-Abelian three-gluon vertex cancels in the sum of the partial amplitudes defining the subleading colour amplitude.

The matrix elements considered in this section have been assumed to contain exclusively final-state partons. Introducing initial-state partons, two in the case of hadron-hadron collisions, merely involves changing the normalization of the state-vectors in the colour-helicity space in order to account for the averaging over initial-state colours [20],

$$|\{\boldsymbol{i}\}\rangle \to \frac{1}{\sqrt{n_1 n_2}}|\{\boldsymbol{i}\}\rangle, \tag{1.31}$$

where $n_{1,2}$ denote the number of colour states which can be accommodated by initial state particles 1 and 2, and thus averaged over; $n_q = n_{\bar{q}} = N$, $n_g = N^2 - 1$.

1.1.3 Hadron-hadron collisions

The previous sections have defined the fundamentals of QCD as a QFT displaying local gauge symmetry, with quarks and gluons as coloured fundamental degrees of freedom. Matrix elements and scattering probabilities may be calculated within the framework of perturbation theory as embodied by the Feynman rules but these rules provide information about the parton-level scattering only. In a hadron collider such as the LHC the degrees of freedom are the colourless hadrons, the dynamics of which cannot be derived within QCD from first principles. In order to calculate in the hadron collider environment a model of hadrons is introduced which naïvely assumes the hadron is a collection of partons, the interactions of which dominate the dynamics of the hadron.

A key assumption of this model is that the partons carry a definite fraction of the hadron's total momentum and thus belong to a momentum distribution. This assumption can be heuristically motivated by considering the hadron-hadron collision in the centre of mass frame [24]. A more realistic model of the hadron includes soft interactions within and between the hadrons both before and after the

collision, non-perturbative effects and a rapidly evolving state-vector describing the creation and annihilation of virtual quarks and gluons. The issue of non-perturbative effects will be suspended until section 1.2 and the reliability of a perturbative picture based upon weakly interacting quarks and gluons is assumed. In the centre of mass frame the incoming hadrons are highly relativistic leading to a Lorentz factor $\gamma \approx 7450$. The boosted kinematics cause two well known effects of special relativity to become evident in the centre of mass frame: the protons are Lorentz-contracted along the beam axis and interactions occurring in the proton's frame appear time-dilated. The effect of these phenomena is that the time it takes for a probe, in this case a parton from the other hadron, to traverse the contracted hadron is far shorter than the time-scale of the dilated virtual interactions. As far as the probe is concerned the hadron's partons appear frozen such that on the time-scale of the collision the hadron appears to exist in a single state with each parton possessing a definite fraction of the proton's total momentum. This intuitive physical picture justifies the assumption that the collision is dominated by parton-level scattering rather than hadron scattering as on the time-scales of the collision the individual partons are not interacting with the rest of the hadron. The effect of soft interactions, characterised by the scale Λ_{QCD} at which hadronic interactions dominate over QCD, are numerically subleading to the partonic interactions which occur at the hard scattering scale, $\sqrt{s}$; they occur over time-scales significantly longer than the hard scattering process and so do not interfere with the parton-level calculation.

The assumptions of the naïve parton model allow the cross section to be written in a factorized form [25],

$$
d\sigma(P_1, P_2) = \sum_{i,j} \int \frac{d\xi_1}{\xi_1} \frac{d\xi_2}{\xi_2} \, f_i(\xi_1) f_j(\xi_2) \, d\hat{\sigma}_{ij}(\xi_1 P_1, \xi_2 P_2) + \mathcal{O}\big(\Lambda_{\text{QCD}}^2/s\big)
\tag{1.32}
$$

where $P_{1,2}$ are the momenta of the incoming hadrons, $\xi_{1,2}$ the fractions of those momenta carried by the partons i, j initiating the hard scattering process, the cross section for which is given by $d\hat{\sigma}_{ij}$, and f_i is the parton distribution function (PDF) which provides information on the average momentum fraction of the hadron carried by partons of type i. The interpretation of this formula in the naïve parton model is

clear: the cross section for a given final-state to be produced in a hadronic collision is given by the cross section for the underlying parton-level sub-process, summed over all sub-processes, with each sub-process carrying a weight dictated by the hadron's PDF corresponding to the probability of a given parton initiating the channel in question. For final-state coloured particles additional hadronization effects produce corrections to this formula which are nevertheless suppressed for sufficiently large hadron-hadron centre of mass energies.

By neglecting soft corrections of $\mathcal{O}\big(\Lambda_{\mathrm{QCD}}^2/s\big)$ a formula for the cross section is obtained which fully factorizes into a partonic cross section and the hadronic PDFs. Given a suitably small coupling constant the partonic cross section can be reliably calculated within perturbation theory using the methods set out in sections 1.1.1-1.1.2. The PDFs are inherently non-perturbative quantities pertaining to the properties of hadrons which are nevertheless universal and can be fitted to data from many processes and even from multiple experiments. The properties of PDFs and their determination with respect to data is covered in more detail in sections 1.4 and 1.6.

1.2   Renormalization of QCD

The subject of renormalization is as rich and fascinating as QFT itself; the subject is integral to both practical calculations and the physical interpretation of results in a vast spectrum of field theories in particle physics and even further afield. This thesis will attempt only to highlight some of the key features necessary for the research presented; more comprehensive treatments of the subject may be found in [26] [27]. Notwithstanding the technical intricacy of the subject, for the purposes of this thesis the issue of renormalization essentially amounts to a proper definition of the theory under consideration.

The fields, coupling constant and gauge-fixing parameter entering the Lagrangian defined in section 1.1.1 simply parameterize the theory and are not fixed measurable quantities. In an interacting QFT quantum corrections to physical observables contain self interactions of the fields; in the perturbative picture these self interac-

tions are displayed as closed loops in Feynman diagrams. The quantum corrections to the classical theory generate dynamical contributions to the parameters of the Lagrangian. In the case of a renormalizable theory such as QCD, these quantum contributions only cause shifts to the existing parameterization of the theory rather than generating new terms in the Lagrangian, as would be the case for a non-renormalizable theory[2].

The reparameterization of the bare Lagrangian due to quantum corrections is mathematically described by rescaling the fields, coupling constant and gauge-fixing parameter by overall multiplicative factors:

$$
\begin{aligned}
\boldsymbol{\psi}_0(x) &= Z_2^{1/2} \, \boldsymbol{\psi}(x), \\
\boldsymbol{A}_{0,\mu}(x) &= Z_3^{1/2} \, \boldsymbol{A}_\mu(x), \\
\boldsymbol{\eta}_0(x) &= Z_\eta^{1/2} \, \boldsymbol{\eta}(x), \\
g_0 &= Z_g \, g, \\
\lambda_0 &= Z_3 \, \lambda,
\end{aligned}
\tag{1.33}
$$

where the bare quantities on the left hand side are those previously used to define the Lagrangian in section 1.1.1 and those on the right hand side are the renormalized parameters of the theory. The quantum corrections are perturbatively described by loop integrals over momenta with arbitrarily high magnitudes, yielding divergent contributions to the multiplicative renormalization factors. By absorbing all divergent behaviour into the renormalization of the bare parameters of the theory, the Green's functions, from which physical observables are derived, depend only on

---

[2]A simple example of this point is seen by considering a Lorentz invariant massless scalar "ϕ^3" theory in d dimensions. The one-loop self-energy graph has degree of divergence of $d - 4$. Differentiating with respect to the external momentum yields a degree of divergence one unit smaller with each differentiation, and so if $d = 8$ five derivatives are taken to render the graph finite. Integrating this quantity with respect to the momentum five times yields five constants of integration, of which two are zero by Lorentz invariance leaving only terms with the structure $c_1 + c_3 p^2 + c_5 (p^2)^2$. The divergences proportional to the c_3 and c_1 terms can be absorbed by renormalizing the kinetic and interaction terms in the Lagrangian respectively. The c_5 term would require a term in the Lagrangian quartic in the field's derivative, not present in the original Lagrangian thus demonstrating the theory's non-renormalizability in $d = 8$.

renormalized quantities and are rendered finite to all orders in perturbation theory.

The absolute normalization of the parameters in a renormalizable theory are not predicted within the theory. An intuitive understanding of why this might be is given by Wilson's interpretation of a renormalizable theory as a low energy effective theory to a more complete high energy theory [28]. In this picture the theory contains an additional parameter, Λ, the momentum scale at which the high energy theory is naturally defined. The high energy theory will in general be characterised by a non-renormalizable Lagrangian which explicitly depends on Λ. It is one of the more profound discoveries in QFT that in a general non-renormalizable Lagrangian, only those terms which are renormalizable are significant at relatively low energies, with the non-renormalizable terms suppressed by powers of Λ [18].

In this picture, the absolute normalization of the theory's parameters would require knowledge of the unknown high energy theory to which the renormalizable theory is an approximation in the low energy limit. This interpretation implies that the absolute normalization of the theory's parameters cannot be calculated within a renormalizable theory and must be inferred from experiment defined at a given momentum scale. The purely renormalizable theory is obtained by sending the high momentum scale $\Lambda \to \infty$. This limit appears to be unjustifiable as it effectively removes one of the theory's degrees of freedom, Λ; however it has already been noted that in such a limit the theory can only be well defined upon normalizing the theory's parameters to experiment at an arbitrary momentum scale, μ, denoted the renormalization scale. Ignorance of the high energy physics characterised by Λ is traded for the arbitrary nature of the renormalization scale μ.

In a higher order calculation, integrals over unconstrained loop momenta sample arbitrarily high momentum scales even if the external momenta are held at laboratory scales. In a general theory a subset of the possible diagrams will yield divergent integrals and are formally ill-defined quantities. In a renormalizable theory this subset of diagrams is severely restricted such that the theory is rendered finite order-by-order in perturbation theory but there are an infinite number of ill-defined diagrams belonging to this restricted class nonetheless. In order to perform the renormalization of a theory and demonstrate its finiteness in perturbative cal-

culations it is generally desirable to quantify the divergence such that it can be directly manipulated by employing a *regulator*[3]. The regulator of choice for QCD is *dimensional regularization* whereby the theory is defined in d-dimensions rather than the physical four [29]. Extending the dimension of the space and the notion of integration to non-integer values is non-trivial but consistent as shown by [30] and for practical purposes amounts to considering d to be a continuous variable. Following the rules of d-dimensional integration, the solution to a given loop integral is in fact a well defined analytic function in d dimensions with poles at $d = 4$ displaying the divergence known to exist for a class of diagrams. By allowing $d = 4 - 2\epsilon$ and expanding whichever function is being calculated as a Laurent series in ϵ the divergences of the loop integration are revealed as poles in the small parameter ϵ.

In practical perturbative calculations, the renormalization of the theory's parameters is performed by trivially rewriting the multiplicative factors,

$$Z_i \;=\; 1 + (Z_i - 1) \tag{1.34}$$

such that the original form of the Lagrangian is split into two contributions: the *basic* Lagrangian written purely in terms of renormalized quantities and the *counterterm* Lagrangian written in terms of renormalized parameters and a set of counterterms defined in terms of the multiplicative Z-factors,

$$\mathcal{L} \;=\; \mathcal{L}_{\text{basic}} + \mathcal{L}_{\text{c.t.}} \tag{1.35}$$

In QCD this partitioning of the Lagrangian yields the counterterm Lagrangian[4],

$$\begin{aligned}
\mathcal{L}_{\text{c.t}} \;=\; & -\frac{1}{4}\delta_3(\partial_\mu \boldsymbol{A}_\nu - \partial_\nu \boldsymbol{A}_\mu)^2 + \delta_2 \bar{\boldsymbol{\psi}}(i\slashed{\partial})\boldsymbol{\psi} \\
& +\; g\delta_g \bar{\boldsymbol{\psi}}(\boldsymbol{t}\cdot\slashed{\boldsymbol{A}})\boldsymbol{\psi} - g\delta_3^{\triangle}(\partial_\mu \boldsymbol{A}_\nu)\cdot(\boldsymbol{A}^\mu \wedge \boldsymbol{A}^\nu) \\
& +\; \frac{1}{4}g^2\delta_3^{\square}(\boldsymbol{A}_\mu \wedge \boldsymbol{A}_\nu)^2 + \delta_\eta \partial_\mu \bar{\boldsymbol{\eta}}\cdot\partial^\mu \boldsymbol{\eta} + g\delta_\eta^{\triangle}\boldsymbol{A}_\mu\cdot(\partial^\mu \bar{\boldsymbol{\eta}}\wedge \boldsymbol{\eta})
\end{aligned} \tag{1.36}$$

---

[3]The fact that regularization is desirable rather than necessary is demonstrated by the BPHZ, or zero-momentum, scheme of renormalization. [26]

[4]There is no counterterm for the gauge-fixing term in this definition of the counterterm Lagrangian. Such a term is zero due to the renormalization factor for the gauge parameter being as described in (1.33). Justification for renormalizing the gauge parameter in this way is evident when considering the finiteness of the renormalized BRST transformation of the $\bar{\eta}$ field.

where $\delta_i^\triangle$ and $\delta_i^\square$ denote the counterterms for the three- and four-point vertices for the relevant fields respectively and the traces over colour indices have been performed for clarity. The counterterms for the field renormalizations are trivial and given by,

$$
\begin{aligned}
\delta_2 &= Z_2 - 1, \\
\delta_3 &= Z_3 - 1, \\
\delta_\eta &= Z_\eta - 1,
\end{aligned}
\tag{1.37}
$$

whereas the counterterms for each interaction vertex involve multiple fields and have the more complicated forms,

$$
\begin{aligned}
\delta_g &= Z_g Z_2 Z_3^{1/2} - 1, \\
\delta_3^\triangle &= Z_g Z_3^{3/2} - 1, \\
\delta_3^\square &= Z_g^2 Z_3^2 - 1, \\
\delta_\eta^\triangle &= Z_g Z_2 Z_3^{1/2} - 1.
\end{aligned}
\tag{1.38}
$$

With the Lagrangian in this form, renormalizing the theory's parameters is equivalent to shifting the values of the counterterms away from zero.

The absolute normalization of the theory's parameters are fixed using several renormalization conditions, defined at the arbitrary renormalization scale μ. In this procedure there are two particular freedoms for the normalization of the theory: the finite value a given Green's function is normalized to as stipulated by the renormalization conditions and the momentum scale at which this normalization is defined.

The first consideration comes down to the size of the finite contribution to the counterterm which may be arbitrarily added without affecting the cancellation of the singularities. Adding or subtracting a finite contribution to the counterterm simply moves a finite quantity between the basic and counterterm Lagrangians and so leaves the functional integral unaltered. A systematic choice for the finite contribution to the counterterms defines the *renormalization scheme*, e.g., the *minimal subtraction* (MS) scheme is defined such that the finite pieces of the counterterms are zero, removing only the singularities defined as poles in ϵ when working in dimensional regularization.

As previously mentioned, the arbitrary partitioning of a finite quantity between the basic and counterterm Lagrangians leaves the functional integral invariant and so physical predictions of the theory are independent of the renormalization scheme chosen. This argument for scheme independence is only true at the level of the full theory. When approximating the full theory using a perturbative expansion the calculation of a physical quantity may display a residual scheme dependence due to the perturbative expansion being an asymptotic series and that series being truncated at a finite order. Although non-zero, the scheme dependence for a quantity calculated at $\mathcal{O}(\alpha_s^n)$, where $\alpha_s = g_s^2/4\pi$, is formally non-zero at $\mathcal{O}(\alpha_s^{n+1})$.

One scheme which is popular when performing higher order perturbative corrections is the *modified minimal subtraction* scheme ($\overline{\text{MS}}$) in which finite contributions occurring systematically order-by-order in the loop expansion are moved into the counterterm Lagrangian, thus removing them from the renormalized quantities and simplifying the results of calculations. For practical calculations this scheme amounts to working in the MS scheme and redefining the dimensional regularization parameter to be $\bar{\epsilon}$,

$$\bar{\epsilon} \;\; = \;\; \frac{1}{\bar{C}(\epsilon)} \, \epsilon \tag{1.39}$$

where $\bar{C}(\epsilon) = e^{-\gamma\epsilon}(4\pi)^\epsilon$ and γ is the Euler-Mascheroni constant.

The second freedom in the normalization of the theory is the arbitrary momentum scale, μ, at which the renormalization conditions apply. It is of course possible to renormalize the theory at an equally arbitrary yet different momentum scale, μ'. Clearly any physical observable is invariant under a shift of the arbitrary renormalization scale. For a dimensionless observable dependent on a single physical momentum scale s, the observable must be a function of (s/μ^2) to be dimensionally correct, where additional μ dependence enters via the renormalized coupling α_s due to the renormalization conditions. Such an observable's invariance under a continuous shift in the renormalization scale is given mathematically in the form of a differential equation,

$$\mu^2 \frac{\mathrm{d}}{\mathrm{d}\mu^2} R\big(s/\mu^2, \alpha_s(\mu^2)\big) \;\; = \;\; 0. \tag{1.40}$$

Expanding the exact differential and employing the convenient variable $t = \ln(s/\mu^2)$

yields,

$$\left[-\frac{\partial}{\partial t} + \beta(\alpha_s(\mu^2)) \frac{\partial}{\partial \alpha_s(\mu^2)} \right] R(e^t, \alpha_s(\mu^2)) = 0 \tag{1.41}$$

where $\beta(\alpha_s(\mu^2))$ is the QCD β-function which describes the variation of the coupling with a variation of the scale and is defined as,

$$\beta(\alpha_s(\mu^2)) = \mu^2 \frac{\partial \alpha_s(\mu^2)}{\partial \mu^2}. \tag{1.42}$$

Variation in the coupling allows (1.41) to be satisfied for any change in μ by exactly compensating with a change in α_s. The general solution to (1.42) for a change in scale between μ^2 and s is given by,

$$t = \int_{\alpha_s(\mu^2)}^{\alpha_s(s)} \frac{\mathrm{d}\alpha_s(\mu'^2)}{\beta(\alpha_s(\mu'^2))}, \tag{1.43}$$

For a suitably small value of the coupling the β-function can be expanded in α_s as a perturbative series,

$$\frac{1}{2\pi} \beta(\alpha_s(\mu^2)) = -\beta_0 \left(\frac{\alpha_s(\mu^2)}{2\pi} \right)^2 - \beta_1 \left(\frac{\alpha_s(\mu^2)}{2\pi} \right)^3 + \mathcal{O}(\alpha_s(\mu^2)^4). \tag{1.44}$$

By retaining only the first term in this series (1.42) can be approximately solved, resulting in the 1-loop running coupling,

$$\alpha_s(s) = \frac{\alpha_0}{1 + \alpha_0 \bar{\beta}_0 t}, \tag{1.45}$$

where $\alpha_0 = \alpha_s(\mu^2)$ and $\bar{\beta}_0 = \beta_0/2\pi$. Retaining higher terms in the perturbative expansion of the β-function provide higher loop corrections to this solution. The leading order coefficient is given by,

$$\beta_0 = \frac{11N - 2N_F}{6} \tag{1.46}$$

where for QCD $N = 3$ and N_F denotes the number of active quark flavours such that,

$$\beta_0 > 0 \qquad \text{for} \qquad N_F \leq 16, \tag{1.47}$$

which is certainly the case for the Standard Model at LHC energies.

Two aspects of this solution are immediately apparent: the behaviour of $\alpha_s(s)$ in the limit $s \to \infty$, $t \to \infty$ and the limit $s \to \mu^2 e^{-1/\bar{\beta}_0 \alpha_0}$, $t \to -1/\bar{\beta}_0 \alpha_0$. In the high

September 24, 2012

momentum scale limit the coupling decreases, an effect known as *asymptotic freedom*. It has been assumed at several points in this thesis that the coupling constant for QCD is suitably small such that perturbation theory can be reliably used to approximate the full theory; asymptotic freedom states that even if this assumption were not true at some scale, at a sufficiently high energy scale the assumption would hold. The utility of this result for scattering experiments such as the LHC is that within the parton model, not only can the cross section be factorized into a partonic cross section and hadronic PDFs but the partonic cross section can be reliably calculated within perturbation theory for sufficiently high centre of mass energy collisions. This goes some way to justifying the naïve parton model's assumption that a relativistic hadron can be considered as a weakly interacting collection of partons.

The second feature of this solution is the behaviour of the solution as $t \to -1/\bar{\beta}_0\alpha_0$. In this limit the denominator of (1.45) tends to zero and the coupling diverges to infinity. This result should not be interpreted as the physical coupling diverging at such a scale but rather evidence for the breakdown of a perturbative solution's reliability. The solution given by (1.45) is obtained by approximating the β-function as a perturbation series which is only valid in the small coupling limit[5].

A solution to (1.41) is given by,

$$R\big(e^t, \alpha_s(\mu^2)\big) \;=\; R\big(1, \alpha_s(s)\big) \tag{1.48}$$

such that the scale dependence of the observable is described entirely by the scale dependence of the running coupling. To demonstrate this consider the notation $\alpha = \alpha_s(\mu^2)$, $\alpha^* = \alpha_s(s)$, $\beta = \beta(\alpha)$, $\beta^* = \beta(\alpha^*)$ for clarity. Equation (1.41) written in the new variables is simply,

$$\left[-\frac{\partial}{\partial t} + \beta\frac{\partial}{\partial\alpha}\right] R(1, \alpha^*) \;=\; 0 \tag{1.49}$$

The fact that (1.48) provides a solution to this equation can be seen by first evalu-

---

[5]The analytic behaviour of the QCD coupling in the low energy limit remains an open problem; in particular the emergence of a linear inter-quark potential is necessary for *confinement*, the phenomenon whereby quarks are confined to colourless hadrons

ating the partial derivative of (1.43) with respect to t,

$$1 = \frac{\partial \alpha^*}{\partial t} \frac{1}{\beta^*} \tag{1.50}$$

then consider differentiating (1.43) with respect to α,

$$0 = \frac{\partial \alpha^*}{\partial \alpha} \frac{1}{\beta^*} - \frac{1}{\beta} \tag{1.51}$$

rearranging these equations yields,

$$\beta^* = \frac{\partial \alpha^*}{\partial t} \quad \& \quad \frac{\partial \alpha^*}{\partial \alpha} = \frac{\beta^*}{\beta} \tag{1.52}$$

which can be used to rewrite (1.49) in the form,

$$\left[-\beta^* \frac{\partial}{\partial \alpha^*} + \frac{\beta \cdot \beta^*}{\beta} \frac{\partial}{\partial \alpha^*} \right] R(1, \alpha^*) = 0, \tag{1.53}$$

such that any function which is purely a function of $\alpha^* = \alpha_s(s)$ satisfies this equation, in particular $R\big(1, \alpha_s(s)\big)$. This function can be expanded as a perturbative series in $\alpha_s(s)$,

$$R\big(1, \alpha_s(s)\big) = r_1 \alpha_s(s) + r_2 \alpha_s(s)^2 + \mathcal{O}(\alpha_s(s)^3). \tag{1.54}$$

Expanding (1.45) as a geometric progression allows $\alpha_s(s)$ to be written purely in terms of the coupling at a different scale[6] $\alpha_0 = \alpha_s(\mu^2)$ and the logarithm of the two kinematic scales, t,

$$\alpha_s(s) = \alpha_0 \sum_{n=0}^{\infty} \left[-\alpha_0 \bar{\beta}_0 t \right]^n, \tag{1.55}$$

such that by using the running coupling, the logarithms of different scales occurring in perturbation theory are automatically resummed. It is necessary in a fixed order calculation to keep track of all contributions to the observable entering at the same order in the expansion parameter. For a leading-order calculation is suffices to retain the first coefficient in (1.54) and the first term in the expansion for the running coupling,

$$R\big(1, \alpha_s(s)\big)_{\mathrm{LO}} = r_1 \alpha_0, \tag{1.56}$$

---

[6]The reference scale is commonly taken to be the mass of the Z^0 boson, $\mu^2 = M_Z$, due to the decreased experimental uncertainty on α_s at this scale

where no logarithms are present as would be expected from a leading-order calculation which doesn't require renormalization. At NLO the next term in the perturbation expansion for R is required, along with the NLO correction to the running coupling,

$$R\big(1, \alpha_s(s)\big)_{\text{NLO}} \;=\; \big(r_2 - \bar{\beta}_0 t\big)\, \alpha_0^2. \tag{1.57}$$

At NNLO it is necessary to solve (1.42) by including the NNLO corrections to the perturbative expansion of the β-function. By including the β_1 term and solving the β-function equation (1.42) an expression for the running coupling is obtained.

$$\frac{1}{\alpha} - \frac{1}{\alpha_0} + \xi \ln\left(\frac{\alpha(1 + \xi\alpha_0)}{\alpha_0(1 + \xi\alpha)}\right) - \bar{\beta}_0 t = 0, \tag{1.58}$$

where $\xi = \beta_1/(2\pi\beta_0)$. This implicit equation can be solved numerically to provide a value for the coupling at NNLO accuracy.

In principle the observable can be considered without fixing the scale to perform the resummation of the logarithms as has been described previously. For an arbitrary renormalization scale μ a dimensionless observable can be expanded in $\alpha_s(\mu^2)$, provided the coupling is suitably small at such a scale,

$$R\big(e^t, \alpha_s(\mu^2)\big) \;=\; \sum_{k=1}^{\infty} r_k(s/\mu^2)\alpha_s^k(\mu^2). \tag{1.59}$$

Inserting the perturbative expansion for R into (1.41) yields,

$$\sum_k \left(\mu^2 \frac{\partial r_k}{\partial \mu^2}\alpha_s^k(\mu^2) + 2k\beta r_k \alpha_s^{k-1}(\mu^2)\right) \;=\; 0. \tag{1.60}$$

Noting that $\beta = -\beta_0\alpha_s^2(\mu^2) + \mathcal{O}\big(\alpha_s^3(\mu^2)\big)$, the term proportional to the jth power of α_s is given by,

$$\alpha_s^j(\mu^2) \left[\mu^2 \frac{\partial r_j}{\partial \mu^2} - 2\beta_0(j-1)r_{j-1} - 2\frac{\beta_1}{2\pi}(j-2)r_{j-2} - \cdots\right] \;=\; 0. \tag{1.61}$$

From this equation it is clear that the scale variation of the term r_j is compensated by a sum over lower order terms up to r_{j-1}. Given these considerations, the scale variation of R truncated at order j (which may be interpreted as an estimate of the theoretical uncertainty on a calculation, or at least an estimate for one aspect of the uncertainty), is formally of order $j + 1$ and in principle decreases order-by-order in perturbation theory.

1.3 Infrared Behaviour of QCD Amplitudes

The renormalization procedure is primarily concerned with the removal of singularities present in perturbative calculations, the task for which the practice was devised. It should be noted that systematically removing the UV singularities via renormalization is a natural by-product of properly defining the theory with renormalization conditions, a concern which would have to be addressed even if no UV singularities were present in the theory's scattering amplitudes. From this perspective the presence of UV singularities, i.e., divergent behaviour of loop integrals in the high momentum limit, is somewhat artificial and an artefact of the theory being ill-defined.

For theories involving massless particles[7], divergences in calculations may also arise for a set of kinematic configurations. This set of limiting behaviour is given by configurations involving partons whose momenta are not large with respect to the centre of mass energy scale and are generically called infrared (IR) configurations. These configurations can involve internal or external particles becoming soft (vanishing energy) or collinear with another parton.

To demonstrate the IR behaviour of higher order corrections, the process $q\bar{q} \to X$ will be considered, where X is taken to be a generic colourless final-state such as a Drell-Yan pair or multiple vector boson production etc. This process displays all relevant classes of IR behaviour at NLO so it is a convenient example to consider. In addition to demonstrating the concepts of this chapter the process also forms the basis for the NNLO calculation presented in chapter 3. The leading-order cross section is given by,

$$\mathrm{d}\sigma_{q\bar{q}}^{LO} \;=\; \mathcal{N}\,\mathcal{N}_{LO} \int \mathrm{d}\Phi_X \; M_2^0(1_q, 2_{\bar{q}}; X), \tag{1.62}$$

where $M_2^0(1_q, 2_{\bar{q}}; X)$ is the single squared colour-ordered amplitude present at leading-order containing all dependence on non-QCD couplings and dynamics. The quantity $\mathcal{N}$ denotes the overall factors such as initial-state spin and colour averaging, hadron-

---

[7]This argument pertains to both exactly massless particles such as gluons or effectively massless particles in the high energy scattering limit such as the light quarks at the LHC.
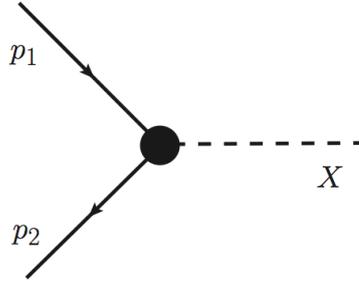
Figure 1.2: The diagram for the process $q\bar{q} \to X$ at leading-order, $\mathcal{O}(\alpha_s^0)$, with the dashed line representing the colourless final-state X, which may consist of more than one colourless particle coupling directly to the quarks.

hadron flux and QCD coupling,

$$
\mathcal{N} = \frac{1}{2s_{12}} \frac{1}{4 \cdot N^2} \left(\frac{\alpha_s}{2\pi} \right) \bar{C}(\epsilon),
\tag{1.63}
$$

with $\bar{C}(\epsilon) = (4\pi)^\epsilon e^{-\epsilon\gamma}$, $s_{12} = (p_1 + p_2)^2$ and $\mathcal{N}_{LO} = N$ denotes the leading-order colour factor. The form of the final-state phase space integral depends on the details of the colourless final-state and is not relevant for this discussion.

1.3.1 Virtual IR singularities

The IR singularity structure of renormalized virtual amplitudes has been systematically studied and is understood completely at the one- and two-loop level required for calculations up to NNLO accuracy.

One-loop singularities

Following the work of Catani [31], the singular parts of a one-loop amplitude, written as a vector in colour space, are governed by the equation,

$$
|\mathcal{M}_n^{(1)}(\mu^2, \epsilon, \{p_i\})\rangle = \boldsymbol{I}^{(1)}(\mu^2, \epsilon, \{p_i\}) \, |\mathcal{M}_n^{(0)}(\mu^2, \{p_i\})\rangle + |\mathcal{M}_n^{(1),f}(\mu^2, \{p_i\})\rangle
\tag{1.64}
$$

where $|\mathcal{M}_n^{(1),f}\rangle$ is an IR finite contribution in the limit $\epsilon \to 0$ and the IR singularity operator is defined as,

$$
\boldsymbol{I}^{(1)}(\mu^2, \epsilon, \{p_i\}) = \frac{e^{\gamma\epsilon}}{2\Gamma(1-\epsilon)} \sum_{i=1}^{n} \frac{1}{\boldsymbol{T}_i^2} \mathcal{V}_i(\epsilon) \sum_{j \neq i} \boldsymbol{T}_i \cdot \boldsymbol{T}_j \left(\frac{\rho\mu^2}{s_{ij}} \right)^\epsilon,
\tag{1.65}
$$

where the unitarity phase is denoted ρ with the value -1 when both particles in the pair are incoming or outgoing and +1 otherwise. The operators $\boldsymbol{T}_i$ satisfy the following properties [20],

$$
\begin{aligned}
(T_i)_{bc}^a &= t_{bc}^a & i &\in \{q_{\text{final}}, \bar{q}_{\text{initial}}\}, \\
(T_i)_{bc}^a &= -t_{bc}^a & i &\in \{q_{\text{initial}}, \bar{q}_{\text{final}}\}, \\
(T_i)_{bc}^a &= f_{abc} & i &\in \{g\} \\
\boldsymbol{T}_i \cdot \boldsymbol{T}_j &= \boldsymbol{T}_j \cdot \boldsymbol{T}_i & i &\neq j, \\
\boldsymbol{T}_i^2 &= \frac{N^2 - 1}{2N} & i &\in \{q, \bar{q}\}, \\
\boldsymbol{T}_i^2 &= N & i &\in \{g\},
\end{aligned}
\tag{1.66}
$$

in addition to the property of colour conservation for the amplitude,

$$
\sum_{i=1}^{n} \boldsymbol{T}_i \, |\boldsymbol{\mathcal{M}}_n\rangle = 0. \tag{1.67}
$$

The singular function is given by,

$$
\mathcal{V}_i(\epsilon) = \boldsymbol{T}_i^2 \frac{1}{\epsilon^2} + \gamma_i \frac{1}{\epsilon}, \tag{1.68}
$$

where,

$$
\begin{aligned}
\gamma_i &= \frac{3}{2} \frac{(N^2 - 1)}{2N} & i &\in \{q, \bar{q}\}, \\
\gamma_i &= \beta_0 & i &\in \{g\}.
\end{aligned}
\tag{1.69}
$$

Applying this method to the process $q\bar{q} \to X$ involves extracting the IR poles of the diagram shown in figure 1.3. For this process there are only two coloured particles, the quarks, with associated operators $\boldsymbol{T}_q$ and $\boldsymbol{T}_{\bar{q}}$ such that $\boldsymbol{T}_q^2 = \boldsymbol{T}_{\bar{q}}^2 = -\boldsymbol{T}_q \cdot \boldsymbol{T}_{\bar{q}} = C_F \cdot \boldsymbol{I}$ from colour conservation[8]. Applying this information to (1.65) yields an expression for the IR singularity operator,

$$
\boldsymbol{I}^{(1)}(\mu^2, \epsilon, 1_q, 2_{\bar{q}}) = -\frac{(N^2 - 1)}{2N} \frac{e^{\gamma\epsilon}}{\Gamma(1 - \epsilon)} \left[\frac{1}{\epsilon^2} + \frac{3}{2\epsilon} \right] \left(-\frac{\mu^2}{s_{12}} \right)^{\epsilon} \boldsymbol{I}. \tag{1.70}
$$

---

[8]Here the symbol $\boldsymbol{I}$ refers to the identity matrix in colour space and should not be confused with the IR singularity operator $\boldsymbol{I}^{(1)}$.
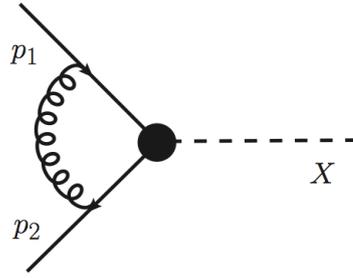
Figure 1.3: The NLO virtual diagram for the process $q\bar{q} \to X$

The poles of the squared matrix element are therefore given by,

$$\langle \mathcal{M}_2^{(0)} | \boldsymbol{I}^{(1)}(\epsilon) | \mathcal{M}_2^{(0)} \rangle \;=\; -\frac{(N^2-1)}{2N} \frac{e^{\gamma\epsilon}}{\Gamma(1-\epsilon)} \left[\frac{1}{\epsilon^2} + \frac{3}{2\epsilon} \right] \left(-\frac{\mu^2}{s_{12}} \right)^{\epsilon} |\mathcal{M}_2^0(1_q, 2_{\bar{q}}; X)|^2 \tag{1.71}$$

An alternative strategy is to work with colour ordered partial amplitudes as described in section 1.1.2. In this picture the IR singularity operator is no longer a matrix in colour space but a scalar, composed as a sum of two particle IR colour-ordered singularity operators, summed over colour-connected pairs in the colour-ordered amplitude. The one-loop squared matrix element is given by the projection of the one-loop partial amplitude onto the tree-level partial amplitude,

$$M_n^1 \;=\; \langle \mathcal{M}_n^1 | \mathcal{M}_n^0 \rangle + \langle \mathcal{M}_n^0 | \mathcal{M}_n^1 \rangle. \tag{1.72}$$

For a generic one loop squared matrix element the pole structure is described by the colour-ordered IR singularity operator in the following way,

$$\mathcal{P}oles \left[M_n^1(1, \cdots, n) \right] \;=\; 2\boldsymbol{I}_n^{(1)}(\epsilon; 1, \cdots, n) \, M_n^0(1, \cdots, n). \tag{1.73}$$

The colour-ordered singularity operator is given as a sum of two particle singularity operators over the set of neighbouring colour-connected pairs, $\mathcal{C}$,

$$\boldsymbol{I}_n^{(1)}(\epsilon; 1, \cdots, n) \;=\; \sum_{i,j \in \mathcal{C}} \boldsymbol{I}_{ij}^{(1)}(\epsilon, s_{ij}) \tag{1.74}$$

where the two particle colour-ordered IR singularity operators are defined for each combination of partons and the various possible colour structures [32],

$$\boldsymbol{I}_{q\bar{q}}^{(1)}(\epsilon, s_{q\bar{q}}) \;=\; -\frac{e^{\gamma\epsilon}}{2\Gamma(1-\epsilon)} \left[\frac{1}{\epsilon^2} + \frac{3}{2\epsilon} \right] \Re \left(-\frac{\mu^2}{s_{q\bar{q}}} \right)^{\epsilon},$$

$$
\begin{aligned}
\boldsymbol{I}_{qg}^{(1)}(\epsilon, s_{qg}) &= -\frac{e^{\gamma\epsilon}}{2\Gamma(1-\epsilon)}\left[\frac{1}{\epsilon^2}+\frac{5}{3\epsilon}\right]\Re\left(-\frac{\mu^2}{s_{qg}}\right)^{\epsilon}, \\
\boldsymbol{I}_{gg}^{(1)}(\epsilon, s_{gg}) &= -\frac{e^{\gamma\epsilon}}{2\Gamma(1-\epsilon)}\left[\frac{1}{\epsilon^2}+\frac{b_0}{\epsilon}\right]\Re\left(-\frac{\mu^2}{s_{gg}}\right)^{\epsilon}, \\
\boldsymbol{I}_{q\bar{q},F}^{(1)}(\epsilon, s_{q\bar{q}}) &= 0, \\
\boldsymbol{I}_{qg,F}^{(1)}(\epsilon, s_{qg}) &= \frac{e^{\gamma\epsilon}}{2\Gamma(1-\epsilon)}\frac{1}{6\epsilon}\Re\left(-\frac{\mu^2}{s_{qg}}\right)^{\epsilon}, \\
\boldsymbol{I}_{gg,F}^{(1)}(\epsilon, s_{q\bar{q}}) &= -\frac{e^{\gamma\epsilon}}{2\Gamma(1-\epsilon)}\frac{b_{0,F}}{\epsilon}\Re\left(-\frac{\mu^2}{s_{gg}}\right)^{\epsilon}.
\end{aligned}
\tag{1.75}
$$

In these expressions the colour decomposition of β_0 is used,

$$
\beta_0 = b_0 N + b_{0,F} N_F,
\tag{1.76}
$$

where $b_0 = 11/6$ and $b_{0,F} = -1/3$. This description of the IR singularity structure can be applied to the same example as previously considered. Only one colour-ordering exists for the process $qq \to X$ at one loop so carrying out the sum over internal colour degrees of freedom belonging to the virtual gluon allows the full squared amplitude to be written in terms of the colour stripped squared partial amplitude,

$$
|\boldsymbol{\mathcal{M}}_2^{(1)}(1_q, 2_{\bar{q}}; X)|^2 = \frac{(N^2-1)}{2N}\,\mathcal{N}_{LO}\,M_2^1(1_q, 2_{\bar{q}}; X).
\tag{1.77}
$$

Following equations (1.74) and (1.75) the poles of the one-loop colour ordered matrix element are given by,

$$
\mathcal{P}oles\left[M_2^1(1_q, 2_{\bar{q}}; X)\right] = 2\boldsymbol{I}_{q\bar{q}}^{(1)}(\epsilon, s_{12})\,M_2^0(1_q, 2_{\bar{q}}; X)
\tag{1.78}
$$

leading to an expression for the poles of the full squared matrix element,

$$
\mathcal{P}oles\left[|\boldsymbol{\mathcal{M}}_2^{(1)}(1_q, 2_{\bar{q}}; X)|^2\right] = \frac{(N^2-1)}{2N}\,2\boldsymbol{I}_{q\bar{q}}^{(1)}(\epsilon, s_{12})\,\mathcal{N}_{LO}\,M_2^0(1_q, 2_{\bar{q}}; X),
\tag{1.79}
$$

which can be compared with the expression found in (1.71)[9].

---

[9]The expressions differ only by imaginary factors which cancel in the overall calculation so extracting only the real component of $(-\mu^2/s_{ij})^{\epsilon}$ is sufficient. [32]

Two-loop singularities

The IR poles of a two-loop amplitude obey a factorization formula similar to the case at one-loop given by [31],

$$
\begin{aligned}
|\mathcal{M}_n^{(2)}(\mu^2, \epsilon, \{p_i\})\rangle &= \boldsymbol{I}^{(2)}(\mu^2, \epsilon, \{p_i\}) \, |\mathcal{M}_n^{(0)}(\mu^2, \{p_i\})\rangle + |\mathcal{M}_n^{(2),f}(\mu^2, \{p_i\})\rangle \\
&\quad + \boldsymbol{I}^{(1)}(\mu^2, \epsilon, \{p_i\}) \, |\mathcal{M}_n^{(1)}(\mu^2, \epsilon, \{p_i\})\rangle,
\end{aligned} \tag{1.80}
$$

where $|\mathcal{M}_n^{(2),f}\rangle$ is a finite function in the limit $\epsilon \to 0$. Note that the last line of (1.82) is not the same as $\left[\boldsymbol{I}^{(1)}\right]^2 |\mathcal{M}_n^{(0)}\rangle$ due to the premultiplication of the finite contribution in (1.64) by the IR singularity operator. As in the one-loop case the full amplitude can be written in terms of colour-ordered partial amplitudes. The two-loop squared matrix element contains the projection of the two-loop partial amplitude onto the tree-level partial amplitude and the self-interference of the one-loop partial amplitude,

$$
M_n^2 = \langle \mathcal{M}_n^2 | \mathcal{M}_n^0 \rangle + \langle \mathcal{M}_n^0 | \mathcal{M}_n^2 \rangle + \langle \mathcal{M}_n^1 | \mathcal{M}_n^1 \rangle \tag{1.81}
$$

The IR poles of an n-parton squared colour-ordered matrix element are given by [31],

$$
\begin{aligned}
\mathcal{P}oles\left[M_n^2(1, \cdots, n) \right] &= 2\boldsymbol{I}_n^{(1)}(\epsilon; 1, \cdots, n)\left(M_n^1(1, \cdots, n) - \frac{\beta_0}{\epsilon} \, M_n^0(1, \cdots, n) \right) \\
&\quad - 2\left[\boldsymbol{I}_n^{(1)}(\epsilon; 1, \cdots, n)\right]^2 M_n^0(1, \cdots, n) \\
&\quad + 2e^{-\gamma\epsilon}\frac{\Gamma(1-2\epsilon)}{\Gamma(1-\epsilon)}\left(\frac{\beta_0}{\epsilon} + K\right) \boldsymbol{I}_n^{(1)}(2\epsilon; 1, \cdots, n) \, M_n^0(1, \cdots, n) \\
&\quad + 2\boldsymbol{H}^{(2)}(\epsilon) \, M_n^0(1, \cdots, n).
\end{aligned} \tag{1.82}
$$

The constant K has the following colour decomposition,

$$
K = k_0 N + k_{0,F} N_F \tag{1.83}
$$

with the coefficients given by,

$$
k_0 = \frac{67}{18} - \frac{\pi^2}{6} \qquad k_{0,F} = -\frac{5}{9}. \tag{1.84}
$$

The hard radiation functions $\boldsymbol{H}^{(2)}(\epsilon)$ depend on the partonic content of the matrix element and may also be decomposed into various colour factors. Using this formula the poles of any two-loop squared matrix element can be isolated.

1.3.2 IR behaviour of real radiative corrections

The IR poles of a virtual matrix element are expressed immediately as a Laurent expansion in ϵ when calculating in dimensional regularization, either through use of the formulae of the previous section or by direct analytic loop integration in $d = 4 - 2\epsilon$ dimensions. QCD matrix elements, which are functions of Lorentz invariants constructed from external momenta, also exhibit divergent behaviour when a number of these invariants vanish. A general Lorentz invariant variable for massless partons is given by,

$$s_{ij} = (p_i + p_j)^2 = 2p_i \cdot p_j. \tag{1.85}$$

This quantity can vanish when either p_i or $p_j \to 0$, the soft limit, or when $p_i \cdot p_j = E_i E_j \big(1 - \cos(\theta)\big) \to 0$, the collinear limit when the spatial angle between partons $\theta \to 0$. Such configurations are unavoidable in practical calculations because the definition of the cross section involves integration of the final state external momenta over all phase space configurations, which inevitably receives contributions from soft and collinear regions of phase space.

Given that such configurations are generally unavoidable, the divergent behaviour depends on the form of the integrand, the IR divergent part of which is the squared matrix element. For a general amplitude the divergent behaviour is characterised by inverse powers of vanishing invariants such that the matrix element numerically diverges. In the case of colour-ordered partial amplitudes, the divergent behaviour is simplified such that the squared amplitude only contains inverse powers of invariants for colour-connected partons, those adjacent in the colour-ordering. For example, consider the tree level five gluon squared colour-ordered amplitude summed over helicities [33],

$$M_5^0(1_g, 2_g, 3_g, 4_g, 5_g) \;\; \propto \;\; \sum_{i=1}^{5} \sum_{j>i} \frac{s_{ij}^4}{s_{12}s_{23}s_{34}s_{45}s_{51}}. \tag{1.86}$$

This expression clearly demonstrates that the divergent IR behaviour is restricted to colour-connected partons. The full amplitude is formed from a sum of colour-ordered amplitudes such that following the sum over permutations divergences appear in all partonic channels, not just the colour-connected ones. The fact that

IR divergences for colour-ordered amplitudes are restricted to colour-connected partons reflects the structure of IR singularities for colour-ordered virtual amplitudes described by (1.74).

Single unresolved limits: tree-level

The single unresolved limits of colour-ordered matrix elements involve partons becoming soft or collinear with colour-adjacent partons. Although treated as massless, quarks are not able to become soft due to the fact that they are fermions constituting a conserved current. In the limit that a final-state quark's momentum becomes soft the matrix element vanishes such that the limit does not contribute to the phase space integral. The same is not true of gluons which as bosons do not obey a current conservation equation and do produce a contribution in the soft limit. In this limit the squared matrix element factorizes into a universal soft function and a reduced matrix element with the gluon pinched out. For a tree-level squared matrix element the factorization is given by [34],

$$M_{n+1}^0(\cdots, i, j_g, k, \cdots) \xrightarrow{j_g \to 0} S_{ijk} \; M_n^0(\cdots, i, k, \cdots). \tag{1.87}$$

The soft function does not depend on the species of parton neighbouring the soft gluon, i.e., the same function applies when the soft gluon is bookended by gluons or quarks, depending only on their momenta,

$$S_{ijk} = \frac{2s_{ik}}{s_{ij}s_{jk}}. \tag{1.88}$$

In the collinear limit where two partons i, j can be described by a single composite parton K, a generic squared matrix element factorizes according to [35],

$$M_{n+1}^0(\cdots, i, j, \cdots) \xrightarrow{i||j} \frac{1}{s_{ij}} P_{ij \to K}(z) \; M_n^0(\cdots, K, \cdots), \tag{1.89}$$

where z denotes the fraction of K's momentum carried by parton i. Unlike the case of soft divergences, the details of the splitting functions $P_{ij \to K}$ depend on the partons involved in the collinear limit and are collected here for completeness:

$$P_{qg \to Q} = \frac{1 + (1-z)^2 - \epsilon z^2}{z},$$

$$\begin{aligned}
P_{q\bar{q} \to G} &= \frac{z^2 + (1-z)^2 - \epsilon}{1 - \epsilon}, \\
P_{gg \to G} &= 2\left(\frac{z}{1-z} + \frac{1-z}{z} + z(1-z) \right),
\end{aligned} \tag{1.90}$$

with other splitting functions related by C-parity, $P_{\bar{q}g \to \bar{Q}} = P_{qg \to Q}$.

The discussion so far has concerned final-state partons becoming unresolved with one another. When a final state gluon becomes soft and is colour adjacent to one or more initial state partons, the matrix element factorization proceeds as in the final-state case; the only modification is that the Lorentz invariants must take into account the crossing of initial-state partons. i.e., for a final state parton i and initial state parton 1, $s_{1i} = (p_1 - p_i)^2 = -2p_1 \cdot p_i$. When the collinear limit involves initial-state partons the factorization formula (1.89) holds but the Altarelli-Parisi splitting functions are modified. For two final-state partons i, j coalescing to form a single composite parton k, as shown in figure 1.4(a), the kinematics are given by,

$$p_i = zp_k \qquad p_j = (1-z)p_k \tag{1.91}$$

whereas for a final state parton j becoming collinear with an initial state parton $\hat{i}$, where the hat denotes initial state,

$$p_j = zp_i \qquad p_k = (1-z)p_i \tag{1.92}$$

The different definition of z in the initial-final collinear configuration alters the definition of the splitting functions. The initial-final splitting functions are related to the final-final splitting functions by [36]:

$$\begin{aligned}
P_{gq \leftarrow Q}(z) &= \frac{1}{1-z}\frac{1}{1-\epsilon}P_{qg \to Q}(1-z), \\
P_{qg \leftarrow Q}(z) &= \frac{1}{1-z}P_{qg \to Q}(z), \\
P_{q\bar{q} \leftarrow G}(z) &= \frac{1-\epsilon}{1-z}P_{q\bar{q} \to G}(z), \\
P_{gg \leftarrow G}(z) &= \frac{1}{1-z}P_{gg \to G}(z)
\end{aligned} \tag{1.93}$$

Angular terms

The splitting functions defined previously are spin averaged splitting functions. The full splitting functions carry a dependence on the spin indices of the parent parton.

(a) (b)
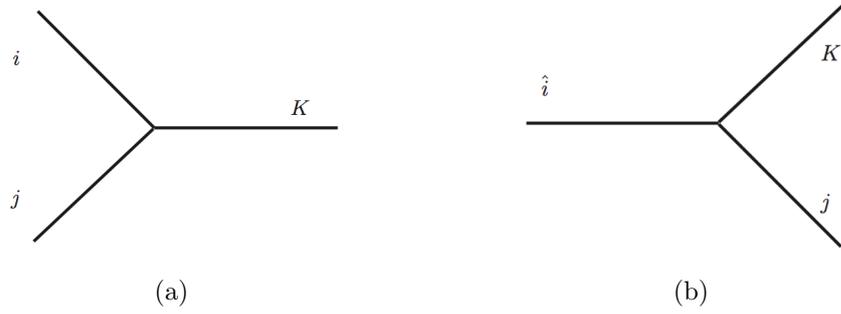
Figure 1.4

A massless fermion carries helicity $s = \pm 1$ and in the case of a parent quark the full splitting function is related to the spin averaged splitting function by,

$$P^{ss'}_{qg \to Q}(z) = \delta_{ss'} P_{qg \to Q}(z), \qquad (1.94)$$

where s and s' are the helicity indices of the parent quark in the splitting amplitude and its conjugate amplitude respectively. As the helicity dependence of the splitting function is simply the identity matrix in spin space no helicity correlations are present in the quark-initiated splitting functions and the spin averaged splitting functions completely describe the factorization of the appropriate matrix elements. In the case of splitting functions with a vector particle as the parent parton the spin is labelled by a Lorentz index $\mu = 1, \cdots, d$. The full splitting functions are tensorial in nature and given by [37]:

$$P^{\mu\nu}_{q\bar{q} \to G}(z, k_\perp) = -g^{\mu\nu} + 4z(1-z)\frac{k_\perp^\mu k_\perp^\nu}{k_\perp^2}$$

$$P^{\mu\nu}_{gg \to G}(z, k_\perp) = -2\left[g^{\mu\nu}\left(\frac{z}{1-z} + \frac{1-z}{z}\right) + 2(1-\epsilon)z(1-z)\frac{k_\perp^\mu k_\perp^\nu}{k_\perp^2}\right], \quad (1.95)$$

where $k_\perp^\mu$ is the component of momentum perpendicular to the collinear splitting axis. The momenta of the collinear partons can be parameterized in terms of $k_\perp$ and a light-like vector n such that $p_K \cdot n = k_\perp \cdot n = 0$,

$$p_i = zp_K + k_\perp + \xi_1 n,$$

$$p_j = (1-z)p_K - k_\perp + \xi_2 n. \qquad (1.96)$$

Requiring that the momenta remain on-shell fixes the constants to be [20],

$$\xi_1 = -\frac{1}{z}\frac{k_\perp^2}{2p_K \cdot n} \qquad \xi_2 = -\frac{1}{1-z}\frac{k_\perp^2}{2p_K \cdot n} \qquad (1.97)$$

In the collinear limit involving the splitting of a parent gluon, the factorization of the matrix element including all spin-dependent effects is given by,

$$M^0_{n+1}(\cdots, i, j, \cdots) \xrightarrow{i||j} \frac{1}{s_{ij}} P^{\mu\nu}_{ij \to K_g}(z, k_\perp)\, M^0_{n,\mu\nu}(\cdots, K_g, \cdots),$$

$$= \frac{1}{s_{ij}} P_{ij \to K_g}(z)\, M^0_n(\cdots, K_g, \cdots) + \text{ang.} \qquad (1.98)$$

The angular terms contain the ϕ-dependence of the tensorial splitting function and are proportional to $\cos(2\phi)$. As such when integrating over the ϕ variable in the final-state phase space integral any angular dependence vanishes. When dealing with quantities at the integrand level before integration over ϕ, the angular dependence must be taken into account. Given the functional dependence of the angular terms, if two phase space points related by an azimuthal rotation $\Delta\phi = \pi/2$ are systematically paired up, then the angular terms for the respective matrix elements will cancel exactly. This strategy has been implemented when studying the single collinear limits involving vector parent partons.

Single unresolved limits: loop-level

For NNLO calculations it is also necessary to consider the single unresolved limits of one-loop squared matrix elements. At one loop new universal singular functions are required which enter via modified factorization formulae. In the soft limit a one-loop colour-ordered matrix element factorizes according to [38],

$$M^1_{n+1}(\cdots, i, j, k, \cdots) \xrightarrow{j \to 0} S_{ijk}\, M^1_n(\cdots, i, k, \cdots) + S^1_{ijk}(\epsilon)\, M^0_n(\cdots, i, k, \cdots),$$

$$(1.99)$$

where $S^1_{ijk}(\epsilon)$ is the one-loop soft radiation function [39]. An analogous formula holds for the collinear factorization of the one-loop matrix elements,

$$M^1_{n+1}(\cdots, i, j, \cdots) \xrightarrow{i||j} \frac{1}{s_{ij}} P_{ij \to K}(z)\, M^1_n(\cdots, K, \cdots)$$

$$+ \frac{1}{s_{ij}} P^1_{ij \to K}(\epsilon, z)\, M^0_n(\cdots, K, \cdots), \qquad (1.100)$$

where the one-loop splitting functions are collected in [40].

Double unresolved limits

At NNLO the cross section includes a double-real radiative correction at tree-level which opens the final-state phase space up to an $(n + 2)$-parton phase space. The subsequent final-state phase space integration includes regions of phase space in which two partons can become simultaneously unresolved. In the double unresolved limits, the colour-ordered matrix element also factorize, with the details of the factorization pattern dictated by the colour-connections of the unresolved partons. In general the double unresolved radiation that can occur can be classified into three patterns, schematically depicted in figure 1.5:

- Colour-connected double unresolved partons. Both unresolved partons are adjacent in the colour ordering and share a common pair of hard radiating partons between which they are radiated.

- Almost colour-connected double unresolved partons. The unresolved partons are separated by one hard parton in the colour ordering. Each unresolved parton is radiated between a hard pair of radiators such that the hard parton separating the unresolved partons acts as a shared radiator.

- Colour-disconnected double unresolved partons. The unresolved partons are separated by more than one hard parton in the colour ordering. Each unresolved parton is radiated between a distinct pair of hard radiators.
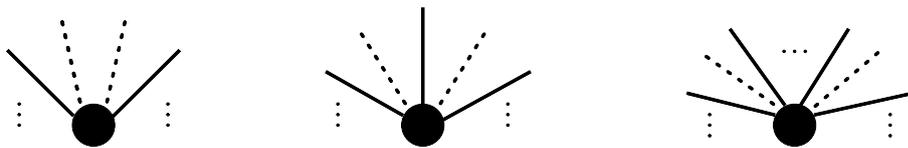
Figure 1.5: The three distinct radiation patterns at NNLO with solid and dashed lines representing hard and unresolved partons respectively. Colour-connected (l), almost colour-connected (c), colour disconnected (r).

At NNLO the means available for partons to become unresolved are the same as at NLO, soft and collinear partons; however there are new combinations of these basic unresolved configurations which generate genuinely NNLO behaviour. Within

the patterns of double unresolved radiation, described previously, the character of that unresolved radiation can be broadly classified into three classes:

- Soft: double unresolved soft radiation involves two partons becoming simultaneously soft and can be defined for colour-connected, almost colour-connected and colour disconnected configurations.

- Collinear: In the colour-connected configuration the situation whereby two partons become unresolved via collinear limits with neighbouring hard partons is called the *triple collinear* limit. In almost colour-connected and colour disconnected configurations two partons becoming collinear with distinct hard partons is referred to as the *double collinear* limit.

- Soft-collinear: the configuration whereby one parton is allowed to go soft whilst another becomes collinear can occur for all three colour configrations.

In each case the squared colour-ordered matrix elements obey factorization formulae similar to those at NLO involving either iterations of NLO singular functions or new NNLO singular functions, depending on the colour configuration under consideration.

Double soft behaviour

In the colour-connected configuration both soft particles are radiated between a common pair of hard radiators. When both soft partons are gluons the tree-level colour-ordered matrix elements factorize according to [41],

$$M_{n+2}^0(\cdots, i, j_g, k_g, l, \cdots) \overset{j,k \to 0}{\longrightarrow} S_{ijkl}\, M_n^0(\cdots, i, l, \cdots), \qquad (1.101)$$

where the identities of the hard partons does not affect the form of S_{ijkl}, just as for the case for radiation of a single soft gluon. In massless QCD it is also possible for a quark-antiquark pair to become soft simultaneously due to a soft gluon splitting into a quark-antiquark pair. In this case the factorization involves a universal function distinct from that of the soft gluon factorization [32],

$$M_{n+2}^0(\cdots, i, j_q, k_{\bar{q}}, l, \cdots) \overset{j,k \to 0}{\longrightarrow} S_{il}(j_q, k_{\bar{q}})\, M_n^0(\cdots, i, l, \cdots) \qquad (1.102)$$

In the almost colour-connected and colour disconnected limits the factorization patterns is an iteration of that at NLO, involving no new universal functions:

$$M_{n+2}^0(\cdots, i, j_g, k, l_g, m, \cdots) \xrightarrow{j,l \to 0} S_{ijk} \, S_{klm} \, M_n^0(\cdots, i, m, \cdots),$$

$$M_{n+2}^0(\cdots, i, j_g, k, \cdots, l, m_g, n, \cdots) \xrightarrow{j,m \to 0} S_{ijk} \, S_{lmn} \, M_n^0(\cdots, i, k, \cdots, l, n, \cdots).$$

(1.103)

The explicit forms of S_{ijkl} and $S_{il}(j_q, k_{\bar{q}})$ may be found in [ ].

Collinear behaviour

In the colour connected configuration the double unresolved limit is the triple collinear limit. Generally a squared colour-ordered matrix element in the triple collinear limit factorizes according to [42],

$$M_{n+2}^0(\cdots, i, j, k, \cdots) \xrightarrow{i\|j\|k} P_{ijk \to I}(x, y, z) \, M_n^0(\cdots, I, \cdots), \qquad (1.104)$$

were I denotes the composite parton and x, y, z are the fractions of parton I's momentum carried by the three daughter partons, i, j, k respectively. As with the single collinear splitting functions, the form of the triple collinear splitting functions depend on the species of parton involved in the collinear limit, making a total of seven distinct splitting functions,

$$
\begin{array}{ccc}
P_{ggg \to G} & P_{q\bar{q}g \to G} & P_{q\bar{q}g \to \tilde{G}}, \\
P_{qgg \to Q} & P_{q\tilde{g}\tilde{g} \to Q} & P_{q\bar{q}'q' \to Q}^{\text{ident}}, \\
& P_{q\bar{q}'q' \to Q}^{\text{non-ident}}.
\end{array}
$$

(1.105)

The splitting functions $P_{q\bar{q}g \to \tilde{G}}$ and $P_{q\tilde{g}\tilde{g} \to Q}$ occur for matrix elements whose gluons have been symmetrized over. Generally such amplitudes occur at sub-leading colour where the square of a coherent sum of colour-ordered amplitudes may be written as an incoherent sum of colour-ordered amplitudes containing Abelian gluons, as demonstrated in section 1.1.2. These splitting functions are also present at leading colour in SU(N) gauge theories with matter in the adjoint representation, such as $\mathcal{N} = 1$ supersymmetric QCD (SQCD), where the gluon and gluino are in the adjoint representation. This allows a triple collinear limit between a fermion and two gluons

which are not colour connected, seen in the colour ordering as $(\cdots, g, \tilde{g}, g, \cdots) \to (\cdots, \tilde{G}, \cdots)$. In QCD the fermions appear adjacent in the colour ordering, never separated by a gluon so such configurations are not possible. A full collection of triple collinear splitting functions may be found in [32].

The double collinear limit occurs when two partons are collinear with distinct hard partons and not with one another. This configuration is an iteration of the NLO single collinear limit and factorizes accordingly,

$$M_{n+2}^0(\cdots, i, j, \cdots, k, l \cdots) \xrightarrow{i||j,\ k||l} \frac{1}{s_{ij}} P_{ij \to I}(z_1) \frac{1}{s_{kl}} P_{kl \to K}(z_2)\ M_n^0(\cdots, I, \cdots, K, \cdots)$$

(1.106)

Soft-collinear behaviour

At NNLO the iteration of the soft and collinear unresolved limits permits a double unresolved limit combining the two in which one parton goes soft and another becomes collinear simultaneously. In the colour-connected limit both unresolved configurations occur between a common set of radiators and the squared colour-ordered matrix element factorizes to product of a single collinear splitting function and the soft-collinear factor [42],

$$M_{n+2}^0(\cdots, i, j, k, l \cdots) \xrightarrow{j \to 0,\ k||l} S_{i,jkl} \frac{1}{s_{kl}} P_{kl \to K}(z)\ M_n^0(\cdots, i, K, \cdots) \quad (1.107)$$

where K is the composite parton formed from the collinear partons. The cases where the soft parton is not colour connected to the collinear pair the squared colour-ordered matrix element factorizes according to an iteration of the single unresolved limits,

$$M_{n+2}^0(\cdots, i, j, k, \cdots, l, m \cdots) \xrightarrow{j \to 0,\ l||m} S_{ijk} \frac{1}{s_{lm}} P_{lm \to L}(z)\ M_n^0(\cdots, i, k, \cdots, L, \cdots)$$

(1.108)

Less singular configurations

The collection of unresolved limits in the previous sections are not exhaustive as the matrix elements may tend to a finite value or contain divergences in a number of unresolved limits. Such limits are however not relevant for the calculation of

the cross section as the phase space integration also carries factors of the vanishing invariants. In the case of the irrelevant unresolved limits the squared matrix elements are not singular enough to overcome the vanishing integration measure and so do not generate IR singular contributions when integrated over the appropriate phase space region.

1.3.3 Final-state singularity cancellation

In previous sections it has been shown that virtual amplitudes possess IR singularities which are expressed as a Laurent expansion in the dimensional regularization parameter ϵ. In the calculation of real emission processes IR divergences are encountered at the integrand level of the final-state phase space integral. It is well known due to the original work of Bloch and Nordsieck [43], with later developments from Kinoshita [44], Lee and Nauenberg [45] (KLN), that all IR singularities and divergences cancel in the physical cross section when summed over all physically degenerate configurations. From this perspective, the IR divergences found in real emission processes make perfect sense; the regions of phase space where the cross section diverges are those associated with configurations with unresolved radiation. By definition these configurations cannot contribute in an observable way to the final-state of which they are the unresolved limit and should instead be considered to contribute to the final-state with fewer particles that they tend to in the unresolved limit.

To genuinely compare the virtual contribution for a given final-state to the real contribution which tends to that final-state in the unresolved limit, the phase space associated with the unresolved particle must be integrated over analytically. In doing so the IR divergences are properly quantified and the remaining final-state phase space is identical to that of the virtual contribution. If the analytic integration is performed in $d = 4 - 2\epsilon$ dimensions, then the divergences at the integrand level manifest themselves as poles in ϵ upon integration, allowing for direct combination with the virtual contribution.

The process of performing the phase space integration analytically in d dimensions has been the subject of intense study for the last several decades and will be

the primary focus of this thesis. The NLO correction to an n-parton final-state at the LHC will receive a virtual n-parton contribution and a real $(n+1)$-parton contribution which are integrated over their respective phase spaces,

$$\mathrm{d}\sigma_{ij}^{NLO} \;\;=\;\; \int_{\Phi_n} \mathrm{d}\sigma_{ij}^{V} + \int_{\Phi_{n+1}} \mathrm{d}\sigma_{ij}^{R}, \tag{1.109}$$

where i and j denote the partons in the initial-state. If the unresolved regions of the $(n+1)$-parton phase space can be integrated over analytically then the IR divergent integrand can be integrated to produce an IR singular function multiplying a finite n-parton phase space integral. At NNLO the cross section receives contributions from the double virtual two-loop n-parton final-state contribution, the real-virtual one-loop $(n+1)$-parton contribution and the double real $(n+2)$-parton contribution,

$$\mathrm{d}\sigma_{ij}^{NNLO} \;\;=\;\; \int_{\Phi_n} \mathrm{d}\sigma_{ij}^{VV} + \int_{\Phi_{n+1}} \mathrm{d}\sigma_{ij}^{RV} + \int_{\Phi_{n+2}} \mathrm{d}\sigma_{ij}^{RR}. \tag{1.110}$$

In the case of an NNLO calculation, integrating the real-virtual and double real contributions analytically over the single- and double-unresolved phase space regions respectively yields the poles in ϵ required to cancel the explicit singularities coming from the loop integrals in the one- and two-loop contributions. The details how this cancellation is achieved are explained in more depth in chapter 2.

It should be noted that the IR singularity cancellation obtained by summing over physically degenerate final-states serves to cancel the virtual singularities against those generated by final-state partons becoming soft or collinear with other final-state partons. For hadronic collisions (the relevant case for the LHC) additional singularities persist, originating in final-state partons becoming collinear with initial-state partons. The cancellation of these singularities will be explained in section 1.4 as the natural consequence of properly defining the observable under consideration, as was the case with the UV poles in renormalization and the final-state IR poles discussed here.

To demonstrate the final-state IR pole cancellation the example of NLO corrections to the process $q\bar{q} \to X$ is once again considered. The singularity structure of the virtual contribution has already been discussed in section 1.3.1, the main result being,

$$\mathcal{P}oles\left[M_2^{(1)}(1_q, 2_{\bar{q}}; X)\right] \;\;=\;\; 2\boldsymbol{I}_{q\bar{q}}^{(1)}(\epsilon, s_{12})\, M_2^0(1_q, 2_{\bar{q}}; X). \tag{1.111}$$
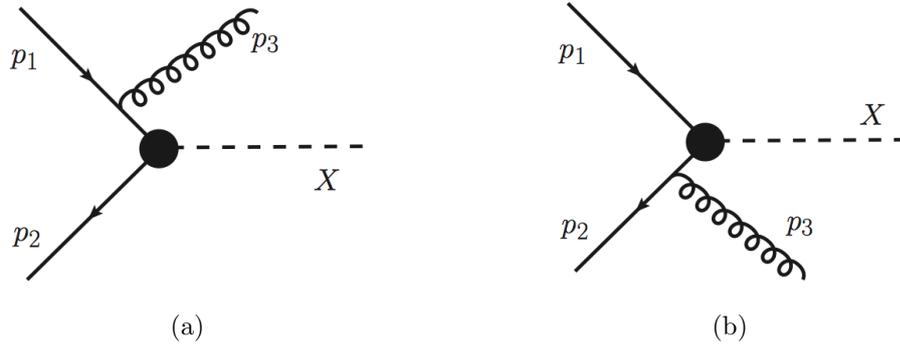
Figure 1.6: The two diagrams contributing to the NLO real radiative correction to the process $q\bar{q} \to X$.

The virtual cross section is given by,

$$d\sigma_{q\bar{q}}^V = \mathcal{N} \, \mathcal{N}_{LO} \, \frac{N^2 - 1}{2N} \int d\Phi_X \, M_2^1(1_q, 2_{\bar{q}}; X), \qquad (1.112)$$

and so the singularity structure of the virtual cross section factors out of the phase space integral yielding,

$$\mathcal{P}oles\big[d\sigma_{q\bar{q}}^V\big] = 2\boldsymbol{I}_{q\bar{q}}^{(1)}(\epsilon, s_{12}) \, \frac{N^2 - 1}{2N} \, d\sigma_{q\bar{q}}^{LO} \qquad (1.113)$$

The diagrams constituting the single real radiative correction to this process are shown in figure 1.6. For a single radiated gluon there is only one colour-ordered amplitude and the total amplitude is given by,

$$|\boldsymbol{\mathcal{M}}_3^{(0)}(1_q, 3_g, 2_{\bar{q}}; X)|^2 = \frac{(N^2 - 1)}{2N} \, \mathcal{N}_{LO} \, M_3^0(1_q, 3_g, 2_{\bar{q}}; X), \qquad (1.114)$$

such that the real emission cross section has the form,

$$d\sigma_{q\bar{q}}^R = \mathcal{N} \, \mathcal{N}_{LO} \, \frac{N^2 - 1}{2N} \int d\Phi_{X+1} \, M_3^0(1_q, 3_g, 2_{\bar{q}}; X), \qquad (1.115)$$

where the phase space integral includes the final-state gluon as well as the phase space associated with X. By integrating over the unresolved regions of the gluon's phase space it can be shown[10] that the singularities of the real radiation upon

---

[10]The integration can either be performed directly or via a subtraction method such as antenna subtraction which in the case considered is particularly simple and is elaborated upon in chapter 3.

September 24, 2012

analytic integration are given by,

$$
\begin{aligned}
\mathcal{P}oles\left[\int_1 \mathrm{d}\sigma_{q\bar{q}}^R\right] &= \mathcal{N}\,\mathcal{N}_{LO}\,\frac{N^2-1}{2N}\left\{-2\boldsymbol{I}_{q\bar{q}}^{(1)}(\epsilon, s_{12})\int \mathrm{d}\Phi_X\,M_2^0(1_q, 2_{\bar{q}}; X)\right. \\
&\quad - \frac{1}{\epsilon}\int \mathrm{d}\Phi_X'\,\frac{\mathrm{d}x_2}{x_2}\,p_{qq}^{(0)}(x_2)\,M_2^0(1_q, x_2 2_{\bar{q}}; X) \\
&\quad \left. - \frac{1}{\epsilon}\int \mathrm{d}\Phi_X'\,\frac{\mathrm{d}x_1}{x_1}\,p_{qq}^{(0)}(x_1)\,M_2^0(x_1 1_q, 2_{\bar{q}}; X)\right\}.
\end{aligned}
\tag{1.116}
$$

In the second and third lines of (1.116) the final-state phase space measure is denoted $\mathrm{d}\Phi_X'$ which is related to the phase space measure $\mathrm{d}\Phi_X$ by a rescaling of one of the initial-state parton's momenta, i.e., the total mass of the final-state is rescaled by one of the variables $x_{1,2}$, which are themselves integrated over. The function $p_{qq}^{(0)}(x)$ is as yet undefined and a discussion of the (IR singular) terms proportional to them is deferred until section 1.4. Putting aside these singularities, the first line of (1.116) can be written in the form,

$$
-2\boldsymbol{I}_{q\bar{q}}^{(1)}(\epsilon, s_{12})\,\frac{N^2-1}{2N}\,\mathrm{d}\sigma_{q\bar{q}}^{LO},
\tag{1.117}
$$

which clearly cancels against the IR poles of the virtual contribution as presented in (1.113).

1.4 Factorization and the QCD Improved Parton Model

The factorization formula (1.32) for the naïve parton model describes the cross section for a hadronic collision in terms of the cross section for a partonic collision weighted by a PDF and summed over all partonic sub-processes contributing to the same hadronic process. This model was based upon the assumptions that the hadron may be thought of as a collection of essentially free partons moving in the direction of the hadron's motion, each carrying a definite fraction of the hadron's momentum. Given the more detailed understanding of QCD presented in the previous sections it is clear that such a picture is approximate and only valid for the high centre of mass scattering limit. To make accurate predictions within the parton model for scattering experiments it is essential to develop the model to the same degree of

rigour as the calculation of the hard scattering subprocesses used as the model's input. When performing calculations for high energy colliders, such as the LHC, this requires formulating the parton model within the framework of perturbation theory.

From this perspective the naïve parton model is expected to constitute the leading-order approximation to the more complete perturbative solution. Moving beyond leading-order in perturbation theory involves incorporating interactions order-by-order in the small coupling, i.e., by considering radiative corrections to the leading-order picture. In the naïve parton model the distinction between the parton level process and the hadron is artificial but clear; the partons are considered free and do not interact with the rest of the hadron. Introducing perturbative interactions complicates the distinction between the collection of partons and the non-perturbative hadron, allowing an almost free parton to radiate other partons thus changing the instantaneous distribution of momentum described by the PDF. In terms of the heuristic picture considered when motivating the naïve parton model, QCD radiation from a parton can generate significant transverse momentum either for the radiated parton or for the radiator recoiling against its radiation. These interactions which occur in perturbation theory violate the assumption that the partons travel in the same direction as the hadron with small transverse momentum.

In order to perform perturbative calculations in a meaningful way a momentum scale μ_F is introduced to define the distinction between soft hadronic and hard partonic physics, named the *factorization scale*. Radiated partons with transverse momentum greater than the factorization scale are considered to be part of the hard scattering process whereas those with transverse momentum below the cutoff are considered part of the hadron. This process is essentially the observation that QCD radiation from the incoming partons with small transverse momentum is unobservable and serves only to alter the instantaneous momentum distribution of the hadron. Partitioning what belongs to the hard scattering process and the hadron with a sharp momentum cutoff causes both quantities to depend on the artificial scale, μ_F, such that the hadronic cross section remains independent of the scale.

The process of partitioning the physics into partonic and hadronic contributions,

known as *factorization*, is in direct analogy to the definition of the renormalization scheme whereby the bare Lagrangian is partitioned into the basic Lagrangian and the counter-term Lagrangian, the details of which do not affect the functional integral. In the spirit of this analogy the PDFs entering into (1.32) are referred to as the bare PDFs. In renormalization the physical parameters are related to the bare parameters by a multiplicative Z-factor, into which the UV singularities of the theory can be absorbed by defining the theory at a renormalization scale μ. In a similar fashion the bare PDF, denoted symbolically[11] as $\boldsymbol{f}^0$, can be related to a *physical* PDF, $\boldsymbol{f}$, not by a multiplicative factor but by a convolution with a factorization kernel, by convention denoted $\boldsymbol{\Gamma}^{-1}$ [46] [47].

$$\begin{aligned}
\boldsymbol{f}^0 &= \left[\boldsymbol{f} \otimes \boldsymbol{\Gamma}^{-1}\right], \\
f_i^0(z) &= \int \mathrm{d}x \, \mathrm{d}y \, f_j(x, \mu_F) \, \Gamma_{ji}^{-1}(y, \mu_F) \, \delta(z - xy).
\end{aligned} \tag{1.118}$$

In the case of renormalization the bare parameters are independent of the renormalization scale but both the physical parameters and the renormalization factors depend on the sliding scale in such a way that any dependence cancels in their combination. In the case of factorization the bare PDF is independent of the factorization scale but the physical PDF and the factorization kernel Γ_{ji}^{-1} do depend on the artificial scale in such a way that any dependence cancels in the convolution of the two. If the factorization scale is sufficiently large then the factorization kernel may be expanded as a perturbative series in the QCD coupling. For practical calculations the perturbative expansion is truncated at a finite order and this process of approximation causes the truncated perturbative calculation to display a residual dependence on the factorization scale, just as was the case with the renormalization scale in perturbative calculations.

The factorization kernel has an inverse operator, Γ_{ji} which for suitably small coupling can be expanded as a perturbative series. In symbolic notation,

$$\boldsymbol{\Gamma} = \boldsymbol{I} + \frac{\alpha_s}{2\pi} \boldsymbol{\Gamma}^1 + \left(\frac{\alpha_s}{2\pi}\right)^2 \boldsymbol{\Gamma}^2 + \mathcal{O}(\alpha_s^3) \tag{1.119}$$

---

[11]In this notation the bold quantities are vectors or matrices in the parton flavour space

where the x and μ_F dependence enters through the coefficients Γ_{ji}^k and α_s respectively as can be seen by dropping the symbolic notation,

$$
\begin{aligned}
\Gamma_{ji}(x, \mu_F) &= \delta_{ji}\, \delta(1-x) + \frac{\alpha_s(\mu_F^2)}{2\pi}\, \Gamma_{ji}^1(x) \\
&\quad + \left(\frac{\alpha_s(\mu_F^2)}{2\pi}\right)^2 \Gamma_{ji}^2(x) + \mathcal{O}\big(\alpha_s^3(\mu_F)\big).
\end{aligned}
\tag{1.120}
$$

As the inverse operator of $\boldsymbol{\Gamma}^{-1}$ this operator relates the physical PDF to the bare quantity,

$$
\boldsymbol{f} = \left[\boldsymbol{f}^0 \otimes \boldsymbol{\Gamma}\right]
\tag{1.121}
$$

This expression for $\boldsymbol{\Gamma}$ can be simply inverted to define the perturbative expansion for $\boldsymbol{\Gamma}^{-1}$ to the same order in α_s,

$$
\boldsymbol{\Gamma}^{-1} = \boldsymbol{I} - \frac{\alpha_s}{2\pi}\, \boldsymbol{\Gamma}^1 - \left(\frac{\alpha_s}{2\pi}\right)^2 \left[\boldsymbol{\Gamma}^2 - \left[\boldsymbol{\Gamma}^1 \otimes \boldsymbol{\Gamma}^1\right]\right] + \mathcal{O}(\alpha_s^3)
\tag{1.122}
$$

In an abuse of notation that makes the similarities with renormalization clear, it is possible to define what could be considered to be a mass factorization counterterm,

$$
\boldsymbol{\Gamma}^{-1} = \boldsymbol{I} + \boldsymbol{\delta}_\Gamma
\tag{1.123}
$$

which is in general a non-diagonal matrix in the flavour space of the partons. By redefining the hadronic cross section in terms of the physical PDFs it takes on the symbolic form,

$$
\mathrm{d}\boldsymbol{\sigma} = \boldsymbol{f} \otimes \boldsymbol{\Gamma}^{-1} \cdot \mathrm{d}\boldsymbol{\sigma} \cdot \boldsymbol{\Gamma}^{-1} \otimes \boldsymbol{f}',
\tag{1.124}
$$

where $\boldsymbol{f}$ and $\boldsymbol{f}'$ denote the two physical PDFs. From this expression it is possible to define the *factorized cross section* by absorbing the factorization kernels into its definition,

$$
\mathrm{d}\hat{\boldsymbol{\sigma}} = \boldsymbol{\Gamma}^{-1} \cdot \mathrm{d}\boldsymbol{\sigma} \cdot \boldsymbol{\Gamma}^{-1}.
\tag{1.125}
$$

This process is in analogy to the redefinition of a general operator in the Lagrangian under the field and coupling reparameterization induced by renormalization. Following the analogy with renormalization to its conclusion, it is possible to partition

the factorized cross section into a basic cross section and a counterterm cross section using (1.123),

$$\mathrm{d}\hat{\boldsymbol{\sigma}} \quad = \quad \mathrm{d}\hat{\boldsymbol{\sigma}}_{\mathrm{basic}} + \mathrm{d}\hat{\boldsymbol{\sigma}}_{\mathrm{c.t}}, \tag{1.126}$$

such that

$$\mathrm{d}\hat{\boldsymbol{\sigma}}_{\mathrm{basic}} \quad = \quad \mathrm{d}\boldsymbol{\sigma}, \tag{1.127}$$

which is calculated using the methods and framework set out so far in this chapter and will in general contain IR singularities associated with initial-final collinear configurations, such as those shown explicitly in (1.116) for the example $q\bar{q} \to X$ at NLO. The counterterm cross section has the symbolic form,

$$\mathrm{d}\hat{\boldsymbol{\sigma}}_{\mathrm{c.t}} \quad = \quad \boldsymbol{\delta}_{\Gamma} \cdot \mathrm{d}\boldsymbol{\sigma} \cdot \boldsymbol{I} + \boldsymbol{I} \cdot \mathrm{d}\boldsymbol{\sigma} \cdot \boldsymbol{\delta}_{\Gamma} + \boldsymbol{\delta}_{\Gamma} \cdot \mathrm{d}\boldsymbol{\sigma} \cdot \boldsymbol{\delta}_{\Gamma}, \tag{1.128}$$

where the form of $\boldsymbol{\delta}_{\Gamma}$ is trivially inferred from (1.122). Just as in renormalization the counterterms can now be adjusted order by order in perturbation theory to remove any initial-state collinear singularities present in the basic cross section. The choice of *factorization scheme* determines the size of the finite piece of the basic cross section also absorbed into the definition of the physical PDF on top of the singular contribution.

By expanding the factorization counterterms and the unfactorized cross section as a perturbative series the counterterm cross section has the form,

$$\mathrm{d}\boldsymbol{\sigma}_{\mathrm{c.t}} = \frac{\alpha_s}{2\pi} \, \mathrm{d}\boldsymbol{\sigma}_{NLO}^{MF} + \left(\frac{\alpha_s}{2\pi}\right)^2 \, \mathrm{d}\boldsymbol{\sigma}_{NNLO}^{MF} + \mathcal{O}(\alpha_s^3). \tag{1.129}$$

These terms are traditionally called mass factorization contributions are defined in terms of the factorization kernels,

$$\begin{aligned}
\mathrm{d}\boldsymbol{\sigma}_{NLO}^{MF} \quad &= \quad -\left[\boldsymbol{\Gamma}^1 \cdot \mathrm{d}\boldsymbol{\sigma}_{LO} \cdot \boldsymbol{I} + \boldsymbol{I} \cdot \mathrm{d}\boldsymbol{\sigma}_{LO} \cdot \boldsymbol{\Gamma}^1\right] \\
\mathrm{d}\boldsymbol{\sigma}_{NNLO}^{MF} \quad &= \quad -\Big[\boldsymbol{\Gamma}^2 \cdot \mathrm{d}\boldsymbol{\sigma}_{LO} \cdot \boldsymbol{I} + \boldsymbol{I} \cdot \mathrm{d}\boldsymbol{\sigma}_{LO} \cdot \boldsymbol{\Gamma}^2 - \left[\boldsymbol{\Gamma}^1 \otimes \boldsymbol{\Gamma}^1\right] \cdot \mathrm{d}\boldsymbol{\sigma}_{LO} \cdot \boldsymbol{I} \\
&\qquad - \boldsymbol{I} \cdot \mathrm{d}\boldsymbol{\sigma}_{LO} \cdot \left[\boldsymbol{\Gamma}^1 \otimes \boldsymbol{\Gamma}^1\right] - \boldsymbol{\Gamma}^1 \cdot \mathrm{d}\boldsymbol{\sigma}_{LO} \cdot \boldsymbol{\Gamma}^1 \\
&\qquad + \boldsymbol{\Gamma}^1 \cdot \mathrm{d}\boldsymbol{\sigma}_{NLO} \cdot \boldsymbol{I} + \boldsymbol{I} \cdot \mathrm{d}\boldsymbol{\sigma}_{NLO} \cdot \boldsymbol{\Gamma}^1\Big].
\end{aligned} \tag{1.130}$$

The factorized perturbative cross sections as matrices in flavour space up to NNLO are therefore given by,

$$\mathrm{d}\hat{\boldsymbol{\sigma}}_{LO} = \mathrm{d}\boldsymbol{\sigma}_{LO}, \tag{1.131}$$

$$\mathrm{d}\hat{\boldsymbol{\sigma}}_{NLO} = \mathrm{d}\boldsymbol{\sigma}_{NLO} + \mathrm{d}\boldsymbol{\sigma}_{NLO}^{MF},$$

$$\mathrm{d}\hat{\boldsymbol{\sigma}}_{NNLO} = \mathrm{d}\boldsymbol{\sigma}_{NNLO} + \mathrm{d}\boldsymbol{\sigma}_{NNLO}^{MF}. \tag{1.132}$$

The details of the mass factorization counterterms, especially within the context of antenna subtraction, will be covered in greater depth in chapter 2.

Introducing the factorization scale and including radiation from initial-state partons, as required by QCD, the hadronic cross section in the *QCD improved parton model*, including all scale dependence, is summarized in the following formula,

$$\mathrm{d}\hat{\sigma}(P_1, P_2) = \sum_{i,j} \int \frac{\mathrm{d}\xi_1}{\xi_1} \frac{\mathrm{d}\xi_2}{\xi_2} \, f_i(\xi_1, \mu_F) f_j(\xi_2, \mu_F)$$

$$\times \quad \mathrm{d}\hat{\sigma}_{ij}(\xi_1 P_1, \xi_2 P_2, \alpha_s(\mu^2), \alpha_s(\mu_F^2), s/\mu^2, s/\mu_F^2). \tag{1.133}$$

To demonstrate the utility of this model the example of NLO corrections to the process $q\bar{q} \rightarrow X$ is considered in the context of the QCD improved parton model. It has been demonstrated in section 1.3.3 that the IR singularities of the virtual contribution to the cross section partially cancel against the real radiation contribution upon analytic integration over the radiated particle's unresolved phase space. The remaining singular contributions were shown in (1.116). In the QCD improved parton model at NLO an additional contribution to the cross section must be calculated, the mass factorization contribution. Following the definitions and results of this section the NLO mass factorization contribution for this example is given by,

$$\mathrm{d}\boldsymbol{\sigma}_{NLO}^{MF} = -\boldsymbol{\Gamma}^1 \cdot \mathrm{d}\boldsymbol{\sigma}_{LO} \cdot \boldsymbol{I} - \boldsymbol{I} \cdot \mathrm{d}\boldsymbol{\sigma}_{LO} \cdot \boldsymbol{\Gamma}^1. \tag{1.134}$$

For the process $q\bar{q} \rightarrow X$ there is only one non-zero element in the leading-order cross section's flavour matrix, $\mathrm{d}\sigma_{q\bar{q}}^{LO}$. Consequently only one factorization kernel is relevant to this calculation, $\boldsymbol{\Gamma}_{qq}^1$, which in the $\overline{\mathrm{MS}}$ factorization scheme is given by[12],

$$\boldsymbol{\Gamma}_{qq}^1 = -\frac{N^2 - 1}{2N} \frac{1}{\epsilon} \, p_{qq}^{(0)}(x). \tag{1.135}$$

---

[12] Although just an element of the flavour matrix, $\boldsymbol{\Gamma}_{qq}^1$ remains boldface as it contains colour

Dropping the symbolic notation and substituting this expression for the factorization kernel into the formula for the NLO mass factorization cross section yields,

$$
\mathrm{d}\sigma_{q\bar{q},NLO}^{MF}(\xi_1 P_1, \xi_2 P_2) = \frac{1}{\epsilon}\frac{N^2-1}{2N}\bigg\{ \int \frac{\mathrm{d}x_1}{x_1}\, p_{qq}^{(0)}(x_1)\, \mathrm{d}\sigma_{q\bar{q}}^{LO}(x_1\xi_1 P_1, \xi_2 P_2)
$$
$$
+ \int \frac{\mathrm{d}x_2}{x_2}\, p_{qq}^{(0)}(x_2)\, \mathrm{d}\sigma_{q\bar{q}}^{LO}(\xi_1 P_1, x_2\xi_2 P_2) \bigg\}.
$$
$$(1.136)$$

It is straightforward to see that when this expression is combined with that of the basic cross section, given in (1.116), the remaining poles cancel[13] such that the fully renormalized and factorized cross section using physical PDFs is UV and IR finite up to NLO for the example considered here. The collinear factorization theorem [48] extends this analysis to all orders in perturbation theory. An all-order analysis of factorization is an extremely complicated field of study and is far from complete, specifically in the case of hadronic collisions as has been demonstrated by recent developments [49].

For convenience the scale is frequently set such that $\mu_F = \mu$ where μ is the renormalization scale. It was shown in section 1.2 that by introducing a running coupling constant, the UV logarithms which occur in the hard scattering cross section at higher orders in perturbation theory are automatically resummed. The fully factorized cross section when computed in perturbation theory will contain logarithms with the argument s/μ_F^2 in a similar fashion. By introducing a running PDF which can be evolved to any scale from the factorization scale at which it is defined, the logarithms associated with a perturbative calculation can be resummed. The differential equation governing the evolution of the physical PDF can be inferred from (1.121) and is given in symbolic form as,

$$
\mu^2 \frac{\partial \boldsymbol{f}}{\partial \mu^2} = \frac{\alpha_s}{2\pi}\big[\boldsymbol{p} \otimes \boldsymbol{f}\big],
$$
$$(1.137)$$

---

factors. The symbol Γ^1 is reserved for colour stripped factorization kernels, for more details see appendix A.

[13]An issue not considered here is that for a full cancellation to occur, the QCD coupling associated with the mass factorization terms and the basic cross section should be equal. This is not the case in general as they are evaluated at different scales however the difference is formally of $\mathcal{O}(\alpha_s^2)$ and so does not affect the NLO singularity cancellation.

where $\boldsymbol{p}$ denotes a splitting function which is in general a matrix in flavour space. In terms of components this equation is given by,

$$
\begin{aligned}
\mu^2 \frac{\partial}{\partial \mu^2} f_i(x, \mu^2) &= \frac{\alpha_s(\mu^2)}{2\pi} \int_0^1 \mathrm{d}y \int_0^1 \mathrm{d}z \; p_{ij}(z) \; f_j(y, \mu^2) \; \delta(x - yz), \\
&= \frac{\alpha_s(\mu^2)}{2\pi} \int_x^1 \frac{\mathrm{d}y}{y} \; p_{ij}(x/y) \; f_j(y, \mu^2),
\end{aligned}
\tag{1.138}
$$

where the splitting function has the perturbative expansion,

$$
p_{ij}(x) = p_{ij}^{(0)}(x) + \frac{\alpha_s}{2\pi} \; p_{ij}^{(1)}(x) + \mathcal{O}(\alpha_s^2)
\tag{1.139}
$$

This equation is known as the Dokshitzer-Gribov-Lipatov-Alterelli-Parisi (DGLAP) evolution equation [35] [50] [51], the solutions of which allow a PDF defined at a given momentum scale to be evolved to another scale within the perturbative regime[14].

Using the DGLAP equation for the scale variation of the PDFs and the fact that the hadronic cross section is independent of the factorization scale, the scale variation of the factorized cross section is given by,

$$
\mu^2 \frac{\partial}{\partial \mu^2} \mathrm{d}\hat{\boldsymbol{\sigma}} = \frac{\alpha_s}{2\pi} \left[\boldsymbol{p} \otimes \mathrm{d}\hat{\boldsymbol{\sigma}} \cdot \boldsymbol{I} + \boldsymbol{I} \cdot \mathrm{d}\hat{\boldsymbol{\sigma}} \otimes \boldsymbol{p} \right].
\tag{1.140}
$$

Solving this equation yields the full logarithmic dependence of the cross section on the scale variation within the perturbative regime.

1.5 Jets and their cross sections

QCD as a gauge field theory of quarks and gluons is well defined and, at least perturbatively, well understood. Much of the theoretical development since QCD's invention has gone towards calculating a more accurate hard cross section, the main tasks of which involve performing loop integrals and extracting IR singularities from phase

---

[14]DGLAP evolution is valid for moving between momentum scales for a fixed value of x which, although valid for a large range is not too small. For evolution to small x at moderate momentum scales, logs of the form $\ln(1/x)$ must be taken into account. Incorporating small x physics into PDF evolution is the focus of the Balitsky-Fadin-Kuraev-Lipatov (BFKL) [52] [53] and Gribov-Levin-Ryskin (GLR) [54] evolution equations.

space integrals. This emphasis on the perturbative hard cross section is permitted because of the factorization of the hadronic cross section into non-perturbative PDFs and a perturbative partonic cross section in high energy hadronic collisions. A framework is necessary when probing collisions of coloured particles due to confinement; no coloured particles exist outside of colourless bound states so any calculation must rely on a model for calculation such as the QCD improved parton model. An additional consequence of confinement is that no coloured particle is ever observed in an experimental detector as any coloured particle rapidly hadronizes into colourless bound states.

The result of this low energy colour censorship is that the basic experimental QCD objects at a particle collider are not quarks and gluons but objects called *jets*, loosely defined as a collimated density of hadrons described by a total 4-momentum. A proper jet definition is necessary for a consistent theoretical description as well as the correct identification of jets in the detectors at colliders. In order to define a jet a set of appropriate variables should first be defined which simplify the task of defining jets at hadron colliders. In a hadronic collision the partonic centre of mass frame is in general boosted relative to the hadronic centre of mass frame along the beam axis. To reflect this fact it is convenient to formulate the physics in terms of variables which are invariant or transform simply under such boosts. Two variables which are obviously invariant under longitudinal boosts are the azimuthal angle, ϕ, which circulates around the beam axis and the two components of momentum transverse to the beam axis, from which the transverse momentum variable is defined as the modulus of the momentum in the transverse plane,

$$p_t \;=\; \sqrt{p_x^2 + p_y^2}. \tag{1.141}$$

Due to length contraction in the direction of travel, a boost in the z direction transforms the polar angle between frames. If a point along a track in the detector has coordinates (r, z) where r is the radial displacement from the beam axis in the transverse plane, then the polar angle is given by,

$$\theta \;=\; \arctan(r/z). \tag{1.142}$$

In a boosted frame the displacement along the beam axis is Lorentz contracted
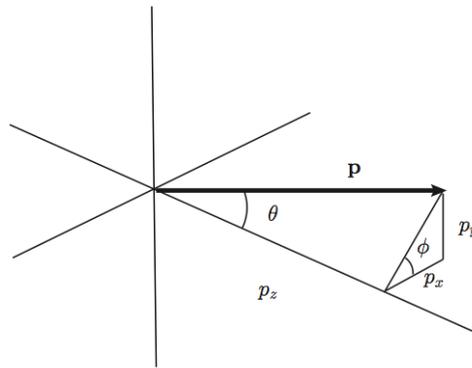
Figure 1.7: A schematic depiction of the relevant variables in a collider environment.

causing the polar angle to widen,

$$\theta' \;=\; \arctan(r\gamma/z), \tag{1.143}$$

such that as $\beta = |v| \to 1$, $\theta' \to \pi/2$. An alternative coordinate when studying relativistic kinematics is the *rapidity*. The rapidity is essentially a hyperbolic angle which reflects the underlying hyperbolic geometry of relativity and so transforms simply under Lorentz boosts. In terms of the object's energy and momentum along the beam axis the rapidity is defined as,

$$y \;=\; \frac{1}{2}\ln\!\left(\frac{E + p_z}{E - p_z}\right), \tag{1.144}$$

Projecting the 3-momentum onto the beam axis and noting that $|\boldsymbol{p}| = \beta E$, the rapidity can be written in terms of the polar angle,

$$y \;=\; \frac{1}{2}\ln\!\left(\frac{1 + \beta\cos\theta}{1 - \beta\cos\theta}\right). \tag{1.145}$$

Using the invariant transverse coordinates and rapidity the 4-momentum of an object can be written in the form,

$$p \;=\; \big(m_t\cosh y,\, p_t\sin\phi,\, p_t\cos\phi,\, m_t\sinh y\big), \tag{1.146}$$

where the transverse mass, $m_t = \sqrt{p_t^2 + m^2}$ is also invariant under boosts along the beam axis. One advantage of using rapidity over the polar angle is that under a Lorentz boost in the direction of the beam axis, values of rapidity transform simply as an addition of a constant. The energy and momentum between two relatively

September 24, 2012

boosted frames are related by $E' = \gamma(E + \beta p_z)$ and $p'_z = \gamma(p_z + \beta E)$, leading to the change in rapidity,

$$y' = y + \tfrac{1}{2}\ln\left(\frac{1+\beta}{1-\beta}\right), \tag{1.147}$$

such that differences in rapidity are invariant under a Lorentz boost between frames in the z direction, i.e., $\Delta y' = \Delta y$. At the LHC the hadrons making up a jet are severely boosted with respect to the laboratory frame so it is often useful to use *pseudorapidity* as a variable, to which rapidity tends in the relativistic limit $\beta \to 1$,

$$\eta = -\ln\big(\tan(\theta/2)\big). \tag{1.148}$$

The maximal rapidity accessible at a collider is given by $y_{\mathrm{max}} = \ln(\sqrt{s}/m)$, where m is the minimum invariant mass of the object. For an operating centre of mass energy of 3.5, 7, 8 and 14 TeV the maximum rapidity is approximately 5.9, 8.9, 9.0 and 9.5 respectively. Similarly if the process of interest involves a high mass resonance decaying into jets then the invariant mass of the jets (for sufficiently low jet multiplicity) will be large, $m \approx \mathcal{O}(1\text{TeV})$. Searches for high mass resonances with a small number of jets are therefore confined to studying jets in the central region.

Having defined the appropriate kinematic variables for measuring jets it is necessary to define what constitutes a jet in a theoretically consistent way. The definition of a jet is not unique and is determined through use of a *jet algorithm*. Jet algorithms broadly fall into two classes, *sequential recombination* and *cone* algorithms, both of which have been used at hadron colliders and will be briefly discussed in the following sections. A comprehensive survey of the field of jet algorithms can be found at [55].

1.5.1 Sequential recombination algorithms

Sequential recombination algorithms start with a partonic final-state, calculate a distance measure between the partons, apply a set of selection criteria and combine partons into a composite particle based on the selection criteria. Once all composite particles pass the selection criteria the algorithm stops and the resulting composite

particles are identified as jets. The general algorithm for jets at hadron colliders follows the steps:

1. Calculate the distance measure, d_{ij} between all final state partons and d_{iB} between final state particles and the beam axis,

2. Find the minimal distance measure,

3. If the minimal measure is a d_{ij} combine particles i and j into a single composite particle and return to step 1,

4. If the minimal distance measure is a d_{iB} record particle i as a jet and remove from the set of particles,

5. Terminate when no particles remain.

The quantity which differentiates between the main jet algorithms is the distance measure used to set the recombination criteria. Generally this can be written in the form,

$$
\begin{aligned}
d_{ij} &= \min(p_{t,i}^{2p}, p_{t,j}^{2p})\frac{\Delta R_{ij}^2}{R^2}, \\
d_{iB} &= p_{t,i}^{2p},
\end{aligned}
\tag{1.149}
$$

where $\Delta R_{ij}^2 = (\Delta y_{ij})^2 + (\Delta \phi_{ij})^2$ and R is a parameter defining the radial extent of the jet when idealized as a cone in y-ϕ coordinates. The value of the constant p defines the specific algorithm with $p = 1, 0, -1$ defining the k_t [56] [57], Cambridge/Aachen [58] [59] and anti-k_t [60] algorithms respectively. The minimum function simply returns whichever of its two arguments is smallest, e.g., in the case of the k_t algorithm the squared transverse momentum of two particles is read in and it selects the one with the smallest value.

An alternative measure would simply be the product of the two transverse momenta, $p_{t,i} \cdot p_{t,j}$ similar to the measure used at LEP for the JADE algorithm [61]. One problem with this measure is that two well separated particles with small p_t (soft and back-to-back), could generate a small distance measure and be recombined. Selecting only the minimum of the two ensures that the distance measure for two particles in such a configuration will generally be larger than between one of those
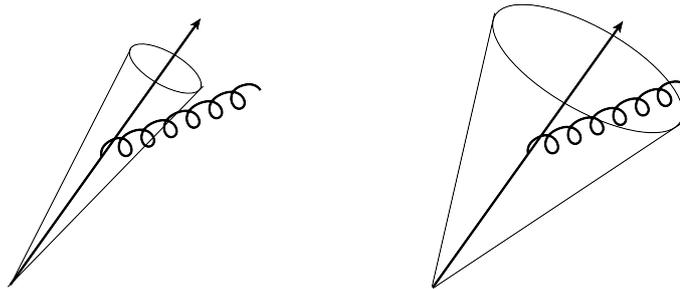
Figure 1.8: Two identical fragmentations can be treated differently for jet definitions with different jet radii.

particles and a nearby hard particle with which it is recombined using the k_t algorithm. This distance measure eliminates the formation of *phantom* jets, formed from many well separated soft particles, by the jet algorithm. The Cambridge/Aachen algorithm has no dependence on the p_t^2 of the particles, clustering purely on the basis of how collinear two particles are, so will never cluster two soft well separated particles. The anti-k_t algorithm has an inverse dependence on the p_t^2 of the particles so soft particles are generally discriminated against as the algorithm favours collinear pairs. The p_t dependence of the k_t, Cambridge/Aachen and anti-k_t algorithms cause the jets to grow outwards from soft, p_t-independent and hard particles respectively.

The other main parameter specifying a jet algorithm is the jet radius, R. There is no unique value for the jet radius and different values have different disadvantages. A small jet radius is more likely to define a particle which fragments (either perturbatively or after hadronization from the decay of unstable hadrons), into two particles as two jets whereas a large jet radius will consider essentially all radiation from a particle to be part of the same jet. This effect may cause an inaccurate reading of the jet energy due to the leaking of radiation from a small jet radius. When it comes to resolving many hard partons however, a smaller jet radius allows a finer resolution whereas a large jet radius would cluster many hard partons and not resolve the physics generating the multiple hard partons. The opposite effect to radiative leaking is radiation from the underlying event leaking into the jet. In this case a small jet radius is useful as it is less likely to capture energy from the underlying event than a jet with a large jet radius.

The choice of jet radius is influenced by these two competing effects, with the radiative leaking serving to reduce the total energy of the jet and the underlying event acting in opposition. In order to gain the best resolution for the physics being probed the jet radius should reflect the relative impact of these competing contributions. i.e., for low p_t the underlying event can dominate over the radiative effects and so a small jet radius will minimise the effect of the underlying event without losing too much to radiative leaking. Similarly at high p_t the underlying event is negligible compared to the large amount of QCD radiation so a larger jet radius is desirable to control the effect of radiative leaking. In practice at the LHC the two experiments ATLAS and CMS use the anti-k_t algorithm with fixed values for the jet radius: 0.4 or 0.6 for ATLAS and 0.5 or 0.7 for CMS. It should be noted that the optimum jet radius is not necessarily at any of these points for a specific observable and in particular for high mass resonance searches using dijet data at the LHC the optimum jet radius can be significantly greater than one [62].

1.5.2 Infrared safety

The most important aspect for any jet algorithm is that the jets produced by the algorithm are robust to IR radiation, that is soft and collinear radiative corrections. The key issue is that soft or collinear radiation should not alter the final distribution of jets produced by the jet algorithm. As has been discussed in previous sections, it is well known that the IR singularities of virtual contributions to the cross section cancel against the IR singularities generated by integrating the real emission contribution over its unresolved phase space. If the jet algorithm is not insensitive to such IR radiation then the virtual and unresolved IR configurations will contribute to different jet multiplicity cross sections and the singularities associated with the respective contributions will not cancel, invalidating perturbation theory. The finite resolution and threshold energy of a detector mean that, irrespective of the jet algorithm, the deep IR configurations will contribute to the same cross sections. The manner in which the detector's energy and spatial resolution ensures IR safety is however a complicated and detector dependent issue, making it difficult to compare theoretical predictions and experimental results. For these reasons IR safe jet al-
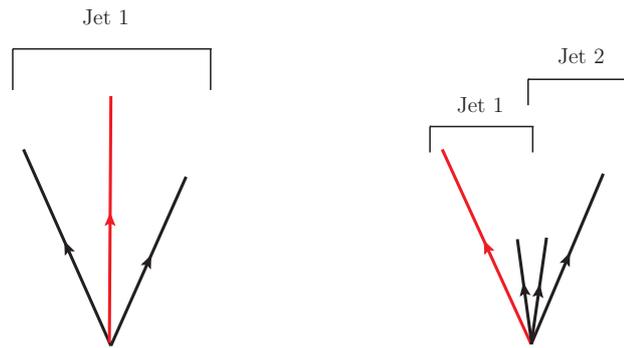
Figure 1.9: A seeded iterative jet algorithm is sensitive to collinear splittings which affect the definition of the hardest seed, the lines highlighted red.

gorithms are essential to understanding experimental results involving jets in the collider environment.

Sequential recombination algorithms are generally IR safe because any soft or collinear radiation will generate a small distance measure and be recombined with a hard parton at the initial stages of the algorithm's run, not affecting the final configuration of jets. A simple counter-example are algorithms which identify the hardest parton as a seed for a proto-jet which can then accumulate surrounding particles to form a jet. Such an algorithm is not IR safe as a splitting of the hardest parton into two collinear partons sharing the momentum may mean the hardest particle is no longer either of the daughter particles of the original hardest particle [55]. In this situation the definition of the hardest seed is very susceptible to collinear splittings and subsequent iterations may split an otherwise single jet into many jets, changing the set of stable final jets. Another example of an IR unsafe algorithm is one which defines a proto-jet as a cone of fixed radius around a seed such that all particles within that cone are summed to form a new seed until a jet is formed that is stable to any further iterations. The issue of IR safety in this case comes about when a soft parton is emitted between two hard partons, forming a stable cone that incorporates the soft particle and the two hard particles into a single jet rather than the two jets without the soft emission.

1.5.3   Cone algorithms

The first jet algorithm [63] was a cone algorithm and they continue to be used extensively today. Unlike sequential recombination algorithms which follow the pattern of QCD radiation by clustering particles into a jet by reversing the sequential branching, cone algorithms are a top down approach to defining jets. As a consequence of this approach cone algorithms have often been compromised by issues of IR safety, especially the class of cone algorithms requiring hard seeds to initiate the jets for the reasons outlined in the previous section. As these infrared unsafe algorithms and their various fixes [64] (which are often ad hoc and not a comprehensive solution) are no longer widely used they will not be discussed further here.

The most widely used cone algorithm today is IR safe and just as valid as any sequential recombination algorithm, called the Seedless Infrared Safe Cone (SIS-Cone) algorithm [65]. This algorithm avoids the problems associated with iterating a proto-jet from a seed by not choosing any particle as a special initial seed. For each subset of particles a total momentum axis is calculated and a cone of set radius is defined surrounding the subset's axis. If exactly the same particles in the subset lie within the cone then it is defined as a stable cone. Following the definition of the stable cones a *split-merge* procedure is performed which removes any overlap between stable cones. The split-merge procedure measures the amount of p_t shared between two proto-jet cones in their overlap, denoted $p_{t,\text{shared}}$; if the fraction of momentum between the overlap and the softest jet is above a critical value, typically 0.75, then the proto-jets are merged into a jet. i.e., if two proto-jets, called h and s (where proto-jet h is harder than s) share part of each other's cone, the overlap fraction is defined as,

$$\frac{p_{t,\text{shared}}}{p_{t,s}} \;\; = \;\; f \tag{1.150}$$

If the overlap momentum falls short of the critical fraction then the shared momentum is redistributed to the cone who's centre is closer in angle. By ensuring that the soft stable cones don't affect the outcome of the split-merge procedure the SISCone algorithm provides an IR safe cone algorithm.

1.6 QCD at NNLO: motivation and application

The previous sections have provided the theoretical framework for QCD within the collider environment necessary to define the calculations contained in this thesis. The framework required to perform these calculations will be discussed in chapter 2 and will focus primarily on the issue of performing the IR singularity cancellation for higher order perturbative corrections. The development of the antenna subtraction method and its application is the main result of this thesis, but ultimately the results of any such calculations are independent of the method used. It is important to consider which calculations are actually worthwhile performing at NNLO accuracy and which observables are sensitive to higher order corrections.

1.6.1 The motivation for NNLO

The motivation for NNLO accuracy comes from both general arguments and process specific considerations. The general considerations are concerned with the theoretical framework of perturbative QCD in the collider environment, whereas the process specific motivation for NNLO strongly depends on how important a particular channel is for phenomenological studies at the LHC.

The structural need for NNLO is well known and has to some extent already been discussed in the previous sections. The most widely quoted method for estimating the theoretical uncertainty is measuring the effect of varying the various unphysical scales present in a calculation. At a hadronic collider such as the LHC the unphysical scales are the renormalization and factorization scales, both of which persist in a truncated perturbative calculation. It has been argued in section 1.4 that as higher order contributions are calculated the dependence on these unphysical scales will systematically decrease. A striking example of this reduction in scale dependence can be seen in figure 1.10 [1] which shows the differential cross section for the production of a stable Z^0 boson in association with some additional hadronic states, as a function of rapidity at the LHC. The bands show the effect of varying the factorization and renormalization scales by a factor of two either side of the conventional value, $\mu_R = \mu_F = \mu$, $M_Z < \mu < 2M_Z$. This example serves to highlight

September 24, 2012
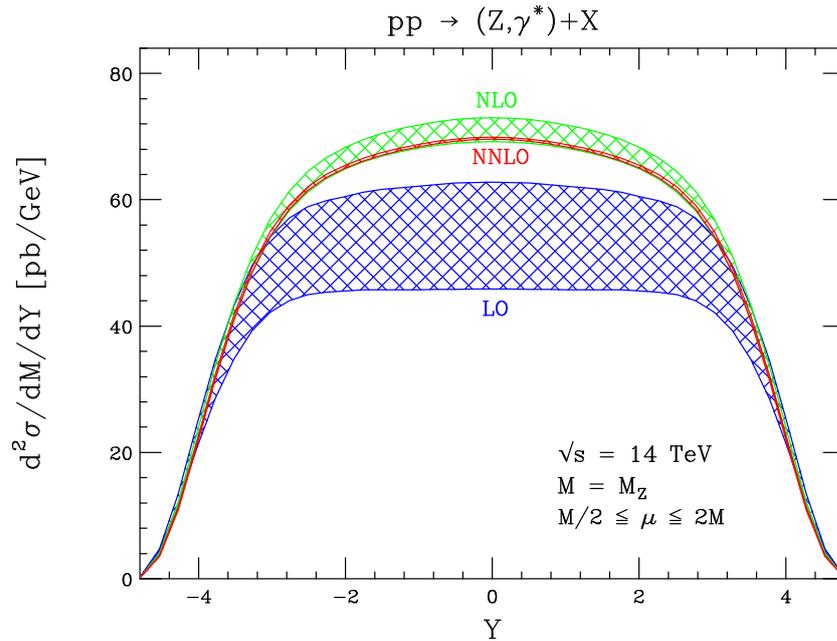
Figure 1.10: The differential cross section for the process $pp \rightarrow Z^0 + X$ where X denotes any additional partons or hadrons [1].

many generic motivations for calculating NNLO corrections.

There are several aspects to the plot in figure 1.10 which demonstrate the motivation for higher order corrections. The most obvious result is that the scale variation of the cross section decreases dramatically as higher order corrections are included. In the central region the scale variation of the leading order result is as much as 30%; this falls to approximately 6% when including the NLO correction and as low as 0.6% for the NNLO result in the same rapidity region [1]. It is also clear that the higher order corrections decrease in size as the perturbative order increases, which indicates that the perturbative series is converging up to NNLO. The convergence of the series can also be seen in the overlap of the respective perturbative contributions. The NLO result does not in fact overlap with the leading order result's theoretical error bands[15] whereas the NNLO result sits comfortably within the (more reliable)

---

[15]This is not in itself that surprising as the leading order result does not have any renormalization scale dependence. Also the variation of the scales over the range $M_Z/2 < \mu < 2M_Z$ is entirely arbitrary. Furthermore, at NLO a new channel is opened up, $q\, g \rightarrow Z\, q$, which is zero at leading order. For a sizeable gluon distribution this new channel can significantly affect the cross section.

NLO theoretical error bands.

A more subtle but important observation is the higher order corrections do not just change the overall normalization of the cross section in a convergent manner; the shape of the distribution is also modified [66]. Higher order corrections contain more dynamical scales for the cross section to be a function of, both virtual and real contributions. In the case of real corrections the final-state phase space is significantly larger and permits more complicated final states. Both of these effects can change the normalization and the shape of a distribution, for example allowing higher rapidity jets to be produced. This is seen in figure 1.10 where the leading order cross section is essentially flat in rapidity but the NLO and NNLO corrections produce a broad peak in the central region.

One of the strongest motivations for performing NNLO calculations is to constrain the PDFs at NNLO. The determination of a PDF not only requires knowledge of the PDF running to the desired order in α_s, but a global fit to data must be performed. The observables used to constrain the PDFs must be calculated to the same order in perturbation theory for a meaningful determination of the PDF. The processes used for the fit will constrain different PDFs, for example the deep inelastic scattering (DIS) data from HERA (or indeed vector boson + jet data from the LHC) probe the quark distributions but provide much looser constraints on the gluon distribution as the virtual photon probe for DIS (or the vector boson in the $V+$ jet data) does not couple to the gluon at leading order [2]. In order to probe the gluon distribution a hadron collider is the most useful environment as a significant fraction of the hadronic initial state's momentum is carried by gluons. The effect of incorporating the inclusive jet data from the Tevatron runs I and II into the NLO gluon PDF fit can be seen in figure 1.11 where the effect is particularly pronounced at high x values.

The LHC's kinematic reach is far greater than was available to the Tevatron, as shown in figure 1.12, so the jet data currently being collected at the LHC has the capacity, if coupled with a full NNLO calculation, to constrain the gluon density and test QCD over a huge dynamical range.

In section 1.5 the various methods for constructing experimental jets from par-

Gluon distribution at Q² = 10⁴ GeV²
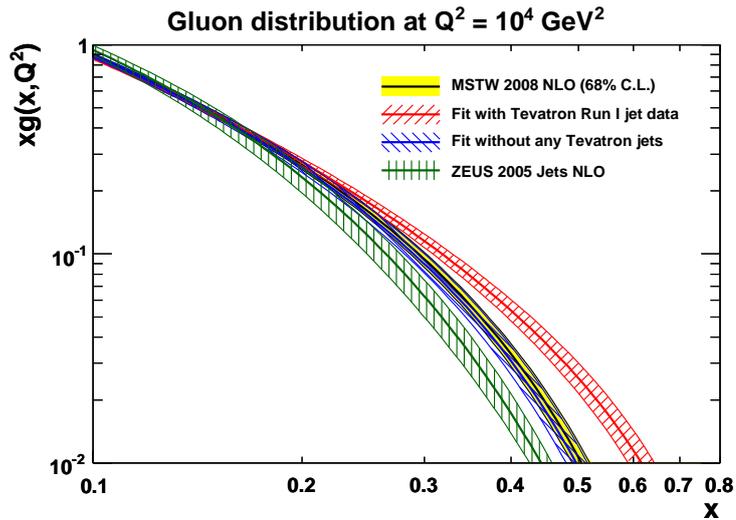
Figure 1.11: A plot of the gluon distribution showing the effect of including Tevatron inclusive jet data [2].

tons were discussed. All the IR safe jet algorithms act on the set of final state momenta present in the partonic matrix element and generate a number of jets based upon their specific criteria. At leading order there is an exact correspondence between partons and jets but at higher orders the additional real radiation can recombine and the jet algorithm becomes non-trivial. At NNLO, in addition to the jet configurations allowed at NLO, three partons present in the matrix element can recombine to form a single jet or two pairs of partons can form two jets. As the number of additional particles in the final state increases, the jets produced by the jet algorithms become more realistic and closer to what is observed in the detector. In this sense higher order corrections begin to unravel the first few emissions of the parton shower but with the full machinery of perturbation theory.

In a similar fashion to the way recombining additional final-state partons improves the description of jets, radiation from initial-state partons also generates a more realistic initial-state [66]. At leading order the total transverse momentum of the initial state, and thus the final state, is zero. Higher perturbative orders allow initial-state radiation which will impart transverse momentum for the initial-state partons and if unobserved can generate a non-zero final-state transverse momentum. Allowing the initial-state radiation to generate transverse momentum for the incoming partons, as QCD dictates it must, can reduce or perhaps even remove the need

(a) Tevatron   (b) LHC
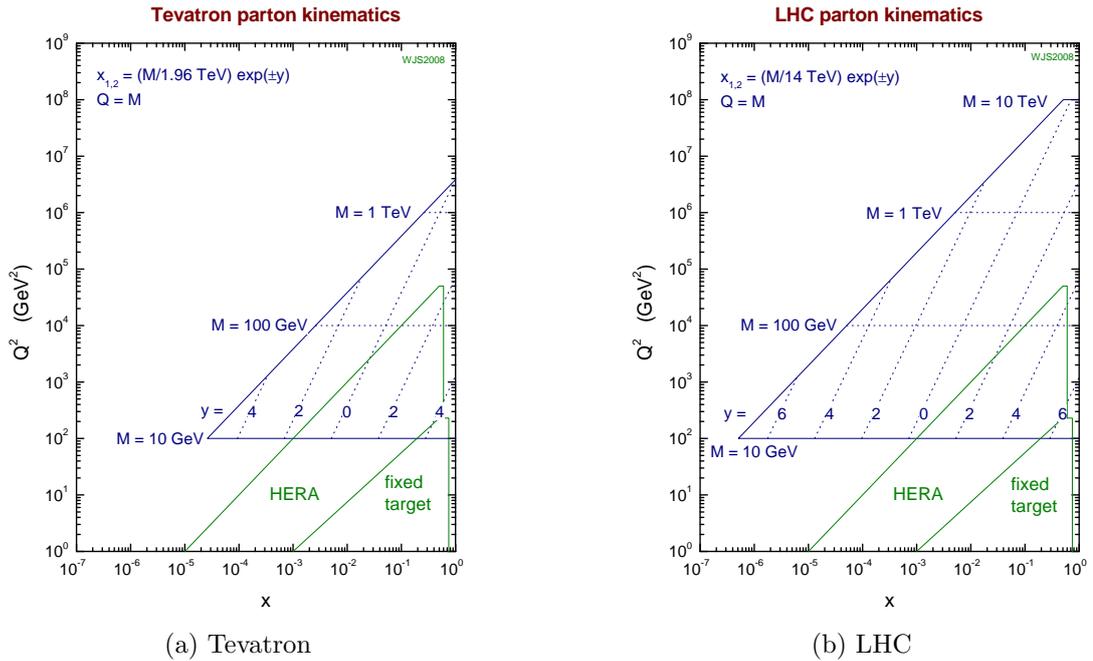
Figure 1.12: The kinematic ranges of the Tevatron and LHC in the x-Q^2 plane [3].

for any intrinsic transverse momentum of the hadron which is sometimes invoked to be able to explain the experimental data. From the point of view of fixed higher order calculations the intrinsic transverse momentum of the hadron is similar to the issues of power law corrections; both effects are invoked to explain the data but both effects can in principle be generated by well motivated higher order perturbative effects. In the case of power law corrections additional powers of $1/\ln(Q^2/\Lambda_{\text{QCD}})$, where Q^2 is a hard scale associated with the partonic cross section, are generated by the multi-loop corrections to the QCD coupling. It is possible for these corrections to mimic any power law contribution and it remains unclear if either intrinsic transverse momentum or power law corrections are generically required, although not ruled out in principle [67].

1.6.2   Seeing NNLO at the LHC

For the LHC NLO accuracy is necessary and, as discussed in the previous section, NNLO is often desirable. It is worthwhile to consider which processes are particularly sensitive to NNLO effects and have the largest impact on the field of phenomenology. Much attention has already been paid to the definition, calculation and properties

of jets in this chapter. Jets are interesting objects in themselves, this coupled with their abundance at the LHC and intimate connection with parton-level QCD makes jet cross sections an attractive observable dominated by QCD effects.

In order to resolve higher order corrections both the theoretical and experimental uncertainties must be brought under control. On the theoretical side the uncertainties may be broadly grouped into perturbative and non-perturbative uncertainties. The perturbative uncertainties associated with a QCD calculation were discussed in the previous section and mainly amount to residual dependence of the cross section on unphysical scales such as the renormalization and factorization scales. In general calculating higher orders in the perturbation series at parton level for relatively large p_t and central rapidities will suffice to reduce the theoretical uncertainty on the partonic cross section[16].

Non-perturbative theoretical uncertainties include the uncertainties on the various partons' distributions within a PDF and disagreements between the competing PDF sets. In addition to the PDF uncertainties, there are hadronization and underlying event effects which have to be successfully modelled to reduce the uncertainty associated with these phenomena. The task of comparing experimental data with the particle-level prediction requires the use of Monte-Carlo (MC) event generators to *unfold* the data back to a particle-level result [68]. The details of the unfolding procedure introduce further sources of error such that even if a high precision calculation is not matched to a parton shower, it will have residual dependence on the parton shower's effect through the MC's interpolation between theory and data. The resulting uncertainty associated with an unfolding procedure is referred to as the Monte-Carlo shape uncertainty. In order to quantify this uncertainty a particle-level MC simulation (which is connected to a detector-level result via a transfer matrix) is re-weighted by a smooth function and reconstructed at the detector level such that the resulting MC generated observable agrees better with the data. The re-weighted and reconstructed MC is then unfolded back to particle-level and compared to the

---

[16]For regions of low momentum transfer or at particle thresholds additional theoretical input in the form of resumed calculations may be required to produce a reliable prediction for the cross section.

re-weighted parton-level MC. With the MC shape uncertainty defined in this way the uncertainty is quantified at the percent level for the unfolding procedure used by the ATLAS collaboration [4].

For jet studies the main experimental uncertainty holding back any comparison to high precision predictions is the Jet Energy Scale (JES) correction. The total 4-momentum of a jet as seen in the calorimeter is given by the sum of the 4-momentum deposited in each calorimeter cell contributing to the jet definition. As discussed in section 1.5, the energy of a jet may be increased by capturing energy from the underlying event, in particular pile-up. In addition to these corrections the detector may contain dead cells and other effects which cause energy loss for the jet. These effects are corrected for by a function of transverse energy and pseudorapidity which is derived from MC simulations of jets. For the 2010 dijet data from CMS based on $34\mathrm{pb}^{-1}$ of data the proportion of the total uncertainty on the cross section due to the JES correction is 60% for a reconstructed dijet mass of $M_{JJ} = 3\mathrm{TeV}$ [69]. For smaller values of the invariant dijet mass this fraction will decrease due to the increasing importance of the underlying event but the JES correction remains the main obstacle to precision physics for high p_t central jets.

The double differential inclusive dijet cross section as a function of the invariant dijet mass, measured by ATLAS, is shown in figure 1.13 as a ratio to the NLO prediction from NLOJet++ using the NLO PDF set CT10 [4]. This measurement of the dijet cross section probes invariant dijet masses of up to 4.6 TeV and for $y^* < 2.5$, where $y^* = |y_1 - y_2|/2$ and $y_{1,2}$ are the rapidities of the leading jets. The data is described reasonably well by the NLO prediction but there are some sizeable discrepancies, in particular with the high invariant mass data, a trend which is seen in both the 2010 and 2011 data and for an increased jet radius of $R = 0.6$ which in principle would be better suited to the high p_t region.

In addition to the dijet cross section, the inclusive jet cross section is the other main observable used in jet studies to test QCD predictions. The inclusive jet cross section as measured by CMS [5] and ATLAS [4] with 2010 data is shown in figures 1.14 and 1.15 respectively. In both instances there is some tension between the NLO prediction and the observed cross section, with the theoretical prediction tending to

(a) 2010, 37pb^{-1} of data

(b) 2011, 4.8fb^{-1} of data, preliminary
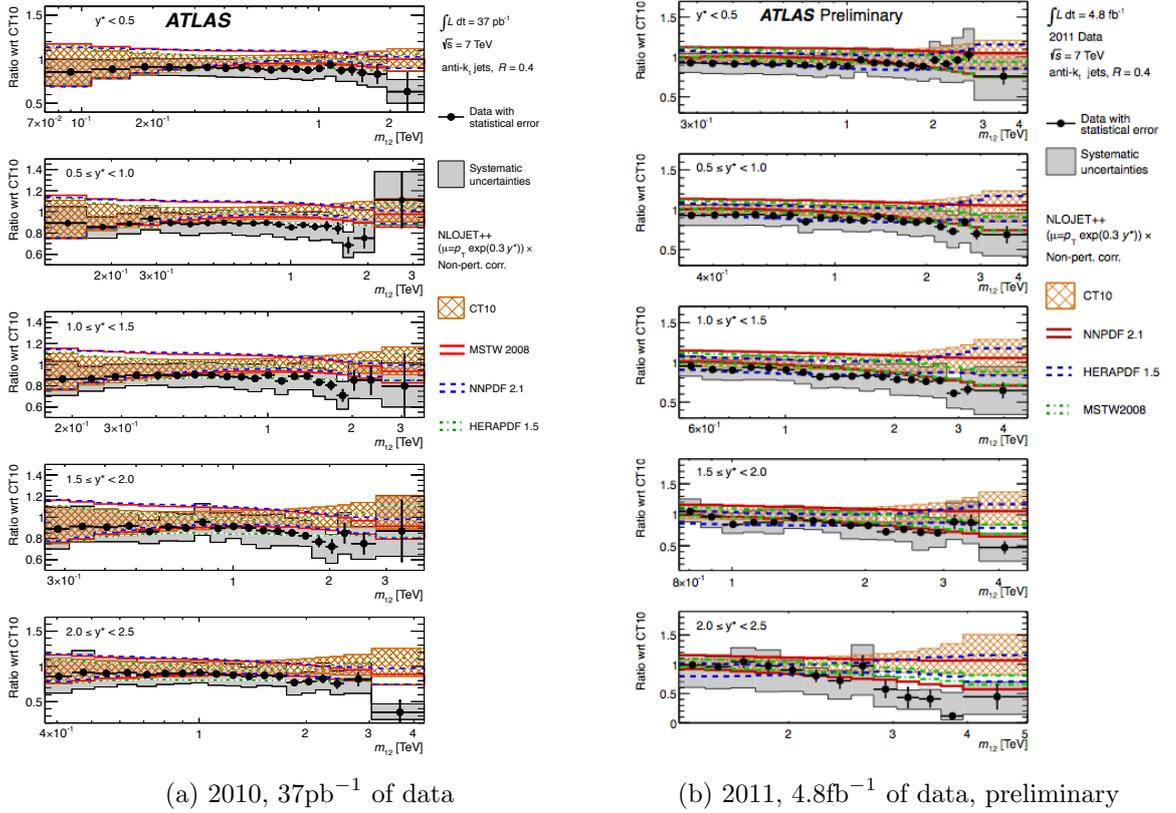
Figure 1.13: The ratio of the double differential dijet cross section as measured by ATLAS to the NLO prediction from NLOJet++ using CT10 NLO PDF set. ATLAS use the anti-k_t algorithm with $R = 0.4$ for this measurement [4].

overshoot the data. At high values of p_t the main source of theoretical error comes from the PDFs and so such a measurement has the potential to constrain the PDFs at large x if the JES uncertainty can be brought within comparable bounds.

A massless QCD calculation of the inclusive jet cross section requires two input parameters: the QCD coupling and the PDFs for the incoming hadrons. As discussed in section 1.2 the value of the coupling can be extrapolated to any momentum scale in the perturbative region by solving the β-function equation for its evolution. An interesting exercise is to turn this process around and use the LHC jet data to extract the QCD coupling that describes the data [70]. The result of this exercise can then be compared with the expectation of the β-function. Any deviation from the QCD evolution, especially at high p_t, may provide indications of non-standard coloured dynamics contributing to the running of α_s at higher orders.

September 24, 2012
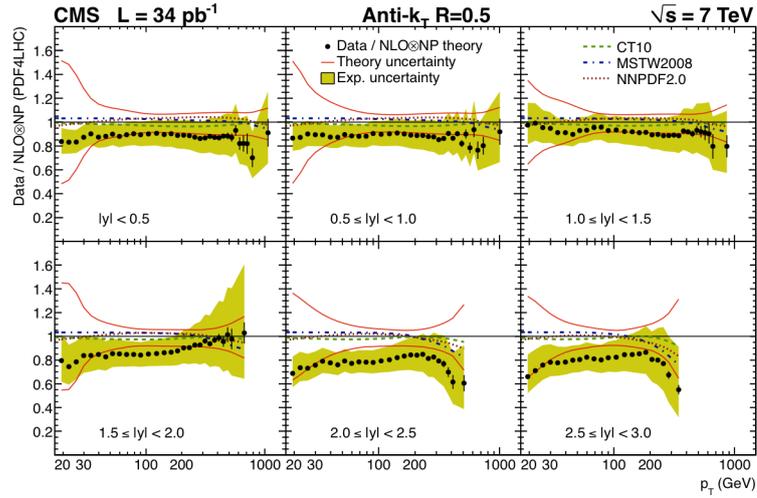
Figure 1.14: The inclusive jet cross section, as measured by CMS, as a ratio to the NLO theoretical prediction [5].

The lack of a single momentum scale at a hadron collider, due to the composite nature of the proton, means that values for the coupling can be extracted over a huge range of momentum scales. When the analysis was performed at the Tevatron by the DØ collaboration [6] the coupling was extracted for the range of the leading jet's p_t of $50 < p_t < 145$ GeV and the results are shown in figure 1.16(a).

The kinematic range of the LHC exceeds that of the Tevatron and a similar analysis compared to an NLO inclusive jet cross section calculation has been recently performed using the 2010 jet data from ATLAS based on 37pb^{-1} of integrated luminosity, [71]. In this study the range of leading jet p_t being probed was increased dramatically to $45 < p_t < 600$ GeV. The results of this extraction are shown in figure 1.16(b) for the various rapidity bins, which include jet rapidities up to $|y| < 4.4$, significantly larger than the Tevatron's reach of $|y| < 1.6$. The limitations on this measurement come from several sources: the statistical uncertainty on high p_t jets, any systematic experimental uncertainties such as the JES, the PDF uncertainties and the renormalization and factorization scale uncertainties. Calculating the inclusive jet cross section to NNLO accuracy could eliminate much of the scale uncertainty in the theoretical calculation whereas the continued running of the LHC will massively increase the high p_t jet data and gradually decrease the JES uncertainty through improved jet calibration. The remaining source of uncertainty is
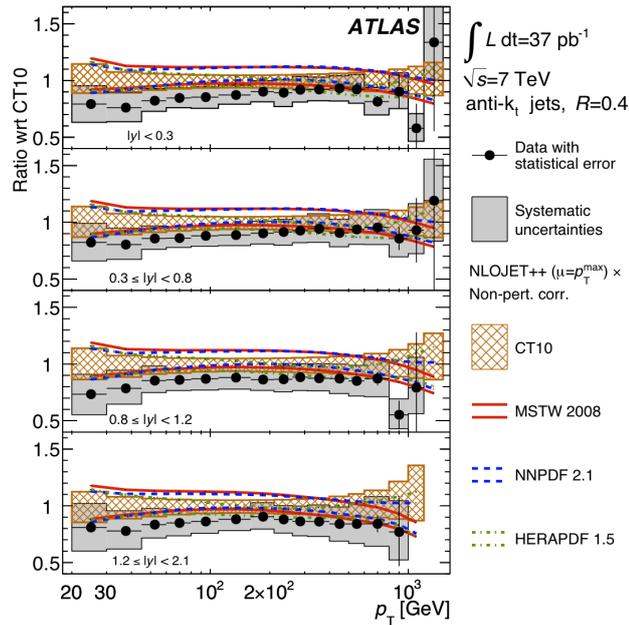
Figure 1.15: The inclusive jet cross section, as measured by ATLAS, as a ratio to the NLO theoretical prediction calculated using NLOJet++ and the CT10 PDF set [4].

the determination of the PDFs, in particular the gluon distribution which is poorly constrained at large x and gives a significant contribution to the jet cross section.

As a hadron collider the LHC is dominated by QCD effects. Jet studies allow these effects to be tested over a large range of validity, but QCD also has a significant effect on the production of colourless particles at the LHC. Colourless particles can be produced in abundance and provide significant Standard Model backgrounds, as in the case of vector boson production in association with one or more jets. Understanding these processes to a high degree of accuracy can have a large impact on LHC phenomenology, e.g., the V+jet cross section can be used to probe the quark PDFs and also provides a significant background to top quark production.

Colourless particle production at the LHC is also important as a background for rare processes such as a Higgs boson decaying into two photons. It has recently been reported [7] [72] that a significant excess is observed in the Higgs searches by both CMS and ATLAS for a reconstructed Higgs mass in the region 125-126 GeV. This observation has been driven to a large extent by an excess in the diphoton channel and so understanding the Standard Model Higgs signal in this channel is
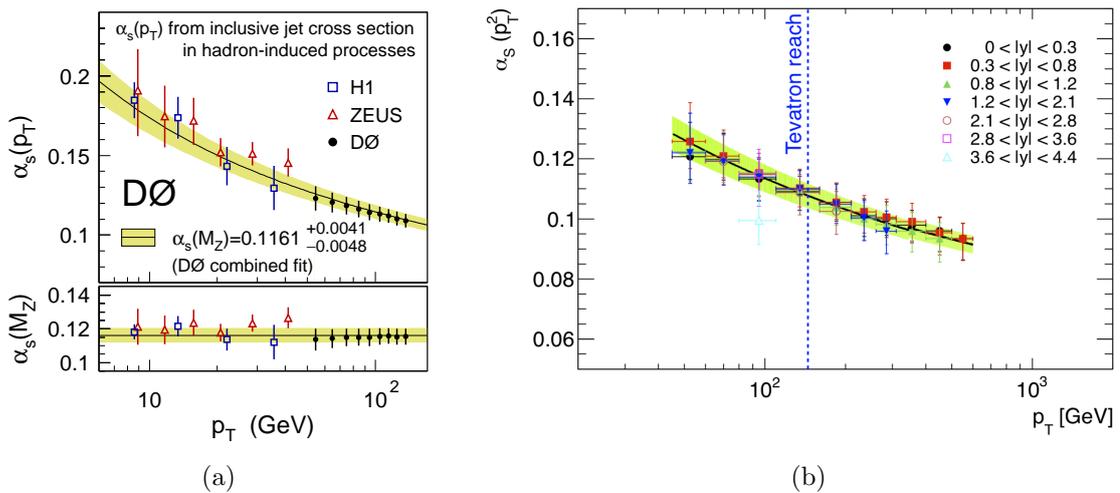
Figure 1.16: Plots showing the extracted value of α_s as a function of leading jet p_t at (a) the Tevatron [6] and (b) ATLAS.

a matter of great importance. In the coming years much experimental attention will be paid to measuring the Higgs cross section, and its associated irreducible backgrounds, to a high degree of accuracy and precision. This effort will be matched on the theoretical side with understanding the data in the context of highly precise theoretical predictions which, if understood properly could lead to hints of Beyond the Standard Model (BSM) Higgs physics, opening up an new frontier for particle physics.
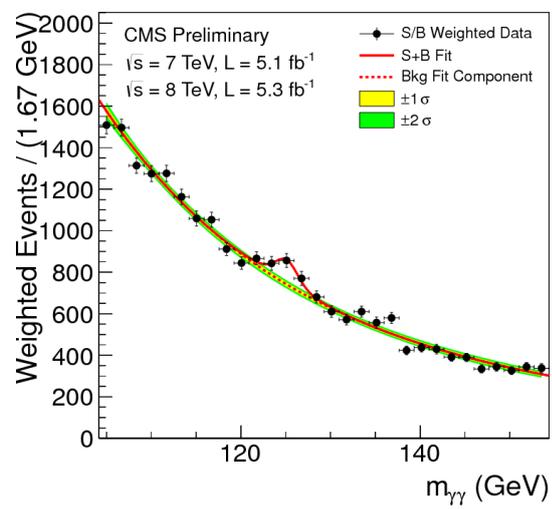
Figure 1.17: The $H \to \gamma\gamma$ channel as measured by CMS based upon a combination of $\sqrt{s} = 7$ TeV and $\sqrt{s} = 8$ TeV data [7].

Chapter 2

Antenna Subtraction

The issue of IR singularities and their cancellation is a generic problem for massless gauge theories such as QCD in the high energy limit. The factorization theorems [48] ensure that the perturbative cross section is ultimately free from singularities and divergences so long as it is properly defined, yet the process of actually performing the singularity cancellation order by order in perturbation theory remains an active field of research. With the knowledge that the IR singularities of the virtual cross section cancel against the IR divergences of the real cross section when analytically integrated over the unresolved phase space, the task is reduced to extracting the implicit singularities from the real contribution's phase space integral such that they are in the same form as the explicit virtual singularities. The method of dimensional regularization is standard in higher order perturbative QCD studies and so the broad task of producing an IR finite observable is reduced to the much more focussed exercise of writing the integral of the real emission over unresolved regions of phase space as a Laurent expansion in the dimensional parameter, ϵ.

In order to perform this task three main strategies have been employed: slicing, sector decomposition and subtraction. The various methods used to perform higher order calculations at NLO or NNLO employ one or more of these basic techniques which are briefly discussed in this section. At NLO all three methods have been implemented by various formalisms, the details of which will not be reproduced here except in the case of antenna subtraction which is the focus of this thesis. Detailed discussions of the application of the alternative methods at NLO can be

found elsewhere: phase space slicing [73–76], Catani-Seymour [20], Frixione-Kunszt-Signer (FKS) [77], sector decomposition [78–81]. At NNLO the antenna subtraction method will be extended and discussed in detail, providing the background and tools for performing the calculations which are the focus of chapters 3, 4 and 5. Details of alternative methods for NNLO calculations may be found in the following references [82–89].

2.1 Basic techniques for singularity isolation

2.1.1 Phase space slicing

The slicing technique has been employed for NLO QCD calculations in addition to extracting poles from double unresolved configurations involving mixed QCD-QED calculations, specifically for the processes $e^+e^- \to 3j$ [74] and $e^+e^- \to \gamma + j$ [76]. The method relies on a detailed understanding of the unresolved limits of the matrix elements, which for colour-ordered squared amplitudes have been discussed in section 1.3.2. The important fact in the context of the slicing method is that the in unresolved limits the colour-ordered squared matrix elements factorize into the direct product of a universal singular function, depending only on the parton directly involved in the singular configuration, and a reduced multiplicity squared matrix element independent of the unresolved momenta.

Schematically, given a set of momenta $\{p\}$, of which a set $\{\mathcal{U}\}$ are involved in an unresolved configuration and the subset $\{\mathcal{V}\}$ actually vanish, i.e., $\{\mathcal{V}\} \subset \{\mathcal{U}\} \subset \{p\}$, the general tree-level factorization formula holds for the squared colour-ordered partial amplitudes,

$$M_n^0(\{p\}) \overset{\{\mathcal{V}\} \text{ unresolved}}{\longrightarrow} \mathcal{F}(\{\mathcal{U}\}) \, M_r^0(\{p\}\backslash\{\mathcal{V}\}), \tag{2.1}$$

where r is the number of resolved particles, i.e., n minus the number of unresolved partons. Here $\mathcal{F}$ is a universal singular function which in the single soft limit is the Eikonal soft function and in the collinear limit is one of the Altarelli-Parisi splitting functions [35]. At loop level a similar factorization formula holds and new one-loop

universal singular functions are required [39],

$$M_n^1(\{p\}; \epsilon) \xrightarrow[\text{unresolved}]{\{\mathcal{V}\}} \mathcal{F}(\{\mathcal{U}\}) \, M_r^1(\{p\}\backslash\{\mathcal{V}\}; \epsilon) + \mathcal{F}^{(1)}(\{\mathcal{U}\}; \epsilon) \, M_r^0(\{p\}\backslash\{\mathcal{V}\}). \quad (2.2)$$

The details of the single unresolved limits of one-loop squared matrix elements are presented in section 1.3.2.

The phase space slicing method partitions the phase space into a set of regions defined by kinematic thresholds. By way of example, consider the process $e^+e^- \rightarrow q\bar{q}g$ with a floating but suitably small threshold, $s_{\min}$ [74]. The soft region of phase space for the gluon can be defined as,

$$s_{qg} < s_{\min} \quad \& \quad s_{\bar{q}g} < s_{\min}. \quad (2.3)$$

Similarly the $q||g$ collinear region can be defined as,

$$s_{qg} < s_{\min} \quad \& \quad s_{\bar{q}g} > s_{\min}, \quad (2.4)$$

and the $\bar{q}||g$ collinear region by,

$$s_{qg} > s_{\min} \quad \& \quad s_{\bar{q}g} < s_{\min}. \quad (2.5)$$

The scale $s_{q\bar{q}}$ is always hard and so the phase space can be considered in the s_{qg}-$s_{\bar{q}g}$ plane as in figure 2.1. In the hard region the matrix elements are finite and well behaved so the hard cross section can be numerically integrated over this region of phase space. In the soft region the squared matrix element is replaced by its factorized form in the exact soft limit,

$$M_3^0(1_q, 3_g, 2_{\bar{q}}) \quad \longrightarrow \quad S_{132} \, M_2^0(1_q, 2_{\bar{q}}). \quad (2.6)$$

In the exact soft limit the three-particle phase space factorizes into a soft phase space and the remaining two-particle phase space,

$$d\Phi_3(p_1, p_2, p_3; Q^2) \quad \longrightarrow \quad d\Phi_2(p_1, p_2; Q^2) \cdot d\Phi_{\text{soft}}(p_1, p_2, p_3) \quad (2.7)$$

where the soft phase space is defined as,

$$d\Phi_{\text{soft}}(p_1, p_2, p_3) \;=\; \frac{(4\pi)^\epsilon}{16\pi^2 \Gamma(1-\epsilon)} \frac{ds_{13} \, ds_{23}}{s_{12}} \left(\frac{s_{13} s_{23}}{s_{12}} \right)^{-\epsilon} \Theta(s_{\min} - s_{13}) \Theta(s_{\min} - s_{23}).$$

$$(2.8)$$

Integrating the soft universal function over the soft phase space analytically and including the dimensionless coupling associated with the gluon emission, $g^2 = \alpha_s \mu^{2\epsilon}$, yields the contribution,

$$
\begin{aligned}
g^2 \int \mathrm{d}\Phi_{\mathrm{soft}}\, S_{132} &= \frac{\alpha_s}{2\pi} \frac{(4\pi\mu^2)^\epsilon}{\Gamma(1-\epsilon)} \frac{1}{s_{12}} \int_0^{s_{\min}} \mathrm{d}s_{13} \int_0^{s_{\min}} \mathrm{d}s_{23} \left(\frac{s_{13}s_{23}}{s_{12}} \right)^{-(1+\epsilon)} \\
&= \frac{\alpha_s}{2\pi} \frac{1}{\Gamma(1-\epsilon)} \frac{1}{\epsilon^2} \left(\frac{4\pi\mu^2}{s_{\min}} \right)^\epsilon \left(\frac{s_{12}}{s_{\min}} \right)^\epsilon
\end{aligned}
\tag{2.9}
$$

In a similar fashion the matrix element and phase space factorize in the collinear limit, when the gluon becomes collinear with either the quark or the anti-quark.

$$
M_3^0(1_q, 3_g, 2_{\bar{q}}) \xrightarrow{q||g} \frac{1}{s_{13}} P_{qg \to Q}(z)\, M_2^0(1_q, 2_{\bar{q}}),
$$

$$
\mathrm{d}\Phi_3(p_1, p_2, p_3; Q^2) \xrightarrow{q||g} \mathrm{d}\Phi_2(p_1, p_2; Q^2) \cdot \mathrm{d}\Phi_{\mathrm{col}}(p_1, p_3, z),
\tag{2.10}
$$

with $z = s_{13}/s_{12}$ and the corresponding formulae for the $\bar{q}||g$ limit are obtained by substituting $1 \leftrightarrow 2$. The collinear phase space is defined as,

$$
\mathrm{d}\Phi_{\mathrm{col}}(p_1, p_3, z) = \frac{(4\pi)^\epsilon}{16\pi^2\Gamma(1-\epsilon)} \, \mathrm{d}s_{13}\mathrm{d}z \left(s_{13}\, z(1-z) \right)^{-\epsilon} \Theta(s_{\min} - s_{13}).
\tag{2.11}
$$

Integrating the splitting function over the collinear phase space yields,

$$
\begin{aligned}
g^2 \int \mathrm{d}\Phi_{\mathrm{col}} \frac{1}{s_{13}} P_{qg \to Q}(z) &= \frac{\alpha_s}{2\pi} \frac{(4\pi\mu^2)^\epsilon}{\Gamma(1-\epsilon)} \int_0^{s_{\min}} \mathrm{d}s_{13}\, s_{13}^{-(1+\epsilon)} \\
&\quad \times \int_0^{\frac{s_{\min}}{s_{12}}} \mathrm{d}z \left[z(1-z) \right]^{-\epsilon} P_{qg \to Q}(z), \\
&= -\frac{\alpha_s}{2\pi} \frac{1}{\Gamma(1-\epsilon)} \frac{1}{\epsilon} \left(\frac{4\pi\mu^2}{s_{\min}} \right)^\epsilon \mathcal{P}_{qg \to Q}\left(\frac{s_{\min}}{s_{12}} \right).
\end{aligned}
\tag{2.12}
$$

The integrated splitting function is given by [74],

$$
\mathcal{P}_{qg \to Q}(x) = \frac{x^{-\epsilon} - 1}{\epsilon} - \frac{3}{4} + \left(-\frac{7}{4} + \frac{\pi^2}{6} \right)\epsilon + \mathcal{O}(\epsilon^2),
\tag{2.13}
$$

where terms of $\mathcal{O}(\epsilon^2)$ and higher are not required as the deepest pole for the rest of the expression is $1/\epsilon$.

By partitioning and factorizing the phase space, understanding the divergent behaviour of the matrix elements and knowing the analytic results for integrating the universal singular functions over unresolved phase space, the ϵ poles of the real
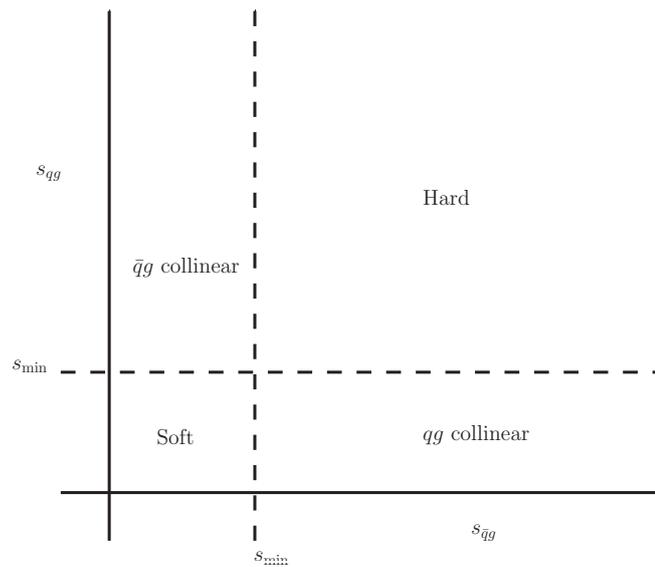
Figure 2.1: A schematic depiction of the various kinematic regions as shown in the s_{qg}-$s_{\bar{q}g}$ plane

emission can be systematically extracted and cancelled against those present in the virtual contribution.

The drawback to the slicing method originates in its use of the theoretical resolution parameter, $s_{\min}$. The method is approximate as the substitution of the full matrix element for the product of the universal singular function and the reduced matrix element, which is made in the region below $s_{\min}$, is strictly valid only in the exact singular limit. The poles are correctly captured by integrating the universal singular functions but a finite systematic theoretical error is introduced due to the mismatch between the exact and approximate matrix elements in the singular regions away from the singularity but below the threshold. The approximate matrix element approaches the exact one in the singular limit and so setting $s_{\min}$ to be suitably small ensures the systematic error is kept to a minimum.

In principle it is desirable to take the floating threshold, $s_{\min}$, to be as small as possible; however in practice an optimum value is chosen. The dependence of the cross section (including real emission in the unresolved regions) on the unphysical parameter $s_{\min}$, through terms of the form $\ln\left(s_{\min}/s_{q\bar{q}}\right)$, ultimately cancels against corresponding terms in the real emission cross section where the additional partons

are resolved. In a Monte Carlo program the hard cross section is evaluated numerically using MC integration and so the cancellation of the unphysical threshold parameter is numerical. If $s_{\min}$ is taken too small then the logarithms containing the $s_{\min}$ dependence, which is separately held in the various contributions to the cross section, generally become large and introduce an error in the numerical cancellation between terms. Balancing these concerns with the systematic error introduced by a non-zero $s_{\min}$ informs the ultimate choice of the unphysical parameter.

2.1.2 Sector decomposition

An alternative strategy to approximating and analytically integrating the cross section in the singular regions is represented by the many implementations of the sector decomposition method [78–81, 90]. For real radiative corrections it is convenient to rescale the available Lorentz invariants to form a set of dimensionless parameters,

$$x_{ij} = \frac{s_{ij}}{s_{\text{hard}}}, \tag{2.14}$$

where s_{hard} denotes the total mass of the final-state, e.g., in e^+e^- annihilation $s_{\text{hard}} = Q^2$. In this way a set of invariant dimensionless parameters can be formed, $x_1 = x_{12}$, $x_2 = x_{13}$, etc. By re-parameterizing the invariants in this way the poles in ϵ can be extracted through use of the identity,

$$x^{-1+a\epsilon} = \frac{1}{a\epsilon}\delta(x) + \sum_{n=0}^{\infty} \frac{(a\epsilon)^n}{n!} \mathcal{D}_n(1-x), \tag{2.15}$$

where the distributions, $\mathcal{D}_n(1-x)$, are defined with respect to integration against a test function,

$$\int_0^1 \mathrm{d}x \ f(x) \ \mathcal{D}_n(1-x) = \int_0^1 \mathrm{d}x \left[\frac{f(x) - f(0)}{x}\right] \ln^n(x). \tag{2.16}$$

In order to extract the poles in this way the singular parameters must be untangled from one other. An example displaying tangled, or *overlapping*, singularities is given by an expression of the form,

$$I = \int_0^1 \mathrm{d}x \int_0^1 \mathrm{d}y \ (x+y)^{-2+\epsilon}. \tag{2.17}$$

The singularities in this expression originate in the divergence of the integrand at $x \to 0$ and $y \to 0$. The integrand is in a non-factorized form so the identity (2.15) cannot be used immediately to extract the poles in ϵ.

The method of sector decomposition solves this issue in an algorithmic fashion by splitting the integration into a set of *Hepp sectors* [91]. For the simple example considered above the two dimensional integral is divided into two sectors: sector H_1 with $x > y$ and sector H_2 with $y > x$ such that $I = H_1 + H_2$ and,

$$
\begin{aligned}
H_1 &= \int_0^1 \mathrm{d}x \int_0^x \mathrm{d}y \ (x+y)^{-2+\epsilon}, \\
H_2 &= \int_0^1 \mathrm{d}y \int_0^y \mathrm{d}x \ (x+y)^{-2+\epsilon}.
\end{aligned}
\tag{2.18}
$$

The innermost integration variable is then rescaled in terms of a new variable, z, i.e., for H_1, $y = xz$ and for H_2, $x = yz$, yielding,

$$
\begin{aligned}
H_1 &= \int_0^1 \mathrm{d}x \ x^{-1+\epsilon} \int_0^1 \mathrm{d}z \ (1+z)^{-2+\epsilon}, \\
H_2 &= \int_0^1 \mathrm{d}y \ y^{-1+\epsilon} \int_0^1 \mathrm{d}z \ (1+z)^{-2+\epsilon}.
\end{aligned}
\tag{2.19}
$$

The integrand involving z is finite over the whole integration range and the divergent behaviour has been factorized into the integrals over x and y which are now in a form amenable to the application of the identity (2.15) to extract the ϵ poles.

In general expressions will contain factors such as $(1-x)$ or $x(1-x)$ which have zeros at $x = 1$ or $x = 0, 1$. In these cases the divergences can be remapped to the origin by a change of variables, or by splitting the integration region further and employing a change of variables to the separate regions. The process of defining sectors, remapping the sectors to the unit hypercube and defining new sub-sectors until all singularities are factorized has been proven to terminate [81] and constitutes the sector decomposition method. The method is versatile and has been applied to extracting singularities from loop integrals as well as phase space integrals. The result of performing an integral using sector decomposition is an expression of the form,

$$
I = \sum_{n=-a}^{b} c_n \epsilon^n + \mathcal{O}(\epsilon^{b+1}),
\tag{2.20}
$$

where a is the depth of the leading pole and b is the order at which the series is terminated, if the quantity being calculated is not multiplied with any other ϵ poles then clearly $b = 0$. The coefficients c_n are finite parameter integrals, as in the case of the z integral in the example above and are generally computed numerically.

2.1.3 Subtraction

Subtraction [92] is a more indirect method for extracting the ϵ poles from an integral, relying on third party quantities, but unlike phase space slicing the method is exact and unlike sector decomposition it is fully analytic. These two facts allow a successful application of the method to be highly accurate and also constitute what could be considered a genuine proof of the singularity cancellation for a physical quantity.

The central idea underpinning all subtraction methods is to define a local counterterm which mimics the behaviour of the physical matrix elements in all IR divergent limits. The general form of the counterterm depends on the specific subtraction formalism being used, however the counterterms of all subtraction methods must fulfil two basic requirements: They must correctly mimic all IR divergent behaviour of the physical cross section and they must be analytically integrable over the unresolved phase space. If a function can be constructed which satisfies these criteria then a contribution to the cross section with n final-state partons can be trivially rewritten,

$$
\underbrace{\int_{\Phi_n} \mathrm{d}\hat{\sigma}_{ij}}_{\text{divergent, non-integrable}} = \underbrace{\int_{\Phi_n} \left[\mathrm{d}\hat{\sigma}_{ij} - \mathrm{d}\hat{\sigma}_{ij}^S \right]}_{\text{finite, numerically integrable}} + \underbrace{\int_{\Phi_n} \mathrm{d}\hat{\sigma}_{ij}^S}_{\text{divergent, analytically integrable}} . \quad (2.21)
$$

By satisfying the necessary requirements of the counterterms the divergent and non-integrable (numerically and analytically) physical cross section is partitioned into a piece which is finite and numerically integrable and a piece which contains all the divergence and is analytically integrable, allowing the poles in ϵ to be extracted.

As (2.21) is a trivial identity no approximation is made and no systematic theoretical error is introduced, unlike in phase space slicing. Similarly the analytic integrability of the counterterms allows the pole cancellation to be carried out analytically, removing any doubt over whether the poles fully cancel which persists

when performing numerical pole cancellation. When cancelling poles numerically it is possible that the cross section will contain terms which are analytically singular but numerically small, e.g., the term $(1/\epsilon)\ln(x)$ where x may be some ratio of kinematic scales close to unity. Such a term is numerically suppressed by the smallness of the logarithm but actually singular and may be difficult to detect when performing the singularity cancellation purely numerically.

The partonic cross section for a general $2 \to n$ scattering process, with two partons in the initial-state, may be expanded as a perturbation series in the small coupling leading to the various different contributions to the cross section,

$$\mathrm{d}\hat{\sigma}_{ij} = \mathrm{d}\hat{\sigma}_{ij}^{LO} + \left(\frac{\alpha_s(\mu^2)}{2\pi}\right)\mathrm{d}\hat{\sigma}_{ij}^{NLO} + \left(\frac{\alpha_s(\mu^2)}{2\pi}\right)^2 \mathrm{d}\hat{\sigma}_{ij}^{NNLO} + \mathcal{O}(\alpha_s(\mu^2)^3). \quad (2.22)$$

For an n-parton leading order final-state the LO, NLO and NNLO contributions have the form,

$$\mathrm{d}\hat{\sigma}_{ij}^{LO} = \int_{\Phi_n} \mathrm{d}\hat{\sigma}_{ij}^{B},$$

$$\mathrm{d}\hat{\sigma}_{ij}^{NLO} = \int_{\Phi_n} \left[\mathrm{d}\hat{\sigma}_{ij}^{V} + \mathrm{d}\hat{\sigma}_{ij,NLO}^{MF}\right] + \int_{\Phi_{n+1}} \mathrm{d}\hat{\sigma}_{ij}^{R},$$

$$\mathrm{d}\hat{\sigma}_{ij}^{NNLO} = \int_{\Phi_n} \left[\mathrm{d}\hat{\sigma}_{ij}^{VV} + \mathrm{d}\hat{\sigma}_{ij,NNLO}^{MF,VV}\right] + \int_{\Phi_{n+1}} \left[\mathrm{d}\hat{\sigma}_{ij}^{RV} + \mathrm{d}\hat{\sigma}_{ij,NNLO}^{MF,RV}\right] + \int_{\Phi_{n+2}} \mathrm{d}\hat{\sigma}_{ij}^{RR},$$

$$(2.23)$$

where the (N)NLO mass factorization contributions $\mathrm{d}\hat{\sigma}_{(N)NLO}^{MF}$ are as defined in section 1.4. The only contribution to the leading order cross section is the tree-level $(n + 2)$-parton Born cross section which is proportional to the squared matrix elements,

$$\mathrm{d}\hat{\sigma}_{ij}^{B} \propto \langle \mathcal{M}_{n+2}^0 | \mathcal{M}_{n+2}^0 \rangle. \quad (2.24)$$

The NLO cross section contains an $(n + 2)$-parton virtual contribution $\mathrm{d}\hat{\sigma}_{ij}^V$, an $(n + 3)$-parton real contribution $\mathrm{d}\hat{\sigma}_{ij}^R$, and the NLO mass factorization contribution $\mathrm{d}\hat{\sigma}_{ij,NLO}^{MF}$ which is integrated over the n-parton phase space. The virtual and real contributions are proportional to the sets of matrix elements,

$$\mathrm{d}\hat{\sigma}_{ij}^{V} \propto \langle \mathcal{M}_{n+2}^0 | \mathcal{M}_{n+2}^1 \rangle + \langle \mathcal{M}_{n+2}^1 | \mathcal{M}_{n+2}^0 \rangle,$$

$$\mathrm{d}\hat{\sigma}_{ij}^{R} \propto \langle \mathcal{M}_{n+3}^0 | \mathcal{M}_{n+3}^0 \rangle. \quad (2.25)$$

The NNLO cross section contains a double virtual, two-loop, contribution $\mathrm{d}\hat{\sigma}_{ij}^{VV}$ which is proportional to the set of $(n+2)$-parton matrix elements,

$$\mathrm{d}\hat{\sigma}_{ij}^{VV} \quad \propto \quad \langle \mathcal{M}_{n+2}^0 | \mathcal{M}_{n+2}^2 \rangle + \langle \mathcal{M}_{n+2}^2 | \mathcal{M}_{n+2}^0 \rangle + \langle \mathcal{M}_{n+2}^1 | \mathcal{M}_{n+2}^1 \rangle. \qquad (2.26)$$

The real-virtual contribution to the NNLO cross section involved the one-loop $(n+3)$-parton matrix elements,

$$\mathrm{d}\hat{\sigma}_{ij}^{RV} \quad \propto \quad \langle \mathcal{M}_{n+3}^0 | \mathcal{M}_{n+3}^1 \rangle + \langle \mathcal{M}_{n+3}^1 | \mathcal{M}_{n+3}^0 \rangle, \qquad (2.27)$$

and the double real contribution is proportional to the tree-level $(n+4)$-parton contributions,

$$\mathrm{d}\hat{\sigma}_{ij}^{RR} \quad \propto \quad \langle \mathcal{M}_{n+4}^0 | \mathcal{M}_{n+4}^0 \rangle. \qquad (2.28)$$

The IR poles in ϵ coming from loop integrals in the virtual cross sections are explicit once the loop integration has been performed analytically in $d = 4 - 2\epsilon$ dimensions. The real emission contributions contain implicit IR divergences at NLO and NNLO which require a local counterterm to be constructed. At NLO only the single real emission contribution is divergent and requires the counterterm, $\mathrm{d}\hat{\sigma}_{ij,NLO}^S$. At NNLO the double real emission contribution requires the counterterm $\mathrm{d}\hat{\sigma}_{ij,NNLO}^S$ and the real-virtual one-loop single real emission contribution requires the counterterm $\mathrm{d}\hat{\sigma}_{ij,NNLO}^{V,S}$, which may also contain explicit ϵ poles.

If a subtraction term can be successfully constructed for each divergent contribution and each of those terms analytically integrated over the unresolved regions of phase space, then the total cross section can be rewritten in a form which is free from explicit IR poles and implicit IR divergence. At NLO the divergence-free cross section is given by,

$$\mathrm{d}\hat{\sigma}_{ij}^{NLO} \quad = \quad \int_{\Phi_{n+1}} \left[\mathrm{d}\hat{\sigma}_{ij}^R - \mathrm{d}\hat{\sigma}_{ij,NLO}^S \right] + \int_{\Phi_n} \left[\mathrm{d}\hat{\sigma}_{ij}^V - \mathrm{d}\hat{\sigma}_{ij,NLO}^T \right]. \qquad (2.29)$$

The first term is free from implicit IR divergence as the subtraction term correctly mimics and subtracts the divergence in all unresolved limits without introducing spurious divergence of its own. The second term in (2.29) contains no implicit divergence (because all n final-state partons are resolved) and no explicit IR ϵ poles

because the virtual subtraction term, given by,

$$\mathrm{d}\hat{\sigma}^T_{ij,NLO} = -\mathrm{d}\hat{\sigma}^{MF}_{ij,NLO} - \int_1 \mathrm{d}\hat{\sigma}^S_{ij,NLO}, \tag{2.30}$$

correctly reproduces the explicit pole structure of the unfactorized virtual contribution to the cross section without introducing spurious poles in ϵ. The integral in (2.30) denotes the integral of the NLO subtraction term over all single unresolved regions of phase space and is in general a sum of integrals over the specific unresolved partons. The result is that the full NLO contribution to the cross section is finite and indeed both brackets in (2.29) are individually finite, allowing each contribution to be implemented in a parton-level Monte Carlo program for numerical evaluation.

At NNLO the same philosophy can be applied to rewriting the cross section in terms of individually finite contributions which can be implemented in a Monte Carlo program. In this case the physical cross section is written in the form,

$$\begin{aligned}
\mathrm{d}\hat{\sigma}^{NNLO}_{ij} &= \int_{\Phi_{n+2}} \left[\mathrm{d}\hat{\sigma}^{RR}_{ij} - \mathrm{d}\hat{\sigma}^S_{ij,NNLO} \right] \\
&+ \int_{\Phi_{n+1}} \left[\mathrm{d}\hat{\sigma}^{RV}_{ij} - \mathrm{d}\hat{\sigma}^T_{ij,NNLO} \right] \\
&+ \int_{\Phi_n} \left[\mathrm{d}\hat{\sigma}^{VV}_{ij} - \mathrm{d}\hat{\sigma}^U_{ij,NNLO} \right].
\end{aligned} \tag{2.31}$$

As was the case at NLO, each bracketed term is IR finite. The first term contains no explicit poles and the implicit divergence is absorbed by the subtraction term. The NNLO double real subtraction term can be further decomposed into terms which can be integrated over just one or both unresolved partons in a single step, denoted $\mathrm{d}\hat{\sigma}^{S,1}_{ij,NNLO}$ and $\mathrm{d}\hat{\sigma}^{S,2}_{ij,NNLO}$ respectively, such that $\mathrm{d}\hat{\sigma}^S_{ij,NNLO} = \mathrm{d}\hat{\sigma}^{S,1}_{ij,NNLO} + \mathrm{d}\hat{\sigma}^{S,2}_{ij,NNLO}$. The real-virtual subtraction term is given by,

$$\mathrm{d}\hat{\sigma}^T_{ij,NNLO} = \mathrm{d}\hat{\sigma}^{V,S}_{ij,NNLO} - \mathrm{d}\hat{\sigma}^{MF,RV}_{ij,NNLO} - \int_1 \mathrm{d}\hat{\sigma}^{S,1}_{ij,NNLO}, \tag{2.32}$$

the various terms in which conspire to cancel all explicit poles and IR divergence of the unfactorized real-virtual cross section. The double virtual cross section doesn't contain any implicit IR divergence and so no two-loop counterterm is required. The explicit ϵ poles of the unfactorized double virtual cross section are then removed by the double virtual subtraction term which is given by,

$$\mathrm{d}\hat{\sigma}^U_{ij,NNLO} = -\mathrm{d}\hat{\sigma}^{MF,VV}_{ij,NNLO} - \int_1 \mathrm{d}\hat{\sigma}^{V,S}_{ij,NNLO} - \int_2 \mathrm{d}\hat{\sigma}^{S,2}_{ij,NNLO}. \tag{2.33}$$

The subtraction formalism as outlined in this section is a method for calculating the cross section without approximation in an analytic fashion and in principle can be applied to any order of the perturbation series. In using subtraction the emphasis is shifted from the ability to integrate the physical cross section, to the ability to integrate the artificially constructed subtraction terms, that is if such a subtraction term can be successfully defined in the first place.

One subtraction method for which all the quantities constituting the subtraction terms have been derived and integrated for calculations up to NNLO (including hadronic initial states) is *antenna subtraction* [32]. Much work in recent years has been focused on deriving and integrating the antenna functions, to be defined in the following section, such that all the tools are now available to construct all the subtraction terms required for a full NNLO calculation [32,36,93–117]. The antenna subtraction formalism will be discussed in detail in the remainder of this chapter with an emphasis on the process of defining the general structure of the various subtraction terms. Understanding how to successfully construct the subtraction terms is the crucial final stage in the antenna subtraction program, now all necessary ingredients have been derived, and will finally allow analytically finite NNLO QCD predictions to be made within a general framework, implemented in a Monte Carlo program.

2.2 Antenna functions

The keystone of the antenna subtraction formalism is the definition and use of *antenna functions*. Antenna functions are constructed from physical matrix elements and contain many of the IR divergences associated with QCD matrix elements. The functions are built from colour-ordered matrix elements and so follow the factorization patterns for colour-ordered matrix elements outlined in section 1.3.2. The factorization pattern requires two partons in the antenna to remain hard and resolved, the radiators, which radiate potentially unresolved partons in a colour-ordered fashion.

The antenna functions are broadly classified according the specifics of the radia-

tor partons in the antenna, which each class being further subdivided according to the quantum numbers of the radiated partons. All antenna functions can be classified into three groups according to the particle type of the radiators: quark-anti-quark, quark-gluon and gluon-gluon antennae. Each class of antennae is derived from an underlying two-parton process, the various QCD radiative corrections to which generate the antenna functions in each class. The physical processes used to calculate the antenna functions are as follows:

- Quark-anti-quark: Derived from the decay of a virtual photon into a massless quark-anti-quark pair and any additional QCD radiation from the quark pair. $\gamma^* \to q \, \bar{q}$ + partons [118].

- Quark-gluon: Derived from the decay of a heavy neutralino into a gluino and gluon in addition to any coloured radiation from the gluon-gluino antenna. $\tilde{\chi} \to \tilde{g} \, g$ + partons [106].

- Gluon-gluon: Derived from the decay of a heavy Higgs boson into a pair of gluons and any subsequent QCD radiation from the gluon pair. $H \to g \, g$ + partons [107].

At NLO the antenna functions are generated by considering QCD real radiative corrections to the underlying processes, i.e., a single gluon emission or a gluon splitting into a quark-anti-quark pair. At NNLO the pattern of radiation is more complicated with a number of new double radiative patterns permitted as well as the one-loop single radiative corrections to the underlying process. The various antennae corresponding to the different partonic channels are summarised in tables 2.1-2.2 and pictorially depicted in figures 2.2-2.3.

The antenna functions are defined mathematically as the ratio of the squared colour-ordered matrix element for the radiative correction to the squared matrix element for the underlying two-parton process. In the case of the tree-level three-parton antennae,

$$X_3^0(i,j,k) \;\; = \;\; \mathcal{S}_{ijk/IK} \frac{M_3^0(i,j,k)}{M_2^0(I,K)}, \tag{2.34}$$

Class	Radiative process	Antennae	
		Tree	1-loop
Quark-anti-quark	$q\,\bar{q} \longrightarrow q\,g\,\bar{q}$	A_3^0	$A_3^1,\ \tilde{A}_3^1,\ \hat{A}_3^1$
Quark-gluon	$q\,g \longrightarrow q\,g\,g$	D_3^0	$D_3^1,\ \hat{D}_3^1$
	$q\,g \longrightarrow q\,q'\,\bar{q}'$	E_3^0	$E_3^1,\ \tilde{E}_3^1,\ \hat{E}_3^1$
Gluon-gluon	$g\,g \longrightarrow g\,g\,g$	F_3^0	$F_3^1,\ \hat{F}_3^1$
	$g\,g \longrightarrow g\,q\,\bar{q}$	G_3^0	$G_3^1,\ \tilde{G}_3^1,\ \hat{G}_3^1$

Table 2.1: The various three-parton tree-level and one-loop antenna functions cate-gorised according to the partonic channels they correspond to.

where $\mathcal{S}_{ijk/IK}$ is a symmetry factor taking into account final-state parton sym-metries and degenerate antenna definitions. The one-loop three-parton antennae are defined in such a way that in the singular limits the antenna is proportional to the one-loop singular function. The colour-ordered matrix elements follow a (tree×loop)+(loop×tree) factorization pattern, as displayed in section 1.3.2, and so to ensure that the antenna function has the desired properties, the (tree×loop) piece is systematically removed from the definition of the antenna [32],

$$X_3^1(i,j,k) \;\; = \;\; \mathcal{S}_{ijk/IK}\frac{M_3^1(i,j,k)}{M_2^0(I,K)} - X_3^0(i,j,k)\frac{M_2^1(I,K)}{M_2^0(I,K)}. \qquad (2.35)$$

The four-parton tree-level antenna functions are defined in a similar fashion to the tree-level tree-parton antennae with an additional radiated parton,

$$X_4^0(i,j,k,l) \;\; = \;\; \mathcal{S}_{ijkl/IL}\frac{M_4^0(i,j,k,l)}{M_2^0(I,L)}. \qquad (2.36)$$

These three definitions suffice to determine all the relevant antenna functions for calculations up to NNLO. The antenna formalism is general and, if desirable, higher multiplicity and higher loop antenna functions can be defined if the matrix elements are available. However for an antenna function to be useful it must also be integrable over the unresolved phase space, a non-trivial requirement.

In addition to the particle content, antenna functions are also broadly classified according to the kinematics of their radiator partons which can be in either the initial- or final-state. When the radiators are both in the final-state, one in the

Class	Radiative process	Antennae
Quark-anti-quark	$q\,\bar{q} \longrightarrow q\,g\,g\,\bar{q}$	$A_4^0,\ \tilde{A}_4^0$
	$q\,\bar{q} \longrightarrow q\,q'\,\bar{q}'\,\bar{q}$	B_4^0
	$q\,\bar{q} \longrightarrow q\,q\,\bar{q}\,\bar{q}$	C_4^0
Quark-gluon	$q\,g \longrightarrow q\,g\,g\,g$	D_4^0
	$q\,g \longrightarrow q\,q'\,\bar{q}'\,g$	$E_4^0,\ \tilde{E}_4^0$
Gluon-gluon	$g\,g \longrightarrow g\,g\,g\,g$	F_4^0
	$g\,g \longrightarrow g\,q\,\bar{q}\,g$	$G_4^0,\ \tilde{G}_4^0$
	$g\,g \longrightarrow q\,\bar{q}\,q'\,\bar{q}'$	H_4^0

Table 2.2: The various four-parton tree-level antenna functions categorised according to the partonic channels they correspond to.

initial-state and one final-state or both in the initial-state, the antenna is referred to as being a final-final, initial-final or initial-initial antenna respectively. In unintegrated form the antenna functions in each configuration are related to one another simply by crossing due to the fact that they are constructed from physical matrix elements. In practice the analytic form of the antenna function is left unaltered and the kinematic variables are crossed into the initial state. If from the set of partons $\{i, j, k, l\}$ partons i and k are crossed into the initial state then the Lorentz invariants are transformed according to:

$$
\begin{aligned}
s_{ij} &\rightarrow -s_{ij} & s_{jk} &\rightarrow -s_{jk}, \\
s_{ik} &\rightarrow +s_{ik} & s_{jl} &\rightarrow +s_{jl}, \\
s_{il} &\rightarrow -s_{il} & s_{kl} &\rightarrow -s_{kl}.
\end{aligned}
\tag{2.37}
$$

If an antenna function contains initial-state partons then the singular limits it contains will be different to the same species of antenna containing only final-state partons. If the initial-state parton becomes collinear with a final-state parton then the splitting function the antenna contains will be an initial-final splitting function, related to the final-final splitting function as shown in (1.93). Due to the initial-state partons having well defined fixed momenta, an initial state parton can never become soft and so the lack of soft initial-state gluons also affects the permitted

(a) A_3^0, A_3^1, $\tilde{A}_3^1$, $\hat{A}_3^1$ (b) D_3^0, D_3^1, $\hat{D}_3^1$ (c) E_3^0, E_3^1, $\hat{E}_3^1$

(d) F_3^0, F_3^1, $\hat{F}_3^1$ (e) G_3^0, G_3^1, $\tilde{G}_3^0$, $\hat{G}_3^1$
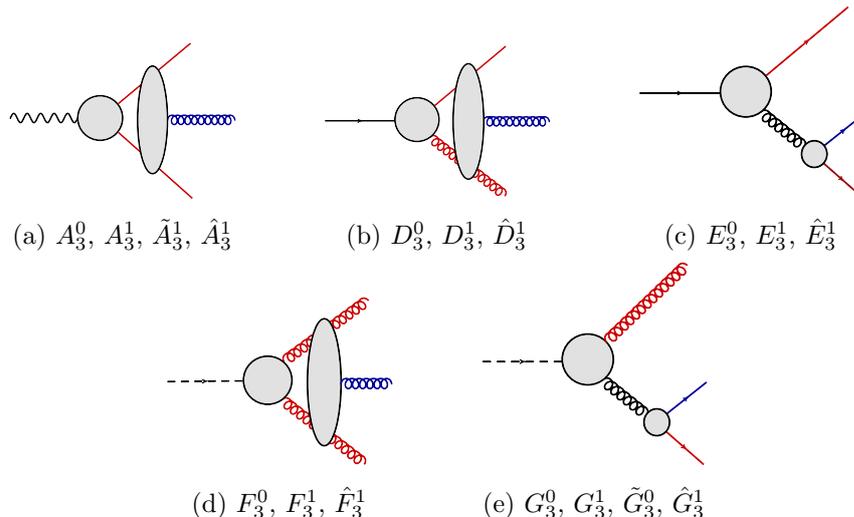
Figure 2.2: The three-parton antenna functions at tree-level and one-loop. Red lines denote hard radiators and blue lines potentially unresolved partons. The grey blobs denote all diagrams generating a given external state.

singularities of the initial-final and initial-initial antenna functions.

It is sometimes convenient to split the antenna functions into sub-antennae which contain fewer singular limits. This can be done by examining the denominators of the terms in the function and partitioning the function to isolate terms only containing certain divergences. For example the three-parton quark-anti-quark antenna is given by,

$$A_3^0(i_q, j_g, k_{\bar{q}}) \;=\; \frac{1}{s_{ijk}}\left(\frac{s_{ij}}{s_{jk}} + \frac{s_{jk}}{s_{ij}} + 2\frac{s_{ik}s_{ijk}}{s_{ij}s_{jk}}\right). \tag{2.38}$$

This antenna contains a quark-gluon collinear limit, an anti-quark-gluon collinear limit and a soft gluon limit. This antenna can be split up into two sub-antennae:

$$A_3^0(i_q, j_g, k_{\bar{q}}) \;=\; a_3^0(i, j, k) + a_3^0(k, j, i), \tag{2.39}$$

where the sub-antenna is given by [32],

$$a_3^0(i, j, k) \;=\; \frac{1}{s_{ijk}}\left(\frac{s_{jk}}{s_{ij}} + 2\frac{s_{ik}s_{ijk}}{(s_{ij} + s_{jk})s_{ij}}\right). \tag{2.40}$$

To obtain the expression in (2.40), the third term in (2.38) is partitioned using *partial fractioning* which exploits the identity,

$$\frac{1}{xy} \;=\; \frac{1}{x+y}\left(\frac{1}{x} + \frac{1}{y}\right), \tag{2.41}$$

to separate the denominator into two terms divergent only in s_{ij} or s_{jk}. The sub-antenna $a_3^0(i, j, k)$ only contains collinear divergence between the partons i and j, not j and k. The soft limit is shared between the two sub-antennae.

An additional complication when defining sub-antennae is that unlike the final-final, initial-final and initial-initial full antennae which are related to one another by crossing, the sub-antennae for the three configurations can be different. Introducing initial-state partons alters the potential divergences present in the antenna and so the antenna is partitioned into sub-antennae differently than in the final-final case; it makes no sense to split up an antenna to isolate a soft gluon limit if that gluon is in the initial-state. For example, consider the three-parton gluonic antenna, $F_3^0(i, j, k)$. In the case of all partons in the final state this antenna can be partitioned into three sub-antennae,

$$F_3^0(i, j, k) = f_3^0(i, j, k) + f_3^0(j, k, i) + f_3^0(k, i, j). \qquad (2.42)$$

The full antenna is divergent when any three of the gluons is soft or any of the colour connected gluons become collinear. By contrast the sub-antenna $f_3^0(i, j, k)$ contains only the soft limit when j becomes soft and only part of the collinear divergence, the rest being shared with the other sub-antennae. If one of the partons is crossed into the initial-state, i.e., $i \rightarrow \hat{i}$, where the hat denotes an initial-state parton, then it is no longer helpful to partition the antenna to isolate the soft i limit as that limit can never be realised. Instead the antenna is partitioned into two initial-final sub-antennae [114],

$$F_3^0(\hat{i}, j, k) = f_3^0(\hat{i}, j, k) + f_3^0(\hat{i}, k, j). \qquad (2.43)$$

The sub-antenna $f_3^0(\hat{i}, j, k)$ now contains the full j soft limit, the full $\hat{i}||j$ collinear limit and shares the $j||k$ limit with the other sub-antenna. In the initial-initial case there is no ambiguity when it comes to defining the hard partons, which are always identified as the initial-state partons, so no partitioning of the antenna is necessary or desirable.

The issue of identifying the hard radiators in an antenna persists at the four-parton level. For initial-initial antennae the choice is unambiguous and the initial-state partons are taken to be the hard radiators and no partitioning of the antenna

(a) A_4^0, $\tilde{A}_4^0$ (b) B_4^0, C_4^0 (c) D_4^0

(d) E_4^0, $\tilde{E}_4^0$ (e) F_4^0 (f) G_4^0, $\tilde{G}_4^0$

(g) H_4^0
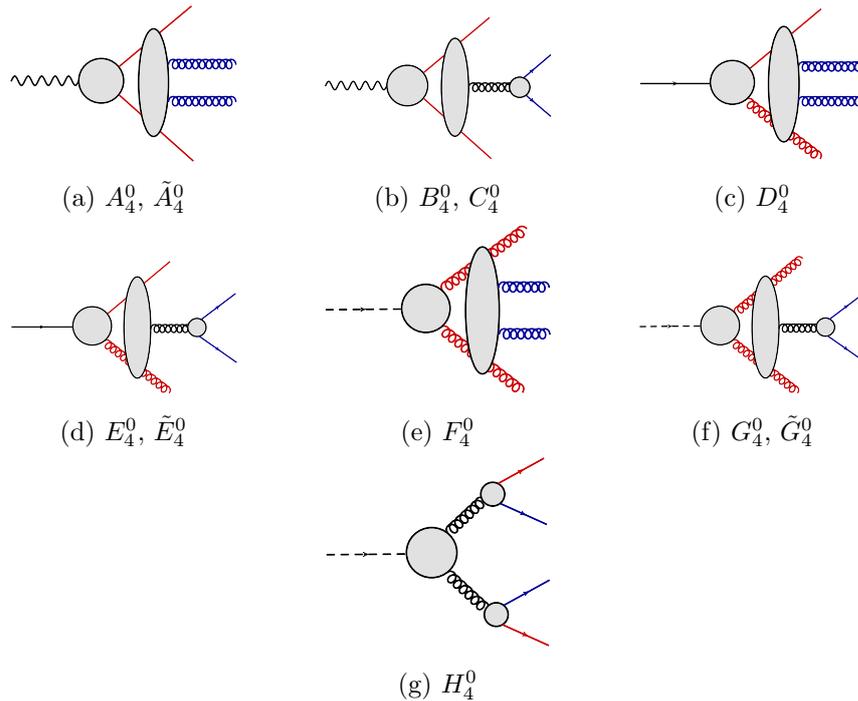
Figure 2.3: The four-parton tree-level antenna functions.

is necessary. As is discussed in section 2.3 the initial-final momentum mapping forms two momenta from an original set of four, including an initial-state parton, $\{\hat{i}, j, k, l\} \rightarrow \{\hat{I}, K\}$. The first hard radiator is always taken to be the initial-state parton, the second can be any of the remaining final-state partons because all choices of hard final-state parton map onto the same two composite momenta. Notwithstanding the robustness of the phase-space map to the choice of hard partons, it may be desirable to partition the antenna further to avoid ambiguities in its divergent limits. This is particularly the case for four-parton antennae involving initial-state gluons, and is also present for three-parton antennae and will be discussed in sections 2.5.1 and 2.6.1. In the case of final-final antennae containing gluons, in particular the F_4^0 and D_4^0 final-final antennae, the choice of hard partons is not immediately obvious as a number of final-state gluons can become soft. As will be discussed in more detail in the next section the final-final phase space map does not resolve this ambiguity as it implicitly identifies two partons as the hard radiators. This means that to capture the full divergence of the antenna many mappings must be employed and the antenna must be partitoned to suit each mapping. The decomposition of the final-final D_4^0 is documented in [108] and the final-final F_4^0 in [114].

	$(n+2)$	$(n+3)$	$(n+4)$
LO	$\mathrm{d}\hat{\sigma}_{ij}^{B}$		
NLO	$\mathrm{d}\hat{\sigma}_{ij}^{V}$	$\mathrm{d}\hat{\sigma}_{ij}^{R}$	
NNLO	$\mathrm{d}\hat{\sigma}_{ij}^{VV}$	$\mathrm{d}\hat{\sigma}_{ij}^{RV}$	$\mathrm{d}\hat{\sigma}_{ij}^{RR}$

Table 2.3: A summary of which cross section contributions sample which sets of momenta up to NNLO, starting from an $(n+2)$-parton Born level contribution.

2.3 Phase space factorization

Antenna subtraction, along with many other subtraction schemes and slicing, relies on two main factorization theorems: matrix element factorization and phase space factorization. As the partonic cross section is formed from matrix elements and integrated over the final-state phase space, both are crucial for the isolation of IR singularities. In unfactorized form the $2 \to n$-particle phase space is given by,

$$
\mathrm{d}\Phi_n(k_1, \cdots, k_n; p_1, p_2) =
$$
$$
\frac{\mathrm{d}^{d-1}k_1}{2E_1(2\pi)^{d-1}} \cdots \frac{\mathrm{d}^{d-1}k_n}{2E_n(2\pi)^{d-1}}(2\pi)^d \delta^d(k_1 + \cdots + k_n - p_1 - p_2),
$$
$$
(2.44)
$$

where the set $\{k_i\}$ denotes the momenta of the final-state partons and $\{p_1, p_2\}$ the incoming partons, the union of the two sets forming an $(n+2)$-parton momentum set. For an $(n+2)$-parton Born-level process the NLO real and virtual corrections are functions of momenta which belong to the $(n+3)$- and $(n+2)$-parton momentum sets respectively. The NNLO double real, real-virtual and double virtual corrections sample momenta from the $(n+4)$-, $(n+3)$- and $(n+2)$-parton momentum sets respectively. The distribution of the cross section contributions among the momentum sets is summarized in table 2.3.

The aim of antenna factorization is to re-parameterize the phase by employing a phase space map which maps the original set of momenta down to a lower multiplicity set of momenta. The original phase space is then rewritten as a direct product of the mapped phase sub-space and an *antenna phase space* which is independent of the mapped momenta and depends only on the momenta of the partons involved

in the antenna function. NNLO calculations with two initial-state partons require final-final, initial-final and initial-initial phase space maps for $(n + 3) \rightarrow (n + 2)$ and $(n + 4) \rightarrow (n + 2)$ mappings, making six maps in total. The kinematics of the final-final, initial-final and initial-initial configurations are different and so although the antenna functions for the three configurations are obtained by crossing, their integrals over the respective antenna phase spaces will generate genuinely distinct functions.

Any phase space map has a few main requirements: A basic requirement is that the composite momenta generated by the map must remain on-shell and respect any symmetries of the original set, i.e., Lorentz symmetry. Another requirement which is necessary for subtraction is that in unresolved limits the set of mapped momenta tend towards the subset of resolved momenta in the original set. Finally the phase space map must allow the original phase space to factorize appropriately. There is a certain amount of freedom in defining the phase space map and any map is valid as long as it satisfies the necessary requirements.

2.3.1 Final-final

In the final-final configuration the $(n + 3) \rightarrow (n + 2)$ map [93] generates the set $\{p_{n+2}\}$ from the original set $\{p_{n+3}\}$. Such a mapping is naturally associated with a three-parton antenna function, $X_3(i, j, k)$, which encapsulates the matrix element's divergent behaviour in the singular limit. The three parton antenna is a function of three momenta, $\{p_i, p_j, p_k\}$ and it is this subset of momenta which are mapped onto two composite momenta, $\{i, j, k\} \rightarrow \{I, J\}$,

$$
\begin{aligned}
p_I &= x_1 p_i + x_2 p_j + x_3 p_k, \\
p_J &= (1 - x_1)p_i + (1 - x_2)p_j + (1 - x_3)p_k.
\end{aligned}
\tag{2.45}
$$

Momentum conservation is trivially maintained by using this form for the composite momenta, i.e., $p_i + p_j + p_k = p_I + p_J$. The parameterization of the composite momenta is given by the functions x_i,

$$
x_1 = \frac{1}{2(s_{ij} + s_{ik})} \left[(1 + \rho)s_{ijk} - 2x_2 s_{jk} \right],
$$

$$x_2 = \frac{s_{jk}}{s_{ij} + s_{jk}},$$

$$x_3 = \frac{1}{2(s_{jk} + s_{ik})}\left[(1-\rho)s_{ijk} - 2x_2 s_{ij}\right],$$

$$\rho = \left[1 + \frac{4x_2(1-x_2)s_{ij}s_{jk}}{s_{ijk}s_{ik}}\right]^{\frac{1}{2}}. \tag{2.46}$$

Using this form for the composite momenta it can be shown that in the soft and collinear limits the composite momenta are reduced to the resolved momenta appropriate for the limit [108]:

$$
\begin{aligned}
j \to 0 \quad &: \qquad p_I \to p_i \qquad\qquad p_J \to p_k, \\
i||j \quad &: \qquad p_I \to p_i + p_j \qquad p_J \to p_k, \\
j||k \quad &: \qquad p_I \to p_i \qquad\qquad p_J \to p_j + p_k.
\end{aligned} \tag{2.47}
$$

Due to the behaviour of the composite momenta in the singular limits it is intuitive to label the composite momenta $\{I, J\} = \{\widetilde{(ij)}, \widetilde{(jk)}\}$, which makes the form of the composite momenta in the singular limits clear. Applying this map to the three momenta involved in the antenna, the full momentum set is mapped according to,

$$\{p_{n+3}\} \quad \longrightarrow \quad \underbrace{\{p_i, p_j, p_k\}}_{\{p_{\text{antenna}}\}} \cup \underbrace{\{p_I, p_J\} \cup \{\{p_{n+3}\}\backslash\{p_i, p_j, p_k\}\}}_{\{p_{n+2}\}}. \tag{2.48}$$

By re-parameterizing the phase space in terms of the new momenta, the entire phase space factorizes into a three-parton antenna phase space and a mapped reduced phase space, echoing the factorization of the matrix elements,

$$
\begin{aligned}
\mathrm{d}\Phi_{n+1}(k_1, \cdots, k_i, k_j, k_k, \cdots, k_{n+1}; p_1, p_2) &= \mathrm{d}\Phi_n(k_1, \cdots, k_I, k_J, \cdots, k_n; p_1, p_2) \\
&\cdot \ \mathrm{d}\Phi_{X_{ijk}}(k_i, k_j, k_k; k_I, k_J).
\end{aligned} \tag{2.49}
$$

Setting $n = 2$ in the above formula and noting that the two-particle phase space is a constant it is clear that the three-parton antenna phase space is proportional to the three-particle phase space,

$$\mathrm{d}\Phi_{X_{ijk}} = P_2^{-1} \cdot \mathrm{d}\Phi_3, \tag{2.50}$$

where the two particle phase space in $d = 4 - 2\epsilon$ dimensions is given by [32],

$$P_2 = 2^{-3+2\epsilon} \pi^{-1+\epsilon} \frac{\Gamma(1-\epsilon)}{\Gamma(2-2\epsilon)}(p_1 + p_2)^{-\epsilon}. \tag{2.51}$$

September 24, 2012

At NNLO in the almost colour-connected and colour disconnected double unresolved configurations the $3 \to 2$ map can be iterated to match the factorization pattern of the matrix elements discussed in section 1.3.2,

$$\{p_{n+4}\} \longrightarrow \{p_{\text{antenna}_1}\} \cup \{p_{n+3}\} \longrightarrow \{p_{\text{antenna}_1}\} \cup \{p_{\text{antenna}_2}\} \cup \{p_{n+2}\}. \quad (2.52)$$

In the colour-connected limit the double unresolved singular function is approximated by a four parton antenna and so a new phase space map is required which maps four momenta down to two composite momenta in a single map. This is achieved by defining a $4 \to 2$ mapping given by, $\{i, j, k, l\} \to \{I, J\}$, such that,

$$
\begin{aligned}
p_I &= x_1 p_i + x_2 p_j + x_3 p_k + x_4 p_l, \\
p_J &= (1 - x_1)p_i + (1 - x_2)p_j + (1 - x_3)p_k + (1 - x_4)p_l. \quad (2.53)
\end{aligned}
$$

In a similar fashion to the $3 \to 2$ map, the parameterization is defined by the functions,

$$
\begin{aligned}
x_1 &= \frac{1}{2(s_{ij} + s_{ik} + s_{il})}\Big[(1 + \rho)s_{ijkl} - x_2(s_{jk} + 2s_{jl}) \\
&\quad - x_3(s_{jk} + 2s_{kl}) + (x_2 - x_3)\left(\frac{s_{ij}s_{kl} - s_{ik}s_{jl}}{s_{il}}\right)\Big], \\
x_2 &= \frac{s_{jk} + s_{jl}}{s_{ij} + s_{jk} + s_{jl}}, \\
x_3 &= \frac{s_{kl}}{s_{ik} + s_{jk} + s_{kl}}, \\
x_4 &= \frac{1}{2(s_{il} + s_{jl} + s_{kl})}\Big[(1 - \rho)s_{ijkl} - x_2(s_{jk} + 2s_{ij}) \\
&\quad - x_3(s_{jk} + 2s_{ik}) - (x_2 - x_3)\left(\frac{s_{ij}s_{kl} - s_{ik}s_{jl}}{s_{il}}\right)\Big]. \quad (2.54)
\end{aligned}
$$

The parameter ρ is defined as,

$$
\begin{aligned}
\rho &= \Big[1 + \frac{(x_2 - x_3)^2}{s_{il}^2 s_{ijkl}^2}\lambda(s_{ij}s_{kl}, s_{il}s_{jk}, s_{ik}s_{jl}) \\
&\quad + \frac{1}{s_{il}s_{ijkl}}\Big(2(x_2(1 - x_3) + x_3(1 - x_2))(s_{ij}s_{kl} + s_{ik}s_{jl} - s_{jk}s_{il}) \\
&\quad + 4x_2(1 - x_2)s_{ij}s_{jl} + 4x_3(1 - x_3)s_{ik}s_{kl}\Big)\Big]^{\frac{1}{2}}, \quad (2.55)
\end{aligned}
$$

where the Källen function is given by,

$$\lambda(x, y, z) = x^2 + y^2 + z^2 - 2(xy + xz + yz). \quad (2.56)$$

September 24, 2012

By studying the behaviour of the x_i functions in the double unresolved singular limits, the behaviour of the composite momenta in those limits can be derived,

$$
\begin{aligned}
j, k \to 0 &: & p_I \to p_i & & p_J \to p_l, \\
i||j||k &: & p_I \to p_i + p_j + p_k & & p_J \to p_l, \\
j||k||l &: & p_I \to p_i & & p_J \to p_j + p_k + p_l, \\
j \to 0,\ k||l &: & p_I \to p_i & & p_J \to p_k + p_l, \\
k \to 0,\ i||j &: & p_I \to p_i + p_j & & p_J \to p_l, \\
i||j,\ k||l &: & p_I \to p_i + p_j & & p_J \to p_k + p_l.
\end{aligned}
\tag{2.57}
$$

Given this behaviour in the singular limits, it is appropriate to label the composite momenta in a way that reflects their behaviour in the unresolved configurations, i.e., $\{I, J\} = \{\widetilde{(ijk)}, \widetilde{(jkl)}\}$. This map clearly identifies the hard partons as partons i and l with the unresolved radiation being partons j and k. Using this mapping in conjunction with the appropriate four-parton antenna function allows the subtraction of IR divergences in a smooth fashion across all configurations where j and k become unresolved.

If the antenna function being used contains more than two potentially unresolved partons then it must be decomposed into sub-antennae which reflect the kinematics of the momentum map, e.g., the gluon-gluon antenna F_4^0 for which any of the gluons may potentially be unresolved and is decomposed into permutations of the sub-antennae $F_{4,a}$ and $F_{4,b}^0$ [114], each of which contain implicitly hard partons which can be matched to the hard partons in the momentum map. A similar situation arises for non-colour-ordered antennae which contain collinear divergences between many non-adjacent partons, such as the final-final $\tilde{A}_4^0$. In these cases the antenna must also be decomposed into sub-antennae, as was performed in [108], to ensure a proper match with the phase space map.

Employing this map to re-parameterize the phase space allows the phase space to be factorized into a four-parton antenna phase space and a mapped reduced phase space,

$$
d\Phi_{n+2}(k_1, \cdots, k_i, k_j, k_k, k_l, \cdots, k_{n+2}; p_1, p_2) = d\Phi_n(k_1, \cdots, k_I, k_J, \cdots, k_n; p_1, p_2)
$$

$$\cdot \quad \mathrm{d}\Phi_{X_{ijkl}}(k_i, k_j, k_k, k_l; k_I, k_J). \quad (2.58)$$

Again setting $n = 2$ shows that the four-parton antenna phase space is proportional to the four-particle phase space,

$$\mathrm{d}\Phi_{X_{ijkl}} = P_2^{-1} \cdot \mathrm{d}\Phi_4. \quad (2.59)$$

The re-parameterization of the original momentum set for colour-connected double unresolved configurations can be summarized by,

$$\{p_{n+4}\} = \underbrace{\{p_i, p_j, p_k, p_l\}}_{p_{\text{antenna}}} \cup \underbrace{\{p_I, p_J\} \cup \{\{p_{n+4}\} \backslash \{p_i, p_j, p_k, p_l\}\}}_{\{p_{n+2}\}} \quad (2.60)$$

It is important to note that the form of the composite momenta given by (2.53) and (2.54) reduces to that of the composite momenta defined by the $3 \rightarrow 2$ map in all single unresolved limits. For example consider the $p_k \rightarrow 0$ limit:

$$p_I \rightarrow x_1 p_i + x_2 p_j + x_4 p_l + \mathcal{O}(p_k),$$

$$p_J \rightarrow (1 - x_1)p_i + (1 - x_2)p_j + (1 - x_4)p_l + \mathcal{O}(p_k), \quad (2.61)$$

where the x_i functions are still those defined for the $4 \rightarrow 2$ map. The behaviour of the x_i functions themselves can be inferred by taking the $k \rightarrow 0$ limit, in which:

$$\lambda(s_{ij}s_{kl}, s_{il}s_{jk}, s_{ik}s_{jl}) \rightarrow 0 + \mathcal{O}(p_k),$$

$$\rho \rightarrow \left[1 + \frac{4x_2(1 - x_2)s_{ij}s_{jl}}{s_{il}s_{ijl}}\right]^{\frac{1}{2}} + \mathcal{O}(p_k),$$

$$x_1 \rightarrow \frac{1}{2(s_{ij} + s_{il})}\left[(1 + \rho)s_{ijl} - 2x_2 s_{jl}\right] + \mathcal{O}(p_k),$$

$$x_2 \rightarrow \frac{s_{jl}}{s_{ij} + s_{jl}} + \mathcal{O}(p_k),$$

$$x_4 \rightarrow \frac{1}{2(s_{jl} + s_{il})}\left[(1 - \rho)s_{ijl} - 2x_2 s_{ij}\right] + \mathcal{O}(p_k). \quad (2.62)$$

Re-labelling the remaining resolved momenta $\{i, j, l\} \rightarrow \{i, j, k\}$, the form of the $4 \rightarrow 2$ composite momenta tend to the form of the $3 \rightarrow 2$ composite momenta. The fact that in single unresolved limits, the $4 \rightarrow 2$ map reproduces the same composite momenta as the $3 \rightarrow 2$ map means that the single unresolved divergent limits of a four-parton antenna can be systematically removed using the product of two three-parton antennae associated with iterated $3 \rightarrow 2$ mappings. The details of how this is achieved will be discussed in section 2.6.

September 24, 2012

2.3.2 Initial-final

Antennae which contain one initial-state parton require a different phase space map as it is inappropriate to use the composite momenta defined for the final-final case as that map will in general map the initial-state parton away from the beam axis. Instead a map is employed which simply rescales the initial-state parton's momentum and maps the remaining final-state partons involved in the antenna to a single composite momentum [36]. For the set of momenta $\{\hat{1}, i, j\}$ of which the initial-final antenna $X_3^0(\hat{1}, i, j)$ is a function, the $3 \to 2$ map is employed such that $\{\hat{1}, i, j\} \to \{\hat{\bar{1}}, I\}$, where,

$$\begin{aligned} \bar{p}_1 &= xp_1, \\ p_I &= p_i + p_j - (1-x)p_1. \end{aligned} \tag{2.63}$$

This form for the momenta ensures momentum conservation, i.e., $p_I - \bar{p}_1 = p_i + p_j - p_1$. The requirement that the composite momenta remain massless fixes the rescaling factor to be,

$$x = \frac{s_{1i} + s_{1j} + s_{ij}}{s_{1i} + s_{1j}}. \tag{2.64}$$

Using this parameterization of the composite momenta it can be shown that in the single unresolved limits [36]:

$$\begin{aligned} i \to 0 &: & \bar{p}_1 &\to p_1 & p_I &\to p_j, \\ \hat{1} \| i &: & \bar{p}_1 &\to p_1 - p_i & p_I &\to p_j, \\ i \| j &: & \bar{p}_1 &\to p_1 & p_I &\to p_i + p_j. \end{aligned} \tag{2.65}$$

To reflect this behaviour the composite momenta may be labelled $\{\hat{\bar{1}}, I\} = \{\hat{\bar{1}}, \widetilde{(ij)}\}$. The full phase space map is summarized as,

$$\{p_{n+3}\} \to \underbrace{\{p_1, p_i, p_j\}}_{\{p_{\text{antenna}}\}} \cup \underbrace{\{\bar{p}_1, p_I\} \cup \{\{p_{n+3}\}\backslash\{p_1, p_i, p_j\}\}}_{\{p_{n+2}\}}. \tag{2.66}$$

The effect of re-parameterizing the momenta in this way allows the phase space to be written as a convolution of a two-particle phase space and a reduced multiplicity mapped phase space,

$$\mathrm{d}\Phi_{n+1}(k_1 \cdots, k_i, k_j, \cdots, k_{n+1}; p_1, p_2) =$$

$$\mathrm{d}\Phi_n(k_1 \cdots, k_I, \cdots, k_n; \bar{p}_1, p_2)\mathrm{d}\Phi_2(k_i, k_j; p_1, q) \frac{Q^2}{2\pi} \frac{\mathrm{d}x}{x}\delta(x - \hat{x})$$

$$(2.67)$$

where the initial-state parton involved in the antenna is taken to have momentum p_1. The momentum $q = p_i + p_j - p_1$ forms the scale $Q^2 = -q^2$. The quantity $\hat{x}$ is given by the fraction defined in (2.64).

The relevant $4 \to 2$ map for the initial-final configuration generalizes the $3 \to 2$ map by adding an extra final-state parton, i.e., $\{\hat{1}, i, j, k\} \to \{\hat{\bar{1}}, I\} = \{\hat{\bar{1}}, \widetilde{(ijk)}\}$, where the bar once again denotes an overall rescaling [36]. The composite momenta are defined by the parameterization,

$$\begin{aligned} \bar{p}_1 &= xp_1, \\ p_I &= p_i + p_j + p_k - (1 - x)p_1, \end{aligned} \qquad (2.68)$$

where, as in the three-parton case, the on-shell condition fixes the rescaling function,

$$x = \frac{s_{1i} + s_{1j} + s_{1k} + s_{ij} + s_{ik} + s_{jk}}{s_{1i} + s_{1j} + s_{1k}}. \qquad (2.69)$$

In the double unresolved limits the composite momenta are reduced to the appropriate resolved momenta,

$$\begin{aligned} i, j \to 0 \quad &: \qquad \bar{p}_1 \to p_1 \qquad\qquad p_I \to p_k, \\ \hat{1}||i||j \quad &: \qquad \bar{p}_1 \to p_1 - p_i - p_j \qquad p_I \to p_k, \\ i||j||k \quad &: \qquad \bar{p}_1 \to p_1 \qquad\qquad p_I \to p_i + p_j + p_k, \\ i \to 0, \ j||k \quad &: \qquad \bar{p}_1 \to p_1 \qquad\qquad p_I \to p_j + p_k, \\ j \to 0, \ \hat{1}||i \quad &: \qquad \bar{p}_1 \to p_1 - p_i \qquad\quad p_I \to p_k, \\ \hat{1}||i, \ j||k \quad &: \qquad \bar{p}_1 \to p_1 - p_i \qquad\quad p_I \to p_j + p_k. \end{aligned} \qquad (2.70)$$

In all single unresolved limits the composite momenta map onto composite momenta of the form generated by a $3 \to 2$ initial-final map as is necessary for the single unresolved limits of the four-parton antenna to be removed by iterated three-parton antenna functions. e.g., consider the $i \to 0$ limit,

$$x \to \frac{s_{1j} + s_{1k} + s_{jk}}{s_{1j} + s_{1k}} + \mathcal{O}(p_i), \qquad (2.71)$$

September 24, 2012

which after re-labelling the momenta $\{1, j, k\} \rightarrow \{1, i, j\}$ is the form of the rescaling factor for the $3 \rightarrow 2$ initial-final map. The map acting on the full momentum set can be summarized as,

$$\{p_{n+4}\} \rightarrow \underbrace{\{p_1, p_i, p_j, p_k\}}_{\{p_{\text{antenna}}\}} \cup \underbrace{\{\bar{p}_1, p_I\} \cup \{\{p_{n+4}\} \backslash \{p_1, p_i, p_j, p_k\}\}}_{\{p_{n+2}\}}. \tag{2.72}$$

This re-parameterization of the momenta allows the phase space to be written in a factorized form as a convolution,

$$d\Phi_{n+2}(k_1 \cdots, k_i, k_j, k_k, \cdots, k_{n+2}; p_1, p_2) =$$
$$d\Phi_n(k_1 \cdots, k_I, \cdots, k_n; \bar{p}_1, p_2) d\Phi_3(k_i, k_j, k_k; p_1, q) \frac{Q^2}{2\pi} \frac{dx}{x} \delta(x - \hat{x}). \tag{2.73}$$

The initial-state parton has again been taken to have momentum p_1 and now the momentum $q = p_i + p_j + p_k - p_1$ such that, $Q^2 = -q^2$. The momentum fraction $\hat{x}$ is simply the quantity defined in (2.69).

2.3.3   Initial-initial

When an antenna function contains two initial-state partons the appropriate phase space map rescales both initial-state partons, which are unambiguously identified as the hard radiators. In the case of the initial-final antennae the composite final-state momentum was defined in a way so as to ensure momentum conservation by including the factor $(1 - x)p_{\hat{i}}$. In the case of an initial-initial three-parton antenna there is no composite final-state momentum involved in the antenna to absorb the overall momentum rescaling and so the whole final-state must be remapped to ensure total momentum conservation [20, 36]. The rescaling of the initial state partons is given by the factors,

$$\begin{aligned} p_1 \rightarrow \bar{p}_1 &= x_1 p_1, \\ p_2 \rightarrow \bar{p}_2 &= x_2 p_2. \end{aligned} \tag{2.74}$$

The rescaled momenta form a vector which lies in the beam axis,

$$\tilde{q} = \bar{p}_1 + \bar{p}_2 \tag{2.75}$$

The total momentum of the n-parton subset of momenta (the final-state momenta with one parton removed) is given by $q = p_1 + p_2 - p_i$, where parton i belongs to the antenna subset. The momentum q will in general not lie in the beam axis so the final state must be transformed in order to achieve this. The rescaling of the massless momenta is a Lorentz invariant process so the transformation of the final-state momenta must belong to the Lorentz group also. A rotation to bring q to the beam axis would require singling out either p_1 or p_2 as the direction to rotate towards and make a symmetrical treatment of the two incoming partons difficult to maintain. The remaining transformations which belong to the Lorentz group are boosts, which to map q onto $\tilde{q}$ are required to be boosts in the transverse plane to the beam axis, i.e., $\Lambda(q)q = \tilde{q}$. As q and $\tilde{q}$ are related via a proper Lorentz boost their invariant squares are equal, $q^2 = \tilde{q}^2$, which yields the result,

$$x_1 x_2 = \frac{s_{12} - s_{1i} - s_{2i}}{s_{12}}. \tag{2.76}$$

The beam axis in the centre of mass frame is defined by the vector $B = \bar{p}_1 - \bar{p}_2$. As a Lorentz invariant, the projection of q onto the beam axis in the boosted and un-boosted frames are equal, $B \cdot q = \tilde{B} \cdot \tilde{q}$. Because the boost is transverse to the beam axis $B = \tilde{B}$ so, $B \cdot q = B \cdot \tilde{q}$. Expanding the vectors B, q and $\tilde{q}$ into their constituent momenta yields the relation,

$$(x_1 - x_2) = \frac{x_1 s_{1i} - x_2 s_{2i}}{s_{12}}. \tag{2.77}$$

Simultaneously solving equations (2.76) and (2.77) fixes the form of the rescaling parameters to be,

$$
\begin{aligned}
x_1 &= \left(\frac{(s_{12} - s_{2i})(s_{12} - s_{1i} - s_{2i})}{s_{12}(s_{12} - s_{1i})} \right)^{\frac{1}{2}}, \\
x_2 &= \left(\frac{(s_{12} - s_{1i})(s_{12} - s_{1i} - s_{2i})}{s_{12}(s_{12} - s_{2i})} \right)^{\frac{1}{2}}.
\end{aligned}
\tag{2.78}
$$

To ensure momentum conservation all the final-state momenta are boosted to a set of mapped momenta, not only the ones involved in the antenna,

$$\tilde{k}_i = k_i - \frac{2k_i \cdot (q + \tilde{q})}{(q + \tilde{q})^2}(q + \tilde{q}) + \frac{2k_i \cdot q}{q^2}\tilde{q}. \tag{2.79}$$

In the single soft and collinear limits the mapped momenta tend towards the appropriate resolved momenta,

$$
\begin{aligned}
i \to 0 \;\; &: \;\; \bar{p}_1 \to p_1 & \bar{p}_2 \to p_2 & \quad \tilde{k}_j \to k_j, \\
\hat{1}\|i \;\; &: \;\; \bar{p}_1 \to p_1 - p_i & \bar{p}_2 \to p_2 & \quad \tilde{k}_j \to k_j, \\
\hat{2}\|i \;\; &: \;\; \bar{p}_1 \to p_1 & \bar{p}_2 \to p_2 - p_i & \quad \tilde{k}_j \to k_j,
\end{aligned}
\tag{2.80}
$$

which can be seen by examining the limits of the $x_{1,2}$, q and $\tilde{q}$ parameters in the limits, e.g., In the $\hat{1}\|i$ limit where $p_i = zp_1$, $x_1 \to (1 - z)$, $x_2 \to 1$ and $\tilde{q} \to q$, which implies the limits listed in (2.84). The fact that the mapped momenta tend to the appropriate resolved momenta in all the unresolved limits allows for a smooth interpolation between all single unresolved limits which matches the multiple singular limits of the initial-initial three-parton antenna functions.

The initial-initial map can be summarized by,

$$
\{p_{n+3}\} \to \underbrace{\{p_1, p_i, p_2\}}_{\{p_{\text{antenna}}\}} \cup \underbrace{\{\bar{p}_1, \bar{p}_2\} \cup \{\tilde{k}_n\}}_{\{p_{n+2}\}},
\tag{2.81}
$$

where $\{\tilde{k}_n\}$ is the set of boosted final-state momenta with parton i removed, i.e., $\{\tilde{k}_n\} = \Lambda \cdot [\{p_{n+3}\} \backslash \{p_1, p_i, p_2\}]$. This parameterization of the momenta allows the phase space to be written in factorized form as a double convolution,

$$
\begin{aligned}
\mathrm{d}\Phi_{n+1}(k_1 \cdots, k_i, \cdots, k_{n+1}; p_1, p_2) \;=\; & [\mathrm{d}k_i] \, \frac{\mathrm{d}x_1}{x_1} \, \frac{\mathrm{d}x_2}{x_2} \, \delta(x_1 - \hat{x}_1) \, \delta(x_2 - \hat{x}_2) \\
& \cdot \; x_1 x_2 \, \mathrm{d}\Phi_n(\tilde{k}_1, \cdots, \tilde{k}_n; \bar{p}_1, \bar{p}_2).
\end{aligned}
\tag{2.82}
$$

The single particle phase space of the final-state parton involved in the antenna is denoted $[\mathrm{d}k_i]$ and the quantities $\hat{x}_i$ ensure the initial-state momenta are properly rescaled to conserve momentum and are given by the form of $x_{1,2}$ given in (2.78).

The extension of the initial-initial map to a $4 \to 2$ map is trivial and only requires the redefinition of q to include the extra parton, i.e., for the map, $\{1, i, j, 2\} \to \{\bar{1}, \bar{2}\}$, $q = p_1 + p_2 - p_i - p_j$, such that in this case,

$$
\begin{aligned}
x_1 &= \left(\frac{(s_{12} - s_{2i} - s_{2j})(s_{12} - s_{1i} - s_{1j} - s_{2i} - s_{2j} + s_{ij})}{s_{12}(s_{12} - s_{1i} - s_{1j})} \right)^{\frac{1}{2}}, \\
x_2 &= \left(\frac{(s_{12} - s_{1i} - s_{2j})(s_{12} - s_{1i} - s_{1j} - s_{2i} - s_{2j} + s_{ij})}{s_{12}(s_{12} - s_{2i} - s_{2j})} \right)^{\frac{1}{2}}.
\end{aligned}
\tag{2.83}
$$

The final-state is given by final-state partons, not including partons i and j, boosted in the same way as in the $3 \to 2$ map but using the modified $x_{1,2}$ and q parameters. In the double unresolved limits the rescaled and boosted momenta behave in the following ways,

$$
\begin{array}{llll}
i, j \to 0 & : & \bar{p}_1 \to p_1 & \bar{p}_2 \to p_2 & \tilde{k}_k \to k_k, \\
\hat{1}||i||j & : & \bar{p}_1 \to p_1 - p_i - p_j & \bar{p}_2 \to p_2 & \tilde{k}_k \to k_k, \\
\hat{2}||i||j & : & \bar{p}_1 \to p_1 & \bar{p}_2 \to p_2 - p_i - p_j & \tilde{k}_k \to k_k, \\
\hat{1}||i, \, j \to 0 & : & \bar{p}_1 \to p_1 - p_i & \bar{p}_2 \to p_2 & \tilde{k}_k \to k_k, \\
\hat{2}||j, \, i \to 0 & : & \bar{p}_1 \to p_1 & \bar{p}_2 \to p_2 - p_j & \tilde{k}_k \to k_k, \\
\hat{1}||i, \, \hat{2}||j & : & \bar{p}_1 \to p_1 - p_i & \bar{p}_2 \to p_2 - p_i & \tilde{k}_k \to k_k & (2.84)
\end{array}
$$

As is the case for the final-final and initial-final maps, the $4 \to 2$ initial-initial mapped momenta collapse onto the mapped momenta of the $3 \to 2$ initial-initial map in all single unresolved limits, allowing the single unresolved limits of the four-parton antenna to be removed through an iteration of three-parton antennae.

The result of the momentum map on the whole set of original momenta can be summarized as,

$$
\{p_{n+4}\} \to \underbrace{\{p_1, p_i, p_j, p_2\}}_{\{p_{\text{antenna}}\}} \cup \underbrace{\{\bar{p}_1, \bar{p}_2\} \cup \{\tilde{k}_n\}}_{\{p_{n+2}\}}, \tag{2.85}
$$

where, $\{\tilde{k}_n\} = \Lambda \cdot [\{p_{n+4}\} \backslash \{p_1, p_i, p_j, p_2\}]$. This parameterization leads to the phase space being written again as a double convolution,

$$
\begin{aligned}
d\Phi_{n+2}(k_1 \cdots, k_i, k_j, \cdots, k_{n+2}; p_1, p_2) &= [dk_i] \, [dk_j] \, \frac{dx_1}{x_1} \frac{dx_2}{x_2} \, \delta(x_1 - \hat{x}_1) \, \delta(x_2 - \hat{x}_2) \\
&\cdot \quad x_1 x_2 \, d\Phi_n(\tilde{k}_1, \cdots, \tilde{k}_n; \bar{p}_1, \bar{p}_2).
\end{aligned} \tag{2.86}
$$

2.4 Integrated antenna functions

Whilst it is necessary for the antenna functions to contain the appropriate singular limits and match the phase space factorization in those limits, the whole programme of antenna subtraction would be derailed if the antennae could not themselves be analytically integrated over the antenna phase space. Before discussing the analytic

integration of the antennae, the integrals defining the integrated antennae should be introduced.

In the final-final three-parton case the phase space factorizes into the direct product of the antenna phase space and a reduced mapped phase space. Integrating the final-final antenna over the antenna phase space and introducing factors of,

$$C(\epsilon) = \frac{(4\pi)^\epsilon e^{-\gamma\epsilon}}{8\pi^2},$$ (2.87)

to account for coupling constant renormalization, gives the form for the integrated antenna [32],

$$\mathcal{X}_3^0(s_{ijk}) = \frac{1}{C(\epsilon)} \int d\Phi_{X_{ijk}} \, X_3^0(i,j,k).$$ (2.88)

The extension of this definition to the four-parton final-final antennae is given by integrating the four-parton antennae against the four-parton antenna phase space introduced in (2.58) [32],

$$\mathcal{X}_4^0(s_{ijkl}) = \frac{1}{[C(\epsilon)]^2} \int d\Phi_{X_{ijkl}} \, X_4^0(i,j,k,l).$$ (2.89)

As previously mentioned, the three- and four-parton final-final antenna phase spaces are proportional to the three- and four-particle phase spaces.

It is important to note that in the case of the four-parton final-final antennae it is sometimes necessary to decompose the antenna into sub-antennae in order to match onto the kinematics of the phase space map. The partial fractioning involved in decomposing the antenna renders the analytic integration of a four-parton sub-antenna highly non-trivial. In order to avoid such integrals the decomposition is performed whilst ensuring that the sum of sub-antennae employed always generates a full four-parton antenna. In this way the full antenna is decomposed appropriately for the numerical implementation of the subtraction process, whilst only requiring that the full four-parton antenna be integrated analytically [114].

In the case of initial-final antenna functions the antenna is related to the final-final antenna by crossing but the phase space factorization is modified. Taking this modification into account, the integrated initial-final antenna function is defined as [36],

$$\mathcal{X}_3^0(s_{1ij}; x_1) = \frac{1}{C(\epsilon)} \int d\Phi_2 \, \frac{Q^2}{2\pi} \, \delta(x_1 - \hat{x}_1) \, X_{3,a}^0(\hat{1}, i, j),$$ (2.90)

where $\hat{x}_1$ is the parameter derived in (2.64) and a denotes the type of particle in the initial-state, i.e., quark or gluon. Extending the definition to the four-parton initial-final antenna gives [111],

$$\mathcal{X}_4^0(s_{1ijk}; x_1) \;\; = \;\; \frac{1}{[C(\epsilon)]^2} \int d\Phi_3 \; \frac{Q^2}{2\pi} \; \delta(x_1 - \hat{x}_1) \; X_{4,a}^0(\hat{1}, i, j, k). \qquad (2.91)$$

The initial-initial antenna functions are integrated over the appropriate phase space to give the integrated initial-initial antenna functions [36],

$$\mathcal{X}_3^0(s_{1i2}; x_1, x_2) \;\; = \;\; \frac{1}{C(\epsilon)} \int [dk_i] \; x_1 x_2 \; \delta(x_1 - \hat{x}_1) \; \delta(x_2 - \hat{x}_2) \; X_{3,ab}^0(\hat{1}, i, \hat{2}),$$
$$(2.92)$$

where a, b denote the types of particle in the initial-state. This definition can be extended to the four-parton initial-initial antennae [113],

$$\mathcal{X}_4^0(s_{1ij2}; x_1, x_2) \;\; = \;\; \frac{1}{[C(\epsilon)]^2} \int [dk_i] \; [dk_i] \; x_1 x_2 \; \delta(x_1 - \hat{x}_1) \; \delta(x_2 - \hat{x}_2) \; X_{4,ab}^0(\hat{1}, i, j, \hat{2}).$$
$$(2.93)$$

The explicit evaluation of integrated antenna functions has received much attention in the last several years and all three- and four-parton antennae relevant for NNLO calculations are now known. The integration relies on rewriting the phase space integral in terms of cut multi-loop diagrams which are then reduced to a set of scalar master integrals by using Integration-By-Parts (IBP) relations [119] amongst other multi-loop tools; the details of which can be found in the literature [111, 113, 120].

2.5 Antenna subtraction at NLO

The field of NLO QCD calculations has advanced significantly in the last decade or so, including the automation of one-loop calculations [121–124] and automated programs for evaluating the phase space integrals of the real emission contribution [20]. The extent of this progress is that for a relatively low number of external legs, NLO massless QCD calculations are now mainly useful as toy calculations to demonstrate a more general method. In this section the antenna subtraction method for NLO calculations will be presented in generality such that its application to the specific calculations of chapters 3, 4 and 5 is clear.

2.5.1 Construction of the real emission subtraction term

The primary goal of any subtraction procedure is to construct a subtraction term, $d\hat{\sigma}$ which absorbs all IR divergence of the cross section without introducing spurious divergence of its own, i.e., the following difference is rendered finite across the entire phase space,

$$\int_{\Phi_{n+1}} \left[d\hat{\sigma}_{ij}^R - d\hat{\sigma}_{ij,NLO}^S \right], \tag{2.94}$$

where $d\hat{\sigma}_{ij}^R$ is the $(n+1)$-parton real correction to an n-parton Born-level process. The real emission takes the form,

$$
\begin{aligned}
d\hat{\sigma}_{ij}^R &= \mathcal{N}_{NLO}^R \frac{\bar{C}(\epsilon)}{C(\epsilon)} d\Phi_{n+1}(k_1, \cdots, k_{n+1}; p_1, p_2) \\
&\times |\mathcal{M}(k_1, \cdots, k_{n+1}; p_1, p_2)|^2 J_n^{(n+1)}(k_1, \cdots, k_n),
\end{aligned}
\tag{2.95}
$$

where $\bar{C}(\epsilon) = 8\pi^2 C(\epsilon)$. The factor $\mathcal{N}$ will in general contain all non-QCD factors and some overall QCD factors such as the overall power of the coupling. The jet finding algorithm, or jet function, is given by $J_n^{(m)}$ which has the interpretation of the function which builds n jets from m partons. Following the discussion in section 1.1.2, the squared matrix element can be decomposed into its various colour structures and the associated colour factor factorized from the squared partial amplitudes. At leading-colour the colour decomposition allows the cross section to be written in the form,

$$
\begin{aligned}
d\hat{\sigma}_{ij}^R &= \mathcal{N}_{NLO}^R N^p \frac{\bar{C}(\epsilon)}{C(\epsilon)} \sum_\sigma d\Phi_{n+1}(k_1, \cdots, k_{n+1}; p_1, p_2) \frac{1}{S_{n+1}} \\
&\times M_{n+1}^0(\sigma(1, \cdots, n+1)) J_n^{(n+1)}(k_1, \cdots, k_n) + \mathcal{O}(1/N^2),
\end{aligned}
\tag{2.96}
$$

where p is the leading power of N and σ denotes permutations of final state partons contributing to the leading-colour cross section.

The sub-leading colour contribution cannot in general be written in this form as an incoherent sum of squared partial amplitudes; however for low multiplicity final-states the sub-leading colour contribution, the square of a coherent sum of QCD partial amplitudes, can often be re-written as an incoherent sum of squared partial amplitudes where a number of gluons behave in an Abelian fashion. In these cases

the squared $U(1) \otimes SU(3)$ partial amplitudes are well suited to antenna subtraction as their IR divergent limits can be understood via matrix element factorization patterns similar to those for pure QCD matrix elements.

Matrix elements containing one Abelian gluon, sometimes called a photon[1], obey the usual QCD factorization formulae in all the unresolved limits of the non-Abelian gluons. The Abelian gluons do not couple to the non-Abelian gluons and only couple to quarks; furthermore they can only be considered colour-connected to the quarks. In this way a subleading colour matrix element can be considered to contain two colour structures: a pure QCD colour structure formed from all quarks and non-Abelian gluons, the factorization properties of which are identical to those of leading colour squared matrix elements, and a QED-like colour structure containing quark pairs and colour dis-connected photons [108]. For example, a matrix element with two-quarks, n-non Abelian gluons and one Abelian gluon, $\tilde{i}$, is denoted $M_{n+3}^0(q, g_1, \cdots, \tilde{g}_i, \cdots, g_n, \bar{q})$ and schematically has the colour structure,

$$(q, 1, \cdots, n, \bar{q}; \tilde{i}) \quad \sim \quad (q, 1, \cdots, n, \bar{q}) \otimes (q, \tilde{i}, \bar{q}). \tag{2.97}$$

The Abelian gluon can have collinear limits with the quarks and also become soft,

$$M_{n+3}^0(q, g_1, \cdots, \tilde{g}_i, \cdots, g_n, \bar{q}) \xrightarrow{i \| q} \frac{1}{s_{qi}} P_{qg \to Q}(z) \, M_{n+2}^0(Q, g_1, \cdots, g_n, \bar{q}),$$

$$M_{n+3}^0(q, g_1, \cdots, \tilde{g}_i, \cdots, g_n, \bar{q}) \xrightarrow{i \to 0} S_{qi\bar{q}} \, M_{n+2}^0(q, g_1, \cdots, g_n, \bar{q}), \tag{2.98}$$

where the collinear limit with the anti-quark is given by exchanging $q \leftrightarrow \bar{q}$. If the subleading colour matrix elements can be re-written in terms of squared matrix elements involving Abelian gluons then the IR divergent limits can be subtracted using antenna functions in an identical fashion to the process at leading colour. Even if the subleading colour contribution cannot be written purely in terms of squared matrix elements with Abelian gluons, as long as the IR divergent limits of the subleading colour matrix elements can be written in terms of the universal singular

---

[1] The term photon is useful as the Abelian gluon behaves in the same way as a photon in the context of QCD i.e., only coupling to quarks, albeit with a rescaled coupling strength compared to the one in QED. The analogy does not extend beyond QCD, e.g., an Abelian gluon does not couple to a W^+ boson.

functions then antenna subtraction can be readily applied. Notwithstanding these complications, the subleading colour contributions will in general contain fewer and less intricate divergent limits than their leading colour counterparts. Furthermore any IR finite contribution to the cross section requires no subtraction and is integrated numerically. The remainder of this section will focus on the leading colour contribution for clarity but it is clear that a similar treatment can be reproduced for subleading colour contributions given the discussion above.

A leading colour contribution to the cross section can be written in the form,

$$
\begin{aligned}
\mathrm{d}\hat{\sigma}_{ij}^R &= \mathcal{N}_{NLO}^R \; N^p \; \frac{\bar{C}(\epsilon)}{C(\epsilon)} \sum_{\mathrm{perms}} \mathrm{d}\Phi_{n+1}(k_1, \cdots, k_{n+1}; p_1, p_2) \frac{1}{S_{n+1}} \\
&\times \; M_{n+1}^0(1, \cdots, n+1) \; J_n^{(n+1)}(k_1, \cdots, k_{n+1}).
\end{aligned} \tag{2.99}
$$

To construct the subtraction term for this contribution the single unresolved limits of the matrix element are considered, where parton j is taken to be the unresolved parton. To reflect the antenna factorization of the squared matrix element, a subtraction term is constructed. When the unresolved parton j has final-state colour connected neighbours, i and k the subtraction term takes the form,

$$
\begin{aligned}
\mathrm{d}\hat{\sigma}_{NLO}^{S,ff} &= \mathcal{N}_{NLO}^R \; N^p \; \frac{\bar{C}(\epsilon)}{C(\epsilon)} \sum_{\mathrm{perms}} \sum_j \mathrm{d}\Phi_{n+1}(k_1, \cdots, k_{n+1}; p_1, p_2) \frac{1}{S_{n+1}} \\
&\times \; X_3^0(i,j,k) \; M_n^0(1, \cdots, I, K, \cdots, n+1) \; J_n^{(n)}(k_1, \cdots, k_I, k_K, \cdots, k_{n+1}).
\end{aligned} \tag{2.100}
$$

The sum over j takes into account all the possible unresolved partons in the colour-ordered matrix element fitting the final-final configuration. The final-final phase space map has been used to ensure the momenta involved in the antenna function are mapped down onto two composite momenta which feed into the reduced matrix element and the jet function. The IR divergence associated with the configuration where j becomes unresolved is mimicked by the appropriate antenna function and, in the singular limit, the subtraction term tends to the value of the real emission cross section.

For hadron-hadron collisions there are two partons in the initial state which have colour connected final-state neighbours that can become unresolved. In these configurations an initial-final antenna is necessary and the initial-final phase space

map is employed to generate the composite momenta for the reduced matrix element and jets function,

$$
\begin{aligned}
\mathrm{d}\hat{\sigma}_{NLO}^{S,if} \;=\;& \mathcal{N}_{NLO}^{R}\, N^p\, \frac{\bar{C}(\epsilon)}{C(\epsilon)} \sum_{\mathrm{perms}} \sum_{j} \sum_{\hat{i}\in\{1,2\}} \mathrm{d}\Phi_{n+1}(k_1,\cdots,k_{n+1};p_1,p_2)\, \frac{1}{S_{n+1}} \\
& \times\; X_{3,a}^0(\hat{i},j,k)\, M_n^0(\hat{\bar{i}},J,\cdots,n+1)\, J_n^{(n)}(k_1,\cdots,k_J,\cdots,k_{n+1}),
\end{aligned}
$$
(2.101)

where the sum over j denotes all final-state partons which are colour connected to an initial-state parton $\hat{i}$, the sum over $\hat{i}$ runs over both initial-state partons and a is the particle type of the initial state parton.

The final configuration which is allowed for hadron-hadron collision is the initial-initial configuration where an unresolved parton is emitted between two initial-state partons. The subtraction term used initial-initial antenna functions and the initial-initial phase space map and is given by,

$$
\begin{aligned}
\mathrm{d}\hat{\sigma}_{NLO}^{S,ii} \;=\;& \mathcal{N}_{NLO}^{R}\, N^p\, \frac{\bar{C}(\epsilon)}{C(\epsilon)} \sum_{\mathrm{perms}} \sum_{j} \mathrm{d}\Phi_{n+1}(k_1,\cdots,k_{n+1};p_1,p_2)\, \frac{1}{S_{n+1}} \\
& \times\; X_{3,ab}^0(\hat{i},j,\hat{k})\, M_n^0(\hat{\bar{i}},\hat{\bar{k}},\cdots,\widetilde{(n+1)})\, J_n^{(n)}(\tilde{k}_1,\cdots,\tilde{k}_{n+1}),
\end{aligned}
$$
(2.102)

where a and b denote the particle type of each incoming parton.

The full subtraction term is a sum of all three contributions,

$$
\mathrm{d}\hat{\sigma}_{ij,NLO}^{S} \;=\; \mathrm{d}\hat{\sigma}_{NLO}^{S,ff} + \mathrm{d}\hat{\sigma}_{NLO}^{S,if} + \mathrm{d}\hat{\sigma}_{NLO}^{S,ii},
$$
(2.103)

such that for DIS $\mathrm{d}\hat{\sigma}_{NLO}^{S,ii} = 0$ and for e^+e^- annihilation $\mathrm{d}\hat{\sigma}_{NLO}^{S,if} = \mathrm{d}\hat{\sigma}_{NLO}^{S,ii} = 0$. At NLO it is possible to write the subtraction terms explicitly for all configurations and for an arbitrary number of partons.

Final-state gluon string

For a string of final-state gluons the subtraction terms is given by a sum over final-final gluonic sub-antennae and their associated reduced matrix elements. For an gluon string containing l gluons in a matrix element,

$$
M_n^0(\cdots,i_1,i_2,i_3,i_4,\cdots,i_i,i_j,i_k,i_l,\cdots),
$$
(2.104)

the subtraction term is given by,

$$
\begin{aligned}
\mathrm{d}\hat{\sigma}_{NLO}^{S,ff,g_1\cdots g_l} \;=\;\; & \mathcal{N}_{NLO}^R \, N^p \, \frac{\bar{C}(\epsilon)}{C(\epsilon)} \sum_{\mathrm{perms}} \mathrm{d}\Phi_{n+1}(k_1,\cdots,k_n;p_1,p_2) \, \frac{1}{S_{n+1}} \Bigg\{ \\[4pt]
& f_3^0(i_1,i_2,i_3) \, M_n^0(\cdots,\widetilde{(i_1 i_2)},\widetilde{(i_2 i_3)},i_4,\cdots,i_i,i_j,i_k,i_l,\cdots) \\[4pt]
& \qquad J_n^{(n)}(k_1,\cdots,k_{(i_1 i_2)},k_{(i_2 i_3)},\cdots,k_n) \\[4pt]
+\;\; & f_3^0(i_2,i_3,i_4) \, M_n^0(\cdots,i_1,\widetilde{(i_2 i_3)},\widetilde{(i_3 i_4)},\cdots,i_i,i_j,i_k,i_l,\cdots) \\[4pt]
& \qquad J_n^{(n)}(k_1,\cdots,k_{(i_2 i_3)},k_{(i_3 i_4)},\cdots,k_n) \\[4pt]
+\;\; & \\[2pt]
& \vdots \\[4pt]
+\;\; & f_3^0(i_i,i_j,i_k) \, M_n^0(\cdots,i_1,i_2,i_3,i_4,\cdots,\widetilde{(i_i i_j)},\widetilde{(i_j i_k)},i_l,\cdots) \\[4pt]
& \qquad J_n^{(n)}(k_1,\cdots,k_{(i_i i_j)},k_{(i_j i_k)},\cdots,k_n) \\[4pt]
+\;\; & f_3^0(i_j,i_k,i_l) \, M_n^0(\cdots,i_1,i_2,i_3,i_4,\cdots,i_i\widetilde{(i_j i_k)},\widetilde{(i_k i_l)},\cdots) \\[4pt]
& \qquad J_n^{(n)}(k_1,\cdots,k_{(i_j i_k)},k_{(i_k i_l)},\cdots,k_n) \Bigg\}.
\end{aligned}
\tag{2.105}
$$

The subtraction term reproduces all single unresolved limits of the gluons in the string except at the ends where the $i_1||i_2$ and $i_k||i_l$ limits are not fully reproduced and the $i_1 \to 0$, $i_l \to 0$ soft limits are absent entirely. In the case of a purely gluonic matrix element the end partons are colour connected due to the colour structure being a trace over all gluons and so the gluon endpoints overlap and all singularities are accounted for. In the case of matrix elements containing quark strings the subtraction terms associated with the quark endpoints will contain the missing soft divergence and share the missing collinear divergence.

Final-state quark string

Introducing quarks alters the available colour structures and thus the colour ordering of the partial amplitudes. In general the colour ordering is made up from strings of quarks with quark endpoints and gluons populating the string. The divergence of the gluon string is subtracted using the subtraction term (2.105) so the only additional limits to take into account are those involving the quark endpoints. For the matrix element containing a quark endpoint,

$$
M_n^0(\cdots;q,i_1,i_2,\cdots,),
\tag{2.106}
$$

the subtraction term is given by,

$$
\begin{aligned}
\mathrm{d}\hat{\sigma}_{NLO}^{S,ff,qg_{i_1}g_{i_2}} = \ & \mathcal{N}_{NLO}^{R} \, N^p \, \frac{\bar{C}(\epsilon)}{C(\epsilon)} \sum_{\text{perms}} \mathrm{d}\Phi_{n+1}(k_1, \cdots, k_n; p_1, p_2) \, \frac{1}{S_{n+1}} \Bigg\{ \\
& d_3^0(q, i_1, i_2) \, M_n^0(\cdots; \widetilde{(qi_1)}, \widetilde{(i_1 i_2)}, \cdots) \\
& J_n^{(n)}(k_1, \cdots, k_{\widetilde{(qi_1)}}, k_{\widetilde{(i_1 i_2)}}, \cdots, k_n) \Bigg\},
\end{aligned}
\tag{2.107}
$$

where a similar formula is obtained for an anti-quark endpoint by substituting $q \leftrightarrow \bar{q}$. This formula correctly subtracts the collinear limits involving the quark with neighbouring gluons as well as the $i_1 \to 0$ soft limit and remaining $i_1 || i_2$ collinear limit not properly accounted for by the gluon string subtraction term.

If only one gluon is present between a quark-antiquark pair then instead of a gluon string of f_3^0 functions bookended by two quark d_3^0 functions, an A_3^0 antenna is used as this matches onto the particle content exactly,

$$
\begin{aligned}
\mathrm{d}\hat{\sigma}_{NLO}^{S,ff,qg_i\bar{q}} = \ & \mathcal{N}_{NLO}^{R} \, N^p \, \frac{\bar{C}(\epsilon)}{C(\epsilon)} \sum_{\text{perms}} \mathrm{d}\Phi_{n+1}(k_1, \cdots, k_n; p_1, p_2) \, \frac{1}{S_{n+1}} \Bigg\{ \\
& A_3^0(q, i, \bar{q}) \, M_n^0(\cdots; \widetilde{(qi)}, \widetilde{(i\bar{q})}; \cdots) \\
& J_n^{(n)}(k_1, \cdots, k_{\widetilde{(qi)}}, k_{\widetilde{(i\bar{q})}}, \cdots, k_n) \Bigg\},
\end{aligned}
\tag{2.108}
$$

If a quark is colour adjacent to a like-flavoured anti-quark in the colour ordering then the additional $q || \bar{q} \to g$ splitting has to be taken into account. This limit not only changes the total number of partons in the final state but also changes the type of matrix element, reducing the number of quarks by two. If the collinear quark-antiquark pair is adjacent to a spectator gluon then the subtraction term is given by,

$$
\begin{aligned}
\mathrm{d}\hat{\sigma}_{NLO}^{S,ff,q\bar{q}} = \ & \mathcal{N}_{NLO}^{R} \, N^p \, \frac{\bar{C}(\epsilon)}{C(\epsilon)} \sum_{\text{perms}} \mathrm{d}\Phi_{n+1}(k_1, \cdots, k_n; p_1, p_2) \, \frac{1}{S_{n+1}} \Bigg\{ \\
& G_3^0(g, q, \bar{q}) \, M_n^0(\cdots; \widetilde{(gq)}, \widetilde{(q\bar{q})}, \cdots) \\
& J_n^{(n)}(k_1, \cdots, k_{\widetilde{(gq)}}, k_{\widetilde{(q\bar{q})}}, \cdots, k_n) \Bigg\}.
\end{aligned}
\tag{2.109}
$$

In the original matrix element the number of fermions is f whereas in the reduced matrix element it is $f' = f - 2$. If the collinear quark-anti-quark pair is adjacent to another quark then the subtraction term is given by,

$$
\mathrm{d}\hat{\sigma}_{NLO}^{S,ff,q\bar{q}} = \mathcal{N}_{NLO}^{R} \, N^p \, \frac{\bar{C}(\epsilon)}{C(\epsilon)} \sum_{\text{perms}} \mathrm{d}\Phi_{n+1}(k_1, \cdots, k_n; p_1, p_2) \, \frac{1}{S_{n+1}} \Bigg\{
$$

$$E_3^0(q', q, \bar{q}) \ M_n^0(\cdots ; \widetilde{(q'q)}, \widetilde{(q\bar{q})}, \cdots)$$
$$J_n^{(n)}(k_1, \cdots, k_{\widetilde{(q'q)}}, k_{\widetilde{(q\bar{q})}}, \cdots, k_n) \Bigg\}. \tag{2.110}$$

where again $f' = f - 2$. In terms of subtracting the divergence it does not matter in practice whether the E_3^0 or G_3^0 antenna is used as they differ only by IR finite terms.

A general subtraction term can be constructed by matching the matrix element's colour structure by gluing together the appropriate subtraction terms. For example consider the NLO subtraction term for the colour ordered matrix element,

$$M_8^0(q_1, g_i, g_j, g_k, \bar{q}_2; Q_3, \bar{Q}_4). \tag{2.111}$$

The subtraction term is given by,

$$\mathrm{d}\hat{\sigma}_{NLO}^S \quad = \quad \mathrm{d}\hat{\sigma}_{NLO}^{S,ff,qg_ig_j} + \mathrm{d}\hat{\sigma}_{NLO}^{S,ff,g_i\cdots g_k} + \mathrm{d}\hat{\sigma}_{NLO}^{S,ff,\bar{q}g_kg_j} + \mathrm{d}\hat{\sigma}_{NLO}^{S,ff,Q\bar{Q}}. \tag{2.112}$$

Initial-final gluon string

When dealing with a gluon string with one gluon crossed into the initial state the initial-final gluonic sub-antenna is used, along with the initial-final phase space map. Consider the matrix element,

$$M_n^0(\cdots, i, j, \hat{1}, k, l, \cdots), \tag{2.113}$$

The divergence of the rest of the gluon string (all gluons not including the initial-state gluon or its neighbours) is subtracted by the two final-state gluon string subtraction terms either side of the initial-state gluon. The initial-final subtraction term is given by,

$$\mathrm{d}\hat{\sigma}_{NLO}^{S,if,g_ig_j\hat{g}_1g_kg_l} \quad = \quad \mathcal{N}_{NLO}^R \ N^p \ \frac{\bar{C}(\epsilon)}{C(\epsilon)} \sum_{\mathrm{perms}} \mathrm{d}\Phi_{n+1}(k_1, \cdots, k_n; p_1, p_2) \ \frac{1}{S_{n+1}} \Bigg\{$$
$$f_3^0(\hat{1}, j, i) \ M_n^0(\cdots, \widetilde{(ij)}\hat{1}, k, l, \cdots) \ J_n^{(n)}(k_1, \cdots, k_{\widetilde{(ij)}}, \cdots, k_n)$$
$$+ \quad f_3^0(\hat{1}, k, l) \ M_n^0(\cdots, i, j, \hat{\bar{1}}, \widetilde{(kl)}, \cdots) \ J_n^{(n)}(k_1, \cdots, k_{\widetilde{(kl)}}, \cdots, k_n) \Bigg\}. \tag{2.114}$$

This subtraction term correctly subtracts the $j \to 0$, $k \to 0$ soft limits, as well as the $j||\hat{1}$, $k||\hat{1}$ collinear limits. The $i \to 0$, $l \to 0$ are completely contained in

the gluon string subtraction terms which are glued to this subtraction term when constructing the full subtraction term. Similarly the $i||j$, $k||l$ collinear limits are shared between this subtraction term and the neighbouring subtraction terms.

Initial-final quark string: Quark initiated

When the end of a quark string is in the initial state, i.e., an incoming quark, the initial-final d_3^0 sub-antenna is used, along with the initial-final momentum map to generate the subtraction term,

$$
\begin{aligned}
\mathrm{d}\hat{\sigma}_{NLO}^{S,if,\hat{q}g_{i_1}g_{i_2}} \;=\;& \mathcal{N}_{NLO}^R \, N^p \, \frac{\bar{C}(\epsilon)}{C(\epsilon)} \sum_{\mathrm{perms}} \mathrm{d}\Phi_{n+1}(k_1,\cdots,k_n;p_1,p_2) \, \frac{1}{S_{n+1}} \\
&\times \; d_3^0(\hat{q},i_1,i_2) \, M_n^0(\cdots;\hat{\bar{q}},\widetilde{(i_1 i_2)},\cdots) \, J_n^{(n)}(k_1,\cdots,k_{\widetilde{(i_1 i_2)}},\cdots,k_n).
\end{aligned}
$$

$$(2.115)$$

This subtraction term contains the full $i_1 \to 0$ soft limit, the full $q||i_1$ collinear limit and part of the $i_1||i_2$ collinear limit which is shared with the neighbouring string's subtraction term to form the full limit. The same partons are able to go soft and collinear in the initial-final d_3^0 antenna as in the final-final d_3^0 antenna and the function is obtained by crossing the quark from the final-final antenna into the initial state.

When only one gluon populates the quark string the initial-final A_3^0 antenna is used to capture the whole string's IR behaviour,

$$
\begin{aligned}
\mathrm{d}\hat{\sigma}_{NLO}^{S,if,\hat{q}g_i\bar{q}} \;=\;& \mathcal{N}_{NLO}^R \, N^p \, \frac{\bar{C}(\epsilon)}{C(\epsilon)} \sum_{\mathrm{perms}} \mathrm{d}\Phi_{n+1}(k_1,\cdots,k_n;p_1,p_2) \, \frac{1}{S_{n+1}} \\
&\times \; A_3^0(\hat{q},i,\bar{q}) \, M_n^0(\cdots;\hat{\bar{q}},\widetilde{(i\bar{q})};\cdots) \, J_n^{(n)}(k_1,\cdots,k_{\widetilde{(i\bar{q})}},\cdots,k_n).
\end{aligned}
$$

$$(2.116)$$

Initial-final quark string: Gluon initiated

The configuration where gluons are crossed into the initial state introduces a new problem which is generic and present in both NLO and NNLO calculations. When an initial-state gluon becomes collinear with a final-state gluon the resulting reduced matrix element contains an initial-state gluon with rescaled momentum. However

when an initial-state gluon becomes collinear with a final-state quark the resulting reduced matrix element contains an initial-state quark with rescaled momentum. One issue for consideration here is which PDF should be attached to the subtraction term. The original matrix element is associated with a gluon PDF whereas the reduced matrix element will be more naturally associated with a quark PDF. If the subtraction is to be successful then it is clear that both terms have to be convoluted with the same PDF, in this case the gluon PDF. Otherwise even if the subtraction term tends to the matrix element in the unresolved limit, the subtraction will be incomplete if both terms are scaled relative to one another by different PDFs.

The main problem in this configuration comes from the gluon initiated D_3^0 antenna. This antenna contains a soft gluon limit for the final-state gluon, a final-final quark-gluon limit, an initial-final gluon-gluon limit and an initial-final quark-gluon limit. The first three of these limits cause the matrix element to collapse onto a reduced matrix element with an initial-state gluon. The last limit, the initial-final quark-gluon limit, causes the matrix element to collapse onto a reduced matrix element containing an initial state quark. The problem arises from the D_3^0 antenna containing all of these limits but the reduced matrix element it is associated with has to have either a quark or a gluon in the initial state with no smooth interpolation between the two functions, unlike the smooth interpolation for the momentum in the different limits.

One solution to this problem is to partition the full D_3^0 antenna into two sub-antennae to isolate the initial-final quark-gluon limit. This was achieved by partial fractioning in [36], yielding,

$$
\begin{aligned}
D_3^0(i_q, \hat{1}_g, j_g) &= d_3^0(i_q, \hat{1}_g; j_g) + d_3^0(i_q, j_g, \hat{1}_g), \\
d_3^0(i_q, \hat{1}_g; j_g) &= \frac{1}{s_{1ij}^2}\left(\frac{2s_{1ij}^2 s_{ij}}{(s_{1i}+s_{1j})s_{1i}} + \frac{s_{ij}s_{1j} + s_{1j}^2}{s_{1i}}\right), \\
d_3^0(i_q, j_g, \hat{1}_g) &= \frac{1}{s_{1ij}^2}\left(\frac{2s_{1ij}^2 s_{ij}}{(s_{1i}+s_{1j})s_{1j}} + \frac{2s_{1ij}^2 s_{1i}}{s_{ij}s_{1j}}\right. \\
&\qquad \left. + \frac{s_{1i}s_{1j} + s_{1j}^2}{s_{ij}} + \frac{2s_{1i}s_{ij}}{s_{1j}} + 5s_{1ij} + s_{ij}\right). \quad (2.117)
\end{aligned}
$$

From these expressions for the sub-antennae it is clear that the antenna $d_3^0(q, \hat{g}; g)$ contains all the $i_q || \hat{1}_g$ collinear limit whilst the $d_3^0(q, g, \hat{g})$ sub-antenna contains the

soft gluon limit, the initial-final gluon-gluon collinear limit and the final-final quark-gluon collinear limit. Using these sub-antennae with the appropriate reduced matrix elements yields the subtraction term for configuration when the quark is adjacent to the initial-state gluon,

$$
\begin{aligned}
\mathrm{d}\hat{\sigma}_{NLO}^{S,if,q_i \hat{g}_1 g_j} \quad = \quad & \mathcal{N}_{NLO}^R \; N^p \; \frac{\bar{C}(\epsilon)}{C(\epsilon)} \sum_{\text{perms}} \mathrm{d}\Phi_{n+1}(k_1, \cdots, k_n; p_1, p_2) \; \frac{1}{S_{n+1}} \\
& d_3^0(i_q, \hat{1}_g; j_g) \; M_n^0(\cdots; \hat{\tilde{1}}_q, \widetilde{(ij)}_g, \cdots) \; J_n^{(n)}(k_1, \cdots, k_{\widetilde{(ij)}}, \cdots, k_n).
\end{aligned}
$$

(2.118)

This subtraction term will properly subtract the $i_q || \hat{1}_g$ collinear limit. The j_g soft and $\hat{1}_g || j_q$ collinear limits are removed by the subtraction term for the initial-final gluon string neighbouring this configuration. If the initial state gluon is separated from the quark by a single final-state gluon then the other sub-antenna is employed,

$$
\begin{aligned}
\mathrm{d}\hat{\sigma}_{NLO}^{S,if,q_i g_j \hat{g}_1} \quad = \quad & \mathcal{N}_{NLO}^R \; N^p \; \frac{\bar{C}(\epsilon)}{C(\epsilon)} \sum_{\text{perms}} \mathrm{d}\Phi_{n+1}(k_1, \cdots, k_n; p_1, p_2) \; \frac{1}{S_{n+1}} \\
& d_3^0(i_q, j_g, \hat{1}_g) \; M_n^0(\cdots; \widetilde{(ij)}_q, \hat{\tilde{1}}_g, \cdots) \; J_n^{(n)}(k_1, \cdots, k_{\widetilde{(ij)}}, \cdots, k_n),
\end{aligned}
$$

(2.119)

which properly subtracts the j_g soft, $i_q || j_g$ and $j_g || \hat{1}_g$ limits.

An alternative strategy is to use the full D_3^0 antenna for the subtraction. This will not capture all collinear limits and will possess some spurious limits however these are both corrected for by using an initial-initial A_3^0 antenna. Consider the configuration in which the quark and the initial-state gluon are separated by a single final-state gluon. The term,

$$
D_3^0(i_q, j_g, \hat{1}_g) \; M_n^0(\cdots; \widetilde{(ij)}_q \hat{\tilde{1}}_g, \cdots),
$$

(2.120)

will correctly subtract the j_g soft, $i_q || j_g$ collinear and $j_g || \hat{1}_g$ collinear limits. However in the limit $i_q || \hat{1}_g$ the antenna function is divergent whereas the colour ordered matrix element is finite because i_q and $\hat{1}_g$ are not colour connected. To correct for this over-subtraction a new term can be introduced,

$$
A_3^0(i_q, \hat{1}_g, \hat{2}) \; M_n^0(\cdots; \tilde{j}_q \hat{\tilde{1}}_g, \cdots).
$$

(2.121)

This term uses an initial-initial antenna function and an initial-initial momentum map. Examining the singular limits of the antenna it is clear that the only IR divergent limit is,

$$A_3^0(i_q, \hat{1}_g, \hat{2}) \xrightarrow{i_q || \hat{1}_g} \frac{1}{s_{1i}} P_{qg \leftarrow Q}(z). \tag{2.122}$$

The A_3^0 antenna usually has the gluon-anti-quark collinear limit as well but in this case because the initial-state partons are essentially constants they can never become soft or collinear with one another so inverse powers of s_{12} are not dangerous when it comes to the phase space integral. In principle the parton entering the rightmost argument of the A_3^0 antenna should be a quark but in practice the parton identity of parton 2 is irrelevant for the subtraction as it is not involved in the singular limits and only affects the subtraction term through the initial-initial map. The only configuration in which this term contributes is the $i_q || \hat{1}_g$ limit and in that limit the mapped momenta used for the reduced matrix elements in (2.120) and (2.121) tend to the same values such that the second parton used for the antenna is a benign spectator. The subtraction term for the configuration under consideration is then,

$$
\begin{aligned}
\mathrm{d}\hat{\sigma}_{NLO}^{S,if,q_i g_j \hat{g}_1} \;=\;& \mathcal{N}_{NLO}^R \, N^p \, \frac{\bar{C}(\epsilon)}{C(\epsilon)} \sum_{\text{perms}} \mathrm{d}\Phi_{n+1}(k_1, \cdots, k_n; p_1, p_2) \, \frac{1}{S_{n+1}} \Bigg\{ \\
& D_3^0(i_q, j_g, \hat{1}_g) \, M_n^0(\cdots; \widetilde{(ij)}_q \hat{\tilde{1}}_g, \cdots) \, J_n^{(n)}(k_1, \cdots, k_{\widetilde{(ij)}}, \cdots, k_n) \\
& - \; A_3^0(i_q, \hat{1}_g, \hat{2}) \, M_n^0(\cdots; \tilde{j}_q \hat{\tilde{1}}_g, \cdots) \, J_n^{(n)}(\tilde{k}_1, \cdots, \tilde{k}_n) \Bigg\}. \tag{2.123}
\end{aligned}
$$

The reduced matrix element attached to the A_3^0 term at first appears to have incorrect arguments, as in the $i_q || \hat{1}_g$ limit it would be expected that the reduced matrix element would inherit an initial-state quark. However this subtraction term is in fact removing a spurious limit of the D_3^0 subtraction term. The arguments of the reduced matrix element for that subtraction term term make no sense in the $i_q || \hat{1}_g$ limit so it is not surprising that the reduced matrix element for the A_3^0 term does not follow the usual pattern of factorization.

The configuration where the initial-state gluon is adjacent to the quark is subtracted using the initial-initial A_3^0 antenna, as this contains exactly the limit necessary without introducing any spurious limits. The difference in this case compared to its previous use is that now the arguments of the reduced matrix element follow

the usual factorization pattern as they have to mimic the physical matrix element rather than an unphysical spurious limit of an artificial subtraction term,

$$
\begin{aligned}
\mathrm{d}\hat{\sigma}_{NLO}^{S,if,q_i\hat{g}_1g_j} \;=\; & \mathcal{N}_{NLO}^R \, N^p \, \frac{\bar{C}(\epsilon)}{C(\epsilon)} \sum_{\text{perms}} \mathrm{d}\Phi_{n+1}(k_1,\cdots,k_n;p_1,p_2) \, \frac{1}{S_{n+1}} \\
& A_3^0(i_q,\hat{1}_g;\hat{2}) \, M_n^0(\cdots;\hat{\tilde{1}}_q,\cdots,\hat{\tilde{2}},\cdots) \, J_n^{(n)}(\tilde{k}_1,\cdots,\tilde{k}_n).
\end{aligned}
$$

(2.124)

Both methods described here, the decomposition into sub-antennae and the combination of full D_3^0 and A_3^0 antennae, succeed in properly subtracting the IR divergence of the quark string endpoints and both are integrable with their integrated forms listed in [36]. In principle there is no preferred choice for which method to use at NLO and in practice both work with similar accuracy.

At NNLO when two antennae are used to remove limits using iterated mappings the small numerical discrepancy between using the initial-final and initial-initial maps can cause sizeable differences between the two methods and inform a choice as to which is better suited. For example consider the subtraction term constructed to remove the $i_q||\hat{1}_g$ and $k_g||\hat{2}_g$ divergence from the string $(i_q,\hat{1}_g,j_g,k_g,\hat{2}_g,\cdots)$. Using the sub-antennae a subtraction term can be constructed,

$$
d_3^0(i_q,\hat{1}_g;j_g) \, f_3^0(\hat{2}_g,k_g,\widetilde{(ji)}_g) \, M_n^0(\cdots,\hat{\tilde{1}}_q,\widetilde{((ji)k)}_g,\hat{\tilde{2}}_g,\cdots),
$$

(2.125)

which in the particular limit being considered tends to the value,

$$
\frac{1}{s_{1i}}P_{qg\leftarrow Q}(x)\frac{1}{s_{2k}}P_{qg\leftarrow Q}(y) \, M_n^0(\cdots,\hat{\tilde{1}}_q,\widetilde{((ji)k)}_g,\hat{\tilde{2}}_g,\cdots).
$$

(2.126)

Generating the subtraction term using the initial-initial A_3^0, as discussed above, gives,

$$
A_3^0(i_q,\hat{1}_g,\hat{2}_g) \, f_3^0(\hat{\tilde{2}}_g,\tilde{k}_g,\tilde{j}_g) \, M_n^0(\cdots,\hat{\tilde{1}}_q,\widetilde{(\tilde{j}\tilde{k})}_g,\hat{\tilde{\tilde{2}}}_g,\cdots),
$$

(2.127)

which in the same limit tends to the value,

$$
\frac{1}{s_{1i}}P_{qg\leftarrow Q}(x)\frac{1}{s_{\bar{2}\tilde{k}}}P_{qg\leftarrow Q}(y) \, M_n^0(\cdots,\hat{\tilde{1}}_q,\widetilde{(\tilde{j}\tilde{k})}_g,\hat{\tilde{\tilde{2}}}_g,\cdots).
$$

(2.128)

Although the initial-final and initial-initial maps drive the momenta to the same values in the unresolved limits, they may converge at different rates. This does not

affect the values of the reduced matrix elements which are relatively insensitive to very small numerical differences in the momenta via the two maps. The discrepancy is generated by the inverse powers of mapped momenta which also become small, i.e., the s_{2k} and $s_{\bar{2}\tilde{k}}$ in the expressions above. Although in the unresolved limit $\bar{2} \to 2$ and $\tilde{k} \to k$, because s_{2k} is also vanishing, any numerical discrepancy between $\{\bar{2}, \tilde{k}\}$ and $\{2, k\}$ is of the same order as the scale s_{2k}, which is very small in this limit, and can cause a significant error which is multiplied due to the reciprocal power of the small invariant.

For these practical concerns it may be advantageous to use the initial-final d_3^0 sub-antennae for iterated subtraction terms at NNLO instead of the difference of two full antennae using different maps. At NLO the iterated antenna structure never arises as only one parton is ever unresolved and so both methods are equivalent. The advantage of the antenna difference method really only shows up for the case of four-parton antennae which suffer the same problems as the initial-final D_3^0 antenna. This issue will be discussed in more detail in section 2.6.1.

If an initial-state quark is adjacent to a final-state quark and a gluon then the crossed version of the final-final G_3^0 antenna is used to construct the subtraction term,

$$
\begin{aligned}
\mathrm{d}\hat{\sigma}_{NLO}^{S,if,\hat{q}_1 q_j} \;=\;& \mathcal{N}_{NLO}^R \, N^p \, \frac{\bar{C}(\epsilon)}{C(\epsilon)} \sum_{\mathrm{perms}} \mathrm{d}\Phi_{n+1}(k_1, \cdots, k_n; p_1, p_2) \, \frac{1}{S_{n+1}} \\
& G_3^0(i_g, \hat{1}_q, j_q) \, M_n^0(\cdots ; \widetilde{(ij)}_g, \hat{\bar{1}}_g, \cdots,) \, J_n^{(n)}(k_1, \cdots, k_{\widetilde{(ij)}}, \cdots, k_n).
\end{aligned}
$$
(2.129)

If the initial-state quark is adjacent to a final-state quark of the same flavour and a final-state quark of a different flavour then the subtraction term is given by,

$$
\begin{aligned}
\mathrm{d}\hat{\sigma}_{NLO}^{S,if,\hat{q}_1 q_j} \;=\;& \mathcal{N}_{NLO}^R \, N^p \, \frac{\bar{C}(\epsilon)}{C(\epsilon)} \sum_{\mathrm{perms}} \mathrm{d}\Phi_{n+1}(k_1, \cdots, k_n; p_1, p_2) \, \frac{1}{S_{n+1}} \\
& E_3^0(i_Q, \hat{1}_q, j_q) \, M_n^0(\cdots ; \widetilde{(ij)}_Q, \hat{\bar{1}}_g, \cdots,) \, J_n^{(n)}(k_1, \cdots, k_{\widetilde{(ij)}}, \cdots, k_n).
\end{aligned}
$$
(2.130)

Initial-initial gluon string

When two initial-state gluons are separated by only one final-state gluon then the subtraction term utilises the full initial-initial gluonic antenna,

$$
\begin{aligned}
\mathrm{d}\hat{\sigma}_{NLO}^{S,ii,\hat{g}_1 g_i \hat{g}_2} \;=\;& \mathcal{N}_{NLO}^R \, N^p \, \frac{\bar{C}(\epsilon)}{C(\epsilon)} \sum_{\mathrm{perms}} \mathrm{d}\Phi_{n+1}(k_1,\cdots,k_n;p_1,p_2) \, \frac{1}{S_{n+1}} \\
& F_3^0(\hat{1}_g, i_g, \hat{2}_g) \, M_n^0(\cdots,\hat{\bar{1}}_g, \hat{\bar{2}}_g, \cdots,) \, J_n^{(n)}(\tilde{k}_1,\cdots,\tilde{k}_n).
\end{aligned}
$$

(2.131)

The antenna requires no decomposition into sub-antennae as only one parton is allowed to become unresolved. The subtraction term properly subtracts the i_g soft, $\hat{1}_g||i_g$ and $\hat{2}_g||i_g$ collinear divergence of the matrix element. The unresolved limits occurring between the initial-state partons and those that bookend the initial-initial system are removed using initial-final subtraction terms as previously discussed.

Initial-initial quark string: Quark-antiquark initiated

If a quark string has both endpoints in the initial-state and more than one gluon populating the string then the subtraction term is the sum of two initial-final quark string subtraction terms with potentially a final-state gluon string between the two if enough gluons populate the string. If only one gluon populates the string with both endpoints in the initial state then the divergences are removed using the initial-initial A_3^0 antenna,

$$
\begin{aligned}
\mathrm{d}\hat{\sigma}_{NLO}^{S,ii,\hat{q}_1 g_i \hat{\bar{q}}_2} \;=\;& \mathcal{N}_{NLO}^R \, N^p \, \frac{\bar{C}(\epsilon)}{C(\epsilon)} \sum_{\mathrm{perms}} \mathrm{d}\Phi_{n+1}(k_1,\cdots,k_n;p_1,p_2) \, \frac{1}{S_{n+1}} \\
& A_3^0(\hat{1}_q, i_g, \hat{2}_{\bar{q}}) \, M_n^0(\cdots;\hat{\bar{1}}_q, \hat{\bar{2}}_{\bar{q}};\cdots,) \, J_n^{(n)}(\tilde{k}_1,\cdots,\tilde{k}_n).
\end{aligned}
$$

(2.132)

Initial-initial quark string: Quark-gluon initiated

If one endpoint of a quark string is in the initial-state and an initial-state gluon is separated from the quark by one final-state gluon then the subtraction term takes the form,

$$
\mathrm{d}\hat{\sigma}_{NLO}^{S,ii,\hat{q}_1 g_i \hat{g}_2} \;=\; \mathcal{N}_{NLO}^R \, N^p \, \frac{\bar{C}(\epsilon)}{C(\epsilon)} \sum_{\mathrm{perms}} \mathrm{d}\Phi_{n+1}(k_1,\cdots,k_n;p_1,p_2) \, \frac{1}{S_{n+1}}
$$

$$D_3^0(\hat{1}_q, i_g, \hat{2}_g) \, M_n^0(\cdots; \hat{\bar{1}}_q, \hat{\bar{2}}_g, \cdots,) \, J_n^{(n)}(\tilde{k}_1, \cdots, \tilde{k}_n). \quad (2.133)$$

The antenna requires no decomposition into sub-antennae as the only parton which can become unresolved is the final-state gluon and the initial-state partons do not suffer from an identity crisis as the final-state gluon does not change the particle type of any initial-state parton.

Initial-initial quark string: Gluon-gluon initiated

For the configuration where a final-state quark is the endpoint of a quark string and adjacent to two initial state gluons the full initial-initial D_3^0 antenna with both gluons in the initial-state has to be decomposed into two sub-antennae. Clearly only one of the initial-state gluons is colour connected to the quark and so only one of the collinear limits is required for the subtraction (no soft limits are present for initial-state gluons). In addition to the unnecessary divergence when the other gluon becomes collinear with the quark, the two limits map onto different matrix elements. In the $i_q||\hat{1}$ case the reduced matrix element has the initial state partons with particle type $\{\hat{\bar{1}}, \hat{\bar{2}}\} = \{q, g\}$ whereas the $i_q||\hat{2}$ limit, also contained in the full D_3^0 antenna, the initial-state particle have the type $\{g, q\}$. The full $D_3^0(i_q, j_g, k_g)$ antenna has no denominators of the form $s_{ij}s_{ik}$ and so it can be decomposed into sub-antennae without the use of partial fractioning. The sub-antenna is given by,

$$d_3^0(i_q, \hat{1}_g; \hat{2}_g) \;=\; \frac{1}{s_{12i}^2}\left(\frac{s_{12}^2}{s_{1i}} + \frac{4s_{2i}^2}{s_{1i}} + \frac{4s_{1i}^2}{s_{12}} + \frac{3s_{12}s_{2i}}{s_{1i}} + \frac{2s_{2i}^3}{s_{12}s_{1i}} + \frac{3s_{2i}s_{1i}}{s_{12}} + 3s_{12} + 9s_{1i}\right),$$

$$(2.134)$$

such that it contains all the $i_q||\hat{1}_g$ collinear divergence. The full antenna is obtained by summing the two sub-antennae, which are related to one another by the substitution $\hat{1} \leftrightarrow \hat{2}$, $D_3^0(i_q, \hat{1}_g, \hat{2}_g) = d_3^0(i_q, \hat{1}_g; \hat{2}_g) + d_3^0(i_q, \hat{2}_g; \hat{1}_g)$. The sub-antenna has been integrated in [36] and the subtraction term for the configuration under consideration is given by,

$$d\hat{\sigma}_{NLO}^{S,ii,q_i\hat{g}_1\hat{g}_2} \;=\; \mathcal{N}_{NLO}^R \, N^p \, \frac{\bar{C}(\epsilon)}{C(\epsilon)} \sum_{\text{perms}} d\Phi_{n+1}(k_1, \cdots, k_n; p_1, p_2) \, \frac{1}{S_{n+1}}$$

$$d_3^0(i_q, \hat{1}_g; \hat{2}_g) \, M_n^0(\cdots; \hat{\bar{1}}_q, \hat{\bar{2}}_g, \cdots,) \, J_n^{(n)}(\tilde{k}_1, \cdots, \tilde{k}_n). \quad (2.135)$$

An alternative strategy is to use the full initial-initial A_3^0 antenna which only contains the IR divergence necessary for this limit. The second initial-state parton in the A_3^0 antenna is supposed to be a quark and in this context would in actual fact be a gluon but this does not affect the divergent limit of the antenna or its integrated form. Using this strategy the subtraction term is given by,

$$
\begin{aligned}
\mathrm{d}\hat{\sigma}_{NLO}^{S,ii,q_i\hat{g}_1\hat{g}_2} \;=\;& \mathcal{N}_{NLO}^R \, N^p \, \frac{\bar{C}(\epsilon)}{C(\epsilon)} \sum_{\mathrm{perms}} \mathrm{d}\Phi_{n+1}(k_1,\cdots,k_n;p_1,p_2) \, \frac{1}{S_{n+1}} \\
& A_3^0(i_q,\hat{1}_g,\hat{2}) \, M_n^0(\cdots;\hat{\bar{1}}_q,\hat{\bar{2}}_g,\cdots,) \, J_n^{(n)}(\tilde{k}_1,\cdots,\tilde{k}_n). \quad (2.136)
\end{aligned}
$$

The fact that the two terms are interchangeable in the context of subtraction can be seen by noticing that the initial-initial d_3^0 sub-antenna and the quark-gluon initiated A_3^0 antennae have the same divergent limits and the same poles upon analytic integration.

2.5.2 NLO mass factorization term

The NLO mass factorization contribution was discussed in detail in section 1.4 where it was shown that in general the contribution has the form,

$$
\begin{aligned}
\mathrm{d}\hat{\sigma}_{ij,NLO}^{MF} \;=\;& -\bar{C}(\epsilon) \left\{ \int \frac{\mathrm{d}x_1}{x_1} \frac{\mathrm{d}x_2}{x_2} \, \delta_{lj} \, \delta(1-x_2) \, \mathbf{\Gamma}_{ki}^1 \, \mathrm{d}\hat{\sigma}_{kl}^B \right. \\
& \left. + \int \frac{\mathrm{d}x_1}{x_1} \frac{\mathrm{d}x_2}{x_2} \, \delta_{ki} \, \delta(1-x_1) \, \mathbf{\Gamma}_{lj}^1 \, \mathrm{d}\hat{\sigma}_{kl}^B \right\} \quad (2.137)
\end{aligned}
$$

When considering $(n+1)$-parton real corrections to an n-jet cross section, the Born cross section is computed from the tree-level n-parton matrix element. Writing the Born cross section out in terms of the matrix elements being integrated over the final-state phase space the mass factorization contribution at NLO is given by,

$$
\begin{aligned}
\mathrm{d}\hat{\sigma}_{ij,NLO}^{MF} \;=\;& \sum_{\mathrm{perms}} \mathrm{d}\Phi_n(k_1,\cdots,k_n;p_1,p_2) \, \bar{C}(\epsilon) \int \frac{\mathrm{d}x_1}{x_1} \frac{\mathrm{d}x_2}{x_2} \frac{1}{S_n} \left\{ \vphantom{\int} \right. \\
& -\delta_{lj} \, \delta(1-x_2) \, \mathbf{\Gamma}_{ki}^1(x_1) \, M_n^0(\cdots,\hat{k},\cdots,\hat{l},\cdots) \, J_n^{(n)}(k_1,\cdots,k_n) \\
& \left. -\delta_{ki} \, \delta(1-x_1) \, \mathbf{\Gamma}_{lj}^1(x_2) \, M_n^0(\cdots,\hat{k},\cdots,\hat{l},\cdots) \, J_n^{(n)}(k_1,\cdots,k_n) \right\}.
\end{aligned}
$$
$$(2.138)$$

In this formula is an implicit sum over k and l, denoting the particle types of the initial-state partons. In practical calculations the matrix elements accompanying

some of the terms in this implicit sum over initial-state partons are zero, e.g., a cross section with a purely gluonic Born cross section will admit a term where one initial-state parton is transformed into a quark but the matrix element for a single quark in an otherwise gluonic process is zero by current conservation. The explicit forms for the various mass factorization kernels and their associated colour decompositions are listed in appendix A.1.

2.5.3 Integration of the real emission subtraction term

Integrating the various subtraction terms over the final-final, initial-final and initial-initial single unresolved antenna phase spaces is trivial once the integrated antennae are known. The unintegrated antennae are replaced by the appropriate integrated antennae and the remaining final-state resolved momenta relabelled. By integrating out the unresolved partons, the many reduced matrix elements undergoing different mappings map onto a common reduced matrix element which allows the sum of many unintegrated subtraction terms to become the factorized product of a single reduced matrix element and a sum of integrated antenna functions.

Final-state gluon string

Integrating the formula for an $(n + 1)$-parton final-state gluon string subtraction term yields the contribution,

$$
\begin{aligned}
\int_1 \mathrm{d}\hat{\sigma}_{NLO}^{S,ff,g_1\cdots g_{n+1}} \;=\;& \mathcal{N}_{NLO}^R \; N^p \; \bar{C}(\epsilon) \int \frac{\mathrm{d}x_1}{x_1} \, \frac{\mathrm{d}x_2}{x_2} \, \frac{1}{S_n} \\
& \sum_{\mathrm{perms}} \mathrm{d}\Phi_n(k_1,\cdots,k_n;p_1,p_2) \, \delta(1-x_1) \, \delta(1-x_2) \\
& \boldsymbol{J}_n^{(1)}(1_g,\cdots,n_g) \, M_n^0(\cdots,1_g,\cdots,n_g,\cdots) \, J_n^{(n)}(\tilde{k}_1,\cdots,\tilde{k}_n),
\end{aligned}
$$

$$(2.139)$$

where the reciprocal power of $C(\epsilon)$ has been absorbed into the definition of the integrated antenna functions, as described in section 2.4. The quantity $\boldsymbol{J}_n^{(1)}$ denotes a sum of integrated antenna functions which factor onto the same matrix element. For an $(n + 1)$-gluon string that upon integration maps into an n-gluon string the

integrated antenna operator is given by,

$$\boldsymbol{J}_n^{(1)}(1, \cdots, n) \;=\; \frac{1}{3}\Big(\mathcal{F}_3^0(s_{12}) + \mathcal{F}_3^0(s_{23}) + \cdots + \mathcal{F}_3^0(s_{(n-1)n})\Big).$$

$$(2.140)$$

The integrated final-final antennae can be written in terms of the colour ordered insertion operators introduced in section 1.3.1 and it is trivial to show that,

$$\mathcal{P}oles\big[\boldsymbol{J}_n^{(1)}(1, \cdots, n)\big] \;=\; -2\boldsymbol{I}_n^{(1)}(\epsilon; 1, \cdots, n),$$

$$(2.141)$$

such that these two quantities differ only by finite terms. The IR singularity structure of the one-loop virtual contributions in terms of the IR insertion operator is well known, so introducing a correspondence between integrated antennae and the insertion operator allows for a direct comparison of the integrated subtraction term and the poles of the one-loop contribution.

Final-state quark string

A final-state quark string with quark endpoint neighbouring final-state gluons upon integration over the unresolved gluon phase space yields,

$$\begin{aligned}
\int_1 \mathrm{d}\hat{\sigma}_{NLO}^{S,ff,q_i g_j g_k} \;=\;& \mathcal{N}_{NLO}^R \, N^p \, \bar{C}(\epsilon) \int \frac{\mathrm{d}x_1}{x_1} \frac{\mathrm{d}x_2}{x_2} \frac{1}{S_n} \\
& \sum_{\text{perms}} \mathrm{d}\Phi_n(k_1, \cdots, k_n; p_1, p_2) \, \delta(1 - x_1) \, \delta(1 - x_2) \\
& \boldsymbol{J}_2^{(1)}(i_q, k_g) \, M_n^0(\cdots; i_q, k_g, \cdots) \, J_n^{(n)}(\tilde{k}_1, \cdots, \tilde{k}_n),
\end{aligned}$$

$$(2.142)$$

where the two-parton integrated antenna string is given by,

$$\boldsymbol{J}_2^{(1)}(i_q, k_g) \;=\; \frac{1}{2}\mathcal{D}_3^0(s_{ik}).$$

$$(2.143)$$

Combining this result with the form of the integrated antenna string for final-state gluons, the integrated subtraction term for a final-state quark string with $(n-1)$ gluons separated by two quarks is given by,

$$\boldsymbol{J}_n^{(1)}(1_q, 2_g, \cdots, (n-1)_g, n_{\bar{q}}) \;=\; \frac{1}{2}\mathcal{D}_3^0(s_{12}) + \frac{1}{3}\mathcal{F}_3^0(s_{23}) + \cdots$$

$$+ \ \frac{1}{3}\mathcal{F}_3^0(s_{(n-2)(n-1)}) + \frac{1}{2}\mathcal{D}_3^0(s_{(n-1)n}). \quad (2.144)$$

If in unintegrated form the quarks are only separated by a single gluon then the subtraction term integrated over the unresolved gluon phase space is given by,

$$
\begin{aligned}
\int_1 \mathrm{d}\hat{\sigma}_{NLO}^{S,ff,q_i g_j \bar{q}_k} \ = \ & \mathcal{N}_{NLO}^R \ N^p \ \bar{C}(\epsilon) \int \frac{\mathrm{d}x_1}{x_1} \frac{\mathrm{d}x_2}{x_2} \frac{1}{S_n} \\
& \sum_{\mathrm{perms}} \mathrm{d}\Phi_n(k_1, \cdots, k_n; p_1, p_2) \ \delta(1-x_1) \ \delta(1-x_2) \\
& \boldsymbol{J}_2^{(1)}(i_q, k_{\bar{q}}) \ M_n^0(\cdots; i_q, k_{\bar{q}}; \cdots) \ J_n^{(n)}(\tilde{k}_1, \cdots, \tilde{k}_n),
\end{aligned}
$$

$$(2.145)$$

where the final-state quark-antiquark integrated antenna string is given by,

$$\boldsymbol{J}_2^{(1)}(i_q, k_{\bar{q}}) \ = \ \mathcal{A}_3^0(s_{ik}). \quad (2.146)$$

Integrating the remaining subtraction terms which take into account the limits when a quark-anti-quark pair become collinear to form a composite gluon are integrated to generate the following contributions to the cross section,

$$
\begin{aligned}
\int_1 \mathrm{d}\hat{\sigma}_{NLO}^{S,ff,g_i q_j \bar{q}_k} \ = \ & \mathcal{N}_{NLO}^R \ N^p \ \bar{C}(\epsilon) \int \frac{\mathrm{d}x_1}{x_1} \frac{\mathrm{d}x_2}{x_2} \frac{1}{S_n} \\
& \sum_{\mathrm{perms}} \mathrm{d}\Phi_n(k_1, \cdots, k_n; p_1, p_2) \ \delta(1-x_1) \ \delta(1-x_2) \\
& \boldsymbol{J}_{2,N_F}^{(1)}(i_g, j_g) \ M_n^0(\cdots, i_g, j_g, \cdots) \ J_n^{(n)}(\tilde{k}_1, \cdots, \tilde{k}_n), \\
\int_1 \mathrm{d}\hat{\sigma}_{NLO}^{S,ff,q_i' q_j \bar{q}_k} \ = \ & \mathcal{N}_{NLO}^R \ N^p \ \bar{C}(\epsilon) \int \frac{\mathrm{d}x_1}{x_1} \frac{\mathrm{d}x_2}{x_2} \frac{1}{S_n} \\
& \sum_{\mathrm{perms}} \mathrm{d}\Phi_n(k_1, \cdots, k_n; p_1, p_2) \ \delta(1-x_1) \ \delta(1-x_2) \\
& \boldsymbol{J}_{2,N_F}^{(1)}(i_q, j_g) \ M_n^0(\cdots, i_{q'}, j_g, \cdots) \ J_n^{(n)}(\tilde{k}_1, \cdots, \tilde{k}_n),
\end{aligned}
$$

$$(2.147)$$

where these terms generally carry a factor of N_F due to the sum over final-state quark flavours being partially evaluated for the N_F quark pairs becoming collinear in the limit. The two final-state two-particle integrated antenna strings are given by,

$$\boldsymbol{J}_{2,N_F}^{(1)}(i_g, j_g) \ = \ \frac{1}{2}\mathcal{G}_3^0(s_{ij}),$$

$$\boldsymbol{J}_{2,N_F}^{(1)}(i_q, j_g) = \frac{1}{2}\mathcal{E}_3^0(s_{ij}). \tag{2.148}$$

For final-state strings of particles there is no mass factorization contribution so the virtual subtraction terms are given directly by the integrated subtraction terms, i.e.,

$$\mathrm{d}\hat{\sigma}_{NLO}^{T,ff} = -\int_1 \mathrm{d}\hat{\sigma}_{NLO}^{S,ff}. \tag{2.149}$$

Initial-final gluon string

When a parton is crossed into the initial-state and the contribution is integrated over the unresolved phase space the integral of the subtraction term contains initial-state collinear singularities. As discussed in section 1.4 these singularities are removed by the process of factorization whereby they cancel in the factorized cross section against the mass factorization contributions to the cross section. For an initial-final gluon string the integrated subtraction term combined with the mass factorization contribution associated with the initial-state parton is given by,

$$\begin{aligned}
\mathrm{d}\hat{\sigma}_{NLO}^{T,if,\hat{g}_1 g_i g_j} = {}& -\mathcal{N}_{NLO}^R \, N^p \, \bar{C}(\epsilon) \int \frac{\mathrm{d}x_1}{x_1} \frac{\mathrm{d}x_2}{x_2} \frac{1}{S_n} \\
& \sum_{\text{perms}} \mathrm{d}\Phi_n(k_1, \cdots, k_n; p_1, p_2) \, \delta(1 - x_2) \\
& \boldsymbol{J}_2^{(1)}(\hat{\bar{1}}_g, j_g) \, M_n^0(\cdots, \hat{\bar{1}}_g, j_g, \cdots) \, J_n^{(n)}(\tilde{k}_1, \cdots, \tilde{k}_n),
\end{aligned} \tag{2.150}$$

where the initial-final integrated antenna string is formed from the integrated initial-final antenna and the mass factorization kernel,

$$\boldsymbol{J}_2^{(1)}(\hat{\bar{1}}_g, j_g) = \frac{1}{2}\mathcal{F}_{3,g}^0(s_{\bar{1}j}) - \frac{1}{2}\Gamma_{gg}^1(x_1). \tag{2.151}$$

This two parton integrated antenna string can be combined with other integrated antenna strings in an additive fashion to encapsulate the ϵ poles of a matrix element containing an initial-state gluon neighbouring final-state gluons. The inclusion of the mass factorization kernel removes any initial-state collinear poles present in the integrated antenna, leaving only genuine final-state IR poles which can be cancelled against the virtual cross section. The integrated antennae can be written in terms of the insertion operators, e.g.,

$$\mathcal{P}oles\big(\mathcal{F}_{3,g}^0(s_{\bar{1}i})\big) = -4\boldsymbol{I}_{gg}^{(1)}(s_{\bar{1}i}) \, \delta(1-x) + \frac{1}{2}s_{\bar{1}i}^{-\epsilon} \, \Gamma_{gg}^1(x), \tag{2.152}$$

and so, noting that the deepest pole of Γ^1_{gg} is $1/\epsilon$, the resulting pole structure of $\boldsymbol{J}^{(1)}_2(\hat{1}_g, j_g)$ matches onto the pole structure of the one-loop virtual gluon cross section as required to ensure the pole cancellation.

Initial-final quark string: Quark initiated

Integrating the subtraction term for a quark string endpoint with an initial-state quark and combining it with the appropriate mass factorization contribution yields the contribution to the cross section,

$$
\begin{aligned}
\mathrm{d}\hat{\sigma}^{T,if,\hat{q}_1 g_i g_j}_{NLO} \quad = \quad & -\mathcal{N}^R_{NLO} \, N^p \, \bar{C}(\epsilon) \int \frac{\mathrm{d}x_1}{x_1} \frac{\mathrm{d}x_2}{x_2} \frac{1}{S_n} \\
& \sum_{\text{perms}} \mathrm{d}\Phi_n(k_1, \cdots, k_n; p_1, p_2) \, \delta(1 - x_2) \\
& \boldsymbol{J}^{(1)}_2(\hat{\bar{1}}_q, j_g) \, M^0_n(\cdots; \hat{\bar{1}}_q, j_g, \cdots) \, J^{(n)}_n(\tilde{k}_1, \cdots, \tilde{k}_n), \quad (2.153)
\end{aligned}
$$

where the initial-final quark-gluon integrated antenna string is given by,

$$
\boldsymbol{J}^{(1)}_2(\hat{\bar{1}}_q, j_g) \quad = \quad \frac{1}{2}\mathcal{D}^0_{3,q}(s_{\bar{1}j}) - \Gamma^1_{qq}(x_1). \tag{2.154}
$$

This two-parton integrated antenna string can be added with other strings for neighbouring partons to generate a contribution which matches the pole structure of the virtual cross section.

If only one gluon populates the quark string and one of the quarks is in the initial state then the integrated antenna string is given by,

$$
\boldsymbol{J}^{(1)}_2(\hat{\bar{1}}_q, i_{\bar{q}}) \quad = \quad \mathcal{A}^0_{3,q}(s_{\bar{1}i}) - \Gamma^1_{qq}(x_1). \tag{2.155}
$$

The configuration where a quark pair become collinear with one of the quarks in the initial-state has a subtraction term which when integrated and combined with the mass appropriate mass factorization terms generates the following integrated antenna strings,

$$
\begin{aligned}
\boldsymbol{J}^{(1)}_{2,q\to g}(i_g, \hat{\bar{1}}_g) \quad &= \quad \mathcal{G}^0_{3,q}(s_{\bar{1}i}) - \Gamma^1_{gq}(x_1), \\
\boldsymbol{J}^{(1)}_{2,N_F}(\hat{\bar{1}}_q, i_g) \quad &= \quad \frac{1}{2}\mathcal{E}^0_{3;q,q'\bar{q}'}(s_{\bar{1}i}). \tag{2.156}
\end{aligned}
$$

The poles of the integrated antennae in the identity changing integrated antenna string, $\boldsymbol{J}^{(1)}_{2,q\to g,N_F}$, are cancelled due to the mass factorization contribution, as expected for identity changing contributions,

$$\mathcal{P}oles\big[\boldsymbol{J}^{(1)}_{2,q\to g}(i_g\hat{\bar{1}}_g)\big] \;=\; 0 \tag{2.157}$$

The remaining term corresponds to an initial-final collinear quark pair neighbouring a non-identical flavoured quark. The integrated subtraction term generates the integrated antenna string,

$$\boldsymbol{J}^{(1)}_{2,q\to g}(i_{q'}\hat{\bar{1}}_g) \;=\; \mathcal{E}^0_{3;q,qq'}(s_{\bar{1}i}) - \Gamma^1_{gq}(x_1), \tag{2.158}$$

where the poles of the antenna are once again cancelled by the mass factorization contribution.

$$\mathcal{P}oles\big[\boldsymbol{J}^{(1)}_{2,q\to g}(i_{q'}\hat{\bar{1}}_g)\big] \;=\; 0 \tag{2.159}$$

Initial-final quark string: Gluon initiated

For the configuration where initial-state gluons are adjacent or almost adjacent to a quark endpoint the divergences can be removed by decomposing the full D^0_3 antenna into two sub-antennae. Both of these sub-antennae have been integrated in [36] and are denoted,

$$\int_1 d^0_3(i_q,\hat{1}_g;j_g) \;=\; \mathcal{D}^0_{3;g,qg}(s_{\bar{1}j}),$$
$$\int_1 d^0_3(i_q,j_g,\hat{1}_g) \;=\; \mathcal{D}^0_{3;g,gq}(s_{\bar{1}j}). \tag{2.160}$$

The subtraction term which removes the initial-state collinear divergence associated with the final-state quark becoming collinear with the initial state gluon is integrated and combined with the appropriate mass factorization term to give,

$$\begin{aligned}
\mathrm{d}\hat{\sigma}^{T,if,q_i\hat{g}_1g_j}_{NLO} \;=\; & -\mathcal{N}^R_{NLO}\, N^p\, \bar{C}(\epsilon) \int \frac{\mathrm{d}x_1}{x_1}\,\frac{\mathrm{d}x_2}{x_2}\,\frac{1}{S_n} \\
& \sum_{\text{perms}} \mathrm{d}\Phi_n(k_1,\cdots,k_n;p_1,p_2)\,\delta(1-x_2) \\
& \boldsymbol{J}^{(1)}_{2,g\to q}(\hat{\bar{1}}_q,j_g)\,M^0_n(\cdots;\hat{\bar{1}}_q,j_g,\cdots)\,J^{(n)}_n(\tilde{k}_1,\cdots,\tilde{k}_n).
\end{aligned} \tag{2.161}$$

Using the integrated sub-antenna the integrated antenna string is given by,

$$\boldsymbol{J}^{(1)}_{2,g\rightarrow q}(\hat{\bar{1}}_q, j_g) \;\; = \;\; \mathcal{D}^0_{3;g,qg}(s_{\bar{1}j}) - \Gamma^1_{qg}(x_1). \tag{2.162}$$

If the alternative strategy of using the initial-initial A^0_3 subtraction term is employed then the factor of $\delta(1 - x_2)$ is removed from the definition of the virtual subtraction term to take into account the fact that an initial-initial antenna has been used. The integrated antenna string is then given by,

$$\boldsymbol{J}^{(1)}_{2,g\rightarrow q}(\hat{\bar{1}}_q, j_g) \;\; = \;\; \mathcal{A}^0_{3,gq}(s_{12}) - \Gamma^1_{qg}(x_1)\delta(1 - x_2). \tag{2.163}$$

By examining the poles of both $\mathcal{D}^0_{3;g,qg}$ and $\mathcal{A}^0_{3,gq}$ it is clear that not only are they identical, but also the poles cancel completely against the mass factorization contribution such that,

$$\mathcal{P}oles\big[\boldsymbol{J}^{(1)}_{2,g\rightarrow q}(\hat{\bar{1}}_q, j_g)\big] \;\; = \;\; 0. \tag{2.164}$$

This is to be expected given that this subtraction term is used purely to remove the initial-state collinear divergence of the initial-state gluon and the final-state quark. The subtraction term for the configuration where the initial-state gluon is separated from the quark by a single gluon is integrated and combined with the mass factorization contribution to give the contribution,

$$\begin{aligned}
\mathrm{d}\hat{\sigma}^{T,if,q_ig_j\hat{g}_1}_{NLO} \;\; = \;\; & -\mathcal{N}^R_{NLO} \, N^p \, \bar{C}(\epsilon) \int \frac{\mathrm{d}x_1}{x_1} \frac{\mathrm{d}x_2}{x_2} \frac{1}{S_n} \\
& \sum_{\text{perms}} \mathrm{d}\Phi_n(k_1, \cdots, k_n; p_1, p_2) \, \delta(1 - x_2) \\
& \boldsymbol{J}^{(1)}_2(i_q, \hat{\bar{1}}) \, M^0_n(\cdots; i_q, \hat{\bar{1}}_q, \cdots) \, J^{(n)}_n(\tilde{k}_1, \cdots, \tilde{k}_n).
\end{aligned} \tag{2.165}$$

Using the integrated sub-antenna the integrated antenna string has the form,

$$\boldsymbol{J}^{(1)}_2(i_q, \hat{\bar{1}}) \;\; = \;\; \mathcal{D}^0_{3;g,gq}(s_{\bar{1}j}) - \frac{1}{2}\Gamma^0_{gg}(x_1). \tag{2.166}$$

If the alternative method whereby the difference of an initial-final D^0_3 and an initial-initial A^0_3 is used to remove the IR divergence, the factor of $\delta(1 - x_2)$ is removed from the integration and the integrated antenna string is given by,

$$\boldsymbol{J}^{(1)}_2(i_q, \hat{\bar{1}}) \;\; = \;\; \mathcal{D}^0_{3;g}(s_{\bar{1}j})\delta(1 - x_2) - \mathcal{A}^0_{3,qg}(s_{12}) - \frac{1}{2}\Gamma^0_{gg}(x_1) - \delta(1 - x_2).$$

$$(2.167)$$

By examining the poles of the individual antennae it is clear that the two expressions for the integrated antenna string share the same poles and match onto the pole structure of the corresponding virtual contribution.

If only one gluon populates the quark string and is also in the initial-state then the integrated antenna string is given by,

$$\boldsymbol{J}_{2,g\to q}^{(1)}(\hat{\bar{1}}_q, i_{\bar{q}}) \;\; = \;\; \mathcal{A}_{3,g}^0(s_{\bar{1}i}) - \Gamma_{qg}^1(x_1), \qquad (2.168)$$

such that the mass factorization contribution completely cancels the poles within this term,

$$\mathcal{P}oles\big[\boldsymbol{J}_{2,g\to q}^{(1)}(\hat{\bar{1}}_q, i_{\bar{q}})\big] \;\; = \;\; 0 \qquad (2.169)$$

Initial-initial gluon string

For a gluon string with two initial state gluons separated by one final-state gluon the integrated subtraction term combined with the appropriate mass factorization terms gives the contribution,

$$
\begin{aligned}
\mathrm{d}\hat{\sigma}_{NLO}^{T,ii,\hat{g}_1 g_i \hat{g}_2} \;\; = \;\; & -\mathcal{N}_{NLO}^R \, N^p \, \bar{C}(\epsilon) \int \frac{\mathrm{d}x_1}{x_1} \frac{\mathrm{d}x_2}{x_2} \frac{1}{S_n} \sum_{\mathrm{perms}} \mathrm{d}\Phi_n(k_1,\cdots,k_n;p_1,p_2) \\
& \boldsymbol{J}_2^{(1)}(\hat{\bar{1}}_g, \hat{\bar{2}}_g) \, M_n^0(\cdots,\hat{\bar{1}}_g, \hat{\bar{2}}_g,\cdots) \, J_n^{(n)}(\tilde{k}_1,\cdots,\tilde{k}_n). \qquad (2.170)
\end{aligned}
$$

The initial-initial gluonic integrated antenna string is given by,

$$\boldsymbol{J}_2^{(1)}(\hat{\bar{1}}_g, \hat{\bar{2}}_g) \;\; = \;\; \mathcal{F}_{3,gg}^0(s_{\bar{1}\bar{2}}) - \frac{1}{2}\Gamma_{gg}^1(x_1)\delta(1-x_2) - \frac{1}{2}\Gamma_{gg}^1(x_2)\delta(1-x_1). \; (2.171)$$

The IR divergences associated with gluons either side of the initial-initial system are removed by initial-final and final-final strings, the integrated forms of which have already been discussed.

Initial-initial quark string: Quark-anti-quark initiated

When both the quark and anti-quark of a quark string are in the initial-state and more than one gluons populates the string, the subtraction term is given by a sum of

initial-final quark strings. If only one gluon populates the string then the integrated subtraction term combined with the mass factorization contribution gives,

$$
\begin{aligned}
\mathrm{d}\hat{\sigma}_{NLO}^{T,ii,\hat{q}_1 g_i \hat{\bar{q}}_2} &= -\mathcal{N}_{NLO}^R \, N^p \, \bar{C}(\epsilon) \int \frac{\mathrm{d}x_1}{x_1} \frac{\mathrm{d}x_2}{x_2} \frac{1}{S_n} \sum_{\text{perms}} \mathrm{d}\Phi_n(k_1, \cdots, k_n; p_1, p_2) \\
&\quad \boldsymbol{J}_2^{(1)}(\hat{\bar{1}}_q, \hat{\bar{2}}_{\bar{q}}) \, M_n^0(\cdots; \hat{\bar{1}}_q, \hat{\bar{2}}_{\bar{q}}; \cdots) \, J_n^{(n)}(\tilde{k}_1, \cdots, \tilde{k}_n),
\end{aligned}
\tag{2.172}
$$

such that,

$$
\boldsymbol{J}_2^{(1)}(\hat{\bar{1}}_q, \hat{\bar{2}}_{\bar{q}}) = \mathcal{A}_{3,q\bar{q}}^0(s_{\bar{1}\bar{2}}) - \Gamma_{qq}^1(x_1)\delta(1-x_2) - \Gamma_{qq}^1(x_2)\delta(1-x_1). \tag{2.173}
$$

Initial-initial quark string: Quark-gluon initiated

The subtraction term for the configuration involving an initial-state quark and gluon separated by a final-state gluon is integrated and combined with the appropriate mass factorization terms to give,

$$
\begin{aligned}
\mathrm{d}\hat{\sigma}_{NLO}^{T,ii,\hat{q}_1 g_i \hat{g}_2} &= -\mathcal{N}_{NLO}^R \, N^p \, \bar{C}(\epsilon) \int \frac{\mathrm{d}x_1}{x_1} \frac{\mathrm{d}x_2}{x_2} \frac{1}{S_n} \sum_{\text{perms}} \mathrm{d}\Phi_n(k_1, \cdots, k_n; p_1, p_2) \\
&\quad \boldsymbol{J}_2^{(1)}(\hat{\bar{1}}_q, \hat{\bar{2}}_g) \, M_n^0(\cdots; \hat{\bar{1}}_q, \hat{\bar{2}}_g, \cdots) \, J_n^{(n)}(\tilde{k}_1, \cdots, \tilde{k}_n),
\end{aligned}
\tag{2.174}
$$

where the integrated antenna string for this configuration is given by,

$$
\boldsymbol{J}_2^{(1)}(\hat{\bar{1}}_q, \hat{\bar{2}}_g) = \mathcal{D}_{3,qg}^0(s_{\bar{1}\bar{2}}) - \Gamma_{qq}^1(x_1)\delta(1-x_2) - \frac{1}{2}\Gamma_{gg}^1(x_2)\delta(1-x_1). \tag{2.175}
$$

Initial-initial quark string: Gluon-gluon initiated

When two initial-state gluons are adjacent to one another and a quark the appropriate subtraction term can be integrated and combined with the mass factorization contribution to generate the term,

$$
\begin{aligned}
\mathrm{d}\hat{\sigma}_{NLO}^{T,ii,\hat{q}_i \hat{g}_1 \hat{g}_2} &= -\mathcal{N}_{NLO}^R \, N^p \, \bar{C}(\epsilon) \int \frac{\mathrm{d}x_1}{x_1} \frac{\mathrm{d}x_2}{x_2} \frac{1}{S_n} \sum_{\text{perms}} \mathrm{d}\Phi_n(k_1, \cdots, k_n; p_1, p_2) \\
&\quad \boldsymbol{J}_{2,g \to q}^{(1)}(\hat{\bar{1}}_q, \hat{\bar{2}}_g) \, M_n^0(\cdots; \hat{\bar{1}}_q, \hat{\bar{2}}_g, \cdots) \, J_n^{(n)}(\tilde{k}_1, \cdots, \tilde{k}_n).
\end{aligned}
\tag{2.176}
$$

In this case the identity changing integrated antenna string can be written using the integrated sub-antenna,

$$
\boldsymbol{J}_{2,g \to q}^{(1)}(\hat{\bar{1}}_q, \hat{\bar{2}}_g) = \mathcal{D}_{3,gg}^0(s_{\bar{1}\bar{2}}) - \Gamma_{qg}^1(x_1)\delta(1-x_2), \tag{2.177}
$$

or the integrated A_3^0 antenna, as discussed in the previous section,

$$\boldsymbol{J}_{2,g\to q}^{(1)}(\hat{\bar{1}}_q, \hat{\bar{2}}_g) \;\; = \;\; \mathcal{A}_{3,qg}^0(s_{\bar{1}\bar{2}}) - \Gamma_{qg}^1(x_1)\delta(1 - x_2). \tag{2.178}$$

The IR poles of both expressions are identical and completely cancel against the mass factorization term, as expected,

$$\mathcal{P}oles\big[\boldsymbol{J}_{2,g\to q}^{(1)}(\hat{\bar{1}}_q, \hat{\bar{2}}_g)\big] \;\; = \;\; 0. \tag{2.179}$$

The single unresolved integrated antenna strings are collected for reference in section B.1 and will be referred to frequently in the rest of this thesis.

2.5.4 Construction of the virtual subtraction term

The virtual subtraction term is constructed from the integrated real subtraction term and the mass factorization contribution. The combination of the two terms into contributions proportional to the integrated antenna strings has been considered in the last section. To form the full virtual subtraction term the various integrated antenna strings are joined together to form a single string per distinct reduced matrix element. For example consider an $(n + 1)$-parton gluonic matrix element, that maps down into the n-parton matrix element $M_n^0(i,\cdots,j,\hat{\bar{1}},\hat{\bar{2}},k,\cdots)$. Once the single unresolved subtraction term for this matrix element has been integrated and combined with the mass factorization terms the resultant virtual subtraction term is given by,

$$\begin{aligned}
\mathrm{d}\hat{\sigma}_{NLO}^T \;\; = \;\; & -\mathcal{N}_{NLO}^R \, N^p \, \bar{C}(\epsilon) \int \frac{\mathrm{d}x_1}{x_1} \frac{\mathrm{d}x_2}{x_2} \frac{1}{S_n} \sum_{\mathrm{perms}} \mathrm{d}\Phi_n(k_1, \cdots, k_n; p_1, p_2) \\
& \boldsymbol{J}_n^{(1)}(i_g\cdots, j_g, \hat{\bar{1}}_g, \hat{\bar{2}}_g, k_g, \cdots) \, M_n^0(i_g\cdots, j_g, \hat{\bar{1}}_g, \hat{\bar{2}}_g, k_g, \cdots) \, J_n^{(n)}(\tilde{k}_1, \cdots, \tilde{k}_n).
\end{aligned}$$
$$\tag{2.180}$$

The full integrated antenna string is formed from the various integrated antenna strings defined in the previous section,

$$\begin{aligned}
\boldsymbol{J}_n^{(1)}(i_g\cdots, j_g, \hat{\bar{1}}_g, \hat{\bar{2}}_g, k_g, \cdots) \;\; = \;\; & \boldsymbol{J}_j^{(1)}(i_g\cdots, j_g)\delta(1 - x_1)\delta(1 - x_2) \\
& + \;\; \boldsymbol{J}_2^{(1)}(j_g, \hat{\bar{1}}_g)\delta(1 - x_2) + \boldsymbol{J}_2^{(1)}(\hat{\bar{1}}_g, \hat{\bar{2}}_g) \\
& + \;\; \boldsymbol{J}_2^{(1)}(\hat{\bar{1}}_g, k_g)\delta(1 - x_1)
\end{aligned}$$

$$+ \quad \boldsymbol{J}_{n-k}^{(1)}(k_g, \cdots, i_g)\delta(1-x_1)\delta(1-x_2). \quad (2.181)$$

Similarly a collection of matrix elements which in their single unresolved limits collapse onto the matrix element $M_n^0(\hat{\bar{1}}_q, i_g, \cdots, j_g, \hat{\bar{2}}_{\bar{q}})$, generate a virtual subtraction term involving,

$$
\begin{aligned}
\boldsymbol{J}_n^{(1)}(\hat{\bar{1}}_q, i_g, \cdots, j_g, \hat{\bar{2}}_{\bar{q}}) &= \boldsymbol{J}_2^{(1)}(\hat{\bar{1}}_q, i_g)\delta(1-x_2) \\
&+ \boldsymbol{J}_{n-2}^{(1)}(i_g, \cdots, j_g)\delta(1-x_1)\delta(1-x_2) \\
&+ \boldsymbol{J}_2^{(1)}(j_g, \hat{\bar{2}}_{\bar{q}})\delta(1-x_1)
\end{aligned}
\quad (2.182)
$$

2.6 Antenna subtraction at NNLO

Extending the analysis presented so far to NNLO is non-trivial but possible within the antenna subtraction formalism. By defining tree-level four-parton and three-parton one-loop antennae, as discussed in section 2.2, the method can accommodate double unresolved tree-level and single unresolved one-loop configurations, which are the genuinely new NNLO ingredients of any calculation.

As discussed in section 2.1.3, within the framework of subtraction a NNLO calculation involves the construction of three subtraction terms for the double real, real-virtual and double virtual, denoted $d\hat{\sigma}_{NNLO}^S$, $d\hat{\sigma}_{NNLO}^T$, $d\hat{\sigma}_{NNLO}^U$ respectively. If all integrated antennae are known then this method is guaranteed to be integrable by construction but the process of assembling a successful subtraction term at each level of the calculation is not as algorithmic as is the case at NLO. Nevertheless a significant amount of structure does exist and is visible when using the antenna subtraction method.

The construction of subtraction terms at the double real, real-virtual and double virtual levels requires an intimate understanding of the explicit infrared singularity structure and implicit infrared divergent behaviour of both the physical matrix elements and the subtraction terms at different levels in the calculation. The structures of these subtraction terms are dictated by two main considerations: the colour connection of partons and explicit IR pole cancellation. The former completely informs the construction of the double real subtraction term as there are no explicit

IR poles to consider; the latter is the sole concern of the double virtual subtraction term which is free from implicit IR divergences. The real-virtual subtraction term contains both explicit poles and implicit divergent behaviour and so its structure must take into account both parton colour connection and explicit pole cancellation.

2.6.1   Gluon initiated processes

Before discussing the general form of the subtraction terms it is useful to consider the case of gluon initiated four-parton antennae, specifically the gluon initiated D_4^0. The issue of gluon initiated quark-gluon antennae has been discussed at NLO for three parton antennae where the problem exists because the full antenna collapses onto two distinct antennae in the different limits contained within the single antenna. One solution to this problem at NLO was to partition the full antenna into two sub-antennae, such that each sub-antenna solely maps onto one of the two distinct two-parton antennae in the various unresolved limits. This strategy proves effective at NLO and at NNLO when considering iterated three-parton antenna configurations.

For double unresolved configurations involving initial-state gluons it is often desirable to use a gluon initiated D_4^0 antenna function. This antenna suffers from the same ambiguity as the gluon initiated three-parton antenna, it maps onto two distinct underlying two-parton antennae in the double unresolved limits. This can be seen by considering the triple collinear limits of the antenna $D_4^0(i_q, \hat{1}_g, j_g, k_g)$. In the $i||\hat{1}||j$ and $k||i||\hat{1}$ limits the antenna maps onto a quark-gluon system with the quark in the initial-state. In the $\hat{1}||j||k$ and $j||k||i$ limits the antenna maps into a quark-gluon system with the gluon in the initial-state.

This problem is unlike the ambiguity inherent to final-final antennae involving many gluons, whereby the antennae had to be decomposed into sub-antennae so the hard partons identified in the phase space map match onto hard partons in the antenna. In that case the sub-antennae all mapped onto the same type of matrix element but the momentum map was different for each term. The sub-antennae did not have to be integrated separately because the decomposition was performed such that the sum of sub-antennae formed a full antenna and only the full antenna required analytic integration. This step is important as the sub-antennae

are generated via a complicated decomposition and contain terms which are by themselves difficult to integrate which are not present in the full antenna. In the case of the gluon initiated quark-gluon antennae this trick of decomposing into sub-antennae but only having to integrate the full antenna fails because the sub-antennae would map onto genuinely different types of matrix element, not ones which differ only by a phase space map. Due to this inherent problem with the different matrix elements the sub-antennae would have to be integrated analytically themselves, which for a four-parton sub-antenna involving three gluons is a highly non-trivial task and may require new master integrals to be computed.

An alternative to the method of generating sub-antennae is to return to the idea of using less divergent antenna functions to isolate a particular limit which factors onto one type of matrix element and a difference of two antenna functions which factor onto the other type of matrix element. This method was shown to be equivalent to the method involving sub-antennae for single unresolved limits at NLO in both unintegrated and integrated form. At NLO it may be desirable to choose the sub-antenna method as fewer terms are required to achieve the same goal; whilst at NNLO for iterated antenna limits the sub-antenna method may be more reliable for numerical reasons, as discussed previously. However for double unresolved limits there is no iterated structure to cause numerical issues[2] and the sub-antenna approach appears to be unviable.

Consider a matrix element containing the configuration where an initial-state gluon is adjacent to the quark, e.g., $M_6^0(i_q, \hat{1}_g, j_g, k_g, \hat{2}_g, l_{\bar{q}})$. This matrix element contains the string of partons which match onto the gluon initiated $D_4^0(i_q, \hat{1}_g, j_g, k_g)$ antenna. Using this antenna to remove the divergence is inappropriate for the reasons already mentioned. Instead, the $i||\hat{1}||j$ quark-gluon triple collinear limit present in the matrix element is subtracted using the initial-initial antenna $A_4^0(i_q, \hat{1}_g, j_g, \hat{2})$.

---

[2]An exception to this statement is in the removal of single unresolved limits of the four parton antenna which will contain iterated antennae and may generate numerical mis-matches between the mappings. These issues are not specific to the problem discussed here and arise generally when spurious limits are removed using an antenna function belonging to a different kinematic configuration.

In the matrix element parton $\hat{2}$ is a gluon whereas the rightmost slot in the A_4^0 antenna is conventionally reserved for a quark. This is not a problem if the reduced matrix element associated with this antenna still treats $\hat{2}$ as a gluon and the phase space map is flavour blind. Furthermore the parton $\hat{2}$ is not involved with any other colour connected double unresolved limits so acts as a benign spectator. The antenna will have single unresolved limits involving $\hat{2}$ but these are removed via the usual procedure and will not in principle cause problems for the subtraction.

The second possible configuration is when the initial-state gluon is separated from the quark by a single final-state gluon, e.g., $M_6^0(i_q, j_g, \hat{1}_g, k_g\hat{2}_g, l_{\bar{q}})$. In this situation the antenna $D_4^0(i_q, j_g, \hat{1}_g, k_g)$ seems appropriate but as well as containing spurious divergent limits, the antenna maps onto two distinct two-parton antennae in the various double unresolved limits. In this case the initial-initial antenna $A_4^0(i_q, j_g, \hat{1}_g, \hat{2})$ is used to remove the $i_q||j_g||\hat{1}_g$ limit, with the remaining limits being removed by using the antenna $F_4^0(j_g, \hat{1}_g, k_g, \hat{2})$.

The third configuration is given by an initial-state gluon separated from the quark by two final-state gluons e.g., $M_6^0(i_q, j_g, k_g, \hat{1}_g, \hat{2}_g, l_{\bar{q}})$ for which the antenna $D_4^0(i_q, j_g, k_g, \hat{1}_g)$ appears suitable but suffers from the same problem as before and so is in fact inappropriate by itself. In this situation the D_4^0 antenna is not completely useless as it contains some of the double unresolved limits of the matrix element, specifically the $j_g, k_g \to 0$ double soft limit, the $i_q||j_g||k_g$ and $j_g||k_g||\hat{1}_g$ triple collinear limits, as well as various soft-collinear limits where partons j and k become unresolved. In all these limits the antenna factors into the quark-gluon antenna with the gluon in the initial-state.

The limits contained in the D_4^0 antenna which collapse onto a quark-gluon antenna with the quark in the initial-state can be removed using the initial-initial A_4^0 type antennae, as these antennae were used in the first example to subtract such limits from the matrix elements themselves. Subtracting the antenna $A_4^0(i_q, \hat{1}_g, k_g, \hat{2})$ from the $D_4^0(i_q, j_g, k_g, \hat{1}_q)$ antenna removes the spurious $i_q||\hat{1}_g||k_g$ limit without introducing additional spurious colour-connected unresolved limits. Similarly subtracting the antenna $\tilde{A}_4^0(i_q, j_g, \hat{1}_g, \hat{2}_g)$ from the D_4^0 antenna removes the $i_q||j_g||\hat{1}_g$ limit without introducing new colour-connected double unresolved limits. In the second case

the antenna used is the subleading colour $\tilde{A}_4^0$ antenna because the gluons $\hat{1}_g$ and j_g are not colour-connected in the D_4^0 antenna.

This strategy for dealing with the unresolved limits of an initial-state gluon separated from a quark endpoint by up to two gluons generalizes the argument made at NLO where an initial-state gluon separated from a quark endpoint by up to one gluon encountered similar problems. The advantage of the method is that no new ingredients are required for its implementation.

2.6.2 Construction of the double real subtraction term

At NNLO the double real radiative $(n+4)$-parton correction to the n-jet final-state, for the process $pp \rightarrow n$ jets, must be included and integrated over the appropriate $(n+2)$-parton phase space. In order for this to be achieved, the IR divergent behaviour of the partonic cross section must be isolated. In the antenna subtraction formalism this is achieved by constructing a subtraction term from three- and four-parton antenna functions and reduced multiplicity matrix elements such that a finite contribution can be numerically evaluated and the explicit IR poles extracted for cancellation against contributions at the real-virtual and double virtual levels.

By construction the double real subtraction term mimics the IR divergence and factorization of the real radiation matrix elements in all relevant single and double unresolved limits. At NNLO there are four colour configurations to consider when constructing the subtraction term for n-jet production:

1. A single unresolved parton but an n-jet selecting observable.

2. Two colour-connected unresolved partons, i.e. two unresolved partons radiated between a single pair of hard radiators.

3. Two almost colour-connected unresolved partons, i.e. two colour disconnected unresolved partons sharing a common radiator.

4. Two colour disconnected unresolved partons, i.e. two colour disconnected unresolved partons with no radiators in common.

The four possible colour configurations for the single and double unresolved limits of the $(n + 4)$-parton matrix elements provide a natural way to divide the subtraction term into sections, as has been emphasised in previous works [32] [108] [114]. It should be noted that although the factorization of the matrix elements is strictly classified according to the colour connection of unresolved partons, the associated subtraction terms readily communicate with one another in most unresolved limits due to the existence and cross cancellation of spurious singularities. These systematic cross cancellations suggest that structures exist in the subtraction term other than those dictated by the colour connection of unresolved partons.

In the following sections an equivalent reorganisation of the double real subtraction term into five subsections is presented,

$$d\hat{\sigma}_{NNLO}^S = d\hat{\sigma}_{NNLO}^{S,a} + d\hat{\sigma}_{NNLO}^{S,b_1} + d\hat{\sigma}_{NNLO}^{S,b_2} + d\hat{\sigma}_{NNLO}^{S,c} + d\hat{\sigma}_{NNLO}^{S,d}, \quad (2.183)$$

where $d\hat{\sigma}_{NNLO}^{S,c}$ now contains the large angle soft contribution that was considered separately in previous works [32] [108] [114]. This manifestation of the subtraction term is broadly organised along the lines of colour connection but is also informed by considering how the double real subtraction terms appear in real-virtual and double virtual subtraction terms. Such an organisation of the double real subtraction term allows a transparent understanding of how various terms from the double real level cascade down the calculation upon integration. Understanding this structure also permits a systematic construction of the double real subtraction term in terms of predictable blocks of terms.

Single unresolved subtraction term, $d\hat{\sigma}_{NNLO}^{S,a}$

The removal of single unresolved limits from $(n + 4)$-parton contribution to the n-jet cross section at NNLO strongly resembles the subtraction term constructed to isolate single unresolved limits from the $(n+4)$-parton contribution to the $(n+1)$-jet cross section at NLO. The two subtraction terms differ only in the number of jets allowed by the jet function,

$$d\hat{\sigma}_{NNLO}^{S,a}(k_1, \cdots, k_{n+2}; p_1, p_2) = d\hat{\sigma}_{NLO}^S(k_1 \cdots, k_{n+2}; p_1, p_2)\Big|_{J_{n+1}^{(n+1)} \to J_n^{(n+1)}}. \quad (2.184)$$
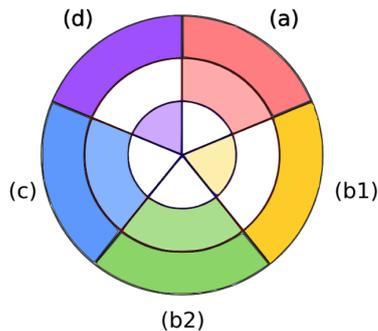
Figure 2.4: A pictorial representation of how the different sections of $\mathrm{d}\hat{\sigma}^S_{NNLO}$ contribute to different levels of the calculation. The inner, middle and outer rings represent the double virtual, real-virtual and double real levels respectively. Sections of $\mathrm{d}\hat{\sigma}^S_{NNLO}$ are labelled (a) $\mathrm{d}\hat{\sigma}^{S,a}_{NNLO}$, $(b1)$ $\mathrm{d}\hat{\sigma}^{S,b_1}_{NNLO}$, $(b2)$ $\mathrm{d}\hat{\sigma}^{S,b_2}_{NNLO}$, (c) $\mathrm{d}\hat{\sigma}^{S,c}_{NNLO}$, (d) $\mathrm{d}\hat{\sigma}^{S,d}_{NNLO}$. Filled segments denote the levels at which the various sections contribute.

The detailed discussion on constructing the NLO subtraction terms given in section 2.5 is then sufficient to construct the single unresolved subtraction term $\mathrm{d}\hat{\sigma}^{S,a}_{NNLO}$. It should be noted that although this section of the subtraction term is constructed to remove single unresolved divergences of the physical matrix elements for n-jet selecting observables it also contains spurious singularities in the almost colour connected and colour disconnected limits, over-subtracting the divergence in each case. These configurations are permitted due to the fact that the reduced matrix elements allow an additional parton to become unresolved and still form n-jets. Nonetheless this contribution is considered to be a well defined collection of subtraction terms because when reintroduced at the real-virtual level upon analytic integration they form a distinct set of terms proportional to the $(n + 3)$-parton matrix elements that explicitly cancel the poles of the one-loop matrix elements and so are naturally grouped together.

Four-parton antenna subtraction term, $\mathrm{d}\hat{\sigma}^{S,b_1}_{NNLO}$

At NNLO there are essential new ingredients in the form of four-parton tree level antenna functions required to faithfully reproduce the colour connected double unresolved divergences of the physical matrix elements. The momentum map associated with a four-parton antenna function is the $(n+4) \to (n+2)$ map for the final-final,

initial-final and initial-initial configurations, as described in sections 2.3.1-2.3.1. The collection of these terms has the form,

$$
\begin{aligned}
\mathrm{d}\hat{\sigma}_{NNLO}^{S,b_1} &= \mathcal{N}^{RR} \sum_{n+2} \mathrm{d}\Phi_{n+2}(k_1, \ldots, k_{n+2}; p_1, p_2) \frac{1}{S_{n+2}} \\
&\times \sum_{j,k} X_4^0(i, j, k, l) \, M_{n+2}^0(\{k_n\}, p_1, p_2) \, J_n^{(n)}(\{k_n\}). \quad (2.185)
\end{aligned}
$$

This term is generic to all three kinematic configurations, with the specific antenna functions and momentum maps depending on which configuration the term belongs to. The four-parton antenna functions display many different types of divergent behaviour including single unresolved and almost colour connected singularities all of which must be properly removed elsewhere in the subtraction term. The analytic integration of the four-parton antenna functions is carried out over the double unresolved antenna phase space and so the terms in $\mathrm{d}\hat{\sigma}_{NNLO}^{S,b_1}$ are reintroduced to the double virtual subtraction term. This is in contrast to the terms introduced to remove the spurious singularities of the four-parton antennae which are added back to the real-virtual subtraction term. For this reason the terms involving four-parton antenna functions are grouped together in the double real subtraction term.

Four-parton single unresolved subtraction term, $\mathrm{d}\hat{\sigma}_{NNLO}^{S,b_2}$

As mentioned in the previous section, four-parton antenna functions contain single unresolved spurious singularities which must be removed to ensure a proper subtraction of the IR divergence in the physical matrix elements. For each four-parton antenna the single unresolved limits are removed by constructing a subtraction term along the lines of $\mathrm{d}\hat{\sigma}_{NNLO}^{S,a}$ but now applying this method to the four-parton antenna function rather than the physical matrix elements. As such the terms are built from three-parton antennae (used to remove the single unresolved limits) multiplied by another three-parton antenna (the remnant of the four-parton antenna after the single unresolved limit is taken) and a reduced matrix element which in the single unresolved limit maps on to the matrix element post-multiplying the four-parton antenna. For a four-parton antenna function this block has the generic form

$$
\mathrm{d}\hat{\sigma}_{NNLO}^{S,b_2} = -\mathcal{N}^{RR} \sum_{n+2} \mathrm{d}\Phi_{n+2}(k_1, \ldots, k_{n+2}; p_1, p_2) \frac{1}{S_{n+2}}
$$

Configuration	X_4^0	$\tilde{X}_4^0$
Final-final	$A_4^0, B_4^0, C_4^0, D_{4,a}^0, E_{4,a}^0, \tilde{E}_4^0, F_{4,a}^0, G_4^0, \tilde{G}_4^0, H_4^0$	$\tilde{A}_4^0, D_{4,c}^0, E_{4,b}^0, F_{4,b}^0,$
Initial-final	$A_4^0, B_4^0, C_4^0, G_4^0, \tilde{G}_4^0, H_4^0$	$\tilde{A}_4^0, D_4^0, E_4^0, F_4^0$
Initial-initial	$A_4^0, B_4^0, C_4^0, D_{4,\text{adj}}^0 F_{4,\text{adj}}^0, G_4^0, \tilde{G}_4^0, H_4^0$	$\tilde{A}_4^0, D_{4,\text{n.adj}}^0, E_4^0, F_{4,\text{n.adj}}^0$

Table 2.4: The classification of the four-parton antenna functions into those containing almost colour connected limits or not. The final state F_4^0, D_4^0 and E_4^0 antennae are decomposed into sub-antennae $D_{4,a}^0$, $D_{4,c}^0$, $E_{4,a}^0$, $E_{4,b}^0$, $F_{4,a}^0$, $F_{4,b}^0$ for numerical implementation.

$$\times \sum_j X_3^0(i,j,k) \, X_3^0(I,K,l) \, M_{n+2}^0(\{k_n\}, p_1, p_2) \, J_n^{(n)}(\{k_n\}),$$

$$(2.186)$$

where the sum is over all partons in the four-parton antenna which admit a single unresolved singularity. As with other sections of the subtraction term this block of terms may contain spurious almost colour connected singularities of its own which can arise when the secondary antenna in (2.186) also contains single unresolved limits. The block of terms associated with each four-parton antenna encapsulates all the single unresolved singularities of the four-parton antenna using the primary antennae of the block. As discussed in section 2.6.3 a collection of terms which correctly mimic the single unresolved limits of the four-parton antenna functions performs a specific role when reintroduced to the real-virtual subtraction term; as such these terms are treated as a distinct grouping in the double real subtraction term.

Almost colour connected subtraction term, $\mathrm{d}\hat{\sigma}_{NNLO}^{S,c}$

The contribution to the subtraction term involving double unresolved almost colour connected unresolved partons is intimately connected to those four-parton antenna functions containing such limits, denoted by $\tilde{X}_4^0$. The classification of the four-parton antenna functions into X_4^0 and $\tilde{X}_4^0$ types is displayed in Table 2.4.

In almost colour connected limits the terms in $\mathrm{d}\hat{\sigma}_{NNLO}^{S,b_2}$ will tend to over-subtract the divergences of the associated $\tilde{X}_4^0$. In the same limits $\mathrm{d}\hat{\sigma}_{NNLO}^{S,a}$ contributes twice

the subtraction required by the matrix elements. Both of these over-subtractions have to be accounted for by $d\sigma_{NNLO}^{S,c}$, which also includes the wide angle soft subtraction term introduced in previous calculations [108] [125].

The terms appropriate for this section can be generated in the following fashion. A final-final double unresolved configuration is considered for clarity but the strategy also applies to initial-final and initial-initial configurations. For each four-parton antenna which contains almost colour connected limits, $\tilde{X}_4^0$, in $d\sigma_{NNLO}^{S,b_1}$ a block of terms in $d\sigma_{NNLO}^{S,c}$ is constructed; for example, the antenna $\tilde{X}_4^0(j,i,k,l)$ with partons i and k unresolved. The antenna is associated with a reduced matrix element, the colour ordering of this matrix element is written down with i and k removed, e.g., if the reduced matrix element is $M_n^0(\dots, a, \widetilde{(j,i,k)}, \widetilde{(i,k,l)}, b, \dots)$ the ordering $(\dots, a, j, l, b, \dots)$, is considered, where j and l are the hard radiators of the antenna. Then consider radiating partons i and k from this underlying ordering in the ordered limit that i is radiated first, followed by k. The second radiation always happens between the antenna's hard radiators whilst the first radiation is allowed to be inserted directly between and one place either side of the antenna's radiators in the colour ordering, with a relative minus sign for these two contributions. Written in terms of antennae this configuration is given by,

$$
\begin{aligned}
+ \quad & \frac{1}{2} X_3^0(j,i,l) \, X_3^0(\widetilde{(j,i)},k,\widetilde{(i,l)}) \, M_n^0(\dots, a, \widetilde{(\widetilde{(j,i)}k)}, \widetilde{(k\widetilde{(i,l)})}, b, \dots) \\
- \quad & \frac{1}{2} X_3^0(a,i,j) \, X_3^0(\widetilde{(j,i)},k,l) \, M_n^0(\dots, \widetilde{(a,i)}, \widetilde{(\widetilde{(j,i)}k)}, \widetilde{(k,l)}, b, \dots) \\
- \quad & \frac{1}{2} X_3^0(l,i,b) \, X_3^0(j,k,\widetilde{(l,i)}) \, M_n^0(\dots, a, \widetilde{(j,k)}, \widetilde{(k\widetilde{(l,i)})}, \widetilde{(i,b)}, \dots) \quad + \ (i \leftrightarrow k).
\end{aligned}
$$

$$(2.187)$$

There is a relative sign between the configurations where both unresolved partons are radiated in region I and the configurations where the first unresolved parton is radiated in either region II or III with the second in region I. The large angle soft terms can also be included in this structure. Two almost colour-connected unresolved partons are removed from the underlying colour ordering and the same radiation pattern of these partons from the underlying colour ordering as in (2.187) is considered. It was shown in [47] that the correct large angle soft terms can also be generated by forcing the first radiation to be between a pair of final state partons,
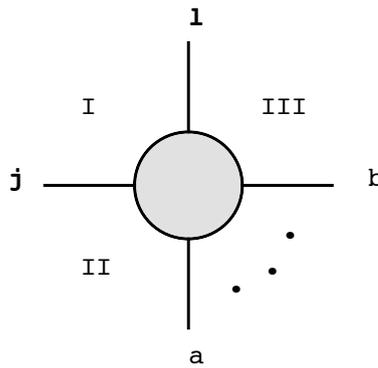
Figure 2.5: The three regions associated with the radiation of the primary unresolved parton. Region I: between the hard radiators of the four-parton antenna, j, l. Region II: one place to the left in the colour ordering between partons a, j. Region III: one place to the right in the colour ordering between partons l, b.

relying on the Lorentz boost invariance of the soft functions and thus removing the need to analytically integrate the soft function over the initial-final or initial-initial antenna phase space. In terms of the pattern of radiation described in (2.187) and figure 2.5 this is understood as the first radiation being between two final state particles in the underlying ordering and the second radiation between the hard radiators in the antenna. In the specific case of six parton scattering amplitudes in double unresolved limits there will only ever be two hard final state partons so the choice of final state partons between which the first unresolved parton is radiated is an unambiguous one.

With the first mapping fixed to be of the final-final type, the secondary antenna (which describes the radiation of the second unresolved parton) has common arguments across all terms, unlike in (2.187) where the arguments depend on the specific mapping inherited from the primary antenna. As a consequence the secondary antenna can be factored out with the reduced matrix element so the large angle soft block has the form,

$$Y \cdot X_3^0(\widetilde{(i,j)}, k, \widetilde{(i,l)}) \ M_n^0(\ldots, a, (\widetilde{(i,j)}k), (\widetilde{k(i,l)}), b, \ldots), \qquad (2.188)$$

where Y is a sum of large angle soft antennae. The structure of this term can be understood with reference to figure 2.5. For each region into which an unresolved

parton can be radiated there is a term in Y given by,

$$-\frac{1}{2}\left[S_{\alpha i\beta} - S_{AIB}\right],$$ (2.189)

where for the example configuration considered in (2.187),

$$
\begin{aligned}
(\alpha,\beta) &= \left\{\left(a,\widetilde{(ij)}\right), \left(\widetilde{(ij)},\widetilde{(il)}\right), \left(\widetilde{(il)},b\right)\right\}, \\
(A,B) &= \left\{\left(a,\widetilde{((ij)k)}\right), \left(\widetilde{((ij)l)},\widetilde{(k(il))}\right), \left(\widetilde{(k(il))},b\right)\right\}.
\end{aligned}
$$ (2.190)

The labels i and I denote the momentum of the unresolved parton i before the first mapping and after the second respectively; unless the secondary antenna is an initial-initial antenna then $i = I$. The pair of soft functions for each region comes with an overall sign depending on which region the primary antenna belongs to, i.e., a relative minus sign for the regions either side of the secondary antenna's radiators. Collecting the terms in (2.187) and the large angle soft terms produces a block for a given four-parton antenna (containing almost colour-connected limits); the sum of such blocks constitutes $d\hat{\sigma}^{S,c}_{NNLO}$,

$$
\begin{aligned}
d\hat{\sigma}^{S,c}_{NNLO} &= \mathcal{N}^{RR} \sum_{n+2} d\Phi_{n+2}(k_1,\ldots,k_{n+2};p_1,p_2)\, \frac{1}{S_{n+2}} \sum_{i,k}\Bigg\{ \\
&+ \frac{1}{2} X^0_3(j,i,l)\, X^0_3(\widetilde{(j,i)},k,\widetilde{(i,l)})\, M^0_n(\ldots,a,\widetilde{((j,i)k)},\widetilde{(k(i,l))},b,\ldots) \\
&- \frac{1}{2} X^0_3(a,i,j)\, X^0_3(\widetilde{(j,i)},k,l)\, M^0_n(\ldots,\widetilde{(a,i)},\widetilde{((j,i)k)},\widetilde{(k,l)},b,\ldots) \\
&- \frac{1}{2} X^0_3(l,i,b)\, X^0_3(j,k,\widetilde{(l,i)})\, M^0_n(\ldots,a,\widetilde{(j,k)},\widetilde{(k(l,i))},\widetilde{(i,b)},\ldots) \\
&- \frac{1}{2}\Bigg[\left(S_{(i,j),i,(i,l)} - S_{((i,j)k)i(k(i,l))}\right) \\
&\qquad - \left(S_{ai(i,j)} - S_{ai((i,j)k)}\right) - \left(S_{bi(i,l)} - S_{bi((i,l)k)}\right)\Bigg] \\
&\quad X^0_3(\widetilde{(i,j)},k,\widetilde{(i,l)})\, M^0_n(\ldots,a,\widetilde{((i,j)k)},\widetilde{(k(i,l))},b,\ldots)\Bigg\},
\end{aligned}
$$ (2.191)

where the sum over i,k denotes the set of almost colour-connected pairs contained within the four-parton antennae in $d\sigma^{S,b_1}_{NNLO}$. The blocks in $d\hat{\sigma}^{S,c}_{NNLO}$ have a common secondary antenna and so when integrated over the single unresolved phase space of the primary antenna will stay together as a block of integrated antenna functions factoring onto a common unintegrated antenna. The structure of this block of terms

in integrated form motivates treating this collection of subtraction terms as a distinct block in the double real contribution.

It should be noted that this block is intimately connected to the presence of almost colour connected limits in a four-parton antenna function. If no such limits exist for a given four-parton antenna in $d\hat\sigma^{S,b_1}_{NNLO}$ then there is no contribution to $d\hat\sigma^{S,c}_{NNLO}$; if a four-parton antenna does contain these limits then the term contributing to $d\hat\sigma^{S,c}_{NNLO}$ is predictable from the information contained in the contribution to $d\hat\sigma^{S,b_1}_{NNLO}$.

Colour disconnected subtraction term, $d\hat\sigma^{S,d}_{NNLO}$

For processes involving six or more coloured particles colour disconnected double unresolved configurations can arise where unresolved partons are separated by more than one hard radiator in the colour ordering. The single unresolved subtraction term $d\hat\sigma^{S,a}_{NNLO}$ admits colour disconnected unresolved limits when the unresolved parton in the antenna is colour disconnected from any other parton in the reduced matrix element which can in principle become unresolved. In the double unresolved limit the antenna will tend to a universal singular function and the reduced matrix element will factorize into another universal function and a further reduced matrix element.

The subtraction terms in $d\hat\sigma^{S,a}_{NNLO}$ take into account all possible unresolved partons and so for each colour disconnected pair of unresolved partons, i and j, where parton i is in the antenna function and j in the reduced matrix element, there is the corresponding subtraction term where j is in the antenna and i in the reduced matrix element. In this double unresolved limit both of these subtraction terms tend to the same value and $d\hat\sigma^{S,a}_{NNLO}$ exactly double-counts the divergence of the matrix elements.

To correct for this over-subtraction a block of terms is introduced with the form,

$$
\begin{aligned}
d\hat\sigma^{S,d}_{NNLO} &= -\mathcal{N}^{RR} \sum_{n+2} d\Phi_{n+2}(k_1,\ldots,k_{n+2};p_1,p_2)\, \frac{1}{S_{n+2}} \\
&\times \sum_{j,m} X_3^0(i,j,k)\, X_3^0(l,m,n)\, M_{n+2}^0(\{k_n\},p_1,p_2)\, J_n^{(n)}(\{k_n\}).
\end{aligned}
$$

(2.192)

where the sum runs over pairs of partons separated by more than one hard parton in the ordering. This term also serves to compensate for the situation where a parton which is colour disconnected from the potentially unresolved parton in the antenna in $d\hat{\sigma}_{NNLO}^{S,a}$ becomes unresolved. In this single unresolved limit the term in $d\hat{\sigma}_{NNLO}^{S,a}$ is divergent but does not match onto any divergence in the matrix elements. Such terms are removed by the terms in $d\hat{\sigma}_{NNLO}^{S,d}$.

The disconnected nature of the terms in $d\sigma_{NNLO}^{S,d}$ allows this block of terms to be analytically integrated over the two disconnected regions of single unresolved antenna phase space. The fact that both unresolved partons can be integrated out directly from the double real level suggests that this contribution should be reintroduced to the double virtual subtraction term and so are kept together as a grouping in the double real contribution

2.6.3 Real-virtual subtraction term

The real-virtual subtraction term must successfully remove the implicit IR divergent behaviour and explicit poles of the one loop $(n+3)$-parton matrix elements. In addition to imitating the physical one-loop matrix elements the real-virtual subtraction term inherits terms from the double real subtraction term upon analytic integration over a single unresolved parton. The a terms will generally introduce both explicit poles and IR divergences which must cancel against other contributions to the real-virtual subtraction term to ensure that $d\sigma_{NNLO}^{RV} - d\sigma_{NNLO}^{T}$ is finite. Taking all these considerations into account leads to a subtraction term for the real-virtual contribution which can be divided into five contributions,

$$d\hat{\sigma}_{NNLO}^{T} = d\hat{\sigma}_{NNLO}^{T,a} + d\hat{\sigma}_{NNLO}^{T,b_1} + d\hat{\sigma}_{NNLO}^{T,b_2} + d\hat{\sigma}_{NNLO}^{T,b_3} + d\hat{\sigma}_{NNLO}^{T,c}. \quad (2.193)$$

The structure and behaviour of each of these terms will be explained in the rest of this section, including whether the terms originate and terminate in the double real, real-virtual and double virtual contribution.

NNLO real-virtual mass factorization term

Recall from section 1.4 that the NNLO mass factorization contribution contains contributions proportional to $d\boldsymbol{\sigma}_{LO}$ and $d\boldsymbol{\sigma}_{NLO}$. When trying to understand which terms contribute to which levels of the NNLO calculation it is instructive to consider the matrix elements involved in each contribution. The terms proportional to $d\boldsymbol{\sigma}_{LO}$ contain $(n+2)$-parton matrix elements and so contribute to the double virtual subtraction term as that contribution involves an n-parton final-state phase space integral. The terms proportional to $d\boldsymbol{\sigma}_{NLO}$ are naturally split into two contributions, $d\boldsymbol{\sigma}_{NLO} = \int_{\Phi_{n+1}} d\boldsymbol{\sigma}_{NLO}^R + \int_{\Phi_n} d\boldsymbol{\sigma}_{NLO}^V$ where the real contribution contains $(n+3)$-parton matrix elements and the virtual contribution contains $(n+2)$-parton contributions. It is then natural for the terms proportional to $d\boldsymbol{\sigma}_{NLO}^R$ to contribute at the real-virtual level and those proportional to $d\boldsymbol{\sigma}_{NLO}^V$ to contribute to the double virtual level, along with the rest of the NNLO mass factorization terms.

An added complication to this issue is the fact that $d\boldsymbol{\sigma}_{NLO}^R$ contains IR divergence in single unresolved regions of phase space and $d\boldsymbol{\sigma}_{NLO}^V$ contains explicit ϵ poles in addition to those carried by the mass factorization kernels. It should be noted that $d\boldsymbol{\sigma}_{NLO}$ is the unfactorized NLO cross section. Therefore in the context of antenna subtraction it can be re-written in the form,

$$d\boldsymbol{\sigma}_{NLO} = \int_{\Phi_{n+1}} \left[d\boldsymbol{\sigma}_{NLO}^R - d\boldsymbol{\sigma}_{NLO}^S \right] + \int_{\Phi_n} \left[d\boldsymbol{\sigma}_{NLO}^V + \int_1 d\boldsymbol{\sigma}_{NLO}^S \right], \quad (2.194)$$

where the first bracketed term is now free from implicit divergence. Both terms in the first bracket depend on the $(n+3)$-parton momentum set and so terms proportional to this quantity are taken to constitute the NNLO real-virtual mass factorization contribution. Writing these terms in less symbolic form reveals,

$$d\hat{\sigma}_{ij,NNLO}^{MF,RV}(\xi_1 H_1, \xi_2 H_2) = -\bar{C}(\epsilon) \int \frac{dx_1}{x_1} \frac{dx_2}{x_2} \Bigg\{$$

$$\delta(1-x_2)\, \Gamma_{ki}^1(x_1) \left[d\hat{\sigma}_{kj,NLO}^R - d\hat{\sigma}_{kj,NLO}^S \right](x_1\xi_1 H_1, x_2\xi_2 H_2)$$

$$+ \quad \delta(1-x_1)\, \Gamma_{lj}^1(x_2) \left[d\hat{\sigma}_{il,NLO}^R - d\hat{\sigma}_{il,NLO}^S \right](x_1\xi_1 H_1, x_2\xi_2 H_2) \Bigg\} \quad (2.195)$$

where ξ_i is the fraction of the incoming hadron's momentum H_i carried by parton i. Rearranging this formula to group terms with a common type of matrix element

allows the mass factorization term to be divided according to,

$$\mathrm{d}\hat{\sigma}_{ij,NNLO}^{MF,RV} = \mathrm{d}\hat{\sigma}_{ij,NNLO}^{MF,RV,a} + \mathrm{d}\hat{\sigma}_{ij,NNLO}^{MF,RV,b}, \qquad (2.196)$$

such that $\mathrm{d}\hat{\sigma}_{ij,NNLO}^{MF,RV,a}$ is proportional to the $(n+3)$-parton matrix elements,

$$\mathrm{d}\hat{\sigma}_{ij,NNLO}^{MF,RV,a}(\xi_1 H_1, \xi_2 H_2) = -\bar{C}(\epsilon) \int \frac{\mathrm{d}x_1}{x_1} \frac{\mathrm{d}x_2}{x_2}$$

$$\left[\delta(1-x_2) \, \Gamma_{ki}^1(x_1) \, \mathrm{d}\hat{\sigma}_{kj,NLO}^R(x_1\xi_1 H_1, x_2\xi_2 H_2) \right.$$

$$\left. + \quad \delta(1-x_1) \, \Gamma_{lj}^1(x_2) \, \mathrm{d}\hat{\sigma}_{il,NLO}^R(x_1\xi_1 H_1, x_2\xi_2 H_2) \right], \qquad (2.197)$$

and $\mathrm{d}\hat{\sigma}_{ij,NNLO}^{MF,RV,b}$ is proportional to the $(n+2)$-parton matrix elements but retains a dependence on the additional parton through the unintegrated antenna functions present in $\mathrm{d}\hat{\sigma}_{NLO}^S$,

$$\mathrm{d}\hat{\sigma}_{ij,NNLO}^{MF,RV,b}(\xi_1 H_1, \xi_2 H_2) = \bar{C}(\epsilon) \int \frac{\mathrm{d}x_1}{x_1} \frac{\mathrm{d}x_2}{x_2}$$

$$\left[\delta(1-x_2) \, \Gamma_{ki}^1(x_1) \, \mathrm{d}\hat{\sigma}_{kj,NLO}^S(x_1\xi_1 H_1, x_2\xi_2 H_2) \right.$$

$$\left. + \quad \delta(1-x_1) \, \Gamma_{lj}^1(x_2) \, \mathrm{d}\hat{\sigma}_{il,NLO}^S(x_1\xi_1 H_1, x_2\xi_2 H_2) \right] \qquad (2.198)$$

It should be noted that the form of $\mathrm{d}\hat{\sigma}_{NNLO}^{MF,RV,a}$ is exactly the same as for $\mathrm{d}\hat{\sigma}_{NLO}^{MF}$ with an additional parton and the replacement $J_n^{(n)} \to J_n^{(n+1)}$. Furthermore the terms are proportional to the $(n+3)$-parton matrix elements unlike any other mass factorization terms.

One loop explicit pole subtraction term, $\mathrm{d}\hat{\sigma}_{NNLO}^{T,a}$

It was emphasised in section 2.6.2 that the construction of $\mathrm{d}\hat{\sigma}_{NNLO}^{S,a}$ follows the same lines as constructing $\mathrm{d}\hat{\sigma}_{NLO}^S$ with a modified jet function and an additional parton. This matches the interpretation of the mass factorization contribution $\mathrm{d}\hat{\sigma}_{NNLO}^{MF,RV,a}$ and so integrating the antennae in $\mathrm{d}\hat{\sigma}_{NNLO}^{S,a}$ and combining with the mass factorization kernels in $\mathrm{d}\hat{\sigma}_{NNLO}^{MF,RV,a}$ will generate precisely the same type of integrated antenna strings seen at NLO for one additional parton. The combination of these two contributions generates the real-virtual subtraction term,

$$\mathrm{d}\hat{\sigma}_{NNLO}^{T,a} = -\mathcal{N}^{RV} \sum_{n+1} \int \frac{\mathrm{d}x_1}{x_1} \frac{\mathrm{d}x_2}{x_2} \, \mathrm{d}\Phi_{n+1}(k_1, \ldots, k_{n+1}; p_1, p_2) \, \frac{1}{S_{n+1}}$$

$$\times \quad \boldsymbol{J}_{n+3}^{(1)}(1,\ldots,n+3) \; M_{n+3}^0(k_1,\ldots,k_{n+1}) \; J_n^{(n+1)}(\{k_{n+1}\}), \quad (2.199)$$

where $\mathcal{N}^{RV} = \bar{C}(\epsilon)\mathcal{N}^{RR}$. It has been previously noted that the poles of the $\boldsymbol{J}_n^{(1)}$ integrated antenna strings are simply related the poles of the colour ordered $\boldsymbol{I}_n^{(1)}$ insertion operator. Using this fact it is clear that the term $\mathrm{d}\hat{\sigma}_{NNLO}^{T,a}$ correctly subtracts the ϵ poles of the real-virtual matrix elements which obey the Catani factorization formula,

$$\mathcal{P}oles\big[M_n^1(1,\cdots,n)\big] \;\; = \;\; 2\boldsymbol{I}_n^{(1)}(1,\cdots,n) \; M_n^0(1,\cdots,n). \qquad (2.200)$$

With the explicit poles of the one-loop matrix elements systematically removed by a suitable combination of the integrated $\mathrm{d}\hat{\sigma}_{NNLO}^{S,a}$ and a distinct piece of the real-virtual mass factorization contribution, the only divergence remaining in the one-loop matrix elements is the implicit single unresolved divergence and any explicit poles associated with the renormalization of the one-loop matrix elements.

Tree $\times$ loop subtraction term, $\mathrm{d}\hat{\sigma}_{NNLO}^{T,b_1}$

One-loop matrix elements factorize in implicit IR singular limits into two terms which can be schematically understood as,

$$1\text{-loop} \quad \longrightarrow \quad (\text{tree} \times \text{loop}) \; + \; (\text{loop} \times \text{tree}).$$

The first term is the product of a tree level singular function factoring onto a one-loop reduced matrix element and is subtracted using the product of a tree level antenna function and a one-loop reduced matrix element. This term by itself removes part of the implicit IR divergence of the one loop matrix elements but introduces explicit poles associated with the one loop $(n+2)$-parton reduced matrix element. The explicit poles of this matrix element can be removed by subtracting the appropriate integrated antenna string and so a subtraction term free from explicit IR poles can be constructed,

$$\mathrm{d}\hat{\sigma}_{NNLO}^{T,b_1} = \mathcal{N}^{RV} \sum_{n+1} \int \frac{\mathrm{d}x_1}{x_1}\frac{\mathrm{d}x_2}{x_2} \; \mathrm{d}\Phi_{n+1}(k_1,\ldots,k_{n+1};p_1,p_2) \; \frac{1}{S_{n+1}}$$

$$\times \sum_j X_3^0(i,j,k)\bigg\{ \delta(1-x_1)\delta(1-x_2) \; M_{n+2}^1(k_1,\ldots,k_n;p_1,p_2)$$

$$+ \, \boldsymbol{J}_{n+2}^{(1)}(1, \ldots, n+2) \, M_{n+2}^0(k_1, \ldots, k_n) \Bigg\} \, J_n^{(n)}(\{k_n\}),$$

$$(2.201)$$

where the sum is over the final state unresolved partons of the physical matrix element. This formula can be applied to final-final, initial-final and initial-initial configurations where in each configuration the appropriate unintegrated antenna function is used, which in turn determines the phase space map. The one-loop matrix element is a reduced matrix element and so to ensure a proper subtraction of the explicit poles the integrated antenna string will have mapped momenta to match.

The term proportional to the one-loop matrix element is entirely introduced at the real-virtual level and so, upon integration over the single unresolved antenna phase space, will be reintroduced to the double virtual level of the calculation. The term proportional to the integrated antenna string, $\boldsymbol{J}_{n+2}^{(1)}$, is introduced to remove the explicit poles of the reduced one-loop matrix element, using the fact that the poles of the integrated antenna string match the poles of the colour-ordered insertion operator. The integrated antenna string is constructed from a string of integrated antennae and the appropriate mass factorization kernels to remove the initial-state collinear explicit poles of the integrated antennae. The mass factorization kernels used to construct the integrated antenna string come naturally from the contribution to the cross section $\mathrm{d}\hat{\sigma}_{NNLO}^{MF,RV,b}$. This can be seen from the definition of $\mathrm{d}\hat{\sigma}_{NNLO}^{MF,RV,b}$ which is proportional to the NLO subtraction term and in turn proportional to the product of a three-parton tree-level antenna and a tree-level $(n+2)$-parton reduced matrix element.

The mass factorization contributions which partially constitute the integrated antenna string do not get reintroduced to the double virtual level upon integration over the antenna phase space, but the integrated antennae which make up the rest of the string do; at first sight this causes the $\boldsymbol{J}_{n+2}^{(1)}$ term to be broken up upon integration. While this is true, it is also clear that the mass factorization terms used to define the integrated antenna string are proportional to the terms belonging to $\mathrm{d}\hat{\sigma}_{NLO}^S$ which have the counterpart in the double virtual cross section given by the

same mass factorization kernels now proportional to $\int_1 d\hat{\sigma}^S_{NLO}$. The second quantity is simply the mass factorization terms used to define $\boldsymbol{J}^{(1)}_{n+2}$ in $d\hat{\sigma}^{T,b_1}_{NNLO}$, integrated over the antenna phase space. These terms are precisely what is needed to generate a full $\boldsymbol{J}^{(1)}_{n+2}$ at the double virtual level when combined with the rest of the terms introduced to form the $\boldsymbol{J}^{(1)}_{n+2}$ in $d\hat{\sigma}^{T,b_1}_{NNLO}$ and are passed down to the double virtual level upon integration. From this analysis it is clear that although the $\boldsymbol{J}^{(1)}_{n+2}$ used in $d\hat{\sigma}^{T,b_1}_{NNLO}$ is broken up upon integration, it is systematically re-assembled at the double virtual level.

loop $\times$ tree subtraction term, $d\hat{\sigma}^{T,b_2}_{NNLO}$

The factorization of one-loop matrix elements in IR limits also requires a term given by a one-loop universal singular function factoring onto a tree-level matrix element. To properly account for this contribution, a subtraction term is constructed from a one-loop antenna function containing the one-loop singular functions and a tree-level reduced matrix element. The one-loop antenna functions contain explicit IR ϵ poles which must be removed to ensure a finite total contribution. This goal is achieved by defining a new integrated antenna string $\bar{\boldsymbol{J}}^{(1)}_n$ which contains the IR explicit poles of the one-loop antenna; the explicit form of this function will be discussed in due course. Assuming such a quantity exists, a block of terms can be constructed to remove the remaining implicit IR divergence from the one-loop matrix elements, which is also free from explicit poles,

$$
\begin{aligned}
d\hat{\sigma}^{T,b_2}_{NNLO} &= \mathcal{N}^{RV} \sum_{n+1} \int \frac{dx_1}{x_1} \frac{dx_2}{x_2} \, d\Phi_{n+1}(k_1, \ldots, k_{n+1}; p_1, p_2) \, \frac{1}{S_{n+1}} \\
&\times \sum_j \left[X^1_3(i,j,k)\delta(1-x_1)\delta(1-x_2) + \bar{\boldsymbol{J}}^{(1)}_3(i,j,k) \, X^0_3(i,j,k) \right] \\
&\times \quad M^0_{n+2}(k_1, \ldots, k_n; p_1, p_2) \, J^{(n)}_n(\{k_n\}), \qquad\qquad (2.202)
\end{aligned}
$$

This subtraction term is again general for all kinematic configurations given the appropriate antenna functions and phase space maps are used. The form of $\bar{\boldsymbol{J}}^{(1)}_3$ can be understood by considering a simple pole cancellation argument. Using the KLN theorem, the explicit poles of a three-parton one-loop physical matrix element constituting a physical cross section cancel against the explicit poles of the four-parton

real radiative correction to the three-parton Born process, after analytic integration over the single unresolved phase space. The three-parton one-loop antenna function is constructed from a one-loop physical matrix element as shown in (2.35). Consider the three-parton one-loop matrix element, used to define the one-loop antenna, as the one-loop correction to a three-parton Born antenna matrix element. Then the tree-level four-parton antenna is the corresponding single real emission correction to the Born-level process. As such, when the four parton antenna function is integrated over all single unresolved regions of phase space, its explicit ϵ poles should cancel against the explicit poles contained in the three-parton one-loop matrix element contributing to the three-parton one-loop antenna function.

The four-parton antenna functions contribute to the double real subtraction term but are not re-introduced to the real-virtual subtraction term because they are integrated over the double unresolved antenna phase space. The quantities needed to generate the $\bar{\boldsymbol{J}}_3^{(1)}$ term contain all the implicit single unresolved divergence of the four-parton antennae and are integrated over the single unresolved antenna phase space to be re-introduced at the real virtual level. This is precisely the definition of the double real subtraction terms collected in $\mathrm{d}\hat{\sigma}_{NNLO}^{S,b_2}$. Integrating this collection of terms over the single unresolved phase space associated with the primary antenna generates a string of integrated antenna functions factoring onto a common secondary unintegrated antenna and a common reduced matrix element[3]. This string of integrated antenna functions will partially cancel the explicit poles of the one-loop antenna.

The other ingredient to the three-parton one-loop antenna is the piece involving the product of a one-loop two-parton reduced matrix element and a three-parton tree-level antenna function, as shown in (2.35). The poles of the ratio of the two-parton one-loop matrix element and the two-parton tree-level matrix element are

---

[3]If the four-parton antenna factors onto different remnant three-parton antennae in different single unresolved limits then several strings will be generated, each of which will match a necessary one-loop three-parton antenna term in the real-virtual subtraction term. The matrix elements will be common to all terms as the original four-parton antenna only factors onto a single matrix element by construction.

given by the poles of the two-parton one-loop antenna functions. The two-parton one-loop antenna functions are presented explicitly in [32] for the final-final configuration, the poles of which are related to the integrated three-parton tree-level antennae. Although not explicitly presented in the literature, the poles of the initial-final and initial-initial two-parton one-loop antennae can be derived from the poles of the integrated three-parton tree-level antennae for the relevant configuration. Using these relations the finite pieces of the initial-final and initial-initial two-parton one-loop antennae need never be calculated as the two-parton one-loop antenna can be systematically replaced with integrated three-parton tree-level antennae for the purposes of subtraction, the finite pieces of which are documented for all kinematic configurations.

When considering initial-final and initial-initial configurations the pole cancellation argument above must be modified for mass factorization terms. As an unintegrated antenna, X_3^1, contains no explicit initial-state collinear poles, whereas the four-parton tree-level matrix elements integrated over the single unresolved phase space will in general contain such poles. This is clear from the form of the terms originating in $\int_1 \mathrm{d}\hat{\sigma}_{NNLO}^{S,b_2}$, some of which will be initial-final or initial-initial integrated antennae containing initial-state collinear poles. For the pole cancellation argument to hold in these configurations the appropriate mass factorization terms should be included, in this case a contribution of the form $\mathrm{d}\hat{\sigma}_{NLO}^{MF}$ for any initial-state partons contained in the Born-level three parton antenna. These terms cannot be derived from the NNLO real-virtual mass factorization contribution and so are put in temporarily in the knowledge that in principle they must cancel elsewhere. Putting in these terms and combining them with the integrated antennae from $\mathrm{d}\hat{\sigma}_{NNLO}^{S,b_2}$ generates an integrated antenna string $\boldsymbol{J}_3^{(1)}$ which completely cancels the ϵ poles of the one-loop three-parton matrix element contained in X_3^1.

The second pole cancellation argument which was made for the final-final case was that by a similar argument the poles of the one-loop two parton antenna are related to the poles of the integrated tree-level three-parton antenna. In the initial-final and initial-initial configurations this argument is again modified to include a mass factorization contribution for any initial-state partons in the Born-level pro-

cess. The mass factorization terms introduced when writing the one-loop two-parton antenna in terms of an integrated tree-level three-parton antenna exactly cancel the mass factorization terms introduced by hand to remove the initial-state collinear poles of the integrated antennas coming from $\int_1 d\hat{\sigma}_{NNLO}^{S,b_2}$. This somewhat lengthy argument can be summarised in the following way,

$$\mathcal{P}oles\big[\bar{\boldsymbol{J}}_3^{(1)}\big] = \mathcal{P}oles\big[\boldsymbol{J}_3^{(1)} + \mathcal{X}_2^1\big] = \mathcal{P}oles\bigg[\sum_j \mathcal{X}_3^0 - \frac{1}{\mathcal{S}}\mathcal{X}_3^0\bigg], \qquad (2.203)$$

where S is a symmetry factor relating the poles of $\mathcal{X}_2^1$ and the final-state singularities of $\mathcal{X}_3^0$.

The terms in $\int_1 d\hat{\sigma}_{NNLO}^{T,b_2}$ proportional to the one-loop antenna are introduced in the real-virtual subtraction term and so must contribute to the double virtual subtraction term upon integration over the single unresolved phase space. The term proportional to $\bar{\boldsymbol{J}}_3^{(1)}$ contains integrated antennae inherited from the double real which terminate in the real-virtual whereas the integrated two-parton one-loop antenna, re-written as an integrated three-parton tree-level antenna, is introduced by hand in the real-virtual and is therefore passed down to the double virtual level. $\bar{\boldsymbol{J}}_3^{(1)}$ itself contains no initial-state collinear poles, and therefore upon integration the double virtual subtraction term inherits the initial-state collinear poles contained in the $\mathcal{X}_3^0$ terms passed down to it.

One-loop renormalisation subtraction term, $d\hat{\sigma}_{NNLO}^{T,b_3}$

When introducing one-loop quantities it is important to ensure they are properly renormalized to guarantee a complete cancellation of explicit poles. In the real-virtual subtraction term two one-loop quantities are introduced: the one-loop reduced matrix elements in (2.201) and the one-loop antenna functions in (2.202). The one-loop matrix elements are renormalised at the renormalisation scale μ^2 whereas the one-loop antenna is renormalised at the mass scale of the antenna s_{ijk}. To account for the effect of renormalisation the substitution is made,

$$X_3^1(i,j,k) \quad \rightarrow \quad X_3^1(i,j,k) + \frac{\beta_0}{\epsilon} C(\epsilon) X_3^0(i,j,k) \left(\left(\frac{s_{ijk}}{\mu^2}\right)^{-\epsilon} - 1\right) \quad (2.204)$$

The systematic inclusion of these terms requires that for each one loop antenna (whose pole structure is proportional to a tree-level antenna) used in the real-virtual

subtraction term a compensating term proportional to β_0 is generated such that a block of subtraction terms is generated of the form,

$$
\begin{aligned}
\mathrm{d}\hat{\sigma}_{NNLO}^{T,b_3} = {} & \mathcal{N}^{RV} \sum_{n+1} \int \frac{\mathrm{d}x_1}{x_1} \frac{\mathrm{d}x_2}{x_2} \, \mathrm{d}\Phi_{n+1}(k_1,\ldots,k_{n+1};p_1,p_2) \frac{1}{S_{n+1}} \\
& \times \sum_j \beta_0 \log\left(\frac{\mu^2}{|s_{ijk}|}\right) X_3^0(i,j,k)\delta(1-x_1)\delta(1-x_2) \\
& \times M_{n+2}^0(k_1,\ldots,k_n;p_1,p_2) \, J_n^{(n)}(\{k_n\}),
\end{aligned}
\tag{2.205}
$$

where the sum mirrors that of (2.202). The colour decomposition of β_0 into b_0 and b_{0,N_F} dictates to which orders in the colour decomposition these terms contribute. The terms in $\mathrm{d}\hat{\sigma}_{NNLO}^{T,b_3}$ originate in the real-virtual subtraction term and so are reintroduced to the double virtual subtraction term when the unintegrated antenna in (2.205) is integrated over the single unresolved antenna phase space.

Integrated almost colour connected subtraction term, $\mathrm{d}\hat{\sigma}_{NNLO}^{T,c}$

The final term which contributes to the real-virtual subtraction term is mostly derived from the analytic integration of $\mathrm{d}\hat{\sigma}_{NNLO}^{S,c}$ over the single unresolved antenna phase space with additional predictable terms to ensure an IR finite contribution.

After integrating out the unresolved parton of the primary antennae in $\mathrm{d}\hat{\sigma}_{NNLO}^{S,c}$ the secondary antennae map onto the same function and can be factored out as a common function for the block at the real-virtual level. Factoring on to this antenna are the three integrated antenna functions and six integrated soft antennae inherited from $\mathrm{d}\hat{\sigma}_{NNLO}^{S,c}$. In order to remove the explicit poles of this combination three additional integrated antennae matching the flavours of those passed down from $\mathrm{d}\hat{\sigma}_{NNLO}^{S,c}$ are introduced. The arguments of these antennae are given by the arguments of their twin terms after these momenta have undergone an additional mapping dictated by the secondary antenna in $\mathrm{d}\hat{\sigma}_{NNLO}^{S,c}$. This choice of arguments ensures that when the secondary antenna contains a divergence the arguments of the integrated antennae map onto each other exactly, causing the difference of integrated antennae to cancel and ensuring the block as a whole does not introduce implicit IR divergent behaviour. The block is then free from explicit poles and divergent behaviour, and so gives a finite contribution at the real-virtual level. For the example

configuration already discussed in the context of $d\hat{\sigma}_{NNLO}^{S,c}$ shown in (2.191), the following block is constructed,

$$
\begin{aligned}
d\hat{\sigma}_{NNLO}^{T,c} &= -\mathcal{N}^{RV} \sum_{n+1} \int \frac{dx_1}{x_1} \frac{dx_2}{x_2} \, d\Phi_{n+1}(k_1, \ldots, k_{n+1}; p_1, p_2) \, \frac{1}{S_{n+1}} \Bigg\{ \\
&\quad \frac{1}{2} \sum_j \Bigg[\bigg(\Big(\mathcal{X}_3^0(s_{ik}) - \mathcal{X}_3^0(s_{(ij)(jk)}) \Big) \\
&\quad - \Big(\mathcal{X}_3^0(s_{ai}) - \mathcal{X}_3^0(s_{a(ij)}) \Big) - \Big(\mathcal{X}_3^0(s_{kb}) - \mathcal{X}_3^0(s_{(kj)b}) \Big) \bigg) \\
&\quad - \bigg(\Big(\mathcal{S}(s_{ik}, s_{ik}, 1) - \mathcal{S}(s_{(ij)(jk)} s_{ik}, x_{(ij)(jk),ik}) \Big) \\
&\quad - \Big(\mathcal{S}(s_{ai}, s_{ik}, x_{ai,ik}) - \mathcal{S}(s_{a(ij)}, s_{ik}, x_{a(ij),ik}) \Big) \\
&\quad - \Big(\mathcal{S}(s_{kb}, s_{ik}, x_{kb,ik}) - \mathcal{S}(s_{(kj)b}, s_{ik}, x_{(kj)b,ik}) \Big) \bigg) \delta(1-x_1)\delta(1-x_2) \Bigg] \Bigg\} \\
&\quad \times \ X_3^0(i,j,k) \ M_{n+2}^0(k_1, \ldots, k_n; p_1, p_2) \ J_n^{(n)}(\{k_n\}). \quad (2.206)
\end{aligned}
$$

To achieve a finite block, three integrated antennae were introduced which after analytic integration over the secondary antenna must be reintroduced at the double virtual level. All other terms inherited from the double real subtraction term terminate at the real-virtual level.

2.6.4 Double virtual subtraction term structure

The double virtual contribution to the $pp \to n$-jet cross section involves the two-loop $(n+2)$-parton matrix elements which have no implicit IR divergence in any regions of the appropriate n-parton phase space. Using the subtraction terms defined in previous sections to remove all implicit IR divergence at the double real and real-virtual levels of the calculation, all that remains is to reintroduce the integrated forms of the appropriate terms to cancel the explicit IR poles of the two-loop contribution.

NNLO double virtual mass factorization terms

Using the symbolic notation of section 1.4, the NNLO mass factorization term is written in the form,

$$
\begin{aligned}
d\boldsymbol{\sigma}_{NNLO}^{MF} &= -\Bigg[\boldsymbol{\Gamma}^2 \cdot d\boldsymbol{\sigma}_{LO} \cdot \boldsymbol{I} + \boldsymbol{I} \cdot d\boldsymbol{\sigma}_{LO} \cdot \boldsymbol{\Gamma}^2 - \big[\boldsymbol{\Gamma}^1 \otimes \boldsymbol{\Gamma}^1 \big] \cdot d\boldsymbol{\sigma}_{LO} \cdot \boldsymbol{I} \\
&\quad - \boldsymbol{I} \cdot d\boldsymbol{\sigma}_{LO} \cdot \big[\boldsymbol{\Gamma}^1 \otimes \boldsymbol{\Gamma}^1 \big] - \boldsymbol{\Gamma}^1 \cdot d\boldsymbol{\sigma}_{LO} \cdot \boldsymbol{\Gamma}^1
\end{aligned}
$$

$$+ \, \boldsymbol{\Gamma}^1 \cdot \mathrm{d}\boldsymbol{\sigma}_{NLO} \cdot \boldsymbol{I} + \boldsymbol{I} \cdot \mathrm{d}\boldsymbol{\sigma}_{NLO} \cdot \boldsymbol{\Gamma}^1 \bigg]. \tag{2.207}$$

It was shown in section 2.6.3 that the unfactorized NLO cross section can be written in the form,

$$\mathrm{d}\boldsymbol{\sigma}_{NLO} \;\; = \;\; \underbrace{\left[\mathrm{d}\boldsymbol{\sigma}_{NLO}^R - \mathrm{d}\boldsymbol{\sigma}_{NLO}^S \right]}_{(n+3)\text{-parton}} + \underbrace{\mathrm{d}\boldsymbol{\sigma}_{NLO}^V + \int_1 \mathrm{d}\boldsymbol{\sigma}_{NLO}^S}_{(n+2)\text{-parton}} \tag{2.208}$$

The terms proportional to the $(n+3)$-parton contributions are used to construct the NNLO real-virtual mass factorization terms, $\mathrm{d}\boldsymbol{\sigma}_{NNLO}^{MF,RV}$, as discussed in section 2.6.3. The remainder of (2.207) then depends on the $(n+2)$-parton momentum set and is used to construct the NNLO double virtual mass factorization contributions. The double virtual mass factorization terms can be divided into two contributions,

$$\mathrm{d}\boldsymbol{\sigma}_{NNLO}^{MF,VV} \;\; = \;\; \mathrm{d}\boldsymbol{\sigma}_{NNLO}^{MF,VV,a} + \mathrm{d}\boldsymbol{\sigma}_{NNLO}^{MF,VV,b}. \tag{2.209}$$

The first term is proportional to the NLO virtual cross section,

$$\mathrm{d}\boldsymbol{\sigma}_{NNLO}^{MF,VV,a} \;\; = \;\; -\boldsymbol{\Gamma}^1 \cdot \mathrm{d}\boldsymbol{\sigma}_{NLO}^V \cdot \boldsymbol{I} - \boldsymbol{I} \cdot \mathrm{d}\boldsymbol{\sigma}_{NLO}^V \cdot \boldsymbol{\Gamma}^1. \tag{2.210}$$

These terms are kept together because they contain mass factorization terms proportional to the one-loop matrix elements and will be naturally grouped with the terms proportional to the one-loop matrix elements inherited from the real-virtual subtraction term upon integration. The second term is proportional to the leading order cross section or the integrated subtraction term, both of which are proportional to the tree-level $(n+2)$-parton matrix elements,

$$\begin{aligned}
\mathrm{d}\boldsymbol{\sigma}_{NNLO}^{MF,VV,b} \;\; = \;\; & -\left[\boldsymbol{\Gamma}^2 - \left[\boldsymbol{\Gamma}^1 \otimes \boldsymbol{\Gamma}^1 \right] \right] \cdot \mathrm{d}\boldsymbol{\sigma}_{LO} \cdot \boldsymbol{I} - \boldsymbol{I} \cdot \mathrm{d}\boldsymbol{\sigma}_{LO} \cdot \left[\boldsymbol{\Gamma}^2 - \left[\boldsymbol{\Gamma}^1 \otimes \boldsymbol{\Gamma}^1 \right] \right] \\
& + \boldsymbol{\Gamma}^1 \cdot \mathrm{d}\boldsymbol{\sigma}_{LO} \cdot \boldsymbol{\Gamma}^1 \\
& - \boldsymbol{\Gamma}^1 \cdot \left(\int_1 \mathrm{d}\boldsymbol{\sigma}_{NLO}^S \right) \cdot \boldsymbol{I} - \boldsymbol{I} \cdot \left(\int_1 \mathrm{d}\boldsymbol{\sigma}_{NLO}^S \right) \cdot \boldsymbol{\Gamma}^1.
\end{aligned} \tag{2.211}$$

Following the discussion in section 2.5 the integrated NLO subtraction term is proportional to a string of integrated antenna functions factoring onto a common matrix element. During a full NLO computation the integrated antennae are combined with the mass factorization contributions to generate integrated antenna strings, $\boldsymbol{J}_{n+2}^{(1)}$.

The NLO cross section contributing to the NNLO mass factorization terms is the unfactorized cross section so the integrated subtraction term in (2.211) is just given by the sum of integrated antennae, not a full $\boldsymbol{J}_{n+2}^{(1)}$. The sum of integrated antennae without the mass factorization kernels is denoted by $\mathcal{Y}$ such that,

$$\mathcal{Y} \;=\; \boldsymbol{J}_{n+2}^{(1)} + \boldsymbol{\Gamma}^1(x_1) + \boldsymbol{\Gamma}^1(x_2). \tag{2.212}$$

Using this definition and the notation $\boldsymbol{\Gamma}^1(x_1) = \boldsymbol{\Gamma}_1^1$, $\boldsymbol{\Gamma}^1(x_2) = \boldsymbol{\Gamma}_2^1$, $\boldsymbol{\Gamma}^2(x_1) = \boldsymbol{\Gamma}_1^2$, $\boldsymbol{\Gamma}^2(x_2) = \boldsymbol{\Gamma}_2^2$, the following relation can be derived,

$$
\begin{aligned}
\frac{1}{2}\boldsymbol{J}_{n+2}^{(1)} \otimes \boldsymbol{J}_{n+2}^{(1)} \;=\;& \frac{1}{2}\mathcal{Y} \otimes \mathcal{Y} - \mathcal{Y} \otimes \boldsymbol{\Gamma}_1^1 - \mathcal{Y} \otimes \boldsymbol{\Gamma}_2^1 \\
&+ \frac{1}{2}\boldsymbol{\Gamma}_1^1 \otimes \boldsymbol{\Gamma}_1^1 + \frac{1}{2}\boldsymbol{\Gamma}_2^1 \otimes \boldsymbol{\Gamma}_2^1 + \boldsymbol{\Gamma}_1^1 \boldsymbol{\Gamma}_2^1.
\end{aligned} \tag{2.213}
$$

Noticing that many of these terms are also present in the NNLO mass factorization contribution allows (2.211) to be re-written in the form,

$$
\begin{aligned}
\mathrm{d}\boldsymbol{\sigma}_{NNLO}^{MF,VV,b} \;=\;& \left(-\boldsymbol{\Gamma}_1^2 - \boldsymbol{\Gamma}_2^2 + \frac{1}{2}\boldsymbol{J}_{n+2}^{(1)} \otimes \boldsymbol{J}_{n+2}^{(1)} - \frac{1}{2}\mathcal{Y} \otimes \mathcal{Y} \right. \\
&\left. + \frac{1}{2}\boldsymbol{\Gamma}_1^1 \otimes \boldsymbol{\Gamma}_1^1 + \frac{1}{2}\boldsymbol{\Gamma}_2^1 \otimes \boldsymbol{\Gamma}_2^1 \right) \mathrm{d}\boldsymbol{\sigma}_{LO}
\end{aligned} \tag{2.214}
$$

This formula can be trivially partitioned into two terms, $\mathrm{d}\boldsymbol{\sigma}_{NNLO}^{MF,VV,b} = \mathrm{d}\boldsymbol{\sigma}_{NNLO}^{MF,VV,b_1} + \mathrm{d}\boldsymbol{\sigma}_{NNLO}^{MF,VV,b_2}$, such that,

$$
\begin{aligned}
\mathrm{d}\boldsymbol{\sigma}_{NNLO}^{MF,VV,b_1} \;=\;& \frac{1}{2}\boldsymbol{J}_{n+2}^{(1)} \otimes \boldsymbol{J}_{n+2}^{(1)} \, \mathrm{d}\boldsymbol{\sigma}_{LO}, \\
\mathrm{d}\boldsymbol{\sigma}_{NNLO}^{MF,VV,b_2} \;=\;& \left(-\boldsymbol{\Gamma}_1^2 - \boldsymbol{\Gamma}_2^2 - \frac{1}{2}\mathcal{Y} \otimes \mathcal{Y} + \frac{1}{2}\boldsymbol{\Gamma}_1^1 \otimes \boldsymbol{\Gamma}_1^1 + \frac{1}{2}\boldsymbol{\Gamma}_2^1 \otimes \boldsymbol{\Gamma}_2^1 \right) \mathrm{d}\boldsymbol{\sigma}_{LO}.
\end{aligned} \tag{2.215}
$$

One-loop matrix element contribution

The first term to be integrated comes from $\mathrm{d}\sigma_{NNLO}^{T,b_1}$ and is the collection of terms proportional to the one-loop matrix element. It should be noted that the mass factorization term $\mathrm{d}\boldsymbol{\sigma}_{NNLO}^{MF,VV,a}$ is proportional to the renormalized virtual cross section. Accordingly the one-loop matrix element should be renormalized by making the substitution,

$$M_{n+2}^1 \to M_{n+2}^1 - \frac{\beta_0}{\epsilon}C(\epsilon)M_{n+2}^0. \tag{2.216}$$

This substitution generates an additional β_0-dependent mass factorization term,

$$\mathrm{d}\boldsymbol{\sigma}_{NNLO}^{MF,VV,a} \to \mathrm{d}\boldsymbol{\sigma}_{NNLO}^{MF,VV,a_1} + \mathrm{d}\boldsymbol{\sigma}_{NNLO}^{MF,VV,a_2}, \tag{2.217}$$

where $\mathrm{d}\boldsymbol{\sigma}_{NNLO}^{MF,VV,a_1}$ has the same form as the un-renormalized $\mathrm{d}\boldsymbol{\sigma}_{NNLO}^{MF,VV,a}$ and $\mathrm{d}\boldsymbol{\sigma}_{NNLO}^{MF,VV,a_2}$ has the form,

$$\mathrm{d}\boldsymbol{\sigma}_{NNLO}^{MF,VV,a_2} = -\frac{\beta_0}{\epsilon} \, \mathrm{d}\boldsymbol{\sigma}_{NLO}^{MF} \tag{2.218}$$

Upon integration, the sum of integrated three-parton tree-level antennae combined with the mass factorization contribution from $\mathrm{d}\boldsymbol{\sigma}_{NNLO}^{MF,VV,a_1}$, generates an integrated antenna string factoring onto a one-loop $(n+2)$-parton matrix element,

$$\mathrm{d}\sigma_{NNLO}^{U,a_1} = -\mathcal{N}^{VV} \sum_n \int \frac{\mathrm{d}z_1}{z_1} \frac{\mathrm{d}z_2}{z_2} \, \mathrm{d}\Phi_n(k_1, \ldots, k_n; p_1, p_2) \frac{1}{S_n}$$
$$\boldsymbol{J}_{n+2}^{(1)}(1, \cdots, n+2) \, M_{n+2}^1(k_1, \ldots, k_n; p_1, p_2) \, J_n^{(n)}(\{k_n\}) \tag{2.219}$$

Integrated β_0 contribution

Integrating the terms in $\mathrm{d}\sigma_{NNLO}^{T,b_3}$ generates a contribution to the double virtual of the form,

$$\mathrm{d}\sigma_{NNLO}^{U,b} = -\mathcal{N}^{VV} \sum_n \int \frac{\mathrm{d}z_1}{z_1} \frac{\mathrm{d}z_2}{z_2} \, \mathrm{d}\Phi_n(k_1, \ldots, k_n; p_1, p_2) \frac{1}{S_n}$$
$$\sum_{\{i,j\}} \frac{\beta_0}{\epsilon} \left(\left(\frac{s_{ij}}{\mu^2} \right)^{-\epsilon} - 1 \right) \mathcal{X}_3^0(s_{ij}) \, M_{n+2}^0(k_1, \ldots, k_n; p_1, p_2) \, J_n^{(n)}(\{k_n\}).$$
$$\tag{2.220}$$

Splitting the bracket in two and combining the second term with $\mathrm{d}\sigma_{NNLO}^{MF,VV,a_2}$ yields,

$$\mathrm{d}\sigma_{NNLO}^{U,b_1} = \mathcal{N}^{VV} \sum_n \int \frac{\mathrm{d}z_1}{z_1} \frac{\mathrm{d}z_2}{z_2} \, \mathrm{d}\Phi_n(k_1, \ldots, k_n; p_1, p_2) \frac{1}{S_n}$$
$$\frac{\beta_0}{\epsilon} \, \boldsymbol{J}_{n+2}^{(1)}(1, \cdots, n+2) \, M_{n+2}^0(k_1, \ldots, k_n; p_1, p_2) \, J_n^{(n)}(\{k_n\}).$$
$$\tag{2.221}$$

The other term is given by,

$$\mathrm{d}\sigma_{NNLO}^{U,b_2} = -\mathcal{N}^{VV} \sum_n \int \frac{\mathrm{d}z_1}{z_1} \frac{\mathrm{d}z_2}{z_2} \, \mathrm{d}\Phi_n(k_1, \ldots, k_n; p_1, p_2) \frac{1}{S_n}$$

$$\sum_{\{ij\}} \frac{\beta_0}{\epsilon} \left(\frac{s_{ij}}{\mu^2}\right)^{-\epsilon} \mathcal{X}_3^0(s_{ij}) \, M_{n+2}^0(k_1, \ldots, k_n; p_1, p_2) \, J_n^{(n)}(\{k_n\}).$$

$$(2.222)$$

At this point is possible to define a piece of the double virtual subtraction term as,

$$
\begin{aligned}
\mathrm{d}\sigma_{NNLO}^{U,A} &= \mathrm{d}\sigma_{NNLO}^{U,a_1} + \mathrm{d}\sigma_{NNLO}^{U,b_1}, \\
&= -\mathcal{N}^{VV} \sum_n \int \frac{\mathrm{d}z_1}{z_1} \frac{\mathrm{d}z_2}{z_2} \, \mathrm{d}\Phi_n(k_1, \ldots, k_n; p_1, p_2) \, \frac{1}{S_n} \left\{ \boldsymbol{J}_{n+2}^{(1)}(1, \cdots, n+2) \right. \\
&\quad \times \left. \left(M_{n+2}^1(k_1, \ldots, k_n; p_1, p_2) - \frac{\beta_0}{\epsilon} M_{n+2}^0(k_1, \ldots, k_n; p_1, p_2) \right) J_n^{(n)}(\{k_n\}) \right\}.
\end{aligned}
$$

$$(2.223)$$

Recalling that the poles of the integrated antenna string are simply related to the poles of Catani's one-loop insertion operator, this contribution to the double virtual cross section contains the pole structure given in the first line of Catani's two-loop factorization formula presented in (1.82).

It is important to note that $\mathrm{d}\sigma_{NNLO}^{U,A}$ does not contain precisely the same poles as the first line of Catani's formula because the difference between $\boldsymbol{J}_n^{(1)}$ and $\boldsymbol{I}_n^{(1)}$ formally of the order ϵ^0. At NLO the poles of the one loop matrix element can be written in terms of an integrated antenna string, the poles of which match the poles of the insertion operator precisely as both quantities factor into a tree-level $\mathcal{O}(\epsilon^0)$ matrix element. At NNLO this is no longer always true as can be seen in the definition of $\mathrm{d}\sigma_{NNLO}^{U,A}$ where both the one-loop matrix element and the factor of β_0/ϵ cause the $\mathcal{O}(\epsilon^0)$ and $\mathcal{O}(\epsilon)$ difference between $\boldsymbol{J}_n^{(1)}$ and $\boldsymbol{I}_n^{(1)}$ to give additional singular contributions. Given these considerations, the pole structure of $\boldsymbol{J}_n^{(1)}$ contains the pole structure of $\boldsymbol{I}_n^{(1)}$, but also receives additional singular contributions which are expected to cancel against similar contributions arising elsewhere in the double virtual subtraction term.

The mass factorization contribution, $\mathrm{d}\boldsymbol{\sigma}_{NNLO}^{MF,VV,b_1}$ is free from initial-state collinear poles and can be systematically isolated to form a contribution to the double virtual subtraction term by itself.

$$\mathrm{d}\hat{\sigma}_{NNLO}^{U,B} = -\mathcal{N}^{VV} \sum_n \int \frac{\mathrm{d}z_1}{z_1} \frac{\mathrm{d}z_2}{z_2} \, \mathrm{d}\Phi_n(k_1, \ldots, k_n; p_1, p_2) \, \frac{1}{S_n}$$

$$\times \quad \frac{1}{2} \boldsymbol{J}_{n+2}^{(1)}(1, \cdots, n+2) \otimes \boldsymbol{J}_{n+2}^{(1)}(1, \cdots, n+2)$$

$$\times \quad M_{n+2}^0(k_1, \ldots, k_n; p_1, p_2) \, J_n^{(n)}(\{k_n\}). \tag{2.224}$$

It is easily seen that this expression contains the pole structure of the second line in (1.82), with additional singular contributions arising from the differences between $\boldsymbol{J}_n^{(1)}$ and $\boldsymbol{I}_n^{(1)}$ at $\mathcal{O}(\epsilon^0)$ and higher orders.

Integrated one-loop antenna contribution

Integrating the term proportional to the one-loop antenna function in $d\sigma_{NNLO}^{T,b_2}$ generates the following term in the double virtual subtraction term,

$$
\begin{aligned}
d\sigma_{NNLO}^{U,c_1} \quad = \quad & -\mathcal{N}^{VV} \sum_n \int \frac{dz_1}{z_1} \frac{dz_2}{z_2} \, d\Phi_n(k_1, \ldots, k_n; p_1, p_2) \, \frac{1}{S_n} \\
& \sum_{\{ij\}} \mathcal{X}_3^1(s_{ij}) \, M_{n+2}^0(k_1, \ldots, k_n; p_1, p_2) \, J_n^{(n)}(\{k_n\}). \tag{2.225}
\end{aligned}
$$

It is noted that upon integration the antennae which generate β_0 terms in the real-virtual subtraction have a pole piece of the form,

$$\mathcal{P}oles\big[\mathcal{X}_3^1(s_{ij})\big] \quad = \quad \cdots - \frac{\beta_0}{\epsilon}\left(\frac{s_{ij}}{\mu^2}\right)^{-\epsilon} \mathcal{X}_3^0(s_{ij}). \tag{2.226}$$

It can therefore be shown that by summing the contributions, $d\sigma_{NNLO}^{U,c_1}$ and $d\sigma_{NNLO}^{U,b_2}$ the poles associated with renormalizing the one-loop antenna are systematically removed by the remainder of the integrated β_0 terms.

Integrated double real contribution

The double virtual subtraction term also receives contributions from terms in the double real subtraction term upon integration, specifically the four-parton antenna terms and the colour disconnected contribution. Integrating the four-parton antenna terms yields the contribution to the double virtual cross section given by,

$$
\begin{aligned}
d\hat{\sigma}_{NNLO}^{U,d_1} \quad = \quad & -\mathcal{N}^{VV} \sum_n \int \frac{dz_1}{z_1} \frac{dz_2}{z_2} \, d\Phi_n(k_1, \ldots, k_n; p_1, p_2) \, \frac{1}{S_n} \\
& \times \sum_{\{i,j\}} \mathcal{X}_4^0(s_{ij}) \, M_{n+2}^0(k_1, \ldots, k_n; p_1, p_2) \, J_n^{(n)}(\{k_n\}) \tag{2.227}
\end{aligned}
$$

The colour disconnected subtraction term is integrated over the unresolved phase space of both three-parton antenna and generates the double virtual term,

$$
\begin{aligned}
\mathrm{d}\hat{\sigma}_{NNLO}^{U,d_2} &= \mathcal{N}^{VV} \sum_n \int \frac{\mathrm{d}z_1}{z_1} \frac{\mathrm{d}z_2}{z_2} \, \mathrm{d}\Phi_n(k_1,\ldots,k_n;p_1,p_2) \, \frac{1}{S_n} \\
&\times \sum_{\{i,j\},\{k,l\}} \mathcal{X}_3^0(s_{ij}) \, \mathcal{X}_3^0(s_{kl}) \, M_{n+2}^0(k_1,\ldots,k_n;p_1,p_2) \, J_n^{(n)}(\{k_n\})
\end{aligned}
$$

(2.228)

where the sum runs over non-overlapping sets of colour-connected partons in the $(n+2)$-parton ordering.

Integrated almost colour connected contribution

Integrating the almost colour connected subtraction term generates products of integrated antenna functions. If two antenna have arguments which are the same colour connected partons i,j, then the product is denoted $\mathcal{X}_3^0(s_{ij}) \otimes \mathcal{X}_3^0(s_{ij})$. If the integrated antennae share a common parton j, the almost colour connected product is denoted $\mathcal{X}_3^0(s_{ij}) \otimes \mathcal{X}_3^0(s_{jk})$. The integral of the terms in $\mathrm{d}\hat{\sigma}_{NNLO}^{T,c}$ which contribute to the double virtual subtraction term has the form,

$$
\begin{aligned}
\mathrm{d}\hat{\sigma}_{NNLO}^{U,e} &= \mathcal{N}^{VV} \sum_n \int \frac{\mathrm{d}z_1}{z_1} \frac{\mathrm{d}z_2}{z_2} \, \mathrm{d}\Phi_n(k_1,\ldots,k_n;p_1,p_2) \, \frac{1}{S_n} \\
&\times \left(-\frac{1}{2} \sum_{\{i,j\}} [\mathcal{X}_3^0(s_{ij}) \otimes \mathcal{X}_3^0(s_{ij})] + \sum_{\{i,j\},\{j,k\}} [\mathcal{X}_3^0(s_{ij}) \otimes \mathcal{X}_3^0(s_{jk})] \right) \\
&\times M_{n+2}^0(k_1,\ldots,k_n;p_1,p_2) \, J_n^{(n)}(\{k_n\}).
\end{aligned}
$$

(2.229)

It can be shown that,

$$
\begin{aligned}
\frac{1}{2}\mathcal{Y} \otimes \mathcal{Y} &= \frac{1}{2} \sum_{\{i,j\}} \mathcal{X}_3^0(s_{ij}) \otimes \mathcal{X}_3^0(s_{ij}) + \sum_{\{i,j\},\{j,k\}} \mathcal{X}_3^0(s_{ij}) \otimes \mathcal{X}_3^0(s_{jk}) \\
&+ \sum_{\{i,j\},\{k,l\}} \mathcal{X}_3^0(s_{ij}) \, \mathcal{X}_3^0(s_{kl}),
\end{aligned}
$$

(2.230)

and so,

$$
\begin{aligned}
\mathrm{d}\hat{\sigma}_{NNLO}^{U,e} + \mathrm{d}\hat{\sigma}_{NNLO}^{U,d_2} &= \mathcal{N}^{VV} \sum_n \int \frac{\mathrm{d}z_1}{z_1} \frac{\mathrm{d}z_2}{z_2} \, \mathrm{d}\Phi_n(k_1,\ldots,k_n;p_1,p_2) \, \frac{1}{S_n} \\
&\times \left(\frac{1}{2}\mathcal{Y} \otimes \mathcal{Y} - \sum_{\{i,j\}} \mathcal{X}_3^0(s_{ij}) \otimes \mathcal{X}_3^0(s_{ij}) \right) \\
&\times M_{n+2}^0(k_1,\ldots,k_n;p_1,p_2) \, J_n^{(n)}(\{k_n\}).
\end{aligned}
$$

(2.231)

$\mathcal{X}$	$\mathcal{A}$	$\mathcal{D}$	$\mathcal{E}$	$\mathcal{F}$	$\mathcal{G}$
$\mathcal{S}_{FF}$	1	1	1	3/2	1/2
$\mathcal{S}_{IF}$	1	1, 1/2	1	1	1/2
$\mathcal{S}_{II}$	1	1/2	$\oslash$	1/2	$\oslash$

Table 2.5: The various symmetry factors needed when translating between $\mathcal{X}_2^1$ and $\mathcal{X}_3^0$ terms. Initial-final and initial-initial antennae may contain different singularities depending on the initial-state partons. The two values for the initial-final $\mathcal{D}$ antenna reflect the quark and gluon initiated antennae respectively. The integrated antennae with no final-state singularities are omitted from this table.

Remaining integrated terms

Only two terms remain to be integrated, both from the real-virtual contribution. The first is the remaining term which is inherited from the real-virtual subtraction term $d\hat{\sigma}_{NNLO}^{T,b_2}$. This term is proportional to a symmetry factor $\mathcal{S}$ which relates the poles of the two-parton one-loop antenna function and the final-state poles of the integrated three-parton antenna. The different values of $\mathcal{S}$ are listed in table 2.5. The integration of this terms yields,

$$
\begin{aligned}
d\hat{\sigma}_{NNLO}^{U,c_2} &= \mathcal{N}^{VV} \sum_n \int \frac{dz_1}{z_1} \frac{dz_2}{z_2} \, d\Phi_n(k_1,\ldots,k_n;p_1,p_2) \, \frac{1}{S_n} \\
&\times \sum_{\{i,j\}} \frac{1}{\mathcal{S}} \, \mathcal{X}_3^0(s_{ij}) \otimes \mathcal{X}_3^0(s_{ij}) \, M_{n+2}^0(k_1,\ldots,k_n;p_1,p_2) \, J_n^{(n)}(\{k_n\}).
\end{aligned}
$$

(2.232)

The last term to integrate is the remainder from $d\hat{\sigma}_{NNLO}^{T,b_1}$ which in un-integrated form is proportional to $\boldsymbol{J}_{n+2}^{(1)}$. When integrated this term generates the contribution to the double virtual cross section,

$$
\begin{aligned}
d\hat{\sigma}_{NNLO}^{U,a_2} &= -\mathcal{N}^{VV} \sum_n \int \frac{dz_1}{z_1} \frac{dz_2}{z_2} \, d\Phi_n(k_1,\ldots,k_n;p_1,p_2) \, \frac{1}{S_n} \\
&\times \left[\mathcal{Y} \otimes \mathcal{Y} \right] M_{n+2}^0(k_1,\ldots,k_n;p_1,p_2) \, J_n^{(n)}(\{k_n\}).
\end{aligned}
$$

(2.233)

Pulling together the various terms generates the subtraction term,

$$
d\hat{\sigma}_{NNLO}^{U,C} = d\hat{\sigma}_{NNLO}^{U,a_2} + d\hat{\sigma}_{NNLO}^{U,b_2} + d\hat{\sigma}_{NNLO}^{U,c_1} + d\hat{\sigma}_{NNLO}^{U,c_2}
$$

$$+ \quad \mathrm{d}\hat{\sigma}_{NNLO}^{U,d_1} + \mathrm{d}\hat{\sigma}_{NNLO}^{U,d_2} + \mathrm{d}\hat{\sigma}_{NNLO}^{U,e} + \mathrm{d}\hat{\sigma}_{NNLO}^{MF,VV,b_2}. \tag{2.234}$$

Writing this subtraction term explicitly yields the form,

$$
\begin{aligned}
\mathrm{d}\hat{\sigma}_{NNLO}^{U,C} \;=\; & -\mathcal{N}^{VV} \sum_n \int \frac{\mathrm{d}z_1}{z_1} \frac{\mathrm{d}z_2}{z_2} \, \mathrm{d}\Phi_n(k_1,\ldots,k_n;p_1,p_2) \, \frac{1}{S_n} \Bigg\{ \\
& \sum_{\{i,j\}} \left(\mathcal{X}_4^0(s_{ij}) + \mathcal{X}_3^1(s_{ij}) + \frac{\beta_0}{\epsilon}\left(\frac{s_{ij}}{\mu^2}\right)^{-\epsilon} \mathcal{X}_3^0(s_{ij}) \right. \\
& \left. + \left(1 - \frac{1}{\mathcal{S}}\right) \mathcal{X}_3^0(s_{ij}) \otimes \mathcal{X}_3^0(s_{ij}) \right) - \mathbf{\Gamma}_1^2 - \mathbf{\Gamma}_2^2 + \frac{1}{2}\mathbf{\Gamma}_1^1 \otimes \mathbf{\Gamma}_1^1 \\
& + \frac{1}{2}\mathbf{\Gamma}_2^1 \otimes \mathbf{\Gamma}_2^1 \Bigg\} \, M_{n+2}^0(k_1,\ldots,k_n;p_1,p_2) \, J_n^{(n)}(\{k_n\}), \tag{2.235}
\end{aligned}
$$

and it is noted that the $\mathcal{Y} \otimes \mathcal{Y}$ terms cancel in the combination. These terms are used to define the double unresolved integrated antenna string $\boldsymbol{J}_{n+2}^{(2)}$, such that,

$$
\begin{aligned}
\mathrm{d}\hat{\sigma}_{NNLO}^{U,C} \;=\; & -\mathcal{N}^{VV} \sum_n \int \frac{\mathrm{d}z_1}{z_1} \frac{\mathrm{d}z_2}{z_2} \, \mathrm{d}\Phi_n(k_1,\ldots,k_n;p_1,p_2) \, \frac{1}{S_n} \sum_{\{i,j\}} \\
& \boldsymbol{J}_{n+2}^{(2)}(1,\cdots,n+2) \, M_{n+2}^0(k_1,\ldots,k_n;p_1,p_2) \, J_n^{(n)}(\{k_n\}), \tag{2.236}
\end{aligned}
$$

Where the double unresolved integrated antenna string is given by,

$$
\begin{aligned}
\boldsymbol{J}_{n+2}^{(2)}(1,\cdots,n+2) \;=\; & \sum_{\{i,j\}} \left\{ \mathcal{X}_4^0(s_{ij}) + \mathcal{X}_3^1(s_{ij}) + \frac{\beta_0}{\epsilon}\left(\frac{s_{ij}}{\mu^2}\right)^{-\epsilon} \mathcal{X}_3^0(s_{ij}) \right. \\
& + \left. \left(1 - \frac{1}{\mathcal{S}}\right) \mathcal{X}_3^0(s_{ij}) \otimes \mathcal{X}_3^0(s_{ij}) \right\} - \mathbf{\Gamma}^2(x_1) - \mathbf{\Gamma}^2(x_2) \\
& + \frac{1}{2}\left[\mathbf{\Gamma}^1 \otimes \mathbf{\Gamma}^1\right](x_1) + \frac{1}{2}\left[\mathbf{\Gamma}^1 \otimes \mathbf{\Gamma}^1\right](x_2), \tag{2.237}
\end{aligned}
$$

and the sum runs over colour connected pairs of partons in the $(n+2)$-parton ordering. The full double virtual subtraction term is given by the sum of all three contributions,

$$\mathrm{d}\hat{\sigma}_{NNLO}^{U} \;=\; \mathrm{d}\hat{\sigma}_{NNLO}^{U,A} + \mathrm{d}\hat{\sigma}_{NNLO}^{U,B} + \mathrm{d}\hat{\sigma}_{NNLO}^{U,C}, \tag{2.238}$$

which when written in terms of single and double unresolved integrated antenna strings is given by,

$$
\begin{aligned}
\mathrm{d}\hat{\sigma}_{NNLO}^{U} \;=\; & -\mathcal{N}^{VV} \sum_n \int \frac{\mathrm{d}z_1}{z_1} \frac{\mathrm{d}z_2}{z_2} \, \mathrm{d}\Phi_n(k_1,\ldots,k_n;p_1,p_2) \, \frac{1}{S_n} \Bigg\{ \\
& \boldsymbol{J}_{n+2}^{(1)}(1,\cdots,n+2)
\end{aligned}
$$

$$\times \left(M_{n+2}^1(k_1, \ldots, k_n; p_1, p_2) - \frac{\beta_0}{\epsilon} M_{n+2}^0(k_1, \ldots, k_n; p_1, p_2) \right) J_n^{(n)}(\{k_n\})$$

$$+ \left(\frac{1}{2} \boldsymbol{J}_{n+2}^{(1)}(1, \cdots, n+2) \otimes \boldsymbol{J}_{n+2}^{(1)}(1, \cdots, n+2) + \boldsymbol{J}_{n+2}^{(2)}(1, \cdots, n+2) \right)$$

$$\times M_{n+2}^0(k_1, \ldots, k_n; p_1, p_2) \, J_n^{(n)}(\{k_n\}) \Bigg\}. \tag{2.239}$$

The first term in this equation is defined in (2.223) and contains the pole structure of the first line in Catani's two-loop factorization formula (1.82) in addition to a set of predictable additional poles. The second term in (2.239) is defined in (2.224) and similarly contains the poles of the second line in (1.82) in addition to a set of predictable extra singularities. The third term introduces the double unresolved integrated antenna string, $\boldsymbol{J}_{n+2}^{(2)}$, and contains a pole structure expected to contain that of the remainder of (1.82), i.e., the terms proportional to $\boldsymbol{I}_{n+2}^{(1)}(2\epsilon)$ and $\boldsymbol{H}^{(2)}(\epsilon)$ and the additional poles present in the first two lines but absent from Catani's formula.

The form of the subtraction term in (2.239) depends on the number and type of particles in the colour ordering of the various matrix elements across the different levels of the calculation. Implicit in the formulation presented above is the assumption that the scattering process contains colour-connected strings of partons long enough to accommodate almost colour-connected and colour-disconnected double unresolved configurations. This is not always the case, in particular for the calculations presented in chapters 3 and 4 where the longest colour-connected strings of partons contain four partons.

In such a configuration, the first term in (2.239) is unchanged as it is the result of single unresolved limits in the one-loop matrix element and is simply given by a two-parton integrated antenna string. The second term comes from the mass factorization contribution and is similarly unchanged. The only place that the almost colour connected and colour disconnected limits contribute is in the double unresolved integrated antenna string, $\boldsymbol{J}_{n+2}^{(2)}$. In the case of the double real matrix elements not containing these limits, the form of $\boldsymbol{J}_{n+2}^{(2)}$ is modified by omitting the term $\mathrm{d}\hat{\sigma}_{NNLO}^{U,e} + \mathrm{d}\hat{\sigma}_{NNLO}^{U,d_2}$ which contributes to $\mathrm{d}\hat{\sigma}_{NNLO}^{U,C}$. Making this adjustment means that the form of $\boldsymbol{J}_{n+2}^{(2)}$ is modified to reflect the lack of almost colour-connected and

colour disconnected configurations. i.e.,

$$
\begin{aligned}
\boldsymbol{J}_{n+2}^{(2)} \quad \longrightarrow \quad & \sum_{\{i,j\}} \left\{ \mathcal{X}_4^0(s_{ij}) + \mathcal{X}_3^1(s_{ij}) + \frac{\beta_0}{\epsilon} \left(\frac{s_{ij}}{\mu^2} \right)^{-\epsilon} \mathcal{X}_3^0(s_{ij}) - \frac{1}{\mathcal{S}} \mathcal{X}_3^0(s_{ij}) \otimes \mathcal{X}_3^0(s_{ij}) \right\} \\
& - \quad \boldsymbol{\Gamma}_1^2 - \boldsymbol{\Gamma}_2^2 + \frac{1}{2} \left[\boldsymbol{\Gamma}_1^1 \otimes \boldsymbol{\Gamma}_1^1 \right] + \frac{1}{2} \left[\boldsymbol{\Gamma}_2^1 \otimes \boldsymbol{\Gamma}_2^1 \right] + \frac{1}{2} \mathcal{Y} \otimes \mathcal{Y}.
\end{aligned}
\tag{2.240}
$$

If desired, this formula can be re-written in terms of integrated antenna strings,

$$
\begin{aligned}
\boldsymbol{J}_{n+2}^{(2)} \quad \longrightarrow \quad & \sum_{\{i,j\}} \left\{ \mathcal{X}_4^0(s_{ij}) + \mathcal{X}_3^1(s_{ij}) + \frac{\beta_0}{\epsilon} \left(\frac{s_{ij}}{\mu^2} \right)^{-\epsilon} \mathcal{X}_3^0(s_{ij}) - \frac{1}{\mathcal{S}} \mathcal{X}_3^0(s_{ij}) \otimes \mathcal{X}_3^0(s_{ij}) \right\} \\
& - \boldsymbol{\Gamma}_1^2 - \boldsymbol{\Gamma}_2^2 + \left[\boldsymbol{\Gamma}_1^1 \otimes \boldsymbol{\Gamma}_1^1 \right] + \left[\boldsymbol{\Gamma}_2^1 \otimes \boldsymbol{\Gamma}_2^1 \right] + \boldsymbol{\Gamma}_1^1 \boldsymbol{\Gamma}_2^1 \\
& + \frac{1}{2} \boldsymbol{J}_{n+2}^{(1)} \otimes \boldsymbol{J}_{n+2}^{(1)} + \boldsymbol{J}_{n+2}^{(1)} \otimes \boldsymbol{\Gamma}_1^1 + \boldsymbol{J}_{n+2}^{(1)} \otimes \boldsymbol{\Gamma}_2^1.
\end{aligned}
\tag{2.241}
$$

The formulation of $\boldsymbol{J}_{n+2}^{(2)}$ in (2.240) or (2.241) will be especially useful in chapters 3 and 4 where $n = 0$ and the double real matrix elements do not generate almost colour-connected or colour disconnected configurations.

Chapter 3

Production of colourless particles via quark scattering

In this chapter the production of one or more colourless particles in a hadronic collision is considered. The NLO and NNLO QCD corrections to the Born-level quark-anti-quark scattering process are calculated using the antenna subtraction method and all IR poles successfully cancelled using the formalism introduced in chapter 2.

3.1 Physical matrix elements for up to four partons

The following matrix elements are those relevant to the production of colourless particles which cannot couple to gluons directly, e.g., $q\bar{q} \to Z^0$, $q\bar{q} \to Z^0 Z^0$, $q\bar{q} \to W^+ W^-$ etc. Generically we discuss the process $q\bar{q} \to X$.

The unrenormalised cross section has a perturbative expansion in terms of the unrenormalised coupling α_s^b given by,

$$
\mathrm{d}\sigma_{ij}^b = \mathrm{d}\sigma_{ij}^{b,LO} + \left(\frac{\alpha_s^b}{2\pi}\right)\mathrm{d}\sigma_{ij}^{b,NLO} + \left(\frac{\alpha_s^b}{2\pi}\right)^2 \mathrm{d}\sigma_{ij}^{b,NNLO} \tag{3.1}
$$

The bare coupling is related to the renormalised coupling evaluated at the renormalisation scale, μ, through the singular multiplicative factor,

$$
\alpha_s^b = Z(\epsilon)\alpha_s(\mu) \tag{3.2}
$$
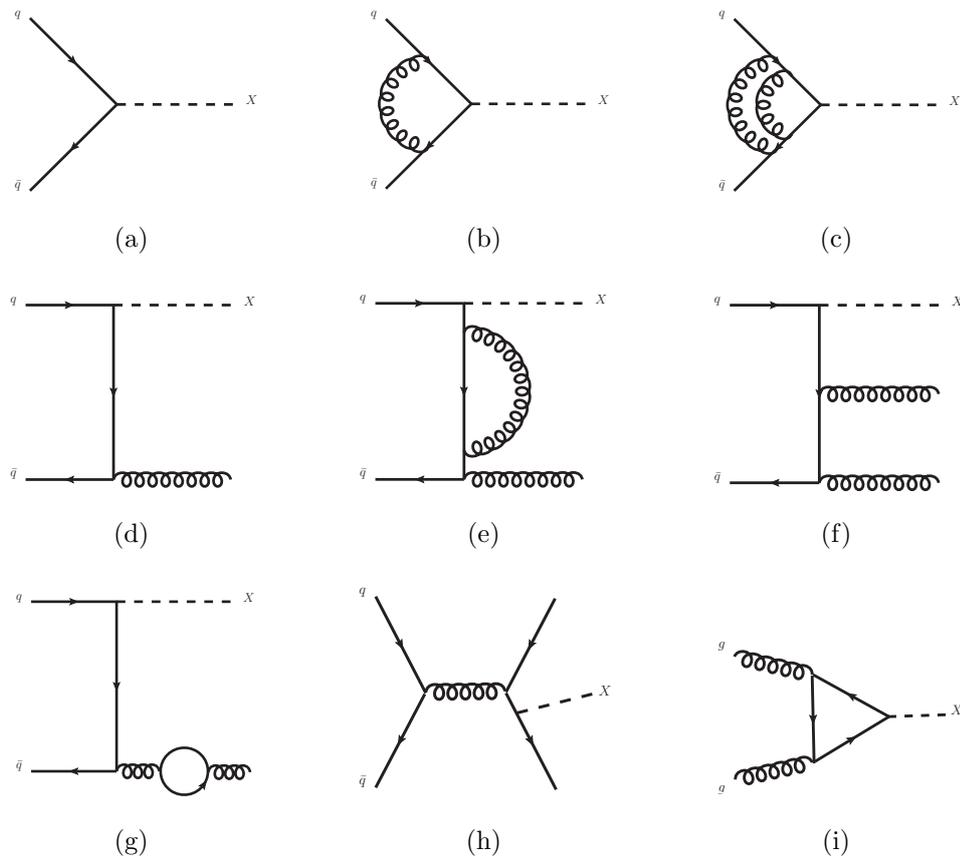
Figure 3.1: A selection of diagrams contributing to the physical matrix elements up to NNLO.

such that all UV divergences in the bare coupling are absorbed into the renormalisation factor,

$$Z(\epsilon) = \frac{1}{\bar{C}}\left[1 - \left(\frac{\alpha_s}{2\pi}\right)\frac{\beta_0}{\epsilon} + \left(\frac{\alpha_s}{2\pi}\right)^2\left(\frac{\beta_0^2}{\epsilon^2} - \frac{\beta_1}{2\epsilon}\right) + \mathcal{O}(\alpha_s^3)\right] \tag{3.3}$$

It should be noted that the leading-order cross section is of order $\mathcal{O}((\alpha_s^b)^0)$ and that each factor of α_s^b in the unrenormalised cross section carries a factor of $\bar{C}(\epsilon)$. Using this information a perturbative expansion for the renormalised cross section is given by,

$$d\sigma_{ij} = d\sigma_{ij}^{LO} + \left(\frac{\alpha_s}{2\pi}\right)d\sigma_{ij}^{NLO} + \left(\frac{\alpha_s}{2\pi}\right)^2 d\sigma_{ij}^{NNLO} \tag{3.4}$$

where the renormalised perturbative contributions are given in terms of the unrenormalised contributions,

$$d\sigma_{ij}^{LO} = d\sigma_{ij}^{b,LO}, \tag{3.5}$$

$$\mathrm{d}\sigma_{ij}^{NLO} = \frac{1}{\overline{C}(\epsilon)}\mathrm{d}\sigma_{ij}^{b,NLO}, \tag{3.6}$$

$$\mathrm{d}\sigma_{ij}^{NNLO} = \frac{1}{\overline{C}(\epsilon)^2}\mathrm{d}\sigma_{ij}^{b,NNLO} - \frac{1}{\overline{C}(\epsilon)}\frac{\beta_0}{\epsilon}\mathrm{d}\sigma_{ij}^{b,NLO}. \tag{3.7}$$

Throughout both this chapter and chapter 4, the decomposition of the physical amplitudes into colour ordered matrix elements proceeds in the same way as for pure QCD processes, except now the colour ordered matrix elements are a sum over all Feynman diagrams for a fixed perturbative order in the various couplings contributing to the same colour ordering defined by the coloured partons. For example, the process $q\bar{q} \to ggZ^0Z^0$ generates thirty Feynman diagrams with both QCD and electroweak couplings. Only two colour structures are present and so all thirty diagrams are distributed amongst the two colour structures, generating two colour ordered amplitudes.

3.1.1 Two parton contribution

The two parton contribution to the cross section enters via the tree-level Born contribution, the one-loop virtual correction and the two-loop double virtual correction. The matrix elements appropriate to all three configurations are given below.

Tree-level:

The tree-level two-parton contribution is calculated from diagrams such as the one shown in figure 3.1 (a), where it is noted that X may represent more than one particle such that the diagram shown represents a class of Feynman diagrams.

$$\begin{aligned}
\mathrm{d}\hat{\sigma}_{q\bar{q}}^{B} &= \mathcal{N}_{q\bar{q}}\mathcal{N}_{LO}\ \mathrm{d}\Phi_{\{X_i\}}(\{p_{X_i}\}; p_1, p_2)\ M_2^0(\hat{1}_q, \hat{2}_{\bar{q}}), \\
\mathrm{d}\hat{\sigma}_{qg}^{B} &= 0, \\
\mathrm{d}\hat{\sigma}_{gg}^{B} &= 0, \tag{3.8}
\end{aligned}$$

where the quark-gluon initiated contribution is zero due to quark current conservation and the gluon-gluon contribution is zero due to the gluons not coupling to colourless particles at tree-level. The set $\{p_{X_i}\}$ denotes the momenta of any colourless particles produced in the scattering process. $\mathcal{N}_{ij}$ contains overall multiplicative

factors due to spin and colour averaging of initial state partons,

$$\mathcal{N}_{ij} \;\; = \;\; \frac{1}{(2s) \cdot 4 \cdot C_i \cdot C_j} \tag{3.9}$$

where $\sqrt{s}$ is the hadron-hadron centre of mass energy and C_i denotes the number of colour states which can be accommodated by an initial-state particle of type i, e.g., $C_q = C_{\bar{q}} = N$, $C_g = N^2 - 1$. The leading-order overall colour factor is given by $\mathcal{N}_{LO} = N$.

One-loop:

The one-loop matrix elements have the form, $\langle \mathcal{M}_2^0 | \mathcal{M}_2^1 \rangle + \langle \mathcal{M}_2^1 | \mathcal{M}_2^0 \rangle$ and so any one-loop amplitude which is projected onto a null tree-level amplitude forms a null matrix element. The class of diagrams contributing to the one-loop amplitudes are represented by figure 3.1 (b).

$$
\begin{aligned}
\mathrm{d}\hat{\sigma}_{q\bar{q}}^V &= \mathcal{N}_{q\bar{q}}\mathcal{N}_{NLO}\,\bar{C}(\epsilon)\left(\frac{\alpha_s}{2\pi}\right)\mathrm{d}\Phi_{\{X_i\}}(\{p_{X_i}\}; p_1, p_2)\, M_2^1(\hat{1}_q, \hat{2}_{\bar{q}}) \\
\mathrm{d}\hat{\sigma}_{qg}^V &= 0 \\
\mathrm{d}\hat{\sigma}_{gg}^V &= 0
\end{aligned}
\tag{3.10}
$$

where the NLO overall colour factor is given by, $\mathcal{N}_{NLO} = C_F\,\mathcal{N}_{LO}$.

Two-loop:

At two loops the matrix elements have the form $\langle \mathcal{M}_2^0 | \mathcal{M}_2^2 \rangle + \langle \mathcal{M}_2^2 | \mathcal{M}_2^0 \rangle + \langle \mathcal{M}_2^1 | \mathcal{M}_2^1 \rangle$ and the cross section can be written in the form,

$$
\begin{aligned}
\mathrm{d}\hat{\sigma}_{q\bar{q}}^{VV} &= \mathcal{N}_{q\bar{q}}\mathcal{N}_{NLO}\,\bar{C}(\epsilon)^2\left(\frac{\alpha_s}{2\pi}\right)^2\mathrm{d}\Phi_{\{X_i\}}(\{p_{X_i}\}; p_1, p_2) \\
&\quad \left\{ N\, M_2^2(\hat{1}_q, \hat{2}_{\bar{q}}) - \frac{1}{N}\,\widetilde{M}_2^2(\hat{1}_q, \hat{2}_{\bar{q}}) + N_F\,\widehat{M}_2^2(\hat{1}_q, \hat{2}_{\bar{q}}) \right\}, \\
\mathrm{d}\hat{\sigma}_{qg}^{VV} &= 0 \\
\mathrm{d}\hat{\sigma}_{gg}^{VV} &= \mathcal{N}_{gg}\mathcal{N}_{NLO}\,\bar{C}(\epsilon)^2\left(\frac{\alpha_s}{2\pi}\right)^2\mathrm{d}\Phi_{\{X_i\}}(\{p_{X_i}\}; p_1, p_2)\, M_2^2(\hat{1}_g, \hat{2}_g)
\end{aligned}
\tag{3.11}
$$

An example two-loop two-parton diagram is shown in figure 3.1 (c). The gluon-gluon initiated channel is non-zero due to the self-interference of the non-zero one-loop amplitude shown in figure 3.1 (i). This contribution is however IR finite, having

no tree-level or one-loop matrix elements to factor onto, and so requires no explicit pole subtraction at the double virtual level.

3.1.2 Three parton contribution

The three-parton contribution to the cross section is given by the real tree-level and the real-virtual one-loop correction to the cross section.

Tree-level:

The tree-level three-parton matrix elements are calculated from the class of diagrams in figure 3.1 (d) and its various crossings.

$$
\begin{aligned}
\mathrm{d}\hat{\sigma}_{q\bar{q}}^{R} &= \mathcal{N}_{q\bar{q}}\mathcal{N}_{NLO}\frac{\bar{C}(\epsilon)}{C(\epsilon)}\left(\frac{\alpha_s}{2\pi}\right)\mathrm{d}\Phi_{\{X_i\}+1}(\{p_{X_i}\},p_3;p_1,p_2) \\
&\qquad\qquad \times M_3^0(\hat{1}_q,3_g,\hat{2}_{\bar{q}})\, J_0^{(1)}(p_3) \\
\mathrm{d}\hat{\sigma}_{qg}^{R} &= \mathcal{N}_{qg}\mathcal{N}_{NLO}\frac{\bar{C}(\epsilon)}{C(\epsilon)}\left(\frac{\alpha_s}{2\pi}\right)\mathrm{d}\Phi_{\{X_i\}+1}(\{p_{X_i}\},p_3;p_1,p_2) \\
&\qquad\qquad \times M_3^0(\hat{1}_q,\hat{2}_g,3_{\bar{q}})\, J_0^{(1)}(p_3) \\
\mathrm{d}\hat{\sigma}_{gg}^{R} &= 0
\end{aligned}
\tag{3.12}
$$

Other non-zero channels are obtained from these processes via an appropriate substitution of labels. e.g., $\mathrm{d}\hat{\sigma}_{\bar{q}q}^{R} = \mathrm{d}\hat{\sigma}_{q\bar{q}}^{R}(q \leftrightarrow \bar{q})$, $\mathrm{d}\hat{\sigma}_{\bar{q}g}^{R} = \mathrm{d}\hat{\sigma}_{qg}^{R}(q \leftrightarrow \bar{q})$ etc.

One-loop:

Diagrams of the type in figure 3.1 (e) are amongst several which generate the one-loop three-parton matrix elements.

$$
\begin{aligned}
\mathrm{d}\hat{\sigma}_{q\bar{q}}^{RV} &= \mathcal{N}_{q\bar{q}}\mathcal{N}_{NLO}\,\frac{\bar{C}(\epsilon)^2}{C(\epsilon)}\left(\frac{\alpha_s}{2\pi}\right)^2\mathrm{d}\Phi_{\{X_i\}+1}(\{p_{X_i}\},p_3;p_1,p_2) \\
&\frac{1}{2}\left\{\ N\, M_3^1(\hat{1}_q,3_g,\hat{2}_{\bar{q}}) - \frac{1}{N}\,\widetilde{M}_3^1(\hat{1}_q,3_g,\hat{2}_{\bar{q}}) + N_F\,\widehat{M}_3^1(\hat{1}_q,3_g,\hat{2}_{\bar{q}})\right\}J_0^{(1)}(p_3), \\
\mathrm{d}\hat{\sigma}_{qg}^{RV} &= \mathcal{N}_{qg}\mathcal{N}_{NLO}\,\frac{\bar{C}(\epsilon)^2}{C(\epsilon)}\left(\frac{\alpha_s}{2\pi}\right)^2\mathrm{d}\Phi_{\{X_i\}+1}(\{p_{X_i}\},p_3;p_1,p_2) \\
&\frac{1}{2}\left\{\ N\, M_3^1(\hat{1}_q,\hat{2}_g,3_{\bar{q}}) - \frac{1}{N}\,\widetilde{M}_3^1(\hat{1}_q,\hat{2}_g,3_{\bar{q}}) + N_F\,\widehat{M}_3^1(\hat{1}_q,\hat{2}_g,3_{\bar{q}})\right\}J_0^{(1)}(p_3), \\
\mathrm{d}\hat{\sigma}_{gg}^{RV} &= 0
\end{aligned}
\tag{3.13}
$$

where $\widetilde{M}_3^1$ and $\widehat{M}_3^1$ denote the squared matrix elements of the sub-leading colour and closed quark-loop contributions respectively. The N_F dependent contribution is generated by diagrams of the type in figure 3.1 (g).

3.1.3 Four parton contribution

The four-parton contribution to the cross section enters via the tree-level double real correction to the Born-level cross section.

3.1.4 Tree-level:

The four-parton tree-level matrix elements are formed from diagrams including those of the type shown in figure 3.1 (f) and (h), along with their various crossings.

$$
\begin{aligned}
\mathrm{d}\hat{\sigma}_{q\bar{q}}^{RR} \;=\; & \mathcal{N}_{q\bar{q}}\mathcal{N}_{NLO}\,\frac{\bar{C}(\epsilon)^2}{C(\epsilon)^2}\left(\frac{\alpha_s}{2\pi}\right)^2 \mathrm{d}\Phi_{\{X_i\}+2}(\{p_{X_i}\},p_3,p_4;p_1,p_2) \\
& \left\{\; \frac{N}{2}\left(\sum_{\{3,4\}} M_4^0(\hat{1}_q,3_g,4_g,\hat{2}_{\bar{q}})\right) - \frac{1}{2N}\,\widetilde{M}_4^0(\hat{1}_q,3_g,4_g,\hat{2}_{\bar{q}}) + N_F\;M_4^0(\hat{1}_q,3_Q,4_{\bar{Q}},\hat{2}_{\bar{q}}) \right. \\
& \left. + \;M_4^0(\hat{1}_q,3_Q,\hat{2}_{\bar{Q}},4_{\bar{q}}) - \frac{1}{N}\,\overline{M}_4^0(\hat{1}_q,3_q,4_{\bar{q}},\hat{2}_{\bar{q}}) \right\}\; J_0^{(2)}(p_3,p_4), \\[6pt]
\mathrm{d}\hat{\sigma}_{qg}^{RR} \;=\; & \mathcal{N}_{qg}\mathcal{N}_{NLO}\,\frac{\bar{C}(\epsilon)^2}{C(\epsilon)^2}\left(\frac{\alpha_s}{2\pi}\right)^2 \mathrm{d}\Phi_{\{X_i\}+2}(\{p_{X_i}\},p_3,p_4;p_1,p_2) \\
& \left\{\; N\left(M_4^0(\hat{1}_q,\hat{2}_g,3_g,4_{\bar{q}}) + M_4^0(\hat{1}_q,3_g,\hat{2}_g,4_{\bar{q}})\right) - \frac{1}{N}\,\widetilde{M}_4^0(\hat{1}_q,\hat{2}_g,3_g,4_{\bar{q}}) \right\}, \\[6pt]
\mathrm{d}\hat{\sigma}_{gg}^{RR} \;=\; & \mathcal{N}_{gg}\mathcal{N}_{NLO}\,\frac{\bar{C}(\epsilon)^2}{C(\epsilon)^2}\left(\frac{\alpha_s}{2\pi}\right)^2 \mathrm{d}\Phi_{\{X_i\}+2}(\{p_{X_i}\},p_3,p_4;p_1,p_2)\;N_F \\
& \left\{\; \sum_{\{1,2\}} N\;M_4^0(3_q,\hat{1}_g,\hat{2}_g,4_{\bar{q}}) - \frac{1}{N}\,\widetilde{M}_4^0(3_q,\hat{1}_g,\hat{2}_g,4_{\bar{q}}) \right\}\; J_0^{(2)}(p_3,p_4) \\[6pt]
\mathrm{d}\hat{\sigma}_{qQ}^{RR} \;=\; & \mathcal{N}_{qQ}\mathcal{N}_{NLO}\,\frac{\bar{C}(\epsilon)^2}{C(\epsilon)^2}\left(\frac{\alpha_s}{2\pi}\right)^2 \mathrm{d}\Phi_{\{X_i\}+2}(\{p_{X_i}\},p_3,p_4;p_1,p_2) \\
& M_4^0(\hat{1}_q,\hat{2}_Q,4_Q,3_q)\;J_0^{(2)}(p_3,p_4) \\[6pt]
\mathrm{d}\hat{\sigma}_{qq}^{RR} \;=\; & \mathcal{N}_{qq}\mathcal{N}_{NLO}\,\frac{\bar{C}(\epsilon)^2}{C(\epsilon)^2}\left(\frac{\alpha_s}{2\pi}\right)^2 \mathrm{d}\Phi_{\{X_i\}+2}(\{p_{X_i}\},p_3,p_4;p_1,p_2) \\
& \frac{1}{2}\left\{\; M_4^0(\hat{1}_q,\hat{2}_Q,4_Q,3_q) + M_4^0(\hat{1}_q,\hat{2}_Q,3_{\bar{Q}},4_{\bar{q}}) - \frac{1}{N}\,\overline{M}_4^0(\hat{1}_q,3_q,\hat{2}_{\bar{q}},4_{\bar{q}}) \right\}\; J_0^{(2)}(p_3,p_4),
\end{aligned}
$$

$$(3.14)$$

$\widetilde{M}_4^0(\hat{1}_q, 3_g, 4_g, \hat{2}_{\bar{q}})$ denotes the sub-leading colour two quark two gluon squared matrix element. The incoherent like-quark flavoured matrix elements are given by,

$$\overline{M}_4^0(\hat{1}_q, 3_q, 4_{\bar{q}}, \hat{2}_{\bar{q}}) = -2\Re\left[\mathcal{M}_4^0(\hat{1}_q, 3_Q, 4_{\bar{Q}}, \hat{2}_{\bar{q}})\mathcal{M}_4^{0,\dagger}(\hat{1}_q, 3_Q, \hat{2}_{\bar{q}}, 4_{\bar{Q}})\right] \quad (3.15)$$

Other contributions to the cross section are obtained from those listed above:

$$\begin{aligned}
\mathrm{d}\sigma_{\bar{q}\bar{q}}^{RR} &= \mathrm{d}\sigma_{qq}^{RR} \\
\mathrm{d}\sigma_{q\bar{Q}}^{RR} &= \mathrm{d}\sigma_{qQ}^{RR} \\
\mathrm{d}\sigma_{qg}^{RR} &= \mathrm{d}\sigma_{gq}^{RR}(\hat{1} \leftrightarrow \hat{2})
\end{aligned} \quad (3.16)$$

3.2 Infrared subtraction at NLO

Following the considerations of section 2.5, the real and virtual subtraction terms can be generated to remove all implicit divergence and explicit poles present in the cross section.

3.2.1 Construction of the NLO real subtraction terms

$$\begin{aligned}
\mathrm{d}\hat{\sigma}_{q\bar{q},NLO}^S &= \mathcal{N}_{q\bar{q}}\mathcal{N}_{NLO}\frac{\bar{C}(\epsilon)}{C(\epsilon)}\left(\frac{\alpha_s}{2\pi}\right)\mathrm{d}\Phi_{\{X_i\}+1}(\{p_X\}, p_3; p_1, p_2) \\
&\qquad\qquad \times A_3^0(\hat{1}, 3, \hat{2})\, M_2^0(\hat{\bar{1}}_q, \hat{\bar{2}}_{\bar{q}})\, J_0^{(1)}(p_3) \\
\mathrm{d}\hat{\sigma}_{qg,NLO}^S &= \mathcal{N}_{qg}\mathcal{N}_{NLO}\frac{\bar{C}(\epsilon)}{C(\epsilon)}\left(\frac{\alpha_s}{2\pi}\right)\mathrm{d}\Phi_{\{X_i\}+1}(\{p_X\}, p_3; p_1, p_2) \\
&\qquad\qquad \times A_3^0(\hat{1}, \hat{2}, 3)\, M_2^0(\hat{\bar{1}}_q, \hat{\bar{2}}_{\bar{q}})\, J_0^{(1)}(p_3) \quad (3.17)
\end{aligned}$$

By examining the IR divergent limits of the three-parton real emission matrix elements in (3.12), it is clear that the subtraction term correctly matches the physical cross section in all single unresolved configurations.

3.2.2 Construction of the NLO virtual subtraction terms

Following the arguments presented in section 2.5, the virtual subtraction term is constructed from the integrated real subtraction terms and the NLO mass factorization contribution. The various elements for this calculation are naturally assembled

in terms of integrated antenna strings to yield the virtual subtraction terms in the form,

$$
\begin{aligned}
\mathrm{d}\hat{\sigma}^T_{q\bar{q},NLO} &= -\mathcal{N}_{q\bar{q}}\mathcal{N}_{NLO}\,\bar{C}(\epsilon)\left(\frac{\alpha_s}{2\pi}\right)\mathrm{d}\Phi_{\{X_i\}}(\{p_X\};\bar{p}_1,\bar{p}_2)\int\frac{\mathrm{d}x_1}{x_1}\frac{\mathrm{d}x_2}{x_2}\\
&\quad\times\boldsymbol{J}^{(1)}_2(\hat{\bar{1}}_q,\hat{\bar{2}}_{\bar{q}})\,M^0_2(\hat{\bar{1}}_q,\hat{\bar{2}}_{\bar{q}})\\
\mathrm{d}\hat{\sigma}^T_{qg,NLO} &= -\mathcal{N}_{qg}\mathcal{N}_{NLO}\,\bar{C}(\epsilon)\left(\frac{\alpha_s}{2\pi}\right)\mathrm{d}\Phi_{\{X_i\}}(\{p_X\};\bar{p}_1,\bar{p}_2)\int\frac{\mathrm{d}x_1}{x_1}\frac{\mathrm{d}x_2}{x_2}\\
&\quad\times\boldsymbol{J}^{(1)}_{2,g\to q}(\hat{\bar{1}}_q,\hat{\bar{2}}_{\bar{q}})\,M^0_2(\hat{\bar{1}}_q,\hat{\bar{2}}_{\bar{q}})
\end{aligned}
$$
$$(3.18)$$

As explained in the previous chapter, the identity changing integrated antenna string, $\boldsymbol{J}^{(1)}_{2,g\to q}(\hat{\bar{1}}_q,\hat{\bar{2}}_{\bar{q}})$, is free from explicit poles. This string is the only contribution to the quark-gluon channel and is necessarily finite as the one-loop contribution is finite, specifically the cross section is zero. The integrated antenna string $\boldsymbol{J}^{(1)}_2(\hat{\bar{1}}_q,\hat{\bar{2}}_{\bar{q}})$ is free from initial-state collinear poles but contains explicit poles which may be written in terms of the colour ordered insertion operator,

$$
\mathcal{P}oles\big[\boldsymbol{J}^{(1)}_2(\hat{\bar{1}}_q,\hat{\bar{2}}_{\bar{q}})\big] = -2\boldsymbol{I}^{(1)}_{q\bar{q}}(s_{\bar{1}\bar{2}})\delta(1-x_1)\delta(1-x_2). \tag{3.19}
$$

This pole structure matches the pole structure of the one-loop squared matrix element and the total cross section is rendered IR finite. Alternatively the poles of the one-loop matrix element can be written in terms of integrated antenna functions allowing for a direct cancellation of the IR explicit poles. Using either approach the final result can be summarized as,

$$
\mathcal{P}oles\left[M^1_2(\hat{1}_q,\hat{2}_{\bar{q}}) - \int\frac{\mathrm{d}x_1}{x_1}\frac{\mathrm{d}x_2}{x_2}\boldsymbol{J}^{(1)}_2(\hat{\bar{1}}_q,\hat{\bar{2}}_{\bar{q}})\,M^0_2(\hat{\bar{1}}_q,\hat{\bar{2}}_{\bar{q}})\right] = 0. \tag{3.20}
$$

3.3   Infrared subtraction at NNLO

Extending the analysis of this process to NNLO involves implementing the formalism of section 2.6 for the processes defined in (3.14). This calculation includes subleading colour matrix elements in the form of squared matrix elements involving Abelian gluons and the discussion in section 2.5 applies when constructing the subtraction terms for these processes.

3.3.1 Construction of the double real subtraction term

Quark-antiquark initial state:

$$
\begin{aligned}
\mathrm{d}\hat{\sigma}_{q\bar{q}}^S &= \mathcal{N}_{q\bar{q}}\mathcal{N}_{NLO}\left(\frac{\alpha_s}{2\pi}\right)^2 \frac{\bar{C}(\epsilon)^2}{C(\epsilon)^2}\, \mathrm{d}\Phi_{\{X_i\}+2}(\{p_{X_i}\}, p_3, p_4; p_1, p_2)\, \Bigg\{ \\
\frac{N}{2}\sum_{\{3,4\}} &\Bigg[\quad d_3^0(\hat{1},3,4)\, M_3^0(\hat{\hat{1}}_q, \widetilde{(3,4)}_g, \hat{2}_{\bar{q}})\, J_0^{(1)}(p_{(3,4)}) \\
&+\ d_3^0(\hat{2},4,3)\, M_3^0(\hat{1}_q, \widetilde{(3,4)}_g, \hat{\hat{2}}_{\bar{q}})\, J_0^{(1)}(p_{(3,4)}) \\
&+\ A_4^0(\hat{1},3,4,\hat{2})\, M_2^0(\hat{\hat{1}}_q, \hat{\hat{2}}_{\bar{q}}) \\
&-\ d_3^0(\hat{1},3,4)\, A_3^0(\hat{\hat{1}}, \widetilde{(3,4)}, \hat{2})\, M_2^0(\hat{\hat{\hat{1}}}_q, \hat{\hat{2}}_{\bar{q}}) \\
&-\ d_3^0(\hat{2},4,3)\, A_3^0(\hat{1}, \widetilde{(3,4)}, \hat{\hat{2}})\, M_2^0(\hat{\hat{1}}_q, \hat{\hat{\hat{2}}}_{\bar{q}}) \Bigg] \\
-\frac{1}{2N} &\Bigg[\quad A_3^0(\hat{1},3,\hat{2})\, M_3^0(\hat{\hat{1}}_q, \tilde{4}_g, \hat{\hat{2}}_{\bar{q}})\, J_0^{(1)}(p_4) \\
&+\ A_3^0(\hat{1},4,\hat{2})\, M_3^0(\hat{\hat{1}}_q, \tilde{3}_g, \hat{\hat{2}}_{\bar{q}})\, J_0^{(1)}(p_3) \\
&+\ \tilde{A}_4^0(\hat{1},3,4,\hat{2})\, M_2^0(\hat{\hat{1}}_q, \hat{\hat{2}}_{\bar{q}}) \\
&-\ A_3^0(\hat{1},3,\hat{2})\, A_3^0(\hat{\hat{1}}, \tilde{4}, \hat{\hat{2}})\, M_2^0(\hat{\hat{\hat{1}}}_q, \hat{\hat{\hat{2}}}_{\bar{q}}) \\
&-\ A_3^0(\hat{1},4,\hat{2})\, A_3^0(\hat{\hat{1}}, \tilde{3}, \hat{\hat{2}})\, M_2^0(\hat{\hat{\hat{1}}}_q, \hat{\hat{\hat{2}}}_{\bar{q}}) \\
&+\ 2\Big(C_4^0(\hat{1},3,4,\hat{2})\, M_2^0(\hat{\hat{1}}_q, \hat{\hat{2}}_{\bar{q}}) + C_4^0(\hat{2},4,3,\hat{1})\, M_2^0(\hat{\hat{1}}_q, \hat{\hat{2}}_{\bar{q}}) \Big) \Bigg] \\
+ &\Bigg[\quad E_3^0(\hat{1},3,\hat{2})\, M_3^0(\hat{\hat{1}}_q, \hat{\hat{2}}_{\bar{q}}, \tilde{3}_{\bar{q}})\, J_0^{(1)}(p_3) \\
&+\ E_3^0(\hat{2},4,\hat{1})\, M_3^0(\tilde{3}_q, \hat{\hat{1}}_g, \hat{\hat{2}}_{\bar{q}})\, J_0^{(1)}(p_3) \\
&+\ B_4^0(\hat{1},3,\hat{2},4)\, M_2^0(\hat{\hat{1}}_q, \hat{\hat{2}}_{\bar{q}}) \\
&-\ E_3^0(\hat{1},3,\hat{2})\, A_3^0(\hat{\hat{1}}, \hat{\hat{2}}, \tilde{3})\, M_2^0(\hat{\hat{\hat{1}}}_q, \hat{\hat{\hat{2}}}_{\bar{q}}) \\
&+\ B_4^0(\hat{2},4,\hat{1},3)\, M_2^0(\hat{\hat{1}}_q, \hat{\hat{2}}_{\bar{q}}) \\
&-\ E_3^0(\hat{2},4,\hat{1})\, A_3^0(\tilde{3}, \hat{\hat{1}}, \hat{\hat{2}})\, M_2^0(\hat{\hat{\hat{1}}}_q, \hat{\hat{\hat{2}}}_{\bar{q}}) \Bigg] \\
+N_F &\Bigg[\quad \frac{1}{2}E_3^0(\hat{1},3,4)\, M_3^0(\hat{\hat{1}}_q, \widetilde{(3,4)}_g, \hat{2}_{\bar{q}})\, J_0^{(1)}(p_{(3,4)}) \\
&+\ \frac{1}{2}E_3^0(\hat{2},4,3)\, M_3^0(\hat{1}_q, \widetilde{(3,4)}_g, \hat{\hat{2}}_{\bar{q}})\, J_0^{(1)}(p_{(3,4)}) \\
&+\ B_4^0(\hat{1},3,4,\hat{2})\, M_2^0(\hat{\hat{1}}_q, \hat{\hat{2}}_{\bar{q}}) \\
&-\ \frac{1}{2}E_3^0(\hat{1},3,4)\, A_3^0(\hat{\hat{1}}, \widetilde{(3,4)}, \hat{2})\, M_2^0(\hat{\hat{\hat{1}}}_q, \hat{\hat{2}}_{\bar{q}})
\end{aligned}
$$

$$- \frac{1}{2} E_3^0(\hat{2}, 4, 3) \ A_3^0(\hat{1}, \widetilde{(3,4)}, \hat{\bar{2}}) \ M_2^0(\hat{\bar{1}}_q, \hat{\bar{\bar{2}}}_{\bar{q}}) \Big] \Big\} \tag{3.21}$$

Quark-gluon initial state:

$$
\begin{aligned}
\mathrm{d}\hat{\sigma}_{qg}^S \ = \ & \mathcal{N}_{qg}\mathcal{N}_{NLO}\left(\frac{\alpha_s}{2\pi}\right)^2 \frac{\bar{C}(\epsilon)^2}{C(\epsilon)^2} \ \mathrm{d}\Phi_{\{X_i\}+2}(\{p_{X_i}\}, p_3, p_4; p_1, p_2) \Bigg\{ \\
& N \ \Big[\ d_3^0(4, 3, \hat{2}) \ M_3^0(\hat{1}_q, \hat{\bar{2}}_g, \widetilde{(3,4)}_{\bar{q}}) \ J_0^{(1)}(p_{(3,4)}) \\
& + \ D_3^0(\hat{1}, 3, \hat{2}) \ M_3^0(\hat{\bar{1}}_q, \hat{\bar{2}}_g, \tilde{4}_{\bar{q}}) \ J_0^{(1)}(p_4) \\
& + \ d_3^0(4, \hat{2}; 3) \ M_3^0(\hat{1}_q, \widetilde{(3,4)}_g, \hat{\bar{2}}_{\bar{q}}) \ J_0^{(1)}(p_{(3,4)}) \\
& + \ A_4^0(\hat{1}, \hat{2}, 3, 4) \ M_2^0(\hat{\bar{1}}_q, \hat{\bar{2}}_{\bar{q}}) \\
& - \ d_3^0(4, 3, \hat{2}) \ A_3^0(\hat{1}, \hat{\bar{2}}, \widetilde{(3,4)}) \ M_2^0(\hat{\bar{1}}_q, \hat{\bar{\bar{2}}}_{\bar{q}}) \\
& + \ A_4^0(\hat{1}, 3, \hat{2}, 4) \ M_2^0(\hat{\bar{1}}_q, \hat{\bar{2}}_{\bar{q}}) \\
& - \ D_3^0(\hat{1}, 3, \hat{2}) \ A_3^0(\hat{\bar{1}}, \hat{\bar{2}}, \tilde{4}) \ M_2^0(\hat{\bar{\bar{1}}}_q, \hat{\bar{\bar{2}}}_{\bar{q}}) \\
& - \ d_3^0(4, \hat{2}; 3) \ A_3^0(\hat{1}, \widetilde{(3,4)}, \hat{\bar{2}}) \ M_2^0(\hat{\bar{1}}_q, \hat{\bar{\bar{2}}}_{\bar{q}}) \Big] \\
& -\frac{1}{N} \ \Big[\ A_3^0(\hat{1}, 3, 4) \ M_3^0(\hat{\bar{1}}_q, \hat{2}_g, \widetilde{(3,4)}_{\bar{q}}) \ J_0^{(1)}(p_{(3,4)}) \\
& + \ A_3^0(\hat{1}, \hat{2}, 4) \ M_3^0(\hat{\bar{1}}_q, \tilde{3}_g, \hat{\bar{2}}_{\bar{q}}) \ J_0^{(1)}(p_3) \\
& + \ \tilde{A}_4^0(\hat{1}, \hat{2}, 3, 4) \ M_2^0(\hat{\bar{1}}_q, \hat{\bar{2}}_{\bar{q}}) \\
& - \ A_3^0(\hat{1}, 3, 4) \ A_3^0(\hat{\bar{1}}, \hat{2}, \widetilde{(3,4)}) \ M_2^0(\hat{\bar{\bar{1}}}_q, \hat{\bar{2}}_{\bar{q}}) \\
& - \ A_3^0(\hat{1}, \hat{2}, 4) \ A_3^0(\hat{\bar{1}}, \tilde{3}, \hat{\bar{2}}) \ M_2^0(\hat{\bar{\bar{1}}}_q, \hat{\bar{\bar{2}}}_{\bar{q}}) \Big] \Bigg\} \tag{3.22}
\end{aligned}
$$

Gluon-gluon initial state:

$$
\begin{aligned}
\mathrm{d}\hat{\sigma}_{gg}^S \ = \ & \mathcal{N}_{gg}\mathcal{N}_{NLO}\left(\frac{\alpha_s}{2\pi}\right)^2 \frac{\bar{C}(\epsilon)^2}{C(\epsilon)^2} \ \mathrm{d}\Phi_{\{X_i\}+2}(\{p_{X_i}\}, p_3, p_4; p_1, p_2) \Bigg\{ \\
& N_F N \sum_{\{\hat{1}, \hat{2}\}} \ \Big[\ d_3^0(3, \hat{1}; 2) \ M_3^0(\hat{\bar{1}}_q, \hat{\bar{2}}_g, \tilde{4}_{\bar{q}}) \ J_0^{(1)}(p_4) \\
& + \ d_3^0(4, \hat{2}; \hat{1}) \ M_3^0(\tilde{3}_q, \hat{\bar{1}}_g, \hat{\bar{2}}_{\bar{q}}) \ J_0^{(1)}(p_3) \\
& + \ A_4^0(3, \hat{1}, \hat{2}, 4) \ M_2^0(\hat{\bar{1}}_q, \hat{\bar{2}}_{\bar{q}}) \\
& - \ d_3^0(3, \hat{1}; 2) \ A_3^0(\hat{\bar{1}}, \hat{\bar{2}}, \tilde{4}) \ M_2^0(\hat{\bar{\bar{1}}}_q, \hat{\bar{2}}_{\bar{q}}) \\
& - \ d_3^0(4, \hat{2}; \hat{1}) \ A_3^0(\tilde{3}, \hat{\bar{1}}, \hat{\bar{2}}) \ M_2^0(\hat{\bar{\bar{1}}}_q, \hat{\bar{\bar{2}}}_{\bar{q}}) \Big]
\end{aligned}
$$

$$
-\frac{N_F}{N} \left[\; d_3^0(3,\hat{1};2) \; M_3^0(\hat{\tilde{1}}_q, \hat{\tilde{2}}_g, \tilde{4}_{\bar{q}}) \; J_0^{(1)}(p_4) \right.
$$

$$
+ \; d_3^0(4,\hat{2};\hat{1}) \; M_3^0(\tilde{3}_q, \hat{\tilde{1}}_g, \hat{\tilde{2}}_{\bar{q}}) \; J_0^{(1)}(p_3)
$$

$$
+ \; \tilde{A}_4^0(3,\hat{1},\hat{2},4) \; M_2^0(\hat{\tilde{1}}_q, \hat{\tilde{2}}_{\bar{q}})
$$

$$
- \; d_3^0(3,\hat{1};2) \; A_3^0(\hat{\tilde{1}}, \hat{\tilde{2}}, \tilde{4}) \; M_2^0(\hat{\tilde{\tilde{1}}}_q, \hat{\tilde{\tilde{2}}}_{\bar{q}})
$$

$$
\left. - \; d_3^0(4,\hat{2};\hat{1}) \; A_3^0(\tilde{3}, \hat{\tilde{1}}, \hat{\tilde{2}}) \; M_2^0(\hat{\tilde{\tilde{1}}}_q, \hat{\tilde{\tilde{2}}}_{\bar{q}}) \right]
$$

$$
(3.23)
$$

Quark-quark (non-identical) initial state:

$$
\mathrm{d}\hat{\sigma}_{qQ}^S \;=\; \mathcal{N}_{q\bar{q}}\mathcal{N}_{NLO}\left(\frac{\alpha_s}{2\pi}\right)^2 \frac{\bar{C}(\epsilon)^2}{C(\epsilon)^2} \, \mathrm{d}\Phi_{\{X_i\}+2}(\{p_{X_i}\}, p_3, p_4; p_1, p_2) \left\{ \right.
$$

$$
E_3^0(\hat{1}, \hat{2}, 4) \; M_3^0(\hat{\tilde{1}}_q, \hat{\tilde{2}}_g, \tilde{3}_{\bar{q}}) \; J_0^{(1)}(p_{\tilde{3}})
$$

$$
+ \; E_3^0(\hat{2}, \hat{1}, 3) \; M_3^0(\hat{\tilde{2}}_q, \hat{\tilde{1}}_g, \tilde{4}_{\bar{q}}) \; J_0^{(1)}(p_{\tilde{4}})
$$

$$
+ \; B_4^0(\hat{1}, \hat{2}, 4, 3) \; M_2^0(\hat{\tilde{1}}_q, \hat{\tilde{2}}_{\bar{q}})
$$

$$
- \; E_3^0(\hat{1}, \hat{2}, 4) \; A_3^0(\hat{\tilde{1}}, \hat{\tilde{2}}, \tilde{3}) M_2^0(\hat{\tilde{\tilde{1}}}_q, \hat{\tilde{\tilde{2}}}_{\bar{q}})
$$

$$
+ \; B_4^0(\hat{2}, \hat{1}, 3, 4) \; M_2^0(\hat{\tilde{1}}_q, \hat{\tilde{2}}_{\bar{q}})
$$

$$
- \; E_3^0(\hat{2}, \hat{1}, 3) \; A_3^0(\hat{\tilde{2}}, \hat{\tilde{1}}, \tilde{4}) M_2^0(\hat{\tilde{\tilde{1}}}_q, \hat{\tilde{\tilde{2}}}_{\bar{q}}) \left. \right\}.
$$

$$
(3.24)
$$

Quark-quark (identical) initial state:

$$
\mathrm{d}\hat{\sigma}_{qq}^S \;=\; \mathcal{N}_{q\bar{q}}\mathcal{N}_{NLO}\left(\frac{\alpha_s}{2\pi}\right)^2 \frac{\bar{C}(\epsilon)^2}{C(\epsilon)^2} \, \mathrm{d}\Phi_{\{X_i\}+2}(\{p_{X_i}\}, p_3, p_4; p_1, p_2) \left\{ \right.
$$

$$
\frac{1}{2} \left\{ \; E_3^0(\hat{1}, \hat{2}, 4) \; M_3^0(\hat{\tilde{1}}_q, \hat{\tilde{2}}_g, \tilde{3}_{\bar{q}}) \; J_0^{(1)}(p_{\tilde{3}}) \right.
$$

$$
+ \; E_3^0(\hat{2}, \hat{1}, 3) \; M_3^0(\hat{\tilde{2}}_q, \hat{\tilde{1}}_g, \tilde{4}_{\bar{q}}) \; J_0^{(1)}(p_{\tilde{4}})
$$

$$
+ \; E_3^0(\hat{1}, \hat{2}, 3) \; M_3^0(\hat{\tilde{1}}_q, \hat{\tilde{2}}_g, \tilde{4}_{\bar{q}}) \; J_0^{(1)}(p_{\tilde{4}})
$$

$$
+ \; E_3^0(\hat{2}, \hat{1}, 4) \; M_3^0(\hat{\tilde{2}}_q, \hat{\tilde{1}}_g, \tilde{3}_{\bar{q}}) \; J_0^{(1)}(p_{\tilde{3}})
$$

$$
+ \; B_4^0(\hat{1}, \hat{2}, 4, 3) \; M_2^0(\hat{\tilde{1}}_q, \hat{\tilde{2}}_{\bar{q}})
$$

$$
- \; E_3^0(\hat{1}, \hat{2}, 4) \; A_3^0(\hat{\tilde{1}}, \hat{\tilde{2}}, \tilde{3}) M_2^0(\hat{\tilde{\tilde{1}}}_q, \hat{\tilde{\tilde{2}}}_{\bar{q}})
$$

$$
+ \; B_4^0(\hat{2}, \hat{1}, 3, 4) \; M_2^0(\hat{\tilde{1}}_q, \hat{\tilde{2}}_{\bar{q}})
$$

$$
- \; E_3^0(\hat{2}, \hat{1}, 3) \; A_3^0(\hat{\tilde{2}}, \hat{\tilde{1}}, \tilde{4}) M_2^0(\hat{\tilde{\tilde{1}}}_q, \hat{\tilde{\tilde{2}}}_{\bar{q}})
$$

$$+ \quad B_4^0(\hat{1}, \hat{2}, 3, 4) \ M_2^0(\hat{\bar{1}}_q, \hat{\bar{2}}_{\bar{q}})$$

$$- \quad E_3^0(\hat{1}, \hat{2}, 3) \ A_3^0(\hat{\bar{1}}, \hat{\bar{2}}, \tilde{4}) M_2^0(\hat{\bar{\bar{1}}}_q, \hat{\bar{\bar{2}}}_{\bar{q}})$$

$$+ \quad B_4^0(\hat{2}, \hat{1}, 4, 3) \ M_2^0(\hat{\bar{1}}_q, \hat{\bar{2}}_{\bar{q}})$$

$$- \quad E_3^0(\hat{2}, \hat{1}, 4) \ A_3^0(\hat{\bar{2}}, \hat{\bar{1}}, \tilde{3}) M_2^0(\hat{\bar{\bar{1}}}_q, \hat{\bar{\bar{2}}}_{\bar{q}}) \Big\}$$

$$- \frac{1}{2N} \ \left\{ \ \left(C_4^0(\hat{1}, 3, 4, \hat{2}) + C_4^0(\hat{2}, 4, 3, \hat{1}) \right) \ M_2^0(\hat{\bar{1}}_q, \hat{\bar{2}}_{\bar{q}}) \right\}. \tag{3.25}$$

3.3.2 Construction of the real-virtual subtraction term

Following the discussion in section 2.6.3, the real-virtual subtraction term is generated from integrating a portion of the double real-subtraction term and including the appropriate NNLO mass factorization terms defined in section **??**. The real-virtual subtraction terms are conveniently formulated in terms of single unresolved integrated antenna strings, the explicit expressions for which can be found in appendix B.1, or inferred from those listed in B.1 given the rules for combining integrated antenna strings.

Quark-antiquark initial state:

$$\mathrm{d}\hat{\sigma}_{q\bar{q}}^T \;=\; \mathcal{N}_{q\bar{q}}\mathcal{N}_{NLO}\left(\frac{\alpha_s}{2\pi}\right)^2 \frac{\bar{C}(\epsilon)^2}{C(\epsilon)} \, \mathrm{d}\Phi_{\{X_i\}+1}(\{p_{X_i}\}, p_3; \bar{p}_1, \bar{p}_2) \int \frac{\mathrm{d}x_1}{x_1}\frac{\mathrm{d}x_2}{x_2} \Bigg\{$$

$$N \ \Bigg\{ \ -\boldsymbol{J}_3^{(1)}(\hat{\bar{1}}_q, 3_g, \hat{\bar{2}}_{\bar{q}}) \ M_3^0(\hat{\bar{1}}_q, \tilde{3}_g, \hat{\bar{2}}_{\bar{q}}) \ J_0^{(1)}(p_3)$$

$$+ A_3^0(\hat{1}, 3, \hat{2}) \Big[M_2^1(\hat{\bar{1}}_q, \hat{\bar{2}}_{\bar{q}})\delta(1 - x_1)\delta(1 - x_2) + \boldsymbol{J}_2^{(1)}(\hat{\bar{1}}_q, \hat{\bar{2}}_{\bar{q}}) \ M_2^0(\hat{\bar{1}}_q, \hat{\bar{2}}_{\bar{q}}) \Big]$$

$$+ \Big[A_3^1(\hat{\bar{1}}, 3, \hat{\bar{2}})\delta(1 - x_1)\delta(1 - x_2) + \bar{\boldsymbol{J}}_3^{(1)}(\hat{\bar{1}}_q, 3_g, \hat{\bar{2}}_{\bar{q}}) \ A_3^0(\hat{1}, 3, \hat{2}) \Big] \ M_2^0(\hat{\bar{\bar{1}}}_q, \hat{\bar{\bar{2}}}_{\bar{q}}) \Big]$$

$$+ b_0 \log\left(\frac{\mu^2}{s_{\bar{1}23}}\right) \ A_3^0(\hat{\bar{1}}, 3, \hat{\bar{2}})\delta(1 - x_1)\delta(1 - x_2) \ M_2^0(\hat{\bar{\bar{1}}}_q, \hat{\bar{\bar{2}}}_{\bar{q}}) \Bigg\}$$

$$- \frac{1}{N} \ \Bigg\{ \ -\boldsymbol{J}_2^{(1)}(\hat{\bar{1}}_q, \hat{\bar{2}}_{\bar{q}}) \ M_3^0(\hat{\bar{1}}_q, 3_g, \hat{\bar{2}}_{\bar{q}}) \ J_0^{(1)}(p_3)$$

$$+ A_3^0(\hat{1}, 3, \hat{2}) \Big[M_2^1(\hat{\bar{1}}_q, \hat{\bar{2}}_{\bar{q}})\delta(1 - x_1)\delta(1 - x_2) + \boldsymbol{J}_2^{(1)}(\hat{\bar{1}}_q, \hat{\bar{2}}_{\bar{q}}) \ M_2^0(\hat{\bar{1}}_q, \hat{\bar{2}}_{\bar{q}}) \Big]$$

$$+ \Big[\tilde{A}_3^1(\hat{\bar{1}}, 3, \hat{\bar{2}})\delta(1 - x_1)\delta(1 - x_2) + \widetilde{\bar{\boldsymbol{J}}}_3^{(1)}(\hat{\bar{1}}_q, 3_{\tilde{g}}, \hat{\bar{2}}_{\bar{q}}) \ A_3^0(\hat{1}, 3, \hat{2}) \Big] \ M_2^0(\hat{\bar{\bar{1}}}_q, \hat{\bar{\bar{2}}}_{\bar{q}}) \Big] \Bigg\}$$

$$+ \ \Bigg\{ \ -\boldsymbol{J}_{2,q\to g}^{(1)}(\hat{\bar{1}}_q, \hat{\bar{2}}_g) \ M_3^0(\hat{\bar{1}}_q, \hat{\bar{2}}_g, 3_{\bar{q}}) \ J_0^{(1)}(p_3)$$

$$-\boldsymbol{J}_{2,q\to g}^{(1)}(\hat{\bar{2}}_q,\hat{\bar{1}}_g)\; M_3^0(3_q,\hat{\bar{1}}_g,\hat{\bar{2}}_{\bar{q}})\; J_0^{(1)}(p_3)$$

$$+\boldsymbol{J}_{2,q\to g}^{(1)}(\hat{\bar{1}}_q,\hat{\bar{2}}_g)\; A_3^0(\hat{\bar{1}},\hat{\bar{2}},3)\; M_2^0(\hat{\bar{\bar{1}}}_q,\hat{\bar{\bar{2}}}_{\bar{q}})$$

$$+\boldsymbol{J}_{2,q\to g}^{(1)}(\hat{\bar{2}}_q,\hat{\bar{1}}_g)\; A_3^0(3,\hat{\bar{1}},\hat{\bar{2}})\; M_2^0(\hat{\bar{\bar{1}}}_q,\hat{\bar{\bar{2}}}_{\bar{q}})\Big\}$$

$$+N_F\;\left\{\;-\boldsymbol{J}_{3,N_F}^{(1)}(\hat{\bar{1}}_q,3_g,\hat{\bar{2}}_{\bar{q}})\; M_3^0(\hat{\bar{1}}_q,3_g,\hat{\bar{2}}_{\bar{q}})\; J_0^{(1)}(p_3)\right.$$

$$+\left[\hat{A}_3^1(\hat{\bar{1}},3,\hat{\bar{2}})\delta(1-x_1)\delta(1-x_2)+\bar{\boldsymbol{J}}_{3,N_F}^{(1)}(\hat{\bar{1}}_q,3_g,\hat{\bar{2}}_{\bar{q}})\; A_3^0(\hat{\bar{1}},3,\hat{\bar{2}})\right]\; M_2^0(\hat{\bar{\bar{1}}}_q,\hat{\bar{\bar{2}}}_{\bar{q}})$$

$$\left.+b_{0,F}\log\left(\frac{\mu^2}{s_{\bar{1}23}}\right)\; A_3^0(\hat{\bar{1}},3,\hat{\bar{2}})\delta(1-x_1)\delta(1-x_2)\; M_2^0(\hat{\bar{\bar{1}}}_q,\hat{\bar{\bar{2}}}_{\bar{q}})\right\}\right\} \qquad (3.26)$$

Several aspects of this formula are worth noting before similar expressions are presented for the other processes. In the colour decomposition (not including overall colour factors), the N^0 contributions all come from the double real subtraction term and are given by identity changing integrated antenna strings. All such strings are free from explicit poles and so no poles are subtracted at $\mathcal{O}(N^0)$. This reflects the lack of one-loop three parton matrix element contributing to the physical cross section at that order.

The $1/N$ contribution contains integrated antenna strings with the final-state gluon omitted. This reflects the fact that the gluon is Abelian and so the effective colour-structure is just a quark-anti-quark pair. In the (loop×tree) term the Abelian gluon enters only through the term,

$$\widetilde{\bar{\boldsymbol{J}}}_3^{(1)}(\hat{\bar{1}}_q,3_{\tilde{g}},\hat{\bar{2}}_{\bar{q}})\;=\;\mathcal{A}_{3,q\bar{q}}^0(s_{\bar{1}2})-\mathcal{A}_{3,q\bar{q}}^0(s_{\bar{1}23}). \qquad (3.27)$$

This term is distinct from $\bar{\boldsymbol{J}}_3^{(1)}(\hat{\bar{1}}_q,3_g,\hat{\bar{2}}_{\bar{q}})$ as the Abelian gluon is not involved in the colour ordering, reflected in the fact that no $\mathcal{D}_3^0$ antenna are included in its definition. The dependence on the Abelian gluon enters only through the mass of the antenna subtracted at the end of (3.27).

In the N_F dependent contribution there is no (tree×loop) contribution due to the lack of a N_F dependent one-loop matrix element with only a quark-anti-quark pair as the coloured external states. Similarly there is no N_F dependent quark-anti-quark two-parton one-loop antenna and so $\bar{\boldsymbol{J}}_{3,N_F}^{(1)}(\hat{\bar{1}}_q,3_g,\hat{\bar{2}}_{\bar{q}})=\boldsymbol{J}_{3,N_F}^{(1)}(\hat{\bar{1}}_q,3_g,\hat{\bar{2}}_{\bar{q}})$.

In order to construct the integrated antenna strings the appropriate mass factorization terms are combined with the integrated antenna functions. In the case

of an identity changing configuration a slight subtlety must be taken into account. In the formula above, the integrated antennae come from the double real subtraction term with colour factor N^0 because that is the colour factor carried by the $M_4^0(\hat{1}_q, 3_Q, \hat{2}_{\bar{Q}}, 4_{\bar{q}})$ contribution to the cross section. The identity changing mass factorization contribution has the form $\mathbf{\Gamma}_{gq}^1 \, \mathrm{d}\sigma_{qg}^R$. According to appendix A.1,

$$\mathbf{\Gamma}_{gq}^1 = \left(\frac{N^2-1}{N}\right)\Gamma_{gq}^1, \tag{3.28}$$

where Γ_{gq}^1 is the colour stripped mass factorization kernel. Factoring out the factor of $\mathcal{N}_{NLO}$ common to both $\mathrm{d}\sigma_{qg}^R$ and the N^0 contribution to $\mathrm{d}\sigma_{qq}^T$, the mass factorization contribution appears to have the wrong colour structure, contributing at N and $1/N$ rather than N^0. The solution is in the initial-state colour averaging factors $\mathcal{N}_{ij}$. Using the relation,

$$\mathcal{N}_{q\bar{q}} = \left(\frac{N^2-1}{N}\right)\mathcal{N}_{qg}, \tag{3.29}$$

it is clear that if the mass factorization contribution is to be proportional to the overall factor of $\mathcal{N}_{q\bar{q}}$ used in (3.26) then the additional factor of $(N^2-1)/N$ is combined with $\mathcal{N}_{qg}$ to generate this overall factor, allowing the identity changing mass factorization terms to contribute at $\mathcal{O}(N^0)$ as required. Similar problems with colour factors arise for other identity changing mass factorization terms, all are solved in the same way as in the example above.

Quark-gluon initial state:

$$
\begin{aligned}
\mathrm{d}\hat{\sigma}_{qg}^T = {} & \mathcal{N}_{qg}\mathcal{N}_{NLO}\left(\frac{\alpha_s}{2\pi}\right)^2 \frac{\bar{C}(\epsilon)^2}{C(\epsilon)} \, \mathrm{d}\Phi_{\{X_i\}+1}(\{p_{X_i}\}, p_3; \bar{p}_1, \bar{p}_2) \int \frac{\mathrm{d}x_1}{x_1}\frac{\mathrm{d}x_2}{x_2} \Bigg\{ \quad (3.30) \\
N \quad & \Bigg\{ -\boldsymbol{J}_3^{(1)}(\hat{\bar{1}}_q, \hat{\bar{2}}_g, 3_{\bar{q}}) \, M_3^0(\hat{\bar{1}}_q, \hat{\bar{2}}_g, 3_{\bar{q}}) \, J_0^{(1)}(p_3) \\
& + A_3^0(\hat{1}, \hat{2}, 3)\left[M_2^1(\hat{\bar{1}}_q, \hat{\bar{2}}_{\bar{q}})\delta(1-x_1)\delta(1-x_2) + \boldsymbol{J}_2^{(1)}(\hat{\bar{1}}_q, \hat{\bar{2}}_{\bar{q}}) \, M_2^0(\hat{\bar{1}}_q, \hat{\bar{2}}_{\bar{q}}) \right] \\
& + \left[A_3^1(\hat{1}, \hat{2}, 3)\delta(1-x_1)\delta(1-x_2) + \bar{\boldsymbol{J}}_3^{(1)}(\hat{\bar{1}}_q, \hat{\bar{2}}_g, 3_{\bar{q}}) \, A_3^0(\hat{1}, \hat{2}, 3) \right] M_2^0(\hat{\bar{1}}_q, \hat{\bar{2}}_{\bar{q}}) \\
& + b_0 \log\left(\frac{\mu^2}{s_{\bar{1}\bar{2}3}}\right) A_3^0(\hat{1}, \hat{2}, 3)\delta(1-x_1)\delta(1-x_2) \, M_2^0(\hat{\bar{1}}_q, \hat{\bar{2}}_{\bar{q}}) \\
& - \boldsymbol{J}_{2, g \to q}^{(1)}(\hat{\bar{2}}_{\bar{q}}, 3_g) \, M_3^0(\hat{\bar{1}}_q, 3_g, \hat{\bar{2}}_{\bar{q}}) \, J_0^{(1)}(p_3)
\end{aligned}
$$

$$+ \boldsymbol{J}^{(1)}_{2,g\to q}(3_g, \hat{\bar{2}}_{\bar{q}}) \, A^0_3(\hat{\bar{1}}_q, 3_g, \hat{\bar{2}}_{\bar{q}}) \, M^0_2(\hat{\bar{\bar{1}}}_q, \hat{\bar{\bar{2}}}_{\bar{q}}) \Big\}$$

$$- \frac{1}{N} \left\{ \; - \boldsymbol{J}^{(1)}_2(\hat{\bar{1}}_q, 3_{\bar{q}}) \, M^0_3(\hat{\bar{1}}_q, \hat{\bar{2}}_g, 3_{\bar{q}}) \, J^{(1)}_0(p_3) \right.$$

$$+ A^0_3(\hat{1}, \hat{2}, 3)\left[M^1_2(\hat{\bar{\bar{1}}}_q, \hat{\bar{\bar{2}}}_{\bar{q}})\delta(1-x_1)\delta(1-x_2) + \boldsymbol{J}^{(1)}_2(\hat{\bar{\bar{1}}}_q, \hat{\bar{\bar{2}}}_{\bar{q}}) \, M^0_2(\hat{\bar{\bar{1}}}_q, \hat{\bar{\bar{2}}}_{\bar{q}}) \right]$$

$$+ \left[\tilde{A}^1_3(\hat{1}, \hat{2}, 3)\delta(1-x_1)\delta(1-x_2) + \widetilde{\boldsymbol{J}}^{(1)}_3(\hat{1}_q, \hat{\bar{2}}_g, 3_{\bar{q}}) \, A^0_3(\hat{1}, \hat{2}, 3) \right] M^0_2(\hat{\bar{\bar{1}}}_q, \hat{\bar{\bar{2}}}_{\bar{q}})$$

$$- \boldsymbol{J}^{(1)}_{2,g\to q}(\hat{\bar{2}}_{\bar{q}}, \hat{\bar{1}}_q) \, M^0_3(\hat{\bar{1}}_q, 3_g, \hat{\bar{2}}_{\bar{q}}) \, J^{(1)}_0(p_3)$$

$$\left. + \boldsymbol{J}^{(1)}_{2,g\to q}(\hat{\bar{2}}_{\bar{q}}, \hat{\bar{1}}_q) \, A^0_3(\bar{1}_q, 3_g, \bar{2}_{\bar{q}}) \, M^0_2(\hat{\bar{\bar{1}}}_q, \hat{\bar{\bar{2}}}_{\bar{q}}) \right\}$$

$$+ N_F \left\{ \; - \boldsymbol{J}^{(1)}_{3,N_F}(\hat{\bar{1}}_q, \hat{\bar{2}}_g, 3_{\bar{q}}) \, M^0_3(\hat{\bar{1}}_q, \hat{\bar{2}}_g, 3_{\bar{q}}) \, J^{(1)}_0(p_3) \right.$$

$$+ \left[\hat{A}^1_3(\hat{1}, \hat{2}, 3) \, \delta(1-x_1)\delta(1-x_2) + \boldsymbol{J}^{(1)}_{3,N_F}(\hat{\bar{1}}_q, \hat{\bar{2}}_g, 3_{\bar{q}}) \, A^0_3(\hat{1}, \hat{2}, 3) \right] M^0_2(\hat{\bar{\bar{1}}}_q, \hat{\bar{\bar{2}}}_{\bar{q}})$$

$$\left. \left. + b_{0,F} \log\left(\frac{\mu^2}{s_{\bar{1}23}} \right) \delta(1-x_1)\delta(1-x_2) \, A^0_3(\hat{1}, \hat{2}, 3) \, M^0_2(\hat{\bar{\bar{1}}}_q, \hat{\bar{\bar{2}}}_{\bar{q}}) \right\} \right\} \tag{3.31}$$

In this formula $\boldsymbol{J}^{(1)}_{3,N_F}(\hat{\bar{1}}_q, \hat{\bar{2}}_g, 3_{\bar{q}}) = \boldsymbol{J}^{(1)}_{2,N_F}(3_{\bar{q}}, \hat{\bar{2}}_g)\delta(1-x_1)$ as there is no N_F dependent initial-initial quark-gluon two-parton string which would be denoted by $\boldsymbol{J}^{(1)}_{2,N_F}(\hat{\bar{1}}_q, \hat{\bar{2}}_g)$.

Gluon-gluon initial state:

$$\mathrm{d}\hat{\sigma}^T_{gg} = \mathcal{N}_{gg}\mathcal{N}_{NLO}\left(\frac{\alpha_s}{2\pi}\right)^2 \frac{\bar{C}(\epsilon)^2}{C(\epsilon)} \, \mathrm{d}\Phi_{\{X_i\}+1}(\{p_{X_i}\}, p_3; \bar{p}_1, \bar{p}_2) \int \frac{\mathrm{d}x_1}{x_1}\frac{\mathrm{d}x_2}{x_2} \Bigg\{$$

$$N_F N \sum_{\{1,2\}} \left\{ \; - \boldsymbol{J}^{(1)}_{2,g\to q}(\hat{\bar{1}}_q, \hat{\bar{2}}_g) \, M^0_3(\hat{\bar{1}}_q, \hat{\bar{2}}_g, 3_{\bar{q}}) \, J^{(1)}_0(p_3) \right.$$

$$- \boldsymbol{J}^{(1)}_{2,g\to q}(\hat{\bar{2}}_q, \hat{\bar{1}}_g) \, M^0_3(3_q, \hat{\bar{1}}_g, \hat{\bar{2}}_{\bar{q}}) \, J^{(1)}_0(p_3)$$

$$+ \boldsymbol{J}^{(1)}_{2,g\to q}(\hat{\bar{1}}_q, \hat{\bar{2}}_g) \, A^0_3(\hat{1}, \hat{2}, 3) \, M^0_2(\hat{\bar{\bar{1}}}_q, \hat{\bar{\bar{2}}}_{\bar{q}})$$

$$\left. + \boldsymbol{J}^{(1)}_{2,g\to q}(\hat{\bar{2}}_q, \hat{\bar{1}}_g) \, A^0_3(3, \hat{1}, \hat{2}) \, M^0_2(\hat{\bar{\bar{1}}}_q, \hat{\bar{\bar{2}}}_{\bar{q}}) \right\}$$

$$- \frac{N_F}{N} \left\{ \; - \boldsymbol{J}^{(1)}_{2,g\to q}(\hat{\bar{1}}_q, \hat{\bar{2}}_g) \, M^0_3(\hat{\bar{1}}_q, \hat{\bar{2}}_g, 3_{\bar{q}}) \, J^{(1)}_0(p_3) \right.$$

$$- \boldsymbol{J}^{(1)}_{2,g\to q}(\hat{\bar{2}}_q, \hat{\bar{1}}_g) \, M^0_3(3_q, \hat{\bar{1}}_g, \hat{\bar{2}}_{\bar{q}}) \, J^{(1)}_0(p_3)$$

$$+ \boldsymbol{J}^{(1)}_{2,g\to q}(\hat{\bar{1}}_q, \hat{\bar{2}}_g) \, A^0_3(\hat{1}, \hat{2}, 3) \, M^0_2(\hat{\bar{\bar{1}}}_q, \hat{\bar{\bar{2}}}_{\bar{q}})$$

$$\left. \left. + \boldsymbol{J}^{(1)}_{2,g\to q}(\hat{\bar{2}}_q, \hat{\bar{1}}_g) \, A^0_3(3, \hat{1}, \hat{2}) \, M^0_2(\hat{\bar{\bar{1}}}_q, \hat{\bar{\bar{2}}}_{\bar{q}}) \right\} \right\}. \tag{3.32}$$

All the terms in this expression are proportional to identity changing integrated antenna strings and so the whole subtraction term is free from explicit poles; this

reflects the absence of one-loop gluon-gluon initiated matrix elements in the physical cross section.

Quark-quark initial state:

The quark-quark initial state with non-identical quarks has the subtraction term given by,

$$
\begin{aligned}
\mathrm{d}\hat{\sigma}^T_{qQ} \;=\; & \mathcal{N}_{q\bar{q}}\mathcal{N}_{NLO}\left(\frac{\alpha_s}{2\pi}\right)^2 \frac{\bar{C}(\epsilon)^2}{C(\epsilon)} \,\mathrm{d}\Phi_{\{X_i\}+1}(\{p_{X_i}\}, p_3; \bar{p}_1, \bar{p}_2)\int \frac{\mathrm{d}x_1}{x_1}\frac{\mathrm{d}x_2}{x_2}\left\{ \right.\\
& -\; \boldsymbol{J}^{(1)}_{2,q\to g}(\hat{\bar{1}}_q, \hat{\bar{2}}_g)\, M^0_3(\hat{\bar{1}}_q, \hat{\bar{2}}_g, \tilde{3}_{\bar{q}})\\
& -\; \boldsymbol{J}^{(1)}_{2,q\to g}(\hat{\bar{2}}_q, \hat{\bar{1}}_g)\, M^0_3(\hat{\bar{2}}_q, \hat{\bar{1}}_g, \tilde{3}_{\bar{q}})\\
& +\; \boldsymbol{J}^{(1)}_{2,q\to g}(\hat{\bar{1}}_q, \hat{\bar{2}}_g)\, A^0_3(\hat{\bar{1}}, \hat{\bar{2}}, 3)\, M^0_2(\hat{\bar{\bar{1}}}_q, \hat{\bar{\bar{2}}}_{\bar{q}})\\
& +\; \left. \boldsymbol{J}^{(1)}_{2,q\to g}(\hat{\bar{2}}_q, \hat{\bar{1}}_g)\, A^0_3(\hat{\bar{2}}, \hat{\bar{1}}, 3)\, M^0_2(\hat{\bar{\bar{1}}}_q, \hat{\bar{\bar{2}}}_{\bar{q}})\right\}.
\end{aligned}
\tag{3.33}
$$

These terms are again all proportional to the identity changing integrated antenna strings and so not only terminate in the real-virtual level of the calculation but are also free from explicit poles. This is expected given the lack of non-zero quark-quark initiated three-parton one-loop processes.

The corresponding term for the identical quark contribution is the same as for the non-identical quarks. This is found by inspection when integrating the respective double real subtraction terms but can also be understood with basic physical intuition. The only divergent single unresolved limits for a quark-quark initiated four-quark matrix element is the initial-final single collinear limit. In this limit both the identical and non-identical quark matrix elements factor onto a two-quark one-gluon matrix element with the gluon in the initial-state. The identical quark matrix elements in principle have twice as many divergent collinear limits than the non-identical matrix elements but the identical quark final-state symmetry factor removes this degeneracy upon integration. The result is that the double real contributions from non-identical and identical quark-quark initial states have the same single unresolved limits and factor onto the same reduced matrix elements; therefore their respective contributions to the real-virtual subtraction term are the same.

$$
\mathrm{d}\hat{\sigma}^T_{qQ} \;=\; \mathrm{d}\hat{\sigma}^T_{qq}
\tag{3.34}
$$

3.3.3 Construction of the double virtual subtraction term

The double virtual subtraction can be generated by following the discussion in section 2.6.4. The result is quoted here in terms of integrated antenna strings, the explicit formulae for which can be found in appendix B.

Quark-antiquark initial state:

$$
\begin{aligned}
\mathrm{d}\hat{\sigma}_{q\bar{q}}^{U} =\ & -\mathcal{N}_{q\bar{q}}\mathcal{N}_{NLO}\left(\frac{\alpha_s}{2\pi}\right)^2 \bar{C}(\epsilon)^2\, \mathrm{d}\Phi_{\{X_i\}}(\{p_{X_i}\}; \bar{p}_1, \bar{p}_2) \int \frac{\mathrm{d}z_1}{z_1}\frac{\mathrm{d}z_2}{z_2}\ \Bigg\{ \\
& N\ \Bigg\{\ \boldsymbol{J}_2^{(1)}(\hat{\bar{1}}_q, \hat{\bar{2}}_{\bar{q}})\Big(M_2^1(\hat{\bar{1}}_q, \hat{\bar{2}}_{\bar{q}}) - \frac{b_0}{\epsilon}M_2^0(\hat{\bar{1}}_q, \hat{\bar{2}}_{\bar{q}})\Big) \\
& \qquad +\ \Big(\frac{1}{2}\boldsymbol{J}_2^{(1)}(\hat{\bar{1}}_q, \hat{\bar{2}}_{\bar{q}}) \otimes \boldsymbol{J}_2^{(1)}(\hat{\bar{1}}_q, \hat{\bar{2}}_{\bar{q}})\ + \boldsymbol{J}_2^{(2)}(\hat{\bar{1}}_q, \hat{\bar{2}}_{\bar{q}})\Big)\, M_2^0(\hat{\bar{1}}_q, \hat{\bar{2}}_{\bar{q}})\Bigg\} \\
& +\ \Bigg\{\ \boldsymbol{J}_{2,q\to g\to q}^{(2)}(\hat{\bar{1}}_q, \hat{\bar{2}}_{\bar{q}})\, M_2^0(\hat{\bar{1}}_q, \hat{\bar{2}}_{\bar{q}})\Bigg\} \\
& -\frac{1}{N}\ \Bigg\{\ \boldsymbol{J}_2^{(1)}(\hat{\bar{1}}_q, \hat{\bar{2}}_{\bar{q}})\, M_2^1(\hat{\bar{1}}_q, \hat{\bar{2}}_{\bar{q}}) \\
& \qquad +\ \Big(\frac{1}{2}\boldsymbol{J}_2^{(1)}(\hat{\bar{1}}_q, \hat{\bar{2}}_{\bar{q}}) \otimes \boldsymbol{J}_2^{(1)}(\hat{\bar{1}}_q, \hat{\bar{2}}_{\bar{q}})\ + \widetilde{\boldsymbol{J}}_2^{(2)}(\hat{\bar{1}}_q, \hat{\bar{2}}_{\bar{q}})\Big)\, M_2^0(\hat{\bar{1}}_q, \hat{\bar{2}}_{\bar{q}})\Bigg\} \\
& +N_F\ \Bigg\{\ -\boldsymbol{J}_2^{(1)}(\hat{\bar{1}}_q, \hat{\bar{2}}_{\bar{q}})\, \frac{b_{0,F}}{\epsilon}\, M_2^0(\hat{\bar{1}}_q, \hat{\bar{2}}_{\bar{q}}) + \boldsymbol{J}_{2,N_F}^{(2)}(\hat{\bar{1}}_q, \hat{\bar{2}}_{\bar{q}})\, M_2^0(\hat{\bar{1}}_q, \hat{\bar{2}}_{\bar{q}})\Bigg\}\Bigg\} \quad (3.35)
\end{aligned}
$$

It is noted that the structures seen in this subtraction term and the explicit forms, listed in appendix B, display the structures discussed in section 2.6.4. Ignoring overall colour factors, the $\mathcal{O}(N)$, $\mathcal{O}(1/N)$ and $\mathcal{O}(N_F)$ contributions correspond to terms in the double virtual physical cross section and are expected to cancel the explicit poles present in these terms. The $\mathcal{O}(N^0)$ contribution does not correspond to any two-loop matrix elements but as it is built from a finite identity changing integrated antenna string this term contains no explicit poles.

Quark-gluon initial state:

$$
\begin{aligned}
\mathrm{d}\hat{\sigma}_{qg}^{U} =\ & -\mathcal{N}_{qg}\mathcal{N}_{NLO}\left(\frac{\alpha_s}{2\pi}\right)^2 \bar{C}(\epsilon)^2\, \mathrm{d}\Phi_{\{X_i\}}(\{p_{X_i}\}; \bar{p}_1, \bar{p}_2) \int \frac{\mathrm{d}z_1}{z_1}\frac{\mathrm{d}z_2}{z_2}\ \Bigg\{ \\
& N\ \Bigg\{\ \boldsymbol{J}_{2,g\to q}^{(1)}(\hat{\bar{1}}_q, \hat{\bar{2}}_{\bar{q}})\Big(M_2^1(\hat{\bar{1}}_q, \hat{\bar{2}}_{\bar{q}}) - \frac{b_0}{\epsilon}\, M_2^0(\hat{\bar{1}}_q, \hat{\bar{2}}_{\bar{q}})\Big) + \boldsymbol{J}_{2,g\to q}^{(2)}(\hat{\bar{1}}_q, \hat{\bar{2}}_{\bar{q}})\, M_2^0(\hat{\bar{1}}_q, \hat{\bar{2}}_{\bar{q}})\Bigg\} \\
& -\frac{1}{N}\ \Bigg\{\ \boldsymbol{J}_{2,g\to q}^{(1)}(\hat{\bar{1}}_q, \hat{\bar{2}}_{\bar{q}})\, M_2^1(\bar{1}_q, \bar{2}_{\bar{q}}) + \widetilde{\boldsymbol{J}}_{2,g\to q}^{(2)}(\hat{\bar{1}}_q, \hat{\bar{2}}_{\bar{q}})\, M_2^0(\hat{\bar{1}}_q, \hat{\bar{2}}_{\bar{q}})\Bigg\}
\end{aligned}
$$

$$+N_F \left\{ -\boldsymbol{J}^{(1)}_{2,g\to q}(\hat{\bar{1}}_q, \hat{\bar{2}}_{\bar{q}}) \frac{b_{0,F}}{\epsilon} M_2^0(\hat{\bar{1}}_q, \bar{\bar{2}}_{\bar{q}}) + \boldsymbol{J}^{(2)}_{2,g\to q,N_F}(\hat{\bar{1}}_q, \hat{\bar{2}}_{\bar{q}}) M_2^0(\hat{\bar{1}}_q, \bar{\bar{2}}_{\bar{q}}) \right\} \qquad (3.36)$$

This subtraction term highlights the fact that although the single unresolved identity changing integrated antenna strings, $\boldsymbol{J}^{(1)}_{2,a\to b}$, are finite, these finite terms factor onto terms containing explicit poles. These poles must therefore cancel against poles in the double unresolved identity changing integrated antenna strings, $\boldsymbol{J}^{(2)}_{2,a\to b}$. The fact that these strings contain explicit poles, unlike the single unresolved identity changing strings can be intuitively understood in terms of unresolved configurations. At NNLO a double unresolved configuration may contain an initial-final collinear limit which changes the identity of the initial-state partons, in addition to a final-state soft or collinear limit. The poles associated with the initial-final limit will indeed cancel against the mass factorization contribution included in the string but the additional unresolved parton will contribute genuine poles to the integrated antenna string.

Gluon-gluon initial state

$$\mathrm{d}\hat{\sigma}^U_{gg} = -\mathcal{N}_{gg}\mathcal{N}_{NLO}\left(\frac{\alpha_s}{2\pi}\right)^2 \bar{C}(\epsilon)^2 \, \mathrm{d}\Phi_{\{X_i\}}(\{p_{X_i}\}; \bar{p}_1, \bar{p}_2) \int \frac{\mathrm{d}z_1}{z_1}\frac{\mathrm{d}z_2}{z_2} \left\{ \right.$$

$$N_F N \left\{ \boldsymbol{J}^{(2)}_{2,g\to q,g\to q}(\hat{\bar{1}}_q, \hat{\bar{2}}_{\bar{q}}) M_2^0(\bar{1}_q, \bar{2}_{\bar{q}}) \right\}$$

$$\left. -\frac{N_F}{N} \left\{ \widetilde{\boldsymbol{J}}^{(2)}_{2,g\to q,g\to q}(\hat{\bar{1}}_q, \hat{\bar{2}}_{\bar{q}}) M_2^0(\bar{1}_q, \bar{2}_{\bar{q}}) \right\} \right\} \qquad (3.37)$$

Quark-quark (non-identical) initial state

$$\mathrm{d}\hat{\sigma}^U_{qQ} = -\mathcal{N}_{qQ}\mathcal{N}_{NLO}\left(\frac{\alpha_s}{2\pi}\right)^2 \bar{C}(\epsilon)^2 \, \mathrm{d}\Phi_{\{X_i\}}(\{p_{X_i}\}; \bar{p}_1, \bar{p}_2) \int \frac{\mathrm{d}z_1}{z_1}\frac{\mathrm{d}z_2}{z_2}$$

$$\boldsymbol{J}^{(2)}_{2,Q\to q}(\hat{\bar{1}}_q, \hat{\bar{2}}_{\bar{q}}) M_2^0(\bar{1}_q, \bar{2}_{\bar{q}}). \qquad (3.38)$$

Quark-quark (identical) initial state

$$\mathrm{d}\hat{\sigma}^U_{qq} = \mathcal{N}_{qq}\mathcal{N}_{NLO}\left(\frac{\alpha_s}{2\pi}\right)^2 \bar{C}(\epsilon)^2 \, \mathrm{d}\Phi_{\{X_i\}}(\{p_{X_i}\}; \bar{p}_1, \bar{p}_2) \int \frac{\mathrm{d}z_1}{z_1}\frac{\mathrm{d}z_2}{z_2}$$

$$\left\{ \boldsymbol{J}^{(2)}_{2,Q\to\bar{q}}(\hat{\bar{1}}_q, \hat{\bar{2}}_{\bar{q}}) M_2^0(\bar{1}_q, \bar{2}_{\bar{q}}) - \frac{1}{N}\boldsymbol{J}^{(2)}_{2,q\to\bar{q}}(\hat{\bar{1}}_q, \hat{\bar{2}}_{\bar{q}}) M_2^0(\bar{1}_q, \bar{2}_{\bar{q}}) \right\}. \qquad (3.39)$$

The explicit forms of the integrated antenna strings are collected in appendix B. When properly defined in terms of the integrated antennae inherited from the double real and real-virtual levels of the calculation and the appropriate mass factorization kernels defined in appendix A, the pole structure of the double virtual subtraction term is expected to match that of the two-loop matrix elements.

Chapter 4

Production of colourless particles via gluon scattering

In chapter 3, the colourless particles were assumed to not couple to gluons at tree-level, only coupling to quarks. This is the case for the production of Z^0 and $W^\pm$ bosons via quark scattering. Quark-gluon or gluon-gluon initiated processes can produce these colourless particles beyond leading order but only by coupling directly to quarks. In this chapter the production of one or more colourless particles via gluon scattering is considered, i.e., the process $pp \to X$, where X represents any colourless particle or particles which couple to gluons rather than quarks. An example is the standard model Higgs boson.

The Higgs couplings to quarks are proportional to the quark mass and so in the massless quark limit the Higgs does not interact with the quarks within the proton at tree-level. As the gluon is strictly massless the Higgs cannot couple directly to gluons either but it can couple indirectly through a quark loop. When computing the quark loop contribution, shown in figure 4.1, all flavours of quark contribute to the loop. The Higgs will not couple strongly to the light quark loops but does couple to the top quark loop due to its large mass.

In the limit that the top quark mass is taken to infinity the contribution from the top quark loop can be integrated out, generating an effective Lagrangian,

$$\mathcal{L}_{\text{eff}} \;=\; C \, H \, \text{Tr}\big[\big(\boldsymbol{t} \cdot \boldsymbol{F}_{\mu\nu}\big)^2\big], \tag{4.1}$$
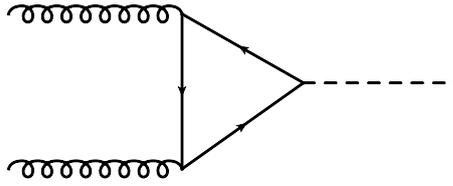
Figure 4.1: The one-loop diagram which allows the Higgs to couple to gluons via a top quark loop.

where to leading order $C = \alpha_s/(6\pi v)$ and is proportional to the strong coupling. $v = 246$ GeV is the vacuum expectation value of the Higgs field. The effective Lagrangian produces interactions between the Higgs and two, three and four gluons. Using this effective theory, Higgs production via tree-level gluon scattering may be calculated, along with the NLO and NNLO corrections to the Born-level process.

4.1 Physical matrix elements for up to four partons

The many Feynman diagrams which contribute to each scattering process may be decomposed into its set of colour ordered amplitudes. These amplitudes contain all non-QCD couplings such that only the QCD coupling (including factors of the effective Higgs-gluon-gluon coupling which contains implicit powers of α_s) and the colour factors common to all diagrams contributing to a particular colour ordered amplitude are stripped out of the amplitudes. The diagrams shown in figure 4.2 reflect this strategy by showing the coloured partons as a genuine Feynman graph with the colourless states being represented by a single dashed line. The presence of the single dashed line in this context means the set of diagrams which dress the coloured partons with colourless particles contributing to the same colour ordered amplitude to the same fixed order in all the relevant couplings. This interpretation of the diagrams in figure 4.2 allows X to represent multiple colourless particles dressing multiple coloured legs and not just the single dashed line coupling to one parton.
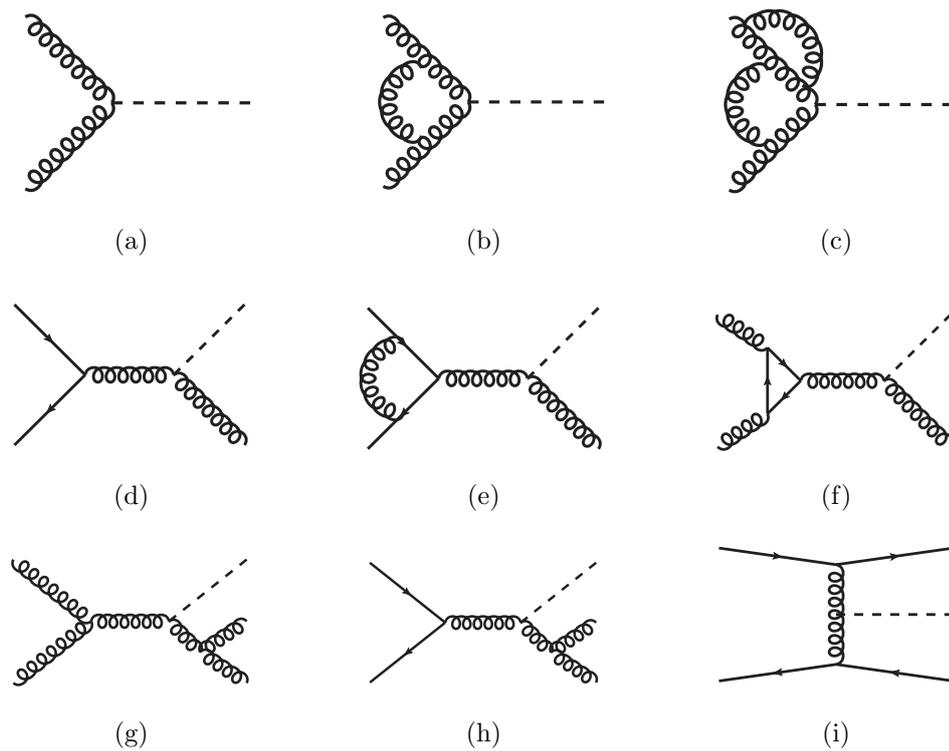
Figure 4.2: A selection of diagrams representing contributions to the physical matrix elements up to NNLO. Dashed lines represent the colourless particle (or particles) X.

4.1.1   Two-parton contribution

Tree-level:

The Born-level process for gluon scattering begins at $\mathcal{O}(\alpha_s^2)$ via the effective Higgs-gluon coupling. To the same order in α_s the quark-initiated process are zero as no direct coupling to massless quarks is permitted. An example diagram for the tree-level two-parton process is shown in figure 4.2 (a).

$$\begin{aligned}
\mathrm{d}\hat{\sigma}_{gg}^{LO} &= 2\mathcal{N}_{gg}\mathcal{N}_{LO} \, \mathrm{d}\Phi_{\{X_i\}}(\{p_{X_i}\}; p_1, p_2) \, M_2^0(\hat{1}_g, \hat{2}_g), \\
\mathrm{d}\hat{\sigma}_{qg}^{LO} &= 0, \\
\mathrm{d}\hat{\sigma}_{q\bar{q}}^{LO} &= 0,
\end{aligned} \tag{4.2}$$

where as before $\mathcal{N}_{ij}$ contains overall multiplicative factors due to spin and colour averaging of initial state partons. The overall factor for this process contains the

leading order colour factor and overall effective coupling,

$$\mathcal{N}_{LO} = \frac{C^{2h}}{2} \, (N^2 - 1),\tag{4.3}$$

where h is the number of effective Higgs-gluon-gluon couplings .

One-loop:

The one-loop corrections to the Born-level processes given by

$$\begin{aligned}
\mathrm{d}\hat{\sigma}^V_{gg} &= \mathcal{N}_{gg}\mathcal{N}_{LO} \, \bar{C}(\epsilon) \left(\frac{\alpha_s}{2\pi}\right) \mathrm{d}\Phi_{\{X_i\}}(\{p_{X_i}\}; p_1, p_2) \\
&\quad \times \left(N \, M_2^1(\hat{1}_g, \hat{2}_g) + N_F \, \widehat{M}_2^1(\hat{1}_g, \hat{2}_g) \right), \\
\mathrm{d}\hat{\sigma}^V_{qg} &= 0, \\
\mathrm{d}\hat{\sigma}^V_{q\bar{q}} &= 0,
\end{aligned}\tag{4.4}$$

where despite the one-loop two-quark amplitude being non-zero, the tree-level two-quark amplitude it projects onto is zero and so provides no contribution to the cross section. An example of a diagram contributing to the one-loop amplitude is given in figure 4.2 (b).

Two-loops:

At two loops the quark-anti-quark initiated channel is non-zero due to the self-interaction of the non-zero one-loop amplitude. The fact that all two-quark tree-level or one-loop matrix elements are zero demonstrates the fact that this two-loop contribution is finite and requires no explicit pole subtraction. The relevant two-loop matrix elements can be obtained from the two-loop gluon form factor, which are presented in renormalized form in [126],

$$\begin{aligned}
\mathrm{d}\hat{\sigma}^{VV}_{gg} &= \mathcal{N}_{gg}\mathcal{N}_{NLO} \, \bar{C}(\epsilon)^2 \left(\frac{\alpha_s}{2\pi}\right)^2 \mathrm{d}\Phi_{\{X_i\}}(\{p_{X_i}\}; p_1, p_2) \\
&\quad \left\{ N \, M_2^2(\hat{1}_g, \hat{2}_g) + N_F \, \widehat{M}_2^2(\hat{1}_g, \hat{2}_g) + \frac{N_F}{N^2}\widehat{\widehat{M}_2^2}(\hat{1}_g, \hat{2}_g) + \frac{N_F^2}{N} \, \widehat{\widehat{M}_2^2}(\hat{1}_g, \hat{2}_g) \right\}, \\
\mathrm{d}\hat{\sigma}^{VV}_{qg} &= 0, \\
\mathrm{d}\hat{\sigma}^{VV}_{q\bar{q}} &= \mathcal{N}_{q\bar{q}}\mathcal{N}_{NLO} \, \bar{C}(\epsilon)^2 \left(\frac{\alpha_s}{2\pi}\right)^2 \mathrm{d}\Phi_{\{X_i\}}(\{p_{X_i}\}; p_1, p_2) \, M_2^2(\hat{1}_q, \hat{2}_{\bar{q}}),
\end{aligned}\tag{4.5}$$

where $\mathcal{N}_{NLO} = N\mathcal{N}_{LO}$. One of the many two-loop diagrams which contribute to the two-loop amplitudes is shown in figure 4.2 (c).

September 24, 2012

4.1.2 Three-parton contribution

Tree-level:

The additional final-state parton in the three-parton contribution opens up the quark-gluon channel, as shown by the diagram in figure 4.2 (d). The various contributions to the NLO cross section are given by,

$$
\begin{aligned}
d\hat{\sigma}_{gg}^R &= \mathcal{N}_{gg}\mathcal{N}_{LO}\frac{\bar{C}(\epsilon)}{C(\epsilon)}\left(\frac{\alpha_s}{2\pi}\right)d\Phi_{\{X_i\}+1}(\{p_{X_i}\},p_3;p_1,p_2)\,2N\,M_3^0(\hat{1}_g,3_g,\hat{2}_g)\,J_0^{(1)}(p_3), \\
d\hat{\sigma}_{qg}^R &= \mathcal{N}_{qg}\mathcal{N}_{LO}\frac{\bar{C}(\epsilon)}{C(\epsilon)}\left(\frac{\alpha_s}{2\pi}\right)d\Phi_{\{X_i\}+1}(\{p_{X_i}\},p_3;p_1,p_2)\,M_3^0(\hat{1}_q,\hat{2}_g,3_{\bar{q}})\,J_0^{(1)}(p_3), \\
d\hat{\sigma}_{q\bar{q}}^R &= \mathcal{N}_{q\bar{q}}\mathcal{N}_{LO}\frac{\bar{C}(\epsilon)}{C(\epsilon)}\left(\frac{\alpha_s}{2\pi}\right)d\Phi_{\{X_i\}+1}(\{p_{X_i}\},p_3;p_1,p_2)\,M_3^0(\hat{1}_q,3_g,\hat{2}_{\bar{q}})\,J_0^{(1)}(p_3).
\end{aligned}
$$

$$(4.6)$$

Unlike for the physical processes discussed in chapter 3, the $d\sigma_{qg}^R$ contribution does admit an initial-state collinear singularity in the configuration where the final-state quark becomes collinear with the initial-state quark. In this configuration the two-particle reduced matrix element is gluonic and non-zero.

The quark-anti-quark initiated channel is non-zero but finite due to the lack of tree-level two-quark matrix element to factor onto in single unresolved limits. Other non-zero channels are obtained from these processes via an appropriate substitution of labels. e.g., $d\hat{\sigma}_{\bar{q}q}^R = d\hat{\sigma}_{q\bar{q}}^R(q \leftrightarrow \bar{q})$.

One-loop:

$$
\begin{aligned}
d\hat{\sigma}_{gg}^{RV} &= \mathcal{N}_{gg}\mathcal{N}_{NLO}\,\frac{\bar{C}(\epsilon)^2}{C(\epsilon)}\left(\frac{\alpha_s}{2\pi}\right)^2 d\Phi_{\{X_i\}+1}(\{p_{X_i}\},p_3;p_1,p_2) \\
&\quad \left\{ 2N\,M_3^1(\hat{1}_g,\hat{2}_g,3_g) + N_F\,\widehat{M_3^1}(\hat{1}_g,\hat{2}_g,3_g) \right\} J_0^{(1)}(p_3), \\
d\hat{\sigma}_{qg}^{RV} &= \mathcal{N}_{qg}\mathcal{N}_{NLO}\,\frac{\bar{C}(\epsilon)^2}{C(\epsilon)}\left(\frac{\alpha_s}{2\pi}\right)^2 d\Phi_{\{X_i\}+1}(\{p_{X_i}\},p_3;p_1,p_2) \\
&\quad \left\{ M_3^1(\hat{1}_q,\hat{2}_g,3_{\bar{q}}) - \frac{1}{N^2}\,\widetilde{M_3^1}(\hat{1}_q,\hat{2}_g,3_{\bar{q}}) + \frac{N_F}{N}\,\widehat{M_3^1}(\hat{1}_q,\hat{2}_g,3_{\bar{q}}) \right\} J_0^{(1)}(p_3), \\
d\hat{\sigma}_{q\bar{q}}^{RV} &= \mathcal{N}_{q\bar{q}}\mathcal{N}_{NLO}\,\frac{\bar{C}(\epsilon)^2}{C(\epsilon)}\left(\frac{\alpha_s}{2\pi}\right)^2 d\Phi_{\{X_i\}+1}(\{p_{X_i}\},p_3;p_1,p_2) \\
&\quad \left\{ M_3^1(\hat{1}_q,3_g,\hat{2}_{\bar{q}}) - \frac{1}{N^2}\,\widetilde{M_3^1}(\hat{1}_q,3_g,\hat{2}_{\bar{q}}) + \frac{N_F}{N}\,\widehat{M_3^1}(\hat{1}_q,3_g,\hat{2}_{\bar{q}}) \right\} J_0^{(1)}(p_3),
\end{aligned}
$$

$$(4.7)$$

where $\widetilde{M}_3^1$ and $\widehat{M}_3^1$ denote the squared matrix elements of the sub-leading colour and closed quark-loop contributions respectively. The contributions to the quark-antiquark initial-state contain no implicit IR divergence because when the final state gluon becomes unresolved the matrix elements factor onto two-quark matrix elements which vanish. An example diagram contributing to the one-loop amplitudes is shown in figure 4.2 (e).

4.1.3 Four-parton contribution

Tree-level:

$$
\begin{aligned}
\mathrm{d}\hat{\sigma}_{gg}^{RR} &= \mathcal{N}_{gg}\mathcal{N}_{NLO} \frac{\bar{C}(\epsilon)^2}{C(\epsilon)^2} \left(\frac{\alpha_s}{2\pi}\right)^2 \mathrm{d}\Phi_{\{X_i\}+2}(\{p_{X_i}\}, p_3, p_4; p_1, p_2)\Bigg\{ \\
&\quad \frac{N}{2}\sum_{\{3,4\}}\left(2M_4^0(\hat{1}_g, \hat{2}_g, 3_g, 4_g) + M_4^0(\hat{1}_g, 3_g, \hat{2}_g, 4_g)\right) \\
&\quad + N_F\sum_{\{1,2\}}M_4^0(3_q, \hat{1}_g, \hat{2}_g, 4_{\bar{q}}) - \frac{N_F}{N^2}\widetilde{M}_4^0(3_q, \hat{1}_g, \hat{2}_g, 4_{\bar{q}})\Bigg\} J_0^{(2)}(p_3, p_4) \\[2mm]
\mathrm{d}\hat{\sigma}_{qg}^{RR} &= \mathcal{N}_{qg}\mathcal{N}_{NLO} \frac{\bar{C}(\epsilon)^2}{C(\epsilon)^2} \left(\frac{\alpha_s}{2\pi}\right)^2 \mathrm{d}\Phi_{\{X_i\}+2}(\{p_{X_i}\}, p_3, p_4; p_1, p_2) \\
&\quad \Bigg\{ \left(M_4^0(\hat{1}_q, \hat{2}_g, 3_g, 4_{\bar{q}}) + M_4^0(\hat{1}_q, 3_g, \hat{2}_g, 4_{\bar{q}})\right) \\
&\quad -\frac{1}{N^2}\widetilde{M}_4^0(\hat{1}_q, \hat{2}_g, 3_g, 4_{\bar{q}})\Bigg\} J_0^{(2)}(p_3, p_4), \\[2mm]
\mathrm{d}\hat{\sigma}_{q\bar{q}}^{RR} &= \mathcal{N}_{q\bar{q}}\mathcal{N}_{NLO} \frac{\bar{C}(\epsilon)^2}{C(\epsilon)^2} \left(\frac{\alpha_s}{2\pi}\right)^2 \mathrm{d}\Phi_{\{X_i\}+2}(\{p_{X_i}\}, p_3, p_4; p_1, p_2) \\
&\quad \Bigg\{ \frac{1}{2}\sum_{\{3,4\}}M_4^0(\hat{1}_q, 3_g, 4_g, \hat{2}_{\bar{q}}) - \frac{1}{2N^2}\widetilde{M}_4^0(\hat{1}_q, 3_g, 4_g, \hat{2}_{\bar{q}}) \\
&\quad +\frac{N_F}{N}M_4^0(\hat{1}_q, 3_Q, 4_{\bar{Q}}, \hat{2}_{\bar{q}}) + \frac{1}{N}M_4^0(\hat{1}_q, 3_Q, \hat{2}_{\bar{Q}}, 4_{\bar{q}}) \\
&\quad -\frac{1}{N^2}\overline{M}_4^0(\hat{1}_q, 3_q, 4_{\bar{q}}, \hat{2}_{\bar{q}})\Bigg\} J_0^{(2)}(p_3, p_4), \\[2mm]
\mathrm{d}\hat{\sigma}_{qQ}^{RR} &= \mathcal{N}_{q\bar{q}}\mathcal{N}_{NLO} \frac{\bar{C}(\epsilon)^2}{C(\epsilon)^2} \left(\frac{\alpha_s}{2\pi}\right)^2 \mathrm{d}\Phi_{\{X_i\}+2}(\{p_{X_i}\}, p_3, p_4; p_1, p_2) \\
&\quad \Bigg\{ \frac{1}{N}M_4^0(\hat{1}_q, \hat{2}_Q, 4_{\bar{Q}}, 3_{\bar{q}}) J_0^{(2)}(p_3, p_4)\Bigg\}, \\[2mm]
\mathrm{d}\hat{\sigma}_{qq}^{RR} &= \mathcal{N}_{q\bar{q}}\mathcal{N}_{NLO} \frac{\bar{C}(\epsilon)^2}{C(\epsilon)^2} \left(\frac{\alpha_s}{2\pi}\right)^2 \mathrm{d}\Phi_{\{X_i\}+2}(\{p_{X_i}\}, p_3, p_4; p_1, p_2)
\end{aligned}
$$

$$\frac{1}{2} \left\{ \frac{1}{N} \left(M_4^0(\hat{1}_q, \hat{2}_Q, 4_{\bar{Q}}, 3_{\bar{q}}) + M_4^0(\hat{1}_q, \hat{2}_Q, 3_{\bar{Q}}, 4_{\bar{q}}) \right) \right.$$
$$\left. - \frac{1}{N^2} \overline{M}_4^0(\hat{1}_q, \hat{2}_{\bar{q}}, 3_{\bar{q}}, 4_{\bar{q}}) \right\} J_0^{(2)}(p_3, p_4).$$

$$(4.8)$$

4.2 Infrared subtraction at NLO

Following the general discussion of chapter 2, the antenna subtraction method can be applied to the NLO real corrections to the Born-level process $g\, g \to X$, where X is typically a Higgs boson.

4.2.1 Construction of the NLO real subtraction terms

$$
\begin{aligned}
\mathrm{d}\hat{\sigma}_{gg,NLO}^S &= \mathcal{N}_{gg}\mathcal{N}_{LO}\,\frac{\bar{C}(\epsilon)}{C(\epsilon)} \left(\frac{\alpha_s}{2\pi}\right) \mathrm{d}\Phi_{\{X_i\}+1}(\{p_X\}, p_3; p_1, p_2) \\
&\quad \times\ 2N\, F_3^0(\hat{1}, 3, \hat{2})\, M_2^0(\hat{\bar{1}}_g, \hat{\bar{2}}_g)\, J_0^{(1)}(p_3) \\
\mathrm{d}\hat{\sigma}_{qg,NLO}^S &= \mathcal{N}_{qg}\mathcal{N}_{LO}\,\frac{\bar{C}(\epsilon)}{C(\epsilon)} \left(\frac{\alpha_s}{2\pi}\right) \mathrm{d}\Phi_{\{X_i\}+1}(\{p_X\}, p_3; p_1, p_2) \\
&\quad \times\ G_3^0(\hat{2}, \hat{1}, 3)\, M_2^0(\hat{\bar{1}}_g, \hat{\bar{2}}_g)\, J_0^{(1)}(p_3)
\end{aligned}
$$

$$(4.9)$$

By examining the single unresolved limits of the matrix elements in (4.6) it can be shown that the subtraction terms presented here correctly mimic the IR divergent behaviour of the cross section in all singular limits.

4.2.2 Construction of the NLO virtual subtraction terms

Integrating the real subtraction terms over the appropriate single unresolved phase space and combining with the mass factorization contributions yields the virtual subtraction terms:

$$
\begin{aligned}
\mathrm{d}\hat{\sigma}_{gg,NLO}^T &= -\mathcal{N}_{gg}\mathcal{N}_{LO}\,\bar{C}(\epsilon) \left(\frac{\alpha_s}{2\pi}\right) \mathrm{d}\Phi_{\{X_i\}}(\{p_X\}; \bar{p}_1, \bar{p}_2) \\
&\quad \times\ \int \frac{\mathrm{d}x_1}{x_1}\frac{\mathrm{d}x_2}{x_2} \left(2N\, \boldsymbol{J}_2^{(1)}(\hat{\bar{1}}_g, \hat{\bar{2}}_g) + N_F\, \boldsymbol{J}_{2,N_F}^{(1)}(\hat{\bar{1}}_g, \hat{\bar{2}}_g)\right) M_2^0(\bar{1}_g, \bar{2}_g), \\
\mathrm{d}\hat{\sigma}_{qg,NLO}^T &= -\mathcal{N}_{qg}\mathcal{N}_{LO}\,\bar{C}(\epsilon) \left(\frac{\alpha_s}{2\pi}\right) \mathrm{d}\Phi_{\{X_i\}}(\{p_X\}; \bar{p}_1, \bar{p}_2)
\end{aligned}
$$

$$\times \quad \int \frac{\mathrm{d}x_1}{x_1} \frac{\mathrm{d}x_2}{x_2} \; \boldsymbol{J}_{2,q\to g}^{(1)}(\hat{\bar{1}}_g, \hat{\bar{2}}_g) \; M_2^0(\hat{\bar{1}}_g, \hat{\bar{2}}_g). \tag{4.10}$$

The integrated antenna string $\boldsymbol{J}_2^{(1)}(\hat{\bar{1}}_g, \hat{\bar{2}}_g)$ is free from initial-state collinear poles and correctly subtracts the explicit pole structure of the corresponding one-loop amplitude in (4.4). The N_F proportional integrated antenna string $\boldsymbol{J}_{2,N_F}^{(1)}(\hat{\bar{1}}_g, \hat{\bar{2}}_g)$ is constructed from the N_F dependent piece of the mass factorization kernel, $\boldsymbol{\Gamma}_{gg}^1$, as shown in appendix B.1. At first sight this seems problematic as the integrated antenna strings should be free from initial-state collinear singularities in order to cancel the genuine poles in the factorized cross section. By looking at the form of $\Gamma_{gg,F}^1$ it is clear that although this term originates in the mass factorization contribution, the singular contribution is just a single pole proportional to $b_{0,F}$ and all x dependence enters through a momentum conserving δ-function. As such, this contribution contains no initial-state collinear splitting functions and can in fact be written in terms of $\boldsymbol{I}_{gg,F}^{(1)}$, which removes the genuine poles from the factorized cross section as required.

The identity changing integrated antenna string is free from explicit poles which reflects the fact that the quark-gluon initiated virtual contribution to the cross section is finite.

4.3 Infrared subtraction at NNLO

Following the general method discussed in chapter 2 and the specific calculations in chapter 3, the double real, real-virtual and double virtual subtraction terms are given as follows:

4.3.1 Construction of the double real subtraction term

With reference to the four-parton tree-level matrix elements listed in (4.8), the double real subtraction terms can be constructed for each contribution to the cross section.

Gluon-gluon initial state:

$$
\begin{aligned}
\mathrm{d}\hat{\sigma}_{gg}^S \;=\;& \mathcal{N}_{gg}\mathcal{N}_{NLO}\left(\frac{\alpha_s}{2\pi}\right)^2 \frac{\bar{C}(\epsilon)^2}{C(\epsilon)^2}\, \mathrm{d}\Phi_{\{X_i\}+2}(\{p_{X_i}\},p_3,p_4;p_1,p_2)\,\Bigg\{ \\
& \frac{N}{2}\sum_{\{3,4\}}\Bigg[\; 2f_3^0(\hat{2},3,4)\,M_3^0(\hat{1}_g,\hat{\bar{2}}_g,\widetilde{(3,4)}_g)\,J_0^{(1)}(p_{(3,4)}) \\
& +\; 2f_3^0(\hat{1},4,3)\,M_3^0(\hat{\bar{1}}_g,2_g,\widetilde{(3,4)},\hat{\bar{2}}_g)\,J_0^{(1)}(p_{(3,4)}) \\
& +\; F_3^0(\hat{1},3,\hat{2})\,M_3^0(\hat{\bar{1}}_g,\hat{\bar{2}}_g,\tilde{4}_g)\,J_0^{(1)}(p_4) \\
& +\; F_3^0(\hat{1},4,\hat{2})\,M_3^0(\hat{\bar{1}}_g,\tilde{3}_g,\hat{\bar{2}}_g)\,J_0^{(1)}(p_3) \\
& +\; 2F_4^0(\hat{1},\hat{2},3,4)\,M_2^0(\hat{\bar{1}}_g,\hat{\bar{2}}_g) \\
& -\; 2f_3^0(\hat{2},3,4)\,F_3^0(\hat{1},\widetilde{(3,4)},\hat{\bar{2}})\,M_2^0(\hat{\bar{1}}_g,\hat{\bar{\bar{2}}}_g) \\
& -\; 2f_3^0(\hat{1},4,3)\,F_3^0(\hat{\bar{1}},\widetilde{(3,4)},\hat{2})\,M_2^0(\hat{\bar{\bar{1}}}_g,\hat{\bar{2}}_g) \\
& +\; F_4^0(\hat{1},3,\hat{2},4)\,M_2^0(\bar{1}_g,\bar{2}_g) \\
& -\; F_3^0(\hat{1},3,\hat{2})\,F_3^0(\hat{\bar{1}},\tilde{4},\hat{\bar{2}})\,M_2^0(\hat{\bar{\bar{1}}}_g,\hat{\bar{\bar{2}}}_g) \\
& -\; F_3^0(\hat{1},4,\hat{2})\,F_3^0(\hat{\bar{1}},\tilde{3},\hat{\bar{2}})\,M_2^0(\hat{\bar{\bar{1}}}_g,\hat{\bar{\bar{2}}}_g)\Bigg] \\
& +N_F\sum_{\{1,2\}}\Bigg[\; d_3^0(3,\hat{1},\hat{2})\,M_3^0(\hat{\bar{1}}_q,\hat{\bar{2}}_g,\tilde{4}_{\bar{q}})\,J_0^{(1)}(p_4) \\
& +\; d_3^0(4,\hat{2},\hat{1})\,M_3^0(\tilde{3}_q,\hat{\bar{1}}_g,\hat{\bar{2}}_{\bar{q}})\,J_0^{(1)}(p_3) \\
& +\; \frac{1}{2}G_3^0(\hat{1},3,4)\,M_3^0(\hat{\bar{1}}_g,\hat{2}_g,\widetilde{(3,4)}_g)\,J_0^{(1)}(p_{(3,4)}) \\
& +\; \frac{1}{2}G_3^0(\hat{2},3,4)\,M_3^0(\hat{1}_g,\hat{\bar{2}}_g,\widetilde{(3,4)}_g)\,J_0^{(1)}(p_{(3,4)}) \\
& +\; G_4^0(\hat{1},3,4,\hat{2})\,M_2^0(\hat{\bar{1}}_g,\hat{\bar{2}}_g) \\
& -\; d_3^0(3,\hat{1},\hat{2})\,G_3^0(\hat{\bar{2}},\hat{\bar{1}},\tilde{4})\,M_2^0(\hat{\bar{\bar{1}}}_g,\hat{\bar{\bar{2}}}_g) \\
& -\; d_3^0(4,\hat{2},\hat{1})\,G_3^0(\hat{\bar{1}},\hat{\bar{2}},\tilde{3})\,M_2^0(\hat{\bar{\bar{1}}}_g,\hat{\bar{\bar{2}}}_g) \\
& -\; \frac{1}{2}G_3^0(\hat{1},3,4)\,F_3^0(\hat{\bar{1}},\hat{2},\widetilde{(3,4)})\,M_2^0(\hat{\bar{\bar{1}}}_g,\hat{\bar{2}}_g) \\
& -\; \frac{1}{2}G_3^0(\hat{2},3,4)\,F_3^0(\hat{1},\hat{\bar{2}},\widetilde{(3,4)})\,M_2^0(\hat{\bar{1}}_g,\hat{\bar{\bar{2}}}_g)\Bigg] \\
& -\frac{N_F}{N^2}\Bigg[\; d_3^0(3,\hat{1},\hat{2})\,\widetilde{M}_3^0(\hat{\bar{1}}_q,\hat{2}_g,\tilde{4}_{\bar{q}})\,J_0^{(1)}(p_4) \\
& +\; d_3^0(4,\hat{2},\hat{1})\,\widetilde{M}_3^0(\tilde{3}_q,\hat{\bar{1}}_g,\hat{\bar{2}}_{\bar{q}})\,J_0^{(1)}(p_4) \\
& +\; \tilde{G}_4^0(\hat{1},3,4,\hat{2})\,M_2^0(\hat{\bar{1}}_g,\hat{\bar{2}}_g) \\
& -\; d_3^0(3,\hat{1},\hat{2})\,G_3^0(\hat{\bar{2}},\hat{\bar{1}},\tilde{4})\,M_2^0(\hat{\bar{\bar{1}}}_g,\hat{\bar{\bar{2}}}_g)
\end{aligned}
$$

$$- \quad d_3^0(4, \hat{2}, \hat{1}) \ G_3^0(\hat{\tilde{1}}, \hat{\tilde{2}}, \tilde{3}) \ M_2^0(\hat{\tilde{\tilde{1}}}_g, \hat{\tilde{\tilde{2}}}_g) \Big] \Big\} \qquad (4.11)$$

Quark-gluon initial state:

$$
\begin{aligned}
\mathrm{d}\hat{\sigma}_{qg}^S \ = \ & \mathcal{N}_{qg}\mathcal{N}_{NLO}\left(\frac{\alpha_s}{2\pi}\right)^2 \frac{\bar{C}(\epsilon)^2}{C(\epsilon)^2} \ \mathrm{d}\Phi_{\{X_i\}+2}(\{p_{X_i}\}, p_3, p_4; p_1, p_2) \Bigg\{ \\
& \Bigg[\quad d_3^0(4, 3, \hat{2}) \ M_3^0(\hat{1}_q, \hat{\tilde{2}}_g, \widetilde{(3, 4)}_{\bar{q}}) \ J_0^{(1)}(p_{(3,4)}) \\
& + \ G_3^0(\hat{2}, \hat{1}, 4) \ M_3^0(\hat{\tilde{1}}_q, \hat{\tilde{2}}_g, \tilde{3}_g) \ J_0^{(1)}(p_3) \\
& + \ D_3^0(\hat{1}, 3, \hat{2}) \ M_3^0(\hat{\tilde{1}}_q, \hat{\tilde{2}}_g, \tilde{4}_{\bar{q}}) \ J_0^{(1)}(p_4) \\
& + \ d_3^0(4, \hat{2}; 3) \ M_3^0(\hat{1}_q, \widetilde{(3, 4)}_g, \hat{\tilde{2}}_{\bar{q}}) \ J_0^{(1)}(p_{(3,4)}) \\
& + \ G_3^0(3, \hat{1}, 4) \ M_3^0(\hat{\tilde{1}}_g, \hat{2}_g, \widetilde{(3, 4)}_g) \ J_0^{(1)}(p_{(3,4)}) \\
& + \ G_4^0(\hat{2}, \hat{1}, 4, 3) \ M_2^0(\hat{\tilde{1}}_g, \hat{\tilde{2}}_g) \\
& - \ d_3^0(4, 3, \hat{2}) \ G_3^0(\hat{\tilde{2}}, \hat{1}, \widetilde{(3, 4)}) \ M_2^0(\hat{\tilde{1}}_g, \hat{\tilde{\tilde{2}}}_g) \\
& - \ G_3^0(\hat{2}, \hat{1}, 4) \ F_3^0(\hat{\tilde{1}}, \hat{\tilde{2}}, \tilde{3}) \ M_2^0(\hat{\tilde{\tilde{1}}}_g, \hat{\tilde{\tilde{2}}}_g) \\
& + \ G_4^0(\hat{2}, 4, \hat{1}, 3) \ M_2^0(\hat{\tilde{1}}_g, \hat{\tilde{2}}_g) \\
& - \ D_3^0(\hat{1}, 3, \hat{2}) \ G_3^0(\hat{\tilde{2}}, \tilde{4}, \hat{\tilde{1}}) \ M_2^0(\hat{\tilde{\tilde{1}}}_g, \hat{\tilde{\tilde{2}}}_g) \\
& - \ d_3^0(4, \hat{2}; 3) \ G_3^0(\tilde{3}, \hat{\tilde{2}}, \hat{\tilde{1}}) \ M_2^0(\hat{\tilde{\tilde{1}}}_g, \hat{\tilde{2}}_g) \\
& - \ G_3^0(\hat{2}, 4, \hat{1}) \ F_3^0(\hat{\tilde{1}}, \hat{\tilde{2}}, \tilde{3}) \ M_2^0(\hat{\tilde{\tilde{1}}}_g, \hat{\tilde{\tilde{2}}}_g) \Bigg] \\
- \frac{1}{N^2} \ & \Bigg[\quad A_3^0(\hat{1}, 3, 4) \ M_3^0(\hat{\tilde{1}}_q, \hat{2}_g, \widetilde{(3, 4)}_{\bar{q}}) \ J_0^{(1)}(p_{(3,4)}) \\
& + \ A_3^0(\hat{1}, \hat{2}, 4) \ M_3^0(\hat{\tilde{1}}_q, \tilde{3}_g, \hat{\tilde{2}}_{\bar{q}}) \ J_0^{(1)}(p_3) \\
& + \ \tilde{G}_4^0(\hat{2}, \hat{1}, 4, 3) \ M_2^0(\hat{\tilde{1}}_g, \hat{\tilde{2}}_g) \\
& - \ A_3^0(\hat{1}, 3, 4) \ G_3^0(\hat{2}, \hat{\tilde{1}}, \widetilde{(3, 4)}) \ M_2^0(\hat{\tilde{\tilde{1}}}_g, \hat{\tilde{2}}_g) \\
& - \ A_3^0(\hat{1}, \hat{2}, 4) \ G_3^0(\tilde{3}, \hat{\tilde{1}}, \hat{\tilde{2}}) \ M_2^0(\hat{\tilde{\tilde{1}}}_q, \hat{\tilde{\tilde{2}}}_{\bar{q}}) \Bigg] \Bigg\} \qquad (4.12)
\end{aligned}
$$

Quark-antiquark initial state:

$$
\begin{aligned}
\mathrm{d}\hat{\sigma}_{q\bar{q}}^S \ = \ & \mathcal{N}_{q\bar{q}}\mathcal{N}_{NLO}\left(\frac{\alpha_s}{2\pi}\right)^2 \frac{\bar{C}(\epsilon)^2}{C(\epsilon)^2} \ \mathrm{d}\Phi_{\{X_i\}+2}(\{p_{X_i}\}, p_3, p_4; p_1, p_2) \Bigg\{ \\
& \frac{1}{2}\sum_{\{3,4\}} \ \Bigg[\quad d_3^0(\hat{1}, 3, 4) \ M_3^0(\hat{\tilde{1}}_q, \widetilde{(3, 4)}_g, \hat{2}_{\bar{q}}) \ J_0^{(1)}(p_{(3,4)})
\end{aligned}
$$

$$
\begin{aligned}
&\quad + \; d_3^0(\hat{2},4,3) \; M_3^0(\hat{1}_q, \widetilde{(3,4)}_g, \hat{\tilde{2}}_{\bar{q}}) \; J_0^{(1)}(p_{(3,4)}) \Big] \\
&-\frac{1}{2N^2} \; \Big[\quad A_3^0(\hat{1},3,\hat{2}) \; M_3^0(\hat{\tilde{1}}_q, \tilde{4}_g, \hat{\tilde{2}}_{\bar{q}}) \; J_0^{(1)}(p_4) \\
&\quad + \; A_3^0(\hat{1},4,\hat{2}) \; M_3^0(\hat{\tilde{1}}_q, \tilde{3}_g, \hat{\tilde{2}}_{\bar{q}}) \; J_0^{(1)}(p_3) \Big] \\
&+\frac{N_F}{N} \; \Big[\quad \frac{1}{2} E_3^0(\hat{1},3,4) \; M_3^0(\hat{\tilde{1}}_q, \widetilde{(3,4)}_g, \hat{2}_{\bar{q}}) \; J_0^{(1)}(p_{(3,4)}) \\
&\quad + \; \frac{1}{2} E_3^0(\hat{2},4,3) \; M_3^0(\hat{1}_q, \widetilde{(3,4)}_g, \hat{\tilde{2}}_{\bar{q}}) \; J_0^{(1)}(p_{(3,4)}) \Big] \\
&+\frac{1}{N} \; \Big[\quad E_3^0(\hat{1},3,\hat{2}) \; M_3^0(\hat{\tilde{1}}_q, \hat{\tilde{2}}_g, \tilde{4}_{\bar{q}}) \\
&\quad + \; E_3^0(\hat{2},4,\hat{1}) \; M_3^0(\tilde{3}_q, \hat{\tilde{1}}_g, \hat{\tilde{2}}_{\bar{q}}) \\
&\quad + \; H_4^0(\hat{1},4,\hat{2},3) \; M_2^0(\hat{\tilde{\tilde{1}}}_g, \hat{\tilde{\tilde{2}}}_g) \\
&\quad - \; E_3^0(\hat{1},3,\hat{2}) \; G_3^0(\hat{\tilde{2}}, \hat{\tilde{1}}, \tilde{4}) \; M_2^0(\hat{\tilde{\tilde{1}}}_g, \hat{\tilde{\tilde{2}}}_g) \\
&\quad - \; E_3^0(\hat{2},4,\hat{1}) \; G_3^0(\hat{\tilde{1}}, \hat{\tilde{2}}, \tilde{3}) \; M_2^0(\hat{\tilde{\tilde{1}}}_g, \hat{\tilde{\tilde{2}}}_g) \Big] \Big] \Big\}
\end{aligned} \tag{4.13}
$$

Non-idential quark-quark initial state:

$$
\begin{aligned}
\mathrm{d}\hat{\sigma}_{qQ}^S \; = \; & \mathcal{N}_{q\bar{q}}\mathcal{N}_{NLO}\left(\frac{\alpha_s}{2\pi}\right)^2 \frac{\bar{C}(\epsilon)^2}{C(\epsilon)^2} \; \mathrm{d}\Phi_{\{X_i\}+2}(\{p_{X_i}\}, p_3, p_4; p_1, p_2) \Big\{ \\
& \frac{1}{N} \; \Big[\quad E_3^0(\hat{1},\hat{2},4) \; M_3^0(\hat{\tilde{1}}_q, \hat{\tilde{2}}_g, \tilde{3}_{\bar{q}}) \; J_0^{(1)}(p_3) \\
&\quad + \; E_3^0(\hat{2},\hat{1},3) \; M_3^0(\hat{\tilde{2}}_q, \hat{\tilde{1}}_g, \tilde{4}_{\bar{q}}) \; J_0^{(1)}(p_4) \\
&\quad + \; H_4^0(\hat{1},3,\hat{2},4) \; M_2^0(\hat{\tilde{\tilde{1}}}_g, \hat{\tilde{\tilde{2}}}_g) \\
&\quad - \; E_3^0(\hat{1},\hat{2},4) \; G_3^0(\hat{\tilde{2}}, \hat{\tilde{1}}, \tilde{3}) \; M_2^0(\hat{\tilde{\tilde{1}}}_g, \hat{\tilde{\tilde{2}}}_g) \\
&\quad - \; E_3^0(\hat{2},\hat{1},3) \; G_3^0(\hat{\tilde{1}}, \hat{\tilde{2}}, \tilde{4}) \; M_2^0(\hat{\tilde{\tilde{1}}}_g, \hat{\tilde{\tilde{2}}}_g) \Big] \Big\}
\end{aligned} \tag{4.14}
$$

Identical quark-quark initial state

$$
\begin{aligned}
\mathrm{d}\hat{\sigma}_{qq}^S \; = \; & \mathcal{N}_{q\bar{q}}\mathcal{N}_{NLO}\left(\frac{\alpha_s}{2\pi}\right)^2 \frac{\bar{C}(\epsilon)^2}{C(\epsilon)^2} \; \mathrm{d}\Phi_{\{X_i\}+2}(\{p_{X_i}\}, p_3, p_4; p_1, p_2) \Big\{ \\
& \frac{1}{2N} \; \Big[\quad E_3^0(\hat{1},\hat{2},4) \; M_3^0(\hat{\tilde{1}}_q, \hat{\tilde{2}}_g, \tilde{3}_{\bar{q}}) \; J_0^{(1)}(p_3) \\
&\quad + \; E_3^0(\hat{2},\hat{1},3) \; M_3^0(\hat{\tilde{2}}_q, \hat{\tilde{1}}_g, \tilde{4}_{\bar{q}}) \; J_0^{(1)}(p_4) \\
&\quad + \; E_3^0(\hat{1},\hat{2},3) \; M_3^0(\hat{\tilde{1}}_q, \hat{\tilde{2}}_g, \tilde{4}_{\bar{q}}) \; J_0^{(1)}(p_4)
\end{aligned}
$$

$$
\begin{aligned}
&+\ E_3^0(\hat{2},\hat{1},4)\ M_3^0(\hat{\bar{2}}_q,\hat{\bar{1}}_g,\tilde{3}_{\bar{q}})\ J_0^{(1)}(p_3)\\
&+\ H_4^0(\hat{1},3,\hat{2},4)\ M_2^0(\hat{\bar{\bar{1}}}_g,\hat{\bar{\bar{2}}}_g)\\
&-\ E_3^0(\hat{1},\hat{2},4)\ G_3^0(\hat{\bar{2}},\hat{\bar{1}},\tilde{3})\ M_2^0(\hat{\bar{\bar{1}}}_g,\hat{\bar{\bar{2}}}_g)\\
&-\ E_3^0(\hat{2},\hat{1},3)\ G_3^0(\hat{\bar{1}},\hat{\bar{2}},\tilde{4})\ M_2^0(\hat{\bar{\bar{1}}}_g,\hat{\bar{\bar{2}}}_g)\\
&+\ H_4^0(\hat{1},4,\hat{2},3)\ M_2^0(\hat{\bar{\bar{1}}}_g,\hat{\bar{\bar{2}}}_g)\\
&-\ E_3^0(\hat{2},\hat{1},4)\ G_3^0(\hat{\bar{1}},\hat{\bar{2}},\tilde{3})\ M_2^0(\hat{\bar{\bar{1}}}_g,\hat{\bar{\bar{2}}}_g)\\
&-\ E_3^0(\hat{1},\hat{2},3)\ G_3^0(\hat{\bar{2}},\hat{\bar{1}},\tilde{4})\ M_2^0(\hat{\bar{\bar{1}}}_g,\hat{\bar{\bar{2}}}_g)\bigg]\bigg\}
\end{aligned}
\tag{4.15}
$$

The remaining subtraction terms can be obtained from those presented in this section via the appropriate relabelling of parton momenta, reflecting the symmetries relating the various matrix elements.

4.3.2 Construction of the real-virtual subtraction term

Integrating the double real subtraction terms over the single unresolved phase space then combining with the one-loop subtraction terms and appropriate mass factorization terms generates the real-virtual subtraction term. As in chapter 3, the following notation is adopted: $\delta_1 = \delta(1-x_1)$, $\delta_2 = \delta(1-x_2)$.

Gluon-gluon initial state:

$$
\begin{aligned}
\mathrm{d}\hat{\sigma}_{gg}^T =\ & \mathcal{N}_{gg}\mathcal{N}_{NLO}\left(\frac{\alpha_s}{2\pi}\right)^2 \frac{\bar{C}(\epsilon)^2}{C(\epsilon)}\ \mathrm{d}\Phi_{\{X_i\}+1}(\{p_{X_i}\},p_3;\bar{p}_1,\bar{p}_2)\int\frac{\mathrm{d}x_1}{x_1}\frac{\mathrm{d}x_2}{x_2}\bigg\{\\
2N\ \bigg\{\ & -\boldsymbol{J}_3^{(1)}(\hat{\bar{1}}_g,\hat{\bar{2}}_g,3_g)\ M_3^0(\hat{\bar{1}}_g,\hat{\bar{2}}_g,3_g)\ J_0^{(1)}(p_3)\\
+\ & F_3^0(\hat{\bar{1}},3,\hat{\bar{2}})\bigg[M_2^1(\hat{\bar{\bar{1}}}_g,\hat{\bar{\bar{2}}}_g)\delta_1\delta_2 + 2\boldsymbol{J}_2^{(1)}(\hat{\bar{\bar{1}}}_g,\hat{\bar{\bar{2}}}_g)\ M_2^0(\hat{\bar{\bar{1}}}_g,\hat{\bar{\bar{2}}}_g)\bigg]\\
+\ & \bigg[F_3^1(\hat{\bar{1}},3,\hat{\bar{2}})\delta_1\delta_2 + \bar{\boldsymbol{J}}_3^{(1)}(\hat{\bar{1}}_g,3_g,\hat{\bar{2}}_g)\ F_3^0(\hat{\bar{1}},3,\hat{\bar{2}})\bigg]M_2^0(\hat{\bar{\bar{1}}}_g,\hat{\bar{\bar{2}}}_g)\\
+\ & b_0\log\left(\frac{\mu^2}{s_{\bar{1}\bar{2}3}}\right)F_3^0(\hat{\bar{1}},3,\hat{\bar{2}})\delta_1\delta_2\ M_2^0(\hat{\bar{\bar{1}}}_g,\hat{\bar{\bar{2}}}_g)\bigg\}\\
+N_F\ \bigg\{\ & -\boldsymbol{J}_{3,N_F}^{(1)}(\hat{\bar{1}}_g,\hat{\bar{2}}_g,3_g)\ M_3^0(\hat{\bar{1}}_g,\hat{\bar{2}}_g,3_g)\ J_0^{(1)}(p_3)\\
+\ & F_3^0(\hat{\bar{1}},3,\hat{\bar{2}})\bigg[\widehat{M_2^1}(\hat{\bar{\bar{1}}}_g,\hat{\bar{\bar{2}}}_g)\delta_1\delta_2 + 2\boldsymbol{J}_{2,N_F}^{(1)}(\hat{\bar{\bar{1}}}_g,\hat{\bar{\bar{2}}}_g)\ M_2^0(\hat{\bar{\bar{1}}}_g,\hat{\bar{\bar{2}}}_g)\bigg]
\end{aligned}
$$

$$
\begin{aligned}
&+ \left[\hat{F}_3^1(\hat{\bar{1}}, 3, \hat{\bar{2}})\delta_1\delta_2 + \bar{\boldsymbol{J}}_{3,N_F}^{(1)}(\hat{\bar{1}}_g, \hat{\bar{2}}_g, 3_g)\, F_3^0(\hat{\bar{1}}, 3, \hat{\bar{2}}) \right] M_2^0(\hat{\bar{\bar{1}}}_g, \hat{\bar{\bar{2}}}_g) \\
&+ b_{0,F} \log\left(\frac{\mu^2}{s_{\bar{1}23}}\right) F_3^0(\hat{\bar{1}}, 3, \hat{\bar{2}})\delta_1\delta_2\, M_2^0(\hat{\bar{\bar{1}}}_g, \hat{\bar{\bar{2}}}_g) \\
&- \boldsymbol{J}_{2,g\to q}^{(1)}(\hat{\bar{1}}_q, \hat{\bar{2}}_g)\, M_3^0(\hat{\bar{1}}_q, \hat{\bar{2}}_g, 3_{\bar{q}}) \\
&- \boldsymbol{J}_{2,g\to q}^{(1)}(\hat{\bar{2}}_q, \hat{\bar{1}}_g)\, M_3^0(3_q, \hat{\bar{1}}_g, \hat{\bar{2}}_{\bar{q}}) \\
&+ \boldsymbol{J}_{2,g\to q}^{(1)}(\hat{\bar{1}}_q, \hat{\bar{2}}_g)\, G_3^0(\hat{\bar{2}}, \hat{\bar{1}}, 3)\, M_2^0(\hat{\bar{\bar{1}}}_g, \hat{\bar{\bar{2}}}_g) \\
&+ \boldsymbol{J}_{2,g\to q}^{(1)}(\hat{\bar{1}}_q, \hat{\bar{2}}_g)\, G_3^0(\hat{\bar{1}}, 3, \hat{\bar{2}})\, M_2^0(\hat{\bar{\bar{1}}}_g, \hat{\bar{\bar{2}}}_g) \Big\} \\
+\frac{N_F}{N^2} \Big\{ &\ \boldsymbol{J}_{2,g\to q}^{(1)}(\hat{\bar{1}}_q, \hat{\bar{2}}_g)\, M_3^0(\hat{\bar{1}}_q, \hat{\bar{2}}_g, 3_{\bar{q}}) \\
&+ \boldsymbol{J}_{2,g\to q}^{(1)}(\hat{\bar{2}}_q, \hat{\bar{1}}_g)\, M_3^0(3_q, \hat{\bar{1}}_g, \hat{\bar{2}}_{\bar{q}}) \\
&- \boldsymbol{J}_{2,g\to q}^{(1)}(\hat{\bar{1}}_q, \hat{\bar{2}}_g)\, G_3^0(\hat{\bar{2}}, \hat{\bar{1}}, 3)\, M_2^0(\hat{\bar{\bar{1}}}_g, \hat{\bar{\bar{2}}}_g) \\
&- \boldsymbol{J}_{2,g\to q}^{(1)}(\hat{\bar{1}}_q, \hat{\bar{2}}_g)\, G_3^0(\hat{\bar{1}}, 3, \hat{\bar{2}})\, M_2^0(\hat{\bar{\bar{1}}}_g, \hat{\bar{\bar{2}}}_g) \Big\} \Big\}
\end{aligned}
\tag{4.16}
$$

Quark-gluon initial state:

$$
\begin{aligned}
\mathrm{d}\hat{\sigma}_{qg}^T ={}& \mathcal{N}_{qg}\mathcal{N}_{NLO}\left(\frac{\alpha_s}{2\pi}\right)^2 \frac{\bar{C}(\epsilon)^2}{C(\epsilon)}\, \mathrm{d}\Phi_{\{X_i\}+1}(\{p_{X_i}\}, p_3; \bar{p}_1, \bar{p}_2) \int \frac{\mathrm{d}x_1}{x_1}\frac{\mathrm{d}x_2}{x_2} \Bigg\{ \\
\Big\{ &-\boldsymbol{J}_3^{(1)}(\hat{\bar{1}}_q, \hat{\bar{2}}_g, 3_{\bar{q}})\, M_3^0(\hat{\bar{1}}_q, \hat{\bar{2}}_g, 3_{\bar{q}})\, J_0^{(1)}(p_3) \\
&+ G_3^0(\hat{\bar{2}}, \hat{\bar{1}}, 3)\left[M_2^1(\hat{\bar{\bar{1}}}_g, \hat{\bar{\bar{2}}}_g)\delta_1\delta_2 + \boldsymbol{J}_2^{(1)}(\hat{\bar{1}}_g, \hat{\bar{2}}_g)\, M_2^0(\hat{\bar{1}}_g, \hat{\bar{2}}_g) \right] \\
&+ \left[G_3^1(\hat{\bar{2}}, \hat{\bar{1}}, 3)\delta_1\delta_2 + \bar{\boldsymbol{J}}_3^{(1)}(\hat{\bar{1}}_q, \hat{\bar{2}}_g, 3_{\bar{q}})\, G_3^0(\hat{\bar{2}}, \hat{\bar{1}}, 3) \right] M_2^0(\hat{\bar{\bar{1}}}_g, \hat{\bar{\bar{2}}}_g) \\
&+ b_0 \log\left(\frac{\mu^2}{s_{\bar{1}23}}\right) G_3^0(\hat{\bar{2}}, \hat{\bar{1}}, 3)\delta_1\delta_2\, M_2^0(\hat{\bar{\bar{1}}}_g, \hat{\bar{\bar{2}}}_g) \\
&- \boldsymbol{J}_{3,q\to g}^{(1)}(\hat{\bar{1}}_g, \hat{\bar{2}}_g, 3_g)\, M_3^0(\hat{\bar{1}}_g, \hat{\bar{2}}_g, 3_g)\, J_0^{(1)}(p_3) \\
&- \boldsymbol{J}_{2,g\to q}^{(1)}(\hat{\bar{2}}_q, 3_g)\, M_3^0(\hat{\bar{1}}_q, 3_g, \hat{\bar{2}}_{\bar{q}})\, J_0^{(1)}(p_3) \\
&+ \boldsymbol{J}_{2,g\to q}^{(1)}(\hat{\bar{2}}_q, 3_g)\, G_3^0(3, \hat{\bar{1}}, \hat{\bar{2}})\, M_2^0(\hat{\bar{\bar{1}}}_g, \hat{\bar{\bar{2}}}_g) \\
&+ 2\boldsymbol{J}_{2,q\to g}^{(1)}(\hat{\bar{1}}_g, \hat{\bar{2}}_g)\, F_3^0(\hat{\bar{1}}, 3, \hat{\bar{2}})\, M_2^0(\hat{\bar{\bar{1}}}_g, \hat{\bar{\bar{2}}}_g) \Big\} \\
-\frac{1}{N^2} \Big\{ &-\boldsymbol{J}_2^{(1)}(\hat{\bar{1}}_q, 3_{\bar{q}})\, M_3^0(\hat{\bar{1}}_q, \hat{\bar{2}}_g, 3_{\bar{q}})\, J_0^{(1)}(p_3) \\
&+ \left[\tilde{G}_3^1(\hat{\bar{2}}, \hat{\bar{1}}, 3)\delta_1\delta_2 + \boldsymbol{J}_2^{(1)}(\hat{\bar{1}}_q, 3_{\bar{q}})\, G_3^0(\hat{\bar{2}}, \hat{\bar{1}}, 3) \right] M_2^0(\hat{\bar{\bar{1}}}_g, \hat{\bar{\bar{2}}}_g) \\
&- \boldsymbol{J}_{2,g\to q}^{(1)}(\hat{\bar{1}}_q, \hat{\bar{2}}_{\bar{q}})\, M_3^0(\hat{\bar{1}}_q, 3_g, \hat{\bar{2}}_{\bar{q}})\, J_0^{(1)}(p_3)
\end{aligned}
$$

$$
\begin{aligned}
&+\;\; \boldsymbol{J}_{2,g\to q}^{(1)}(\hat{\bar{1}}_q, \hat{\bar{2}}_{\bar{q}})\; G_3^0(3, \bar{1}, \bar{2})\; M_2^0(\bar{\bar{1}}_g, \bar{\bar{2}}_g)\Big\} \\
&+\frac{N_F}{N}\;\;\Big\{\;\; G_3^0(\hat{2}, \hat{1}, 3)\Big[\widehat{M}_2^1(\hat{\bar{\bar{1}}}_g, \hat{\bar{\bar{2}}}_g)\delta_1\delta_2 + 2\boldsymbol{J}_{2,N_F}^{(1)}(\hat{\bar{1}}_g, \hat{\bar{2}}_g)\; M_2^0(\hat{\bar{\bar{1}}}_g, \hat{\bar{\bar{2}}}_g)\Big] \\
&\qquad\quad +\;\; \Big[\hat{G}_3^1(\hat{2}, \hat{1}, 3)\delta_1\delta_2 - 2\boldsymbol{J}_{2,N_F}^{(1)}(\hat{\bar{1}}_g, \hat{\bar{2}}_g)\; G_3^0(\hat{2}, \hat{1}, 3)\Big]\; M_2^0(\hat{\bar{\bar{1}}}_g, \hat{\bar{\bar{2}}}_g) \\
&\qquad\quad +\;\; b_{0,F}\log\left(\frac{\mu^2}{s_{\bar{1}\bar{2}3}}\right) G_3^0(\hat{\bar{2}}, \hat{\bar{1}}, 3)\delta_1\delta_2\; M_2^0(\hat{\bar{\bar{1}}}_g, \hat{\bar{\bar{2}}}_g)\Big\}\Big\}
\end{aligned}
\tag{4.17}
$$

Quark-antiquark initial state:

$$
\begin{aligned}
\mathrm{d}\hat{\sigma}_{q\bar{q}}^T \;=\;& \mathcal{N}_{q\bar{q}}\mathcal{N}_{NLO}\left(\frac{\alpha_s}{2\pi}\right)^2 \frac{\bar{C}(\epsilon)^2}{C(\epsilon)}\; \mathrm{d}\Phi_{\{X_i\}+1}(\{p_{X_i}\}, p_3; \bar{p}_1, \bar{p}_2)\int \frac{\mathrm{d}x_1}{x_1}\frac{\mathrm{d}x_2}{x_2}\Big\{ \\
& \qquad -\boldsymbol{J}_3^{(1)}(\hat{\bar{1}}_q, 3_g, \hat{\bar{2}}_{\bar{q}})\; M_3^0(\hat{\bar{1}}_q, 3_g, \hat{\bar{2}}_{\bar{q}})\; J_0^{(1)}(p_3) \\
-\frac{1}{N^2}& \qquad -\boldsymbol{J}_2^{(1)}(\hat{\bar{1}}_q, \hat{\bar{2}}_{\bar{q}})\; M_3^0(\hat{\bar{1}}_q, 3_g, \hat{\bar{2}}_{\bar{q}}) \\
+\frac{N_F}{N}& \qquad -\boldsymbol{J}_{3,N_F}^{(1)}(\hat{\bar{1}}_q, 3_g, \hat{\bar{2}}_{\bar{q}})\; M_3^0(\hat{\bar{1}}_q, 3_g, \hat{\bar{2}}_{\bar{q}})\; J_0^{(1)}(p_3) \\
+\frac{1}{N}& \quad\Big\{\;\; -\boldsymbol{J}_{2,q\to g}^{(1)}(\hat{\bar{1}}_q, \hat{\bar{2}}_g)\; M_3^0(\hat{\bar{1}}_q, \hat{\bar{2}}_g, 3_{\bar{q}})\; J_0^{(1)}(p_3) \\
& \qquad\quad -\boldsymbol{J}_{2,q\to g}^{(1)}(\hat{\bar{2}}_q, \hat{\bar{1}}_g)\; M_3^0(3_q, \hat{\bar{1}}_g, \hat{\bar{2}}_{\bar{q}})\; J_0^{(1)}(p_3) \\
& \qquad\quad +\boldsymbol{J}_{2,q\to g}^{(1)}(\hat{\bar{1}}_q, \hat{\bar{2}}_g)\; G_3^0(\hat{\bar{2}}, \hat{1}, 3)\; M_2^0(\hat{\bar{\bar{1}}}_g, \hat{\bar{\bar{2}}}_g) \\
& \qquad\quad +\boldsymbol{J}_{2,q\to g}^{(1)}(\hat{\bar{2}}_q, \hat{\bar{1}}_g)\; G_3^0(\hat{\bar{1}}, \hat{2}, 3)\; M_2^0(\hat{\bar{\bar{1}}}_g, \hat{\bar{\bar{2}}}_g)\Big\}\Big\}
\end{aligned}
\tag{4.18}
$$

Quark-quark initial state:

The non-identical flavour quark subtraction term is given by,

$$
\begin{aligned}
\mathrm{d}\hat{\sigma}_{qQ}^T \;=\;& \mathcal{N}_{q\bar{q}}\mathcal{N}_{NLO}\left(\frac{\alpha_s}{2\pi}\right)^2 \frac{\bar{C}(\epsilon)^2}{C(\epsilon)}\; \mathrm{d}\Phi_{\{X_i\}+1}(\{p_{X_i}\}, p_3; \bar{p}_1, \bar{p}_2)\int \frac{\mathrm{d}x_1}{x_1}\frac{\mathrm{d}x_2}{x_2}\Big\{ \\
\frac{1}{N}& \quad\Big\{\;\; -\boldsymbol{J}_{2,q\to g}^{(1)}(\hat{\bar{1}}_q, \hat{\bar{2}}_g)\; M_3^0(\hat{\bar{1}}_q, \hat{\bar{2}}_g, 3_{\bar{q}})\; J_0^{(1)}(p_3) \\
& \qquad\quad -\boldsymbol{J}_{2,q\to g}^{(1)}(\hat{\bar{2}}_q, \hat{\bar{1}}_g)\; M_3^0(\hat{\bar{2}}_q, \hat{\bar{1}}_g, 3_{\bar{q}})\; J_0^{(1)}(p_3) \\
& \qquad\quad +\boldsymbol{J}_{2,q\to g}^{(1)}(\hat{\bar{1}}_q, \hat{\bar{2}}_g)\; G_3^0(\hat{\bar{2}}, \hat{1}, 3)\; M_2^0(\hat{\bar{\bar{1}}}_g, \hat{\bar{\bar{2}}}_g) \\
& \qquad\quad +\boldsymbol{J}_{2,q\to g}^{(1)}(\hat{\bar{2}}_q, \hat{\bar{1}}_g)\; G_3^0(\hat{\bar{1}}, \hat{2}, 3)\; M_2^0(\hat{\bar{\bar{1}}}_g, \hat{\bar{\bar{2}}}_g)\Big\}\Big\}
\end{aligned}
\tag{4.19}
$$

Once integrated over the single unresolved phase space and averaged over the final-state symmetry factor, the identical flavour quark-quark subtraction term shares

the same singularity structure as the non-identical flavour subtraction term,

$$\mathrm{d}\hat{\sigma}_{qQ}^T \;=\; \mathrm{d}\hat{\sigma}_{qq}^T. \tag{4.20}$$

4.3.3 Construction of the double virtual subtraction terms

Following the example of chapter 3, the double virtual subtraction terms may be written in terms of single and double unresolved integrated antenna strings. The explicit form of these strings in terms of integrated antennae and mass factorization kernels is given in appendix B.2.

Gluon-gluon initial state:

$$
\begin{aligned}
\mathrm{d}\hat{\sigma}_{gg}^U \;=\; & -\mathcal{N}_{gg}\mathcal{N}_{NLO}\left(\frac{\alpha_s}{2\pi}\right)^2 \bar{C}(\epsilon)^2\,\mathrm{d}\Phi_{\{X_i\}}(\{p_{X_i}\};\bar{p}_1,\bar{p}_2)\int \frac{\mathrm{d}z_1}{z_1}\frac{\mathrm{d}z_2}{z_2}\,\Bigg\{ \\
& N\;\Bigg\{\; 2\boldsymbol{J}_2^{(1)}(\hat{\bar{1}}_g,\hat{\bar{2}}_g)\bigg(\,M_2^1(\hat{\bar{1}}_g,\hat{\bar{2}}_g)-\frac{b_0}{\epsilon}\,M_2^0(\hat{\bar{1}}_g,\hat{\bar{2}}_g)\bigg) \\
& \qquad +\;\bigg(2\boldsymbol{J}_2^{(1)}(\hat{\bar{1}}_g,\hat{\bar{2}}_g)\otimes\boldsymbol{J}_2^{(1)}(\hat{\bar{1}}_g,\hat{\bar{2}}_g)\;+\boldsymbol{J}_2^{(2)}(\hat{\bar{1}}_g,\hat{\bar{2}}_g)\bigg)\,M_2^0(\hat{\bar{1}}_g,\hat{\bar{2}}_g)\Bigg\} \\
& +N_F\;\Bigg\{\;\boldsymbol{J}_2^{(1)}(\hat{\bar{1}}_g,\hat{\bar{2}}_g)\bigg(\,\widehat{M_2^1}(\hat{\bar{1}}_g,\hat{\bar{2}}_g)-\frac{b_0}{\epsilon}\,M_2^0(\hat{\bar{1}}_g,\hat{\bar{2}}_g)\bigg) \\
& \qquad +\;\bigg(\frac{1}{2}\boldsymbol{J}_2^{(1)}(\hat{\bar{1}}_g,\hat{\bar{2}}_g)\otimes\boldsymbol{J}_2^{(1)}(\hat{\bar{1}}_g,\hat{\bar{2}}_g)\;+\boldsymbol{J}_{2,N_F}^{(2)}(\hat{\bar{1}}_g,\hat{\bar{2}}_g)\bigg)\,M_2^0(\hat{\bar{1}}_g,\hat{\bar{2}}_g)\Bigg\} \\
& -\frac{N_F}{N^2}\;\Bigg\{\;\widetilde{\boldsymbol{J}}_{2,N_F}^{(1)}(\hat{\bar{1}}_g,\hat{\bar{2}}_g)\,M_2^0(\bar{1}_g,\bar{2}_g)\Bigg\} \\
& +\frac{N_F^2}{N}\;\Bigg\{\;\boldsymbol{J}_{2,N_F^2}^{(1)}(\hat{\bar{1}}_g,\hat{\bar{2}}_g)\,M_2^0(\bar{1}_g,\bar{2}_g)\Bigg\}\Bigg\}
\end{aligned} \tag{4.21}
$$

Quark-gluon initial state:

$$
\begin{aligned}
\mathrm{d}\hat{\sigma}_{qg}^U \;=\; & -\mathcal{N}_{qg}\mathcal{N}_{NLO}\left(\frac{\alpha_s}{2\pi}\right)^2 \bar{C}(\epsilon)^2\,\mathrm{d}\Phi_{\{X_i\}}(\{p_{X_i}\};\bar{p}_1,\bar{p}_2)\int \frac{\mathrm{d}z_1}{z_1}\frac{\mathrm{d}z_2}{z_2}\,\Bigg\{ \\
& \Bigg\{\;\boldsymbol{J}_{2,q\to g}^{(1)}(\hat{\bar{1}}_g,\hat{\bar{2}}_g)\,\bigg(\,M_2^1(\hat{\bar{1}}_g,\hat{\bar{2}}_g)-\frac{b_0}{\epsilon}\,M_2^0(\hat{\bar{1}}_g,\hat{\bar{2}}_g)\bigg) \\
& \qquad +\;\boldsymbol{J}_{2,q\to g}^{(2)}(\hat{\bar{1}}_g,\hat{\bar{2}}_g)\,M_2^0(\hat{\bar{1}}_g,\hat{\bar{2}}_g)\Bigg\} \\
& -\frac{1}{N^2}\;\Bigg\{\;\widetilde{\boldsymbol{J}}_{2,q\to g}^{(2)}(\hat{\bar{1}}_g,\hat{\bar{2}}_g)\,M_2^0(\hat{\bar{1}}_g,\hat{\bar{2}}_g)\Bigg\} \\
& +\frac{N_F}{N}\;\Bigg\{\;\boldsymbol{J}_{2,q\to g}^{(1)}(\hat{\bar{1}}_g,\hat{\bar{2}}_g)\,\bigg(\,\widehat{M_2^1}(\hat{\bar{1}}_g,\hat{\bar{2}}_g)-\frac{b_{0,F}}{\epsilon}\,M_2^0(\hat{\bar{1}}_g,\hat{\bar{2}}_g)\bigg)
\end{aligned}
$$

$$+ \quad \boldsymbol{J}^{(2)}_{2,q\to g,N_F}(\hat{\bar{1}}_g, \hat{\bar{2}}_g) M_2^0(\hat{\bar{1}}_g, \hat{\bar{2}}_g) \Bigg\} \Bigg\} \tag{4.22}$$

Quark-antiquark initial state:

$$
\begin{aligned}
\mathrm{d}\hat{\sigma}^U_{q\bar{q}} \;=\; & -\mathcal{N}^{NLO}_{q\bar{q}} \left(\frac{\alpha_s}{2\pi} \right)^2 \bar{C}(\epsilon)^2 \, \mathrm{d}\Phi_{\{X_i\}}(\{p_{X_i}\}; \bar{p}_1, \bar{p}_2) \int \frac{\mathrm{d}z_1}{z_1} \frac{\mathrm{d}z_2}{z_2} \\
& \times \;\; \boldsymbol{J}^{(2)}_{2,q\to g,\bar{q}\to g}(\hat{\bar{1}}_g, \hat{\bar{2}}_g) \, M_2^0(\hat{\bar{1}}_g, \hat{\bar{2}}_g).
\end{aligned}
\tag{4.23}
$$

Quark-quark initial state:

The mass factorization contribution for the quark-quark initiated channels is identical to that of the quark-antiquark channel. For the non-identical quark initiated contribution the term inherited from the double real subtraction term is also the same in both cases. In the case of identical quarks the double real subtraction term contains two different unintegrated H_4^0 antennae, which when integrated and divided by the appropriate symmetry factor, produces the same contribution to the cross section as in the quark-anti-quark and non-identical quark-quark initiated channels.

$$
\begin{aligned}
\mathrm{d}\hat{\sigma}^U_{qQ} \;=\; & -\mathcal{N}^{NLO}_{q\bar{q}} \left(\frac{\alpha_s}{2\pi} \right)^2 \bar{C}(\epsilon)^2 \, \mathrm{d}\Phi_{\{X_i\}}(\{p_{X_i}\}; \bar{p}_1, \bar{p}_2) \int \frac{\mathrm{d}z_1}{z_1} \frac{\mathrm{d}z_2}{z_2} \\
& \times \;\; \boldsymbol{J}^{(2)}_{2,q\to g,\bar{q}\to g}(\hat{\bar{1}}_g, \hat{\bar{2}}_g) \, M_2^0(\hat{\bar{1}}_g, \hat{\bar{2}}_g),
\end{aligned}
\tag{4.24}
$$

and $\mathrm{d}\hat{\sigma}^U_{qQ} = \mathrm{d}\hat{\sigma}^U_{qq}$.

Chapter 5

Two Quark Contribution to Dijet Production

The infrared structure of colourless particle production from hadronic collisions has been covered in some detail in previous chapters at both leading and sub-leading colour. The analysis of chapter 2 is applicable to more general calculations than simply colourless final-states and in particular can be used to calculate jet production cross sections for light jets without modification[1].

The calculation of the leading colour contribution to dijet production has previously been performed using the antenna subtraction formalism for purely gluonic channels at both the double real [125] and real-virtual [47] levels. This chapter will extend the antenna subtraction method at NNLO to include quarks and demonstrate the reformulation of the method using integrated antenna strings. The double real correction to dijet production requires six parton matrix elements and any of the four final-state partons can potentially become unresolved. The increased number of coloured particles in the final state allows for almost colour-connected and colour disconnected configurations to arise, unlike the situation for colourless final-states.

The NLO corrections to dijet production involving two quarks will be calculated using the NLO antenna subtraction method before focussing on the leading colour

---

[1]As shown in [112,116], the antenna subtraction formalism can be extended to massive particles for the purposes of heavy quark production by introducing additional massive antennae.

NNLO corrections to the channel $q \, \bar{q} \to g \, g$.

5.1 Matrix elements for up to six partons

At leading colour, the l-loop two-quark m-gluon contribution to the n-jet cross section is given by,

$$
\begin{aligned}
\mathrm{d}\hat{\sigma} \;=\; & \mathcal{N}^l_{m+2} \mathrm{d}\Phi_m(p_3, \ldots, p_{m+2}; p_1, p_2) \frac{1}{m!} \\
& \times \sum_{\sigma \in S_m} M^l_{m+2}(1_q, \sigma(2)_g, \ldots, \sigma(m+1)_g, (m+2)_{\bar{q}}) J^{(m)}_n(p_3, ..., p_{m+2}), \quad (5.1)
\end{aligned}
$$

where, in previous chapters, M^l_{m+2} denotes the l-loop, $(m+2)$-parton, colour-ordered squared matrix element, summed over helicities.

The normalisation factor $\mathcal{N}^l_{m+2}$ includes the average over initial spins and colours and is given by,

$$
\mathcal{N}^l_{m+2} \;=\; \mathcal{N}_{LO} \times \left(\frac{\alpha_s N}{2\pi} \right)^{m+l-2} \frac{\bar{C}(\epsilon)^{m+l-2}}{C(\epsilon)^{m-2}}, \quad (5.2)
$$

where for the $2 \to 2$ Born process,

$$
\mathcal{N}_{LO} \;=\; \frac{1}{2s} \times \frac{1}{4N^2} \times \left(g^2 N \right)^2 \frac{(N^2 - 1)}{N}. \quad (5.3)
$$

The coupling g^2 has been converted into α_s using the factors $C(\epsilon)$ and $\bar{C}(\epsilon)$,

$$
g^2 N C(\epsilon) = \left(\frac{\alpha_s N}{2\pi} \right) \bar{C}(\epsilon). \quad (5.4)
$$

For low multiplicity matrix elements, the sub-leading colour contributions can often be written as an incoherent sum of squared amplitudes, potentially involving Abelian gluons. An example of the antenna subtraction method at sub-leading colour for jet production will be demonstrated for the NLO correction to the $q \, \bar{q} \to g \, g$ subprocess.

5.1.1 Four parton contribution

The four-parton contribution to the cross section includes the tree-level Born cross section, the one-loop virtual and the two-loop double virtual corrections to the Born contribution.

Tree-level:

The Born cross section for the various scattering channels is given by:

$$
\mathrm{d}\hat{\sigma}_{q\bar{q}}^{B} = \mathcal{N}_{LO} \, \mathrm{d}\Phi_2(p_3, p_4; p_1, p_2) \frac{1}{2!} \sum_{\{i,j\}\in\{3,4\}}
$$
$$
\left\{ \left(M_4^0(\hat{1}_q, i_g, j_g, \hat{2}_{\bar{q}}) - \frac{1}{2N^2} \widetilde{M}_4^0(\hat{1}_q, i_g, j_g, \hat{2}_{\bar{q}}) \right) J_2^{(2)}(p_3, p_4) \right\}. \quad (5.5)
$$

The subleading colour contribution, included here for completeness, is formed from the square of a coherent sum of colour-ordered matrix elements,

$$
\widetilde{M}_4^0(\hat{1}_q, i_g, j_g, \hat{2}_{\bar{q}}) = |\mathcal{M}_4^0(\hat{1}_q, i_g, j_g, \hat{2}_{\bar{q}}) + \mathcal{M}_4^0(\hat{1}_q, j_g, i_g, \hat{2}_{\bar{q}})|^2 \quad (5.6)
$$

Here the three gluon coupling involving gluons i and j drops out and this contribution is referred to as having Abelian gluons.

One-loop:

For the purposes of demonstrating the sub-leading colour antenna subtraction method, the full colour decomposition of the one-loop cross section is presented here.

$$
\mathrm{d}\hat{\sigma}_{q\bar{q}}^{V} = \mathcal{N}_4^1 \, \mathrm{d}\Phi_2(p_3, p_4; p_1, p_2) \frac{1}{2!} \sum_{\{i,j\}\in\{3,4\}}
$$
$$
\Big\{ M_4^1(\hat{1}_q, i_g, j_g, \hat{2}_{\bar{q}}) - \frac{1}{N^2}\widetilde{M}_4^1(\hat{1}_q, i_g, j_g, \hat{2}_{\bar{q}}) + \frac{1}{N^4}\widetilde{\widetilde{M}}_4^1(\hat{1}_q, i_g, j_g, \hat{2}_{\bar{q}})
$$
$$
+ \; NN_F \widehat{M}_4^1(\hat{1}_q, i_g, j_g, \hat{2}_{\bar{q}}) - \frac{N_F}{N}\widehat{\widetilde{M}}_4^1(\hat{1}_q, i_g, j_g, \hat{2}_{\bar{q}}) \Big\} J_2^{(2)}(p_i, p_j) \quad (5.7)
$$

where the overall factor is as defined in (5.2),

$$
\mathcal{N}_4^1 = \mathcal{N}_{LO}\left(\frac{\alpha_s N}{2\pi}\right)\bar{C}. \quad (5.8)
$$

The various contributions are formed from the projection of one-loop partial amplitudes onto tree-level amplitudes[2]. The poles of the contributions not proportional to N_F may be expressed in terms of insertion operators, or equivalently in terms of integrated antenna strings,

$$
\mathcal{P}oles\left[M_4^1(\hat{1}_q, i_g, j_g, \hat{2}_{\bar{q}}) \right] = \boldsymbol{J}_4^{(1)}(\hat{1}_q, i_g, j_g, \hat{2}_{\bar{q}}) \, M_4^0(\hat{1}_q, i_g, j_g, \hat{2}_{\bar{q}})
$$

---

[2]In general several one-loop partial amplitudes may contribute to a single term in (5.7)

$$
\begin{aligned}
\mathcal{P}oles\left[\widetilde{M}_4^1(\hat{1}_q, i_g, j_g, \hat{2}_{\bar{q}})\right] &= \boldsymbol{J}_3^{(1)}(\hat{1}_q, j_g, \hat{2}_{\bar{q}})\, \widetilde{M}_4^0(\hat{1}_q, i_g, j_g, \hat{2}_{\bar{q}}) \\
&\quad - \boldsymbol{J}_2^{(1)}(\hat{1}_q, \hat{2}_{\bar{q}})\, M_4^0(\hat{1}_q, i_g, j_g, \hat{2}_{\bar{q}}) \\
\mathcal{P}oles\left[\widetilde{\widetilde{M}_4^1}(\hat{1}_q, i_g, j_g, \hat{2}_{\bar{q}})\right] &= \boldsymbol{J}_2^{(1)}(\hat{1}_q, \hat{2}_{\bar{q}})\, \widetilde{M}_4^0(\hat{1}_q, i_g, j_g, \hat{2}_{\bar{q}})
\end{aligned}
\tag{5.9}
$$

The N_F dependent contributions have pole structures which can be similarly written in terms of N_F dependent integrated antenna strings, but these terms are not considered for this demonstration of the pole cancellation.

Two-loops:

The leading colour contribution to the two-loop quark-anti-quark initiated cross section is given by,

$$
\mathrm{d}\hat{\sigma}_{q\bar{q}}^{VV} = \mathcal{N}_4^2\, \mathrm{d}\Phi_2(p_3, p_4; p_1, p_2)\, \frac{1}{2!} \sum_{\{i,j\}\in\{3,4\}} M_4^2(\hat{1}_q, i_g, j_g, \hat{2}_{\bar{q}})\, J_2^{(2)}(p_i, p_j). \tag{5.10}
$$

As in previous chapters, the two-loop matrix element contains the projection of the two-loop amplitude onto the tree-level amplitude and the self-interference of the one-loop amplitude.

5.1.2 Five parton contribution

The five parton contribution to the cross section is composed of the tree-level single real emission contribution to the NLO cross section and the one-loop real-virtual contribution to the NNLO cross section.

Tree-level:

For the purposes of demonstrating the sub-leading colour NLO antenna subtraction for jet production at NLO, the full colour decomposition of the $q\,\bar{q} \to g\,g$ channel is presented here.

$$
\begin{aligned}
\mathrm{d}\hat{\sigma}_{q\bar{q}}^R = {}& \mathcal{N}_5^0\, \mathrm{d}\Phi_3(p_3, p_4, p_5; p_1, p_2)\, \frac{1}{3!} \sum_{\{i,j,k\}} \left\{ \left[M_5^0(\hat{1}_q, i_g, j_g, k_g, \hat{2}_{\bar{q}}) \right. \right. \\
&\left. \left. - \frac{1}{N^2}\, \widetilde{M}_5^0(\hat{1}_q, i_g, j_g, k_g, \hat{2}_{\bar{q}}) + \left(\frac{N^2+1}{N^4}\right) \widetilde{\widetilde{M}_5^0}(\hat{1}_q, i_g, j_g, k_g, \hat{2}_{\bar{q}}) \right] J_2^{(3)}(p_i, p_j, p_k) \right\}.
\end{aligned}
\tag{5.11}
$$

The sub-leading colour matrix element $\widetilde{M}_5^0(\hat{1}_q, i_g, j_g, k_g, \hat{2}_{\bar{q}})$ is defined in the following way,

$$\widetilde{M}_5^0(\hat{1}_q, i_g, j_g, k_g, \hat{2}_{\bar{q}}) = |\mathcal{M}_5^0(\hat{1}_q, i_g, j_g, k_g, \hat{2}_{\bar{q}}) + \mathcal{M}_5^0(\hat{1}_q, j_g, i_g, k_g, \hat{2}_{\bar{q}})$$
$$+ \mathcal{M}_5^0(\hat{1}_q, j_g, k_g, i_g, \hat{2}_{\bar{q}})|^2, \tag{5.12}$$

such that the gluon i behaves in an Abelian fashion. The most sub-leading contribution is given by the QED-like matrix element, formed by averaging over all colour-ordered matrix elements,

$$\widetilde{\widetilde{M}}_5^0(\hat{1}_q, i_g, j_g, k_g, \hat{2}_{\bar{q}}) = \frac{1}{3!}\left|\sum_{\{i,j,k\}} \mathcal{M}_5^0(\hat{1}_q, i_g, j_g, k_g, \hat{2}_{\bar{q}})\right|^2. \tag{5.13}$$

All gluons in this matrix element are Abelian behaving and are only colour connected to the quark endpoints.

One-loop

The leading colour one-loop contribution to the real-virtual cross section is given by,

$$d\hat{\sigma}_{q\bar{q}}^{RV} = \mathcal{N}_5^1 \, d\Phi_2(p_3, p_4, p_5; p_1, p_2) \frac{1}{3!} \sum_{\{i,j,k\}} M_5^1(\hat{1}_q, i_g, j_g, k_g, \hat{2}_{\bar{q}}) \, J_2^{(2)}(p_i, p_j, p_k). \tag{5.14}$$

5.1.3 Six parton contribution

Tree-level:

At NNLO the only six-parton contribution to dijet production is the tree-level contribution to the double real cross section. At leading colour, the double real radiation contribution from the $q\bar{q} \to gggg$ process is given by,

$$d\hat{\sigma}_{q\bar{q}}^{RR} = \mathcal{N}_6^0 \, d\Phi_4(p_3, \ldots, p_6; p_1, p_2) \frac{1}{4!} \sum_{\{i,j,k,l\}} M_6^0(\hat{1}_q, i_g, j_g, k_g, l_g, \hat{2}_{\bar{q}}) \, J_2^{(4)}(p_i, \ldots, p_l) \tag{5.15}$$

It is convenient to rearrange the 24 amplitudes present in eq. (5.15) into three terms,

$$\sum_{\{i,j,k,l\}} M_6^0(\hat{1}_q, i_g, j_g, k_g, l_g, \hat{2}_{\bar{q}}) = X_6^0(\hat{1}_q, 3_g, 4_g, 5_g, 6_g, \hat{2}_{\bar{q}})$$

$$+ \quad X_6^0(\hat{1}_q, 3_g, 5_g, 4_g, 6_g, \hat{2}_{\bar{q}})$$

$$+ \quad X_6^0(\hat{1}_q, 3_g, 4_g, 6_g, 5_g, \hat{2}_{\bar{q}}), \qquad (5.16)$$

where each X_6^0 contains eight colour ordered squared amplitudes given by the four cyclic permutations of the final state gluons plus their line reversals:

$$
\begin{aligned}
X_6^0(\hat{1}_q, 3_g, 4_g, 5_g, 6_g, \hat{2}_{\bar{q}}) \ = \ & M_6^0(\hat{1}_q, 3_g, 4_g, 5_g, 6_g, \hat{2}_{\bar{q}}) + M_6^0(\hat{1}_q, 6_g, 5_g, 4_g, 3_g, \hat{2}_{\bar{q}}) \\
+ \ & M_6^0(\hat{1}_q, 4_g, 5_g, 6_g, 3_g, \hat{2}_{\bar{q}}) + M_6^0(\hat{1}_q, 3_g, 6_g, 5_g, 4_g, \hat{2}_{\bar{q}}) \\
+ \ & M_6^0(\hat{1}_q, 5_g, 6_g, 3_g, 4_g, \hat{2}_{\bar{q}}) + M_6^0(\hat{1}_q, 4_g, 3_g, 6_g, 5_g, \hat{2}_{\bar{q}}) \\
+ \ & M_6^0(\hat{1}_q, 6_g, 3_g, 4_g, 5_g, \hat{2}_{\bar{q}}) + M_6^0(\hat{1}_q, 5_g, 4_g, 3_g, 6_g, \hat{2}_{\bar{q}}).
\end{aligned}
$$

$$(5.17)$$

It is sufficient to apply the subtraction technique to one block of orderings, the other two are related by symmetry and contribute numerically the same result after integration over the phase space. For the purposes of Monte Carlo integration the entire set of orderings is implemented to restore the full symmetry of the gluon phase space and improve computational efficiency.

5.2 Infrared subtraction at NLO

At NLO, the single real emission cross section contains implicit singularities which may be isolated using the antenna subtraction method as discussed in detail in section 2.5. In the following sections, the NLO subtraction terms are constructed for processes involving two quarks and three gluons with the quarks in the initial state. In order to perform a full pole cancellation against the virtual cross section the additional four-quark and gluon initiated channels must be included. Given the general discussion of section 2.5, constructing these subtraction terms is trivial. Only the $q \, \bar{q} \to ggg$ subtraction terms are presented here by way of example.

5.2.1 Construction of the real subtraction terms

The leading colour subtraction term is given by,

$$
d\hat{\sigma}_{q\bar{q},NLO}^S \ = \ \mathcal{N}_5^0 \ d\Phi_3(p_3, p_4, p_5; p_1, p_2) \ \frac{1}{3!} \sum_{\{i,j,k\}} \Bigg\{
$$

$$
d_3^0(\hat{1}, i, j) \, M_4^0(\hat{\bar{1}}_q, \widetilde{(i,j)}_g, k_g, \hat{2}_{\bar{q}}) \, J_2^{(2)}(p_{(i,j)}, p_k)
$$
$$
+ \quad f_3^0(i, j, k) \, M_4^0(\hat{1}_q, \widetilde{(i,j)}_g, \widetilde{(j,k)}_g, \hat{2}_{\bar{q}}) \, J_2^{(2)}(p_{(i,j)}, p_{(j,k)})
$$
$$
+ \quad d_3^0(\hat{2}, k, j) \, M_4^0(\hat{1}_q, i_g, \widetilde{(j,k)}_g, \hat{\bar{2}}_{\bar{q}}) \, J_2^{(2)}(p_i, p_{(j,k)}) \bigg\} . \tag{5.18}
$$

The subtraction term for the remaining sub-leading colour contributions is constructed by considering the colour structure of the matrix elements in (5.11), following the discussion about sub-leading colour subtraction terms in 2.5.

$$
\mathrm{d}\hat{\sigma}_{q\bar{q},NLO}^S \;=\; \mathcal{N}_5^0 \, \mathrm{d}\Phi_3(p_3, p_4, p_5; p_1, p_2) \, \frac{1}{3!} \sum_{\{i,j,k\}} \bigg\{
$$
$$
-\frac{1}{N^2} \bigg[\; A_3^0(\hat{1}, i, \hat{2}) \, M_4^0(\hat{\bar{1}}_q, \tilde{j}_g, \tilde{k}_g, \hat{\bar{2}}_{\bar{q}}) \, J_2^{(2)}(p_j, p_k)
$$
$$
+ \quad d_3^0(\hat{1}, j, k) \, \widetilde{M_4^0}(\hat{\bar{1}}_q, i_g, \widetilde{(j,k)}_g, \hat{2}_{\bar{q}}) \, J_2^{(2)}(p_i, p_{(j,k)})
$$
$$
+ \quad d_3^0(\hat{2}, k, j) \, \widetilde{M_4^0}(\hat{1}_q, i_g, \widetilde{(j,k)}_g, \hat{\bar{2}}_{\bar{q}}) \, J_2^{(2)}(p_i, p_{(j,k)}) \bigg]
$$
$$
+ \left(\frac{N^2+1}{N^4} \right) \bigg[\; A_3^0(\hat{1}, i, \hat{2}) \, \widetilde{M_4^0}(\hat{\bar{1}}_q, \tilde{j}_g, \tilde{k}_g, \hat{\bar{2}}_{\bar{q}}) \, J_2^{(2)}(p_j, p_k)
$$
$$
+ \quad A_3^0(\hat{1}, j, \hat{2}) \, \widetilde{M_4^0}(\hat{\bar{1}}_q, \tilde{i}_g, \tilde{k}_g, \hat{\bar{2}}_{\bar{q}}) \, J_2^{(2)}(p_i, p_k)
$$
$$
+ \quad A_3^0(\hat{1}, k, \hat{2}) \, \widetilde{M_4^0}(\hat{\bar{1}}_q, \tilde{i}_g, \tilde{j}_g, \hat{\bar{2}}_{\bar{q}}) \, J_2^{(2)}(p_i, p_j) \bigg] \bigg\} . \tag{5.19}
$$

5.2.2 Construction of the virtual subtraction term

Integrating the real subtraction term over the single unresolved phase space and combining with the appropriate NLO mass factorization kernels allows the virtual subtraction term to be constructed from integrated antenna strings. The leading colour virtual subtraction term is given by,

$$
\mathrm{d}\hat{\sigma}_{q\bar{q},NLO}^T \;=\; -\mathcal{N}_4^1 \, \mathrm{d}\Phi_2(p_3, p_4; p_1, p_2) \, \frac{1}{2!} \sum_{\{i,j\}} \int \frac{\mathrm{d}x_1}{x_1} \frac{\mathrm{d}x_2}{x_2}
$$
$$
\boldsymbol{J}_4^{(1)}(\hat{\bar{1}}_q, i_g, j_g, \hat{\bar{2}}_{\bar{q}}) \, M_4^0(\hat{\bar{1}}_q, i_g, j_g, \hat{\bar{2}}_{\bar{q}}) \, J_2^{(2)}(p_i, p_j), \tag{5.20}
$$

where $\boldsymbol{J}_4^{(1)}(\hat{\bar{1}}_q, i_g, j_g, \hat{\bar{2}}_{\bar{q}}) = \boldsymbol{J}_2^{(1)}(\hat{\bar{1}}_q, i_g) + \boldsymbol{J}_2^{(1)}(i_g, j_g) + \boldsymbol{J}_2^{(1)}(j_g, \hat{\bar{2}}_{\bar{q}})$, the explicit form of which can be found in appendix B.1.

Integrating the sub-leading colour subtraction terms and combining with the relevant mass factorization contributions yields the subleading colour virtual sub-

traction terms,

$$
\begin{aligned}
\mathrm{d}\hat{\sigma}^{T}_{q\bar{q},NLO} = {} & -\mathcal{N}^{1}_{4} \, \mathrm{d}\Phi_{2}(p_{3},p_{4};p_{1},p_{2}) \, \frac{1}{2!} \sum_{\{i,j\}} \int \frac{\mathrm{d}x_{1}}{x_{1}} \frac{\mathrm{d}x_{2}}{x_{2}} \\
& -\frac{1}{N^{2}} \Bigg[\quad \boldsymbol{J}^{(1)}_{2}(\hat{\bar{1}}_{q},\hat{\bar{2}}_{\bar{q}}) \, M^{0}_{4}(\hat{\bar{1}}_{q},i_{g},j_{g},\hat{\bar{2}}_{\bar{q}}) \, J^{(2)}_{2}(p_{i},p_{j}) \\
& \qquad\quad + \quad \boldsymbol{J}^{(1)}_{3}(\hat{\bar{1}}_{q},j_{g},\hat{\bar{2}}_{\bar{q}}) \, \widetilde{M}^{0}_{4}(\hat{\bar{1}}_{q},i_{g},j_{g},\hat{\bar{2}}_{\bar{q}}) \, J^{(2)}_{2}(p_{i},p_{j}) \Bigg] \\
& + \left(\frac{N^{2}+1}{N^{4}}\right) \Bigg[\quad \boldsymbol{J}^{(1)}_{2}(\hat{\bar{1}}_{q},\hat{\bar{2}}_{\bar{q}}) \, \widetilde{M}^{0}_{4}(\hat{\bar{1}}_{q},i_{g},j_{g},\hat{\bar{2}}_{\bar{q}}) \, J^{(2)}_{2}(p_{i},p_{j}) \Bigg] \Bigg\}.
\end{aligned}
\tag{5.21}
$$

By grouping terms with a common colour factor and tree-level matrix element, the whole subtraction term can be re-organised into the form,

$$
\begin{aligned}
\mathrm{d}\hat{\sigma}^{T}_{q\bar{q},NLO} = {} & -\mathcal{N}^{1}_{4} \, \mathrm{d}\Phi_{2}(p_{3},p_{4};p_{1},p_{2}) \, \frac{1}{2!} \sum_{\{i,j\}} \int \frac{\mathrm{d}x_{1}}{x_{1}} \frac{\mathrm{d}x_{2}}{x_{2}} \\
& \boldsymbol{J}^{(1)}_{4}(\hat{\bar{1}}_{q},i_{g},j_{g},\hat{\bar{2}}_{\bar{q}}) \, M^{0}_{4}(\hat{\bar{1}}_{q},i_{g},j_{g},\hat{\bar{2}}_{\bar{q}}) \, J^{(2)}_{2}(p_{i},p_{j}) \\
& -\frac{1}{N^{2}} \Bigg[\quad \boldsymbol{J}^{(1)}_{2}(\hat{\bar{1}}_{q},\hat{\bar{2}}_{\bar{q}}) \, M^{0}_{4}(\hat{\bar{1}}_{q},i_{g},j_{g},\hat{\bar{2}}_{\bar{q}}) \, J^{(2)}_{2}(p_{i},p_{j}) \\
& \qquad\quad + \left(\boldsymbol{J}^{(1)}_{3}(\hat{\bar{1}}_{q},j_{g},\hat{\bar{2}}_{\bar{q}}) - \boldsymbol{J}^{(1)}_{2}(\hat{\bar{1}}_{q},\hat{\bar{2}}_{\bar{q}}) \right) \widetilde{M}^{0}_{4}(\hat{\bar{1}}_{q},i_{g},j_{g},\hat{\bar{2}}_{\bar{q}}) \, J^{(2)}_{2}(p_{i},p_{j}) \Bigg] \\
& +\frac{1}{N^{4}} \Bigg[\quad \boldsymbol{J}^{(1)}_{2}(\hat{\bar{1}}_{q},\hat{\bar{2}}_{\bar{q}}) \, \widetilde{M}^{0}_{4}(\hat{\bar{1}}_{q},i_{g},j_{g},\hat{\bar{2}}_{\bar{q}}) \, J^{(2)}_{2}(p_{i},p_{j}) \Bigg] \Bigg\}.
\end{aligned}
\tag{5.22}
$$

Comparing with (5.7) it is clear that this virtual subtraction term, derived from the integrated real subtraction term and the mass factorization kernels, properly subtracts the explicit poles of the non-N_{F} dependent one-loop cross section. The remaining N_{F} dependent explicit poles are subtracted by the N_{F} dependent virtual subtraction term, which is constructed from the N_{F} dependent mass factorization kernels and integrated real subtraction term for four-quark subprocesses.

5.3 Infrared subtraction at NNLO

This section will focus on the leading colour NNLO corrections to the process, $q\,\bar{q} \to g\,g$ involving two quarks. These corrections include the double real tree-level contribution $q\,\bar{q} \to gggg$, the real-virtual one-loop contribution $q\,\bar{q} \to ggg$ and the double virtual two loop contribution $q\,\bar{q} \to g\,g$.

5.3.1 Construction of the double real subtraction term

The leading colour contribution to the squared matrix element is an incoherent sum of squared colour-ordered partial amplitudes. The sum over colour orderings can be partitioned into three blocks of orderings as described in section 5.1.3, such that a subtraction term may be constructed for a block of orderings, rather than the entire squared matrix element. Following the general discussion of section 2.6, the NNLO subtraction term for di-jet production within the block of orderings $X_6^0(\hat{1}_q, 3_g, 4_g, 5_g, 6_g, \hat{2}_{\bar{q}})$ is given by,

$$
\mathrm{d}\hat{\sigma}_{NNLO}^{S,X_6} = \mathcal{N}_6^0 \, \mathrm{d}\Phi_4(p_3, \ldots, p_6; p_1, p_2) \, \frac{1}{4!} \sum_{(ijkl)} \Bigg\{
$$

$$
+ f_3^0(i,j,k) \, M_5^0(\hat{1}, \widetilde{(i,j)}, \widetilde{(j,k)}, l, \hat{2}) \, J_2^{(3)}(p_{(i,j)}, p_{(j,k)}, p_l)
$$

$$
+ f_3^0(j,k,l) \, M_5^0(\hat{1}, i, \widetilde{(j,k)}, \widetilde{(k,l)}, \hat{2}) \, J_2^{(3)}(p_{(i)}, p_{(j,k)}, p_{(k,l)})
$$

$$
+ d_3^0(\hat{1},i,j) \, M_5^0(\hat{\tilde{1}}, \widetilde{(i,j)}, k, l, \hat{2}) \, J_2^{(3)}(p_{(i,j)}, p_k, p_l)
$$

$$
+ d_3^0(\hat{2},l,k) \, M_5^0(\hat{1}, i, j, \widetilde{(k,l)}, \hat{\tilde{2}}) \, J_2^{(3)}(p_i, p_j, p_{(k,l)})
$$

$$
+ f_3^0(l,k,j) \, M_5^0(\hat{1}, \widetilde{(l,k)}, \widetilde{(k,j)}, i, \hat{2}) \, J_2^{(3)}(p_{(l,k)}, p_{(k,j)}, p_i)
$$

$$
+ f_3^0(k,j,i) \, M_5^0(\hat{1}, l, \widetilde{(k,j)}, \widetilde{(j,i)}, \hat{2}) \, J_2^{(3)}(p_l, p_{(k,j)}, p_{(j,i)})
$$

$$
+ d_3^0(\hat{1},l,k) \, M_5^0(\hat{\tilde{1}}, \widetilde{(l,k)}, j, i, \hat{2}) \, J_2^{(3)}(p_{(l,k)}, p_j, p_i)
$$

$$
+ d_3^0(\hat{2},i,j) \, M_5^0(\hat{1}, l, k, \widetilde{(j,i)}, \hat{\tilde{2}}) \, J_2^{(3)}(p_l, p_k, p_{(j,i)})
$$

$$
+ F_{4,a}^0(i,j,k,l) \, M_4^0(\hat{1}, \widetilde{(i,j,k)}, \widetilde{(j,k,l)}, \hat{2}) \, J_2^{(\hat{2})}(p_{(i,j,k)}, p_{(j,k,l)})
$$

$$
+ F_{4,b}^0(i,j,l,k) \, M_4^0(\hat{1}, \widetilde{(i,j,l)}, \widetilde{(j,l,k)}, \hat{2}) \, J_2^{(\hat{2})}(p_{(i,j,k)}, p_{(j,l,k)})
$$

$$
+ F_{4,a}^0(l,k,j,i) \, M_4^0(\hat{1}, \widetilde{(l,k,j)}, \widetilde{(k,j,i)}, \hat{2}) \, J_2^{(\hat{2})}(p_{(l,k,j)}, p_{(k,j,i)})
$$

$$
+ F_{4,b}^0(l,k,i,j) \, M_4^0(\hat{1}, \widetilde{(l,k,i)}, \widetilde{(k,i,j)}, \hat{2}) \, J_2^{(\hat{2})}(p_{(l,k,i)}, p_{(k,i,j)})
$$

$$
+ D_4^0(\hat{1},i,j,k) \, M_4^0(\hat{\tilde{1}}, \widetilde{(i,j,k)}, l, \hat{2}) \, J_2^{(\hat{2})}(p_{(i,j,k)}, p_l)
$$

$$
+ D_4^0(\hat{2},l,k,j) \, M_4^0(\hat{1}, i, \widetilde{(l,k,j)}, \hat{\tilde{2}}) \, J_2^{(\hat{2})}(p_i, p_{(l,k,j)})
$$

$$
- \tilde{A}_4^0(\hat{1},i,k,\hat{2}) \, M_4^0(\hat{\tilde{1}}, \tilde{j}, \tilde{l}, \hat{\tilde{2}}) \, J_2^{(\hat{2})}(p_{\tilde{j}}, p_{\tilde{l}})
$$

$$-f_3^0(i,j,k)\,f_3^0(\widetilde{(i,j)},\widetilde{(j,k)},l)\,M_4^0(\hat{1},((\widetilde{i,j}),(\widetilde{j,k})),((\widetilde{j,k}),l),\hat{2})\,J_2^{(\hat{2})}(p_{((i,j),(j,k))},p_{((j,k),l)})$$

$$-f_3^0(j,k,l)\,f_3^0(i,\widetilde{(j,k)},\widetilde{(k,l)})\,M_4^0(\hat{1},(i,(\widetilde{j,k})),((\widetilde{j,k}),(\widetilde{k,l})),\hat{2})\,J_2^{(\hat{2})}(p_{((i,j),(j,k))},p_{((j,k),l)})$$

$$-f_3^0(i,j,k)\,f_3^0(\widetilde{(i,j)},l,\widetilde{(j,k)})\,M_4^0(\hat{1},((\widetilde{i,j}),l),((\widetilde{j,k}),l),\hat{2})\,J_2^{(\hat{2})}(p_{((i,j),l)},p_{((j,k),l)})$$

$$-f_3^0(l,k,j)\,f_3^0(\widetilde{(l,k)},\widetilde{(k,j)},i)\,M_4^0(\hat{1},((\widetilde{l,k}),(\widetilde{k,j})),((\widetilde{k,j}),i),\hat{2})\,J_2^{(\hat{2})}(p_{((l,k),(k,j))},p_{((k,j),i)})$$

$$-f_3^0(k,j,i)\,f_3^0(l,\widetilde{(k,j)},\widetilde{(j,i)})\,M_4^0(\hat{1},(l,(\widetilde{k,j})),((\widetilde{k,j}),(\widetilde{j,i})),\hat{2})\,J_2^{(\hat{2})}(p_{(k,j)},p_{((k,j),(j,i))})$$

$$-f_3^0(l,k,j)\,f_3^0(\widetilde{(l,k)},i,\widetilde{(k,j)})\,M_4^0(\hat{1},((\widetilde{l,k}),i),((\widetilde{k,j}),i),\hat{2})\,J_2^{(\hat{2})}(p_{((l,k),i)},p_{((k,j),i)})$$

$$-d_3^0(\hat{1},i,j)\,D_3^0(\hat{\hat{1}},\widetilde{(i,j)},k)\,M_4^0(\hat{\bar{\hat{1}}},((\widetilde{i,j}),k),l,\hat{2})\,J_2^{(\hat{2})}(p_{((i,j),k)},p_l)$$

$$-f_3^0(i,j,k)\,D_3^0(\hat{1},\widetilde{(i,j)},\widetilde{(j,k)})\,M_4^0(\hat{\hat{1}},((\widetilde{i,j}),(\widetilde{j,k})),l,\hat{2})\,J_2^{(\hat{2})}(p_{((i,j),(j,k))},p_l)$$

$$-d_3^0(\hat{1},k,j)\,D_3^0(\hat{\hat{1}},\widetilde{(k,j)},i)\,M_4^0(\hat{\bar{\hat{1}}},((\widetilde{k,j}),i),l,\hat{2})\,J_2^{(\hat{2})}(p_{((k,j),i)},p_l)$$

$$-d_3^0(\hat{2},l,k)\,D_3^0(\hat{\hat{2}},\widetilde{(l,k)},j)\,M_4^0(\hat{1},i,((\widetilde{l,k}),j),\hat{\bar{\hat{2}}})\,J_2^{(\hat{2})}(p_{((l,k),j)},p_i)$$

$$-f_3^0(l,k,j)\,D_3^0(\hat{2},\widetilde{(l,k)},\widetilde{(k,j)})\,M_4^0(\hat{1},i,((\widetilde{l,k}),(\widetilde{k,j})),\hat{\hat{2}})\,J_2^{(\hat{2})}(p_i,p_{((l,k),(k,j))})$$

$$-d_3^0(\hat{2},j,k)\,D_3^0(\hat{\hat{2}},\widetilde{(j,k)},l)\,M_4^0(\hat{1},i,((\widetilde{j,k}),l),\hat{\bar{\hat{2}}})\,J_2^{(\hat{2})}(p_i,p_{((j,k),l)})$$

$$+A_3^0(\hat{1},i,\hat{2})\,A_3^0(\hat{\hat{1}},\tilde{k},\hat{\hat{2}})\,M_4^0(\hat{\bar{\hat{1}}},\tilde{\tilde{j}},\tilde{\tilde{l}},\hat{\bar{\hat{2}}})\,J_2^{(\hat{2})}(p_{\tilde{j}},p_{\tilde{l}})$$

$$+A_3^0(\hat{1},k,\hat{2})\,A_3^0(\hat{\hat{1}},\tilde{i},\hat{\hat{2}})\,M_4^0(\hat{\bar{\hat{1}}},\tilde{\tilde{j}},\tilde{\tilde{l}},\hat{\bar{\hat{2}}})\,J_2^{(\hat{2})}(p_{\tilde{\tilde{j}}},p_{\tilde{\tilde{l}}})$$

$$+\frac{1}{2}\,f_3^0(i,l,k)\,f_3^0(\widetilde{(i,l)},j,\widetilde{(l,k)})\,M_4^0(\hat{1},((\widetilde{i,l}),j),((\widetilde{l,k}),j),\hat{2})\,J_2^{(\hat{2})}(p_{((i,l),j)},p_{((l,k),j)})$$

$$-\frac{1}{2}\,d_3^0(\hat{1},l,i)\,f_3^0(\widetilde{(l,i)},j,k)\,M_4^0(\hat{\hat{1}},((\widetilde{i,l}),j),\widetilde{(j,k)},\hat{2})\,J_2^{(\hat{2})}(p_{((i,l),j)},p_{(j,k)})$$

$$-\frac{1}{2}\,d_3^0(\hat{2},l,k)\,f_3^0(i,j,\widetilde{(k,l)})\,M_4^0(\hat{1},\widetilde{(i,j)},(j,\widetilde{(k,l)}),\hat{\hat{2}})\,J_2^{(\hat{2})}(p_{(i,j)},p_{(j,(k,l))})$$

$$-\frac{1}{2}\Big[\,\big(S_{(i,l)l(l,k)}-S_{((i,l),j)l(j,(l,k))}\big)-\big(S_{1l(i,l)}-S_{1l((i,l),j)}\big)-\big(S_{2l(l,k)}-S_{2l(j(l,k))}\big)\,\Big]$$

$$\times f_3^0(\widetilde{(i,l)},j,\widetilde{(l,k)})\,M_4^0(\hat{1},((\widetilde{i,l}),j),(j,\widetilde{(l,k)}),\hat{2})\,J_2^{(\hat{2})}(p_{((i,l),j)},p_{(j,(l,k))})$$

$$+\frac{1}{2}\,f_3^0(l,i,j)\,f_3^0(\widetilde{(l,i)},k,\widetilde{(i,j)})\,M_4^0(\hat{1},((\widetilde{l,i}),k),((\widetilde{i,j}),k),\hat{2})\,J_2^{(\hat{2})}(p_{((l,i),k)},p_{((i,j),k)})$$

$$-\frac{1}{2}\, d_3^0(\hat{1}, i, l)\, f_3^0(\widetilde{(i,l)}, k, j)\, M_4^0(\hat{\tilde{1}}, (\widetilde{(i,l)}, k), \widetilde{(k,j)}, \hat{2})\, J_2^{(\hat{2})}(p_{((i,l),k)}, p_{(k,j)})$$

$$-\frac{1}{2}\, d_3^0(\hat{2}, i, j)\, f_3^0(l, k, \widetilde{(i,j)})\, M_4^0(\hat{1}, \widetilde{(l,k)}, (\widetilde{k, (i,j)}), \hat{\tilde{2}})\, J_2^{(\hat{2})}(p_{(l,k)}, p_{(k,(i,j))})$$

$$-\frac{1}{2}\Bigg[\,\big(S_{(l,i)i(i,j)} - S_{((l,i),k)i(k,(i,j))}\big) - \big(S_{1i(l,i)} - S_{1i((l,i),k)}\big) - \big(S_{2i(i,j)} - S_{2i(k(i,j))}\big)\,\Bigg]$$

$$\times f_3^0(\widetilde{(l,i)}, k, \widetilde{(i,j)})\, M_4^0(\hat{1}, (\widetilde{(l,i)}, k), (\widetilde{k, (i,j)}), \hat{2})\, J_2^{(\hat{2})}(p_{((l,i),k)}, p_{(k,(i,j))})$$

$$+\frac{1}{2}\, d_3^0(\hat{1}, k, j)\, d_3^0(\hat{\tilde{1}}, i, \widetilde{(k,j)})\, M_4^0(\hat{\tilde{\tilde{1}}}, ((\widetilde{k,j}), i), l, \hat{2})\, J_2^{(\hat{2})}(p_{((k,j),i)}, p_l)$$

$$-\frac{1}{2}\, f_3^0(j, k, l)\, d_3^0(\hat{1}, i, \widetilde{(j,k)})\, M_4^0(\hat{\tilde{1}}, (i, \widetilde{(j,k)}), \widetilde{(k,l)}, \hat{2})\, J_2^{(\hat{2})}(p_{(i,(j,k))}, p_{(k,l)})$$

$$-\frac{1}{2}\, A_3^0(\hat{1}, k, \hat{2})\, d_3^0(\hat{\tilde{1}}, \tilde{i}, \tilde{j})\, M_4^0(\hat{\tilde{\tilde{1}}}, \widetilde{(i,j)}, \tilde{l}, \hat{\tilde{2}})\, J_2^{(\hat{2})}(p_{(i,j)}, p_{\tilde{l}})$$

$$-\frac{1}{2}\Bigg[\,\big(S_{1k(j,k)} - S_{\bar{1}k(i,(j,k))}\big) - \big(S_{(j,k)k(k,l)} - S_{(i,(j,k))k(k,l)}\big) - \underbrace{\big(S_{1k2} - S_{\bar{1}k2}\big)}_{0}\,\Bigg]$$

$$\times d_3^0(\hat{1}, i, \widetilde{(j,k)})\, M_4^0(\hat{\tilde{1}}, (i, \widetilde{(j,k)}), \widetilde{(k,l)}, \hat{2})\, J_2^{(\hat{2})}(p_{(i,(j,k))}, p_{(k,l)})$$

$$+\frac{1}{2}\, d_3^0(\hat{1}, i, j)\, d_3^0(\hat{\tilde{1}}, k, \widetilde{(i,j)})\, M_4^0(\hat{\tilde{\tilde{1}}}, ((\widetilde{i,j}), k), l, \hat{2})\, J_2^{(\hat{2})}(p_{((i,j),k)}, p_l)$$

$$-\frac{1}{2}\, f_3^0(j, i, l)\, d_3^0(\hat{1}, k, \widetilde{(j,i)})\, M_4^0(\hat{\tilde{1}}, (k, \widetilde{(j,i)}), \widetilde{(i,l)}, \hat{2})\, J_2^{(\hat{2})}(p_{(k,(j,i))}, p_{(i,l)})$$

$$-\frac{1}{2}\, A_3^0(\hat{1}, i, \hat{2})\, d_3^0(\hat{\tilde{1}}, \tilde{k}, \tilde{j})\, M_4^0(\hat{\tilde{\tilde{1}}}, \widetilde{(k,j)}, \tilde{l}, \hat{\tilde{2}})\, J_2^{(\hat{2})}(p_{(k,j)}, p_{\tilde{l}})$$

$$-\frac{1}{2}\Bigg[\,\big(S_{1i(j,i)} - S_{\bar{1}i(k,(j,i))}\big) - \big(S_{(k,(j,i))i(i,l)} - S_{(j,i)i(i,l)}\big) - \underbrace{\big(S_{1i2} - S_{\bar{1}i2}\big)}_{0}\,\Bigg]$$

$$\times d_3^0(\hat{1}, k, \widetilde{(j,i)})\, M_4^0(\hat{\tilde{1}}, (k, \widetilde{(j,i)}), \widetilde{(i,l)}, \hat{2})\, J_2^{(\hat{2})}(p_{(k,(j,i))}, p_{(i,l)})$$

$$+\frac{1}{2}\, d_3^0(\hat{2}, j, k)\, d_3^0(\hat{\tilde{2}}, l, \widetilde{(j,k)})\, M_4^0(\hat{1}, i, (\widetilde{(j,k)}, l), \hat{\tilde{\tilde{2}}})\, J_2^{(\hat{2})}(p_i, p_{((j,k),l)})$$

$$-\frac{1}{2}\, f_3^0(i, j, k)\, d_3^0(\hat{2}, l, \widetilde{(j,k)})\, M_4^0(\hat{1}, \widetilde{(i,j)}, (\widetilde{l, (j,k)}), \hat{\tilde{2}})\, J_2^{(\hat{2})}(p_{(i,j)}, p_{(l,(j,k))})$$

$$-\frac{1}{2}\, A_3^0(\hat{1}, j, \hat{2})\, d_3^0(\hat{\tilde{2}}, \tilde{l}, \tilde{k})\, M_4^0(\hat{\tilde{1}}, \tilde{i}, \widetilde{(l,k)}, \hat{\tilde{\tilde{2}}})\, J_2^{(\hat{2})}(p_{\tilde{i}}, p_{(l,k)})$$

$$-\frac{1}{2}\Bigg[\,\big(S_{2j(j,k)} - S_{\bar{2}j(l,(j,k))}\big) - \big(S_{(i,j)j(j,k)} - S_{(i,j)j((j,k),l)}\big) - \underbrace{\big(S_{1j2} - S_{1j\bar{2}}\big)}_{0}\,\Bigg]$$

$$\times d_3^0(\hat{2}, l, \widetilde{(j,k)})\, M_4^0(\hat{1}, \widetilde{(i,j)}, (\widetilde{(j,k)}, l), \hat{\tilde{2}})\, J_2^{(\hat{2})}(p_{(i,j)}, p_{((j,k),l)})$$

$$+\frac{1}{2}\, d_3^0(\hat{2}, l, k)\, d_3^0(\hat{\tilde{2}}, j, \widetilde{(l,k)})\, M_4^0(\hat{1}, i, ((\widetilde{l,k}), j), \hat{\tilde{\tilde{2}}})\, J_2^{(\hat{2})}(p_{((l,k),j)}, p_i)$$

$$-\frac{1}{2}\,f_3^0(i,l,k)\,d_3^0(\hat{2},j,\widetilde{(l,k)})\,M_4^0(\hat{1},\widetilde{(i,l)},(j,\widetilde{(l,k)}),\hat{\bar{2}})\,J_2^{(\hat{2})}(p_{(i,l)},p_{(j,(l,k))})$$

$$-\frac{1}{2}\,A_3^0(\hat{1},l,\hat{2})\,d_3^0(\hat{\bar{2}},\tilde{j},\tilde{k})\,M_4^0(\hat{\bar{1}},\tilde{i},\widetilde{(j,k)},\hat{\bar{2}})\,J_2^{(\hat{2})}(p_{\tilde{i}},p_{(j,k)})$$

$$-\frac{1}{2}\left[\,\left(S_{2l(l,k)}-S_{\bar{2}l(j,(l,k))}\right)-\left(S_{(i,l)l((l,k),j)}-S_{(i,l)l(l,k)}\right)-\underbrace{\left(S_{1l2}-S_{1l\bar{2}}\right)}_{0}\,\right]$$

$$\times d_3^0(\hat{2},j,\widetilde{(l,k)})\,M_4^0(\hat{1},\widetilde{(i,l)},((\widetilde{l,k}),j),\hat{\bar{2}})\,J_2^{(\hat{2})}(p_{(i,l)},p_{((l,k),j)})$$

$$-\frac{1}{2}\,A_3^0(\hat{1},i,\hat{2})\,A_3^0(\hat{\bar{1}},\tilde{k},\hat{\bar{2}})\,M_4^0(\hat{\bar{\bar{1}}},\tilde{\tilde{j}},\tilde{\tilde{l}},\hat{\bar{\bar{2}}})\,J_2^{(\hat{2})}(p_{\tilde{\tilde{j}}},p_{\tilde{\tilde{l}}})$$

$$+\frac{1}{2}\,d_3^0(\hat{1},i,j)\,A_3^0(\hat{\bar{1}},k,\hat{2})\,M_4^0(\hat{\bar{\bar{1}}},\widetilde{(i,j)},\tilde{l},\hat{\bar{2}})\,J_2^{(\hat{2})}(p_{\widetilde{(i,j)}},p_{\tilde{l}})$$

$$+\frac{1}{2}\,d_3^0(\hat{2},i,l)\,A_3^0(\hat{1},k,\hat{\bar{2}})\,M_4^0(\hat{\bar{1}},\tilde{j},\widetilde{(i,l)},\hat{\bar{\bar{2}}})\,J_2^{(\hat{2})}(p_{\tilde{j}},p_{\widetilde{(i,l)}})$$

$$+\frac{1}{2}\left[\,\left(S_{1i2}-S_{\bar{1}\tilde{i}\bar{2}}\right)-\left(S_{1i(j,i)}-S_{\bar{1}\tilde{i}\widetilde{(j,i)}}\right)-\left(S_{2i(i,l)}-S_{\bar{2}\tilde{i}\widetilde{(i,l)}}\right)\,\right]$$

$$\times A_3^0(\hat{1},k,\hat{2})\,M_4^0(\hat{\bar{1}},\widetilde{(j,i)},\widetilde{(i,l)},\hat{\bar{2}})\,J_2^{(\hat{2})}(p_{\widetilde{(j,i)}},p_{\widetilde{(i,l)}})$$

$$-\frac{1}{2}\,A_3^0(\hat{1},k,\hat{2})\,A_3^0(\hat{\bar{1}},\tilde{i},\hat{\bar{2}})\,M_4^0(\hat{\bar{\bar{1}}},\tilde{\tilde{j}},\tilde{\tilde{l}},\hat{\bar{\bar{2}}})\,J_2^{(\hat{2})}(p_{\tilde{j}},p_{\tilde{l}})$$

$$+\frac{1}{2}\,d_3^0(\hat{1},k,j)\,A_3^0(\hat{\bar{1}},i,\hat{2})\,M_4^0(\hat{\bar{\bar{1}}},\widetilde{(k,j)},\tilde{l},\hat{\bar{2}})\,J_2^{(\hat{2})}(p_{\widetilde{(k,j)}},p_{\tilde{l}})$$

$$+\frac{1}{2}\,d_3^0(\hat{2},k,l)\,A_3^0(\hat{1},i,\hat{\bar{2}})\,M_4^0(\hat{\bar{1}},\tilde{j},\widetilde{(k,l)},\hat{\bar{\bar{2}}})\,J_2^{(\hat{2})}(p_{\tilde{j}},p_{\widetilde{(k,l)}})$$

$$+\frac{1}{2}\left[\,\left(S_{1k2}-S_{\bar{1}\tilde{k}\bar{2}}\right)-\left(S_{1k(j,k)}-S_{\bar{1}\tilde{k}\widetilde{(j,k)}}\right)-\left(S_{2k(k,l)}-S_{\bar{2}\tilde{k}\widetilde{(k,l)}}\right)\,\right]$$

$$\times A_3^0(\hat{1},i,\hat{2})\,M_4^0(\hat{\bar{1}},\widetilde{(j,k)},\widetilde{(k,l)},\hat{\bar{2}})\,J_2^{(\hat{2})}(p_{\widetilde{(j,k)}},p_{\widetilde{(k,l)}})$$

$$-d_3^0(\hat{1},i,j)\,d_3^0(\hat{2},l,k)\,M_4^0(\hat{\bar{1}},\widetilde{(i,j)},\widetilde{(k,l)},\hat{\bar{2}})\,J_2^{(\hat{2})}(p_{(i,j)},p_{(k,l)})$$

$$-d_3^0(\hat{1},l,k)\,d_3^0(\hat{2},i,j)\,M_4^0(\hat{\bar{1}},\widetilde{(l,k)},\widetilde{(i,j)},\hat{\bar{2}})\,J_2^{(\hat{2})}(p_{(l,k)},p_{(i,j)})\Bigg\} \qquad (5.23)$$

It is interesting to note the appearance of the subleading colour quark-anti-quark antenna $\tilde{A}_4^0$ and the accompanying A_3^0 antennae. The sub-leading colour antenna is introduced to remove spurious singular behaviour of the D_4^0 antenna in the triple collinear limit. Specifically, the D_4^0 antenna contains the IR divergent limit between colour-disconnected gluons,

$$D_4^0(i,j,k,l)\xrightarrow{i\|j\|l}\tilde{P}_{ijl\to Q}(x,y,z), \qquad (5.24)$$

where the antenna tends to the QED-like triple collinear splitting function. This divergent limit has no analogue in the leading colour physical matrix elements and must be removed, a function fulfilled by the $\tilde{A}_4^0$ antenna. The origin of this spurious limit can be seen in the definition of the quark-gluon antennae.

The partons in a quark-gluon antenna are colour connected to colour-adjacent neighbours, which unlike the quark-antiquark antennae, include partons at either end of the antenna, e.g, partons i and l are colour connected in $D_4^0(i, j, k, l)$. This is due to the antenna being derived from colour-ordered matrix elements for the Supersymmetric QCD (SQCD) process $\tilde{\chi} \to \tilde{g}\, g +$ partons where the gluino plays the role of the quark. In SQCD the fermions are in the adjoint representation and so are not restricted to being the endpoints of gluon strings as is the case in non-supersymmetric QCD. The trace colour structure of the gluino-gluon matrix elements allows colour connections to exist between colour disconnected gluons and these configurations give rise to the unphysical divergent limits in the quark-gluon antennae. For pure QCD matrix elements, the quarks always come in quark-antiquark pairs at the end of gluon strings such that no quark can separate two gluons in a colour ordering.

Given the modifications due to the spurious limits of the quark-gluon antennae, the double real subtraction term fits the general structure derived in section 2.6. Due to the non-trivial factorization of the four-parton final-final antennae and the large sum of permutations, it is not straightforward to show that this subtraction term correctly mimics the IR divergent behaviour of the physical cross section. In order to demonstrate its validity, the subtraction term has been tested numerically.

For each IR divergent configuration a set of momenta were generated using RAMBO [127] such that the momenta fulfil a set of constraints defining the unresolved configuration. In this configuration, the ratio of the full physical matrix element to the subtraction term defined above is calculated,

$$R \;=\; \frac{\mathrm{d}\hat{\sigma}^{RR}}{\mathrm{d}\hat{\sigma}^S}. \tag{5.25}$$

This procedure is then repeated for 10,000 different phase space points in the unresolved configuration defined by the constraints. The constraints are then tightened to force the phase space points closer to the unresolved singular point and the ratio
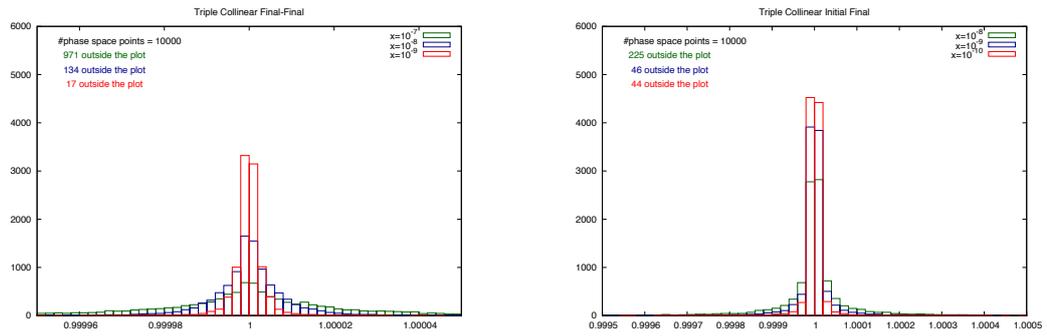
(a) Final-state triple collinear limit between partons i, j, k such that $x = s_{ijk}/s_{12}$.

(b) Triple collinear limit between final-state partons i, j and initial-state parton 1, such that $x = s_{1ij}/s_{12}$.
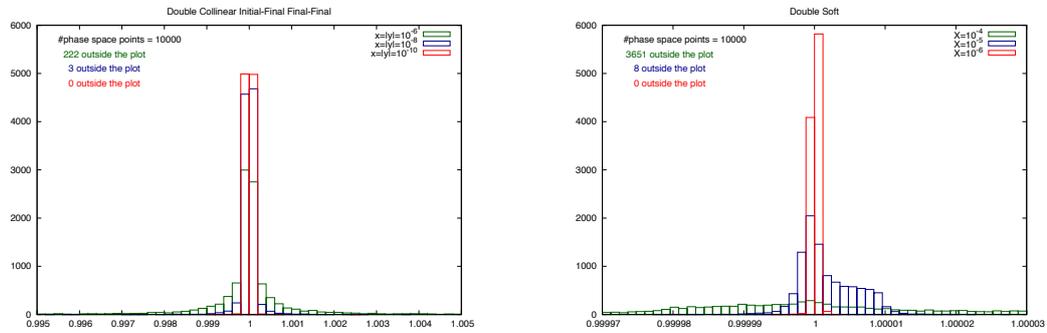

(c) Double collinear limit between final-state partons i, j and the initial-final pair $1, k$ such that $x = s_{ij}/s_{12}$, $y = s_{1k}/s_{12}$

(d) Double soft limit for soft partons i, j such that $x = (s_{12} - s_{ij})/s_{12}$.

Figure 5.1: Plots displaying the convergence of the subtraction term to the physical matrix element in various unresolved limits. The green data is furthest from the singular configuration with the blue data closer to the singular region and the red data the closest.

calculated for another 10,000 points. The procedure is repeated once more for a set of points even closer to the singular point and the histogram of ratios for the three sets of constraints plotted.

The selection of plots from four different unresolved configurations are shown in figure 5.1. In each plot it is shown that as the unresolved singular limit is approached, the distribution of ratios becomes more sharply peaked around one. This provides
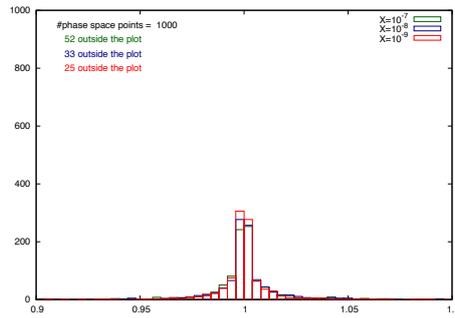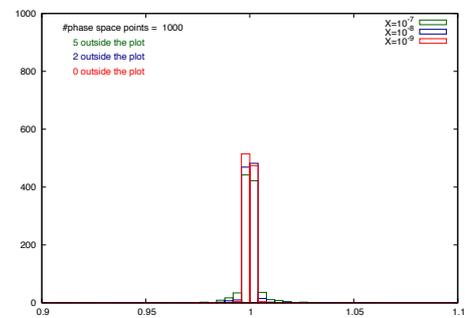
(a) Final-final gluon-gluon collinear limit for the process $gg \to gggg$.
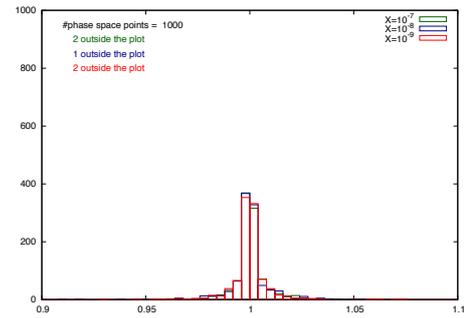
(b) Final-final gluon-gluon collinear limit for the process $q\bar{q} \to gggg$.
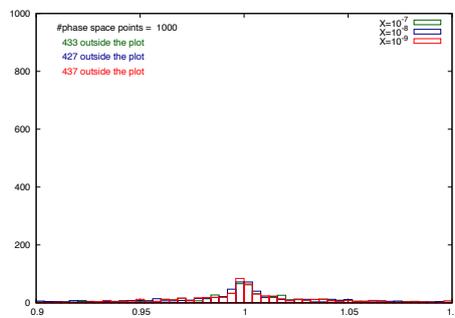
(c) Initial-final gluon-gluon collinear limit for the process $gg \to gggg$.

(d) Initial-final quark-gluon collinear limit for the process $q\bar{q} \to gggg$.

Figure 5.2: Distributions of R without azimuthal angular rotations for single collinear limits of the processes $gg \to gggg$ and $q\bar{q} \to gggg$.

statistical evidence for the convergence of the subtraction term to the physical cross section in the IR divergent limits.

Testing the subtraction term in this way also gives a clear demonstration of the issue of the presence of azimuthal correlations in the single collinear limits. The origin and solution to this problem have been discussed in section 1.3.2, where it was seen that the azimuthal correlations which spoil the subtraction in the single collinear limit arise from splitting functions where a parent gluon splits into two daughter gluons or a quark-anti-quark pair (and the various crossings of this configuration to include initial-state partons). The process $q\bar{q} \to gggg$ contains the

same final state as the process $gg \to gggg$, the antenna subtraction for which has been previously calculated [114]. Therefore by turning off the angular rotations when computing the ratio R, both subtraction terms should display similar behaviour when testing the single collinear limit between two final-state partons. This is seen in figure 5.2 (a) and (b), where it is seen that the subtraction terms for both processes display a broad peak, characteristic of the presence of uncompensated angular terms. An interesting comparison is between the two subtraction terms in the initial-final collinear limit. From the discussions in 1.3.2, it is expected that whilst the collinear limit between an initial-state gluon and a final-state gluon will display azimuthal correlations, the collinear limit between a quark and a gluon will not. This is clearly demonstrated by the plots in figure 5.2 (c) and (d). It is found that the limit involving the initial-state quark is sharply peaked without the need for angular rotations, whereas the corresponding limit in the purely gluonic process displays a broad peak due to azimuthal correlations.

5.3.2 Construction of the real-virtual subtraction term

At leading colour, the real-virtual contribution to the $q\bar{q} \to ggg$ process is given by,

$$
\begin{aligned}
\mathrm{d}\hat{\sigma}_{NNLO}^{RV} &= \mathcal{N}_5^1 \int \mathrm{d}\Phi_3(p_3, \ldots, p_5; \bar{p}_1, \bar{p}_2) \frac{1}{3!} \frac{\mathrm{d}x_1}{x_1} \frac{\mathrm{d}x_2}{x_2} \\
&\times \sum_{P(i,j,k)} M_5^1(\hat{1}_q, i_g, j_g, k_g, \hat{2}_{\bar{q}}) \, J_2^{(3)}(p_3, \ldots, p_5).
\end{aligned}
\tag{5.26}
$$

where the overall factor can be derived from (5.2),

$$
\mathcal{N}_5^1 = \mathcal{N}_{LO} \left(\frac{\alpha_s N}{2\pi} \right)^2 \frac{\bar{C}^2}{C}.
\tag{5.27}
$$

The subtraction term has contributions from the real-virtual subtraction term $\mathrm{d}\hat{\sigma}_{NNLO}^{VS}$, the singly integrated double real subtraction term $\int_1 \mathrm{d}\hat{\sigma}_{NNLO}^{S,1}$ and the mass factorization term $\mathrm{d}\hat{\sigma}_{NNLO}^{MF,RV}$,

$$
\mathrm{d}\hat{\sigma}_{NNLO}^{T} = \mathrm{d}\hat{\sigma}_{NNLO}^{VS} - \int_1 \mathrm{d}\hat{\sigma}_{NNLO}^{S,1} - \mathrm{d}\hat{\sigma}_{NNLO}^{MF,1}.
\tag{5.28}
$$

Following the discussion in section 2.6, the various contributions to the real-virtual subtraction term can be efficiently organised in terms of integrated antenna strings,

$$
\mathrm{d}\hat{\sigma}_{q\bar{q}}^{T} = \mathcal{N}_5^1 \int \mathrm{d}\Phi_3(p_3, \ldots, p_5; \bar{p}_1, \bar{p}_2) \frac{1}{3!} \frac{\mathrm{d}x_1}{x_1} \frac{\mathrm{d}x_2}{x_2} \sum_{P(i,j,k)} \Bigg\{
$$

$$
\begin{aligned}
-\ & \boldsymbol{J}_5^{(1)}(\hat{\bar{1}}_q, i_g, j_g, k_g, \hat{\bar{2}}_{\bar{q}})\ M_5^0(\hat{\bar{1}}_q, i_g, j_g, k_g, \hat{\bar{2}}_{\bar{q}})\ J_2^{(3)}(p_i, p_j, p_k) \\
+\ & d_3^0(\hat{\bar{1}}_q, i_g, j_g)\Bigg[M_4^1(\hat{\bar{\bar{1}}}_q, \widetilde{(ij)}_g, k_g, \hat{\bar{2}}_{\bar{q}})\delta_1\delta_2 \\
& \quad +\ \boldsymbol{J}_4^{(1)}(\hat{\bar{\bar{1}}}_q, \widetilde{(ij)}_g, k_g, \hat{\bar{2}}_{\bar{q}})\ M_4^0(\hat{\bar{\bar{1}}}_q, \widetilde{(ij)}_g, k_g, \hat{\bar{2}}_{\bar{q}}) \Bigg]\ J_2^{(2)}(p_{\widetilde{ij}}, p_k) \\
+\ & f_3^0(i_g, j_g, k_g)\Bigg[M_4^1(\hat{\bar{1}}_q, \widetilde{(ij)}_g, \widetilde{(jk)}_g, \hat{\bar{2}}_{\bar{q}})\delta_1\delta_2 \\
& \quad +\ \boldsymbol{J}_4^{(1)}(\hat{\bar{1}}_q, \widetilde{(ij)}_g, \widetilde{(jk)}_g, \hat{\bar{2}}_{\bar{q}})\ M_4^0(\hat{\bar{1}}_q, \widetilde{(ij)}_g, \widetilde{(jk)}_g, \hat{\bar{2}}_{\bar{q}}) \Bigg]\ J_2^{(2)}(p_{\widetilde{ij}}, p_{\widetilde{jk}}) \\
+\ & d_3^0(\hat{\bar{2}}_{\bar{q}}, k_g, j_g)\Bigg[M_4^1(\hat{\bar{1}}_q, i_g, \widetilde{(kj)}_g, \hat{\bar{\bar{2}}}_{\bar{q}})\delta_1\delta_2 \\
& \quad +\ \boldsymbol{J}_4^{(1)}(\hat{\bar{1}}_q, i_g, \widetilde{(kj)}_g, \hat{\bar{\bar{2}}}_{\bar{q}})\ M_4^0(\hat{\bar{1}}_q, i_g, \widetilde{(kj)}_g, \hat{\bar{\bar{2}}}_{\bar{q}}) \Bigg]\ J_2^{(2)}(p_i, p_{\widetilde{jk}}) \\
+\ & \Bigg[d_3^1(\hat{\bar{1}}_g, i_g, j_g)\delta_1\delta_2 + \bar{\boldsymbol{J}}_3^1(\hat{\bar{1}}_g, i_g, j_g)\ d_3^0(\hat{\bar{1}}_g, i_g, j_g) \Bigg] \\
& \quad \times\ M_4^0(\hat{\bar{\bar{1}}}_q, \widetilde{(ij)}_g, k_g, \hat{\bar{2}}_{\bar{q}})\ J_2^{(2)}(p_{\widetilde{ij}}, p_k) \\
+\ & \Bigg[f_3^1(i_g, j_g, k_g)\delta_1\delta_2 + \bar{\boldsymbol{J}}_3^{(1)}(i_g, j_g, k_g)\ f_3^0(i_g, j_g, k_g) \Bigg] \\
& \quad \times\ M_4^0(\hat{\bar{1}}_q, \widetilde{(ij)}_g, \widetilde{(jk)}_g, \hat{\bar{2}}_{\bar{q}})\ J_2^{(2)}(p_{\widetilde{ij}}, p_{\widetilde{jk}}) \\
+\ & \Bigg[d_3^1(\hat{\bar{2}}_{\bar{q}}, k_g, j_g)\delta_1\delta_2 + \bar{\boldsymbol{J}}_3^{(1)}(\hat{\bar{1}}_q, i_g, \widetilde{(kj)}_g, \hat{\bar{\bar{2}}}_{\bar{q}})\ d_3^0(\hat{\bar{2}}_{\bar{q}}, k_g, j_g) \Bigg] \\
& \quad \times\ M_4^0(\hat{\bar{1}}_q, i_g, \widetilde{(kj)}_g, \hat{\bar{\bar{2}}}_{\bar{q}})\ J_2^{(2)}(p_i, p_{\widetilde{jk}}) \\
-\ & \Bigg[\tilde{A}_3^1(\hat{\bar{1}}, i, \hat{\bar{2}}) + \widetilde{\boldsymbol{J}}_3^{(1)}(\hat{\bar{1}}_q, i_g, \hat{\bar{2}}_{\bar{q}})\ A_3^0(\hat{\bar{1}}, i, \hat{\bar{2}}) \Bigg]\ M_4^0(\hat{\bar{1}}_q, \tilde{j}_g, \tilde{k}_g, \hat{\bar{2}}_{\bar{q}})\ J_2^{(2)}(p_{\tilde{j}}, p_{\tilde{k}}) \\
+\ & b_0 \log\left(\frac{\mu^2}{|s_{1ij}|}\right) d_3^0(\hat{\bar{1}}_g, i_g, j_g)\delta_1\delta_2\ M_4^0(\hat{\bar{\bar{1}}}_q, \widetilde{(ij)}_g, k_g, \hat{\bar{2}}_{\bar{q}}) J_2^{(2)}(p_{\widetilde{ij}}, p_k) \\
+\ & b_0 \log\left(\frac{\mu^2}{s_{ijk}}\right) f_3^0(i_g, j_g, k_g)\delta_1\delta_2\ M_4^0(\hat{\bar{1}}_q, \widetilde{(ij)}_g, \widetilde{(jk)}_g, \hat{\bar{2}}_{\bar{q}}) J_2^{(2)}(p_{\widetilde{ij}}, p_{\widetilde{jk}}) \\
+\ & b_0 \log\left(\frac{\mu^2}{|s_{2kj}|}\right) d_3^0(\hat{\bar{2}}_{\bar{q}}, k_g, j_g)\delta_1\delta_2\ M_4^0(\hat{\bar{1}}_q, i_g, \widetilde{(jk)}_g, \hat{\bar{\bar{2}}}_{\bar{q}}) J_2^{(2)}(p_i, p_{\widetilde{jk}}) \\
+\ & \frac{1}{2}\Bigg[\frac{1}{2}\mathcal{D}_{3,q}^0(s_{\bar{\bar{1}}\widetilde{(ij)}}) - \frac{1}{2}\mathcal{D}_{3,q}^0(s_{\bar{1}j}) - \frac{1}{3}\mathcal{F}_3^0(s_{\widetilde{(ij)}k}) + \frac{1}{3}\mathcal{F}_3^0(s_{jk}) + \mathcal{A}_{3,q\bar{q}}^0(s_{\bar{1}\bar{2}}) - \mathcal{A}_{3,q\bar{q}}^0(s_{\bar{1}\bar{2}}) \\
& \quad +\delta_1\delta_2\Big(\mathcal{S}(s_{\widetilde{(ij)}k}, s_{jk}, x_{\widetilde{(ij)}k,jk}) - \mathcal{S}(s_{jk}, s_{jk}, 1) - \mathcal{S}(s_{\bar{\bar{1}}\widetilde{(ij)}}, s_{jk}, x_{\bar{\bar{1}}\widetilde{(ij)},jk}) \\
& \quad +\mathcal{S}(s_{\bar{1}j}, s_{jk}, x_{\bar{1}j,jk}) \Big) \Bigg]\ d_3^0(\hat{\bar{1}}_q, i_g, j_g)\ M_4^0(\hat{\bar{\bar{1}}}_q, \widetilde{(ij)}_g, k_g, \hat{\bar{2}}_{\bar{q}})\ J_2^{(2)}(p_{\widetilde{ij}}, p_k) \\
+\ & \frac{1}{2}\Bigg[-\frac{1}{2}\mathcal{D}_{3,q}^0(s_{\bar{1}\widetilde{(ij)}}) + \frac{1}{2}\mathcal{D}_{3,q}^0(s_{\bar{1}i}) - \frac{1}{2}\mathcal{D}_{3,q}^0(s_{\bar{2}\widetilde{(jk)}}) + \frac{1}{2}\mathcal{D}_{3,q}^0(s_{\bar{2}k}) + \frac{1}{3}\mathcal{F}_3^0(s_{\widetilde{(ij)}\widetilde{(jk)}}) \\
& \quad -\frac{1}{3}\mathcal{F}_3^0(s_{ik}) + \delta_1\delta_2\Big(-\mathcal{S}(s_{\widetilde{(ij)}\widetilde{(jk)}}, s_{ik}, x_{\widetilde{(ij)}\widetilde{(jk)},ik}) + \mathcal{S}(s_{ik}, s_{ik}, 1)
\end{aligned}
$$

$$+\mathcal{S}(s_{\bar{1}\widetilde{(ij)}},s_{ik},x_{\bar{1}\widetilde{(ij)},ik})-\mathcal{S}(s_{\bar{1}i},s_{ik},x_{\bar{1}i,ik})+\mathcal{S}(s_{\bar{2}\widetilde{(jk)}},s_{ik},x_{\bar{2}\widetilde{(jk)},ik})$$

$$-\mathcal{S}(s_{\bar{2}k},s_{ik},x_{\bar{2}k,ik})\Big)\Big]\ f_3^0(i_g,j_g,k_g)\ M_4^0(\hat{\bar{1}}_q,\widetilde{(ij)}_g,\widetilde{(jk)}_g,\hat{\bar{2}}_{\bar{q}})\ J_2^{(2)}(p_{\widetilde{ij}},p_{\widetilde{jk}})$$

$$+\ \frac{1}{2}\Big[\frac{1}{2}\mathcal{D}_{3,q}^0(s_{\bar{2}\widetilde{(jk)}})-\frac{1}{2}\mathcal{D}_{3,q}^0(s_{\bar{2}j})-\frac{1}{3}\mathcal{F}_3^0(s_{i\widetilde{(jk)}})+\frac{1}{3}\mathcal{F}_3^0(s_{ij})+\mathcal{A}_{3,q\bar{q}}^0(s_{\bar{1}\bar{2}})-\mathcal{A}_{3,q\bar{q}}^0(s_{\bar{1}\bar{2}})$$

$$+\delta_1\delta_2\Big(\mathcal{S}(s_{i\widetilde{(jk)}},s_{ij},x_{i\widetilde{(jk)},ij})-\mathcal{S}(s_{ij},s_{ij},1)$$

$$-\mathcal{S}(s_{\bar{2}\widetilde{(kj)}},s_{ij},x_{\bar{2}\widetilde{(kj)},ij})+\mathcal{S}(s_{\bar{2}j},s_{ij},x_{\bar{2}j,ij})\Big)\Big]$$

$$\times\ d_3^0(\hat{\bar{2}}_{\bar{q}},k_g,j_g)\ M_4^0(\hat{\bar{1}}_q,i_g,\widetilde{(kj)}_g,\hat{\bar{\bar{2}}}_{\bar{q}})\ J_2^{(2)}(p_i,p_{\widetilde{jk}})$$

$$+\ \frac{1}{2}\Big[-\mathcal{A}_{3,q\bar{q}}^0(s_{\bar{1}\bar{2}})+\mathcal{A}_{3,q\bar{q}}^0(s_{\bar{1}\bar{2}})+\frac{1}{2}\mathcal{D}_{3,q}^0(s_{\bar{1}\tilde{j}})-\frac{1}{2}\mathcal{D}_{3,q}^0(s_{\bar{1}j})+\frac{1}{2}\mathcal{D}_{3,q}^0(s_{\bar{2}\tilde{k}})$$

$$-\frac{1}{2}\mathcal{D}_{3,q}^0(s_{\bar{2}k})+\delta_1\delta_2\Big(\mathcal{S}(s_{\bar{\bar{1}}\bar{\bar{2}}},s_{\tilde{j}\tilde{k}},x_{\bar{\bar{1}}\bar{\bar{2}},\tilde{j}\tilde{k}})-\mathcal{S}(s_{\bar{1}\bar{2}},s_{jk},x_{\bar{1}\bar{2},jk})$$

$$-\mathcal{S}(s_{\bar{1}\tilde{j}},s_{\tilde{j}\tilde{k}},x_{\bar{1}\tilde{j},\tilde{j}\tilde{k}})+\mathcal{S}(s_{\bar{1}j},s_{jk},x_{\bar{1}j,jk})-\mathcal{S}(s_{\bar{2}\tilde{k}},s_{\tilde{j}\tilde{k}},x_{\bar{2}\tilde{k},\tilde{j}\tilde{k}})$$

$$+\mathcal{S}(s_{\bar{2}k},s_{jk},x_{\bar{2}k,jk})\Big)\Big]\ A_3^0(\hat{\bar{1}}_q,i_g,\hat{\bar{2}}_{\bar{q}})\ M_4^0(\hat{\bar{\bar{1}}}_q,\tilde{j}_g,\tilde{k}_g,\hat{\bar{2}}_{\bar{q}})\ J_2^{(2)}(p_{\tilde{j}},p_{\tilde{k}})\Big\} \tag{5.29}$$

After integration only those terms introduced at the real-virtual level are passed down to the double virtual subtraction term. Terms of the form $(\mathcal{D}_{3,q}^0\times A_3^0)$ and $(\mathcal{A}_{3,q\bar{q}}^0\times d_3^0)$ which were introduced at the real-virtual level, cancel. This means that the only terms containing the spurious initial-initial antennae to be passed down to the double virtual level are of the form $\tilde{A}_3^1$ and $(\mathcal{A}_{3,q\bar{q}}^0\times A_3^0)$. As demonstrated in the following section, these terms are combined with the integrated spurious four-parton antenna $\tilde{\mathcal{A}}_4^0$ in the double virtual subtraction term.

5.3.3 Construction of the double virtual subtraction term

Following the discussion in section 2.6.4 and the explicit examples in chapters 3 and 4, the double virtual subtraction term can be constructed from the remaining terms from the double real level, those terms introduced at the real-virtual level and the appropriate double virtual mass factorization contribution. The resultant double virtual subtraction term can be written in terms of single and double unresolved integrated antenna strings, fitting the structure already seen in chapters 3 and 4 for the simpler calculations presented there.

$$\mathrm{d}\hat{\sigma}_{q\bar{q}}^U\ =\ -\mathcal{N}_4^2\ \mathrm{d}\Phi_2(p_3,p_4;p_1,p_2)\ \frac{1}{2!}\sum_{\{i,j\}\in\{3,4\}}\Big\{$$

$$
\boldsymbol{J}_4^{(1)}(\hat{\bar{1}}_q, i_g, j_g, \hat{\bar{2}}_{\bar{q}}) \left(M_4^1(\hat{\bar{1}}_q, i_g, j_g, \hat{\bar{2}}_{\bar{q}}) - \frac{b_0}{\epsilon} M_4^1(\hat{\bar{1}}_q, i_g, j_g, \hat{\bar{2}}_{\bar{q}}) \right)
$$

$$
+ \quad \frac{1}{2} \, \boldsymbol{J}_4^{(1)}(\hat{\bar{1}}_q, i_g, j_g, \hat{\bar{2}}_{\bar{q}}) \otimes \boldsymbol{J}_4^{(1)}(\hat{\bar{1}}_q, i_g, j_g, \hat{\bar{2}}_{\bar{q}}) \, M_4^0(\hat{\bar{1}}_q, i_g, j_g, \hat{\bar{2}}_{\bar{q}})
$$

$$
+ \quad \boldsymbol{J}_4^{(2)}(\hat{\bar{1}}_q, i_g, j_g, \hat{\bar{2}}_{\bar{q}}) \, M_4^0(\hat{\bar{1}}_q, i_g, j_g, \hat{\bar{2}}_{\bar{q}}) \Bigg\} \, J_2^{(2)}(p_i, p_j). \tag{5.30}
$$

The explicit form of the single unresolved integrated antenna string can be derived from the strings listed in section B.1, whereas the form of the double unresolved integrated antenna string is listed in section B.2. The explicit poles of this subtraction term are expected to match those of the two-loop amplitude, thus rendering the leading colour NNLO correction to $q\,\bar{q} \to g\,g$ scattering finite at all stages of the calculation.

It is interesting to compare the form of the double virtual subtraction term for this calculation with the leading colour subtraction term for the $e^+e^- \to 3j$ antenna subtraction calculation [108]. Although the e^+e^- annihilation calculation involves only final-state partons, the integrated form of the subtraction terms is expected to closely follow the $q\bar{q} \to gg$ double virtual subtraction term up to mass factorization contributions. The double virtual subtraction term as presented in [108] can be reformulated in terms of final-state integrated antenna strings to fit the double virtual structure discussed in section 2.6,

$$
\mathrm{d}\hat{\sigma}^U \quad = \quad \mathcal{N} \, \mathrm{d}\Phi_3(p_1, p_2, p_3, q^2) \Bigg\{
$$

$$
\boldsymbol{J}_3^{(1)}(1_q, 3_g, 2_{\bar{q}}) \left(M_3^1(1_q, 3_g, 2_{\bar{q}}) - \frac{b_0}{\epsilon} M_3^0(1_q, 3_g, 2_{\bar{q}}) \right)
$$

$$
+ \quad \frac{1}{2} \, \boldsymbol{J}_3^{(1)}(1_q, 3_g, 2_{\bar{q}}) \otimes \boldsymbol{J}_3^{(1)}(1_q, 3_g, 2_{\bar{q}}) \, M_3^0(1_q, 3_g, 2_{\bar{q}})
$$

$$
+ \quad \boldsymbol{J}_3^{(2)}(1_q, 3_g, 2_{\bar{q}}) \, M_3^0(1_q, 3_g, 2_{\bar{q}}) \Bigg\} \, J_3^{(3)}(p_1, p_2, p_3). \tag{5.31}
$$

The single unresolved integrated antenna string is listed in section B.1. The double unresolved integrated antenna string for the relevant final-state partons is given by,

$$
\boldsymbol{J}_3^{(2)}(1_q, 3_g, 2_{\bar{q}}) \quad = \quad -\frac{1}{2}\mathcal{D}_4^0(s_{13}) + \frac{1}{2}\mathcal{D}_4^0(s_{23}) - \frac{1}{2}\tilde{\mathcal{A}}_4^0(s_{12})
$$

$$
+ \quad \frac{1}{2}\mathcal{D}_3^1(s_{13}) + \frac{1}{2}\mathcal{D}_3^1(s_{23}) - \tilde{\mathcal{A}}_3^1(s_{12})
$$

$$
+ \quad \frac{1}{2}\frac{b_0}{\epsilon}\mathcal{D}_3^0(s_{13}) + \frac{1}{2}\frac{b_0}{\epsilon}\mathcal{D}_3^0(s_{23}) - \frac{1}{4}\mathcal{D}_3^0(s_{13}) \otimes \mathcal{D}_3^0(s_{13})
$$

$$- \ \frac{1}{4} \mathcal{D}_3^0(s_{23}) \otimes \mathcal{D}_3^0(s_{23}) + \frac{1}{2} \mathcal{A}_3^0(s_{12}) \otimes \mathcal{A}_3^0(s_{12}). \tag{5.32}$$

The $\otimes$ symbol here just denotes trivial multiplication and the factor $\mathcal{N}$ carries all overall colour factors, QCD coupling and non-QCD factors. It is clear that similar combinations of integrated antennae occur in the double unresolved integrated antenna string generated in the $q\bar{q} \to gg$ calculation. For future research it would be interesting to calculate the analogue of this process for hadronic initial states, the leading colour contribution to $q\bar{q} \to V + g$ and compare the double unresolved integrated antenna string for that calculation. In particular it remains an open question whether the double unresolved integrated antenna strings obey the same combination rules that the single unresolved integrated antenna strings obey, i.e. establishing whether or not the following equality holds,

$$\boldsymbol{J}_4^{(2)}(\hat{\bar{1}}_q, i_g, j_g, \hat{\bar{2}}_{\bar{q}}) \ = \ \boldsymbol{J}_2^{(2)}(\hat{\bar{1}}_q, i_g) + \boldsymbol{J}_2^{(2)}(i_g, j_g) + \boldsymbol{J}_2^{(2)}(j_g, \hat{\bar{2}}_{\bar{q}}). \tag{5.33}$$

In this equation the $\boldsymbol{J}_2^{(2)}(\hat{\bar{1}}_q, i_g)$ contains a suitable partition of the spurious initial-initial antennae in (5.32) and $\boldsymbol{J}_2^{(2)}(i_g, j_g)$ can be calculated from the NNLO leading colour correction to the process $H \to gg$.

Chapter 6

Discussion, Conclusions and Outlook

The research presented in this thesis aims to address two main issues in the field of precision QCD calculations: the extension of the antenna subtraction formalism to hadronic initial states including quark processes, and uncovering the general structure of NNLO calculations within the antenna framework.

The issue of introducing quarks to scattering processes with hadronic initial states presents the antenna subtraction formalism with both practical and theoretical challenges. One of the great advantages of the antenna approach to subtraction is its generality. The method is to a large degree independent of the specific calculation being performed, that information is instead held in the choice of antenna function used in a particular calculation.

When extending the method to include quarks, the appropriate substitution of antenna functions is often sufficient. A clear example of this is the double real subtraction term for the process $q\bar{q} \to gggg$ presented in chapter 5. The analogous process involving only gluons is the double real subtraction term for the process $gg \to gggg$ in the "X_6 topology" (where the initial-state gluons are colour adjacent); the antenna subtraction term for this process has been previously calculated and presented in [125]. Comparing the two subtraction terms, it is clear that many of the terms are related by a simple substitution of quarks for gluons in the antenna functions and matrix elements. For example, the initial-

final and initial-initial four-parton antennae undergo the following substitutions, $F_4^0(1,i,j,k) \to D_4^0(1,i,j,k)$, $F_4^0(1,i,2,k) \to \tilde{A}_4^0(1,i,k,2)$. The latter substitution is interesting as it demonstrates nicely that the spurious limits removed using the $\tilde{A}_4^0$ antenna are not specific to the D_4^0 antenna, but a result of the more general problem of unresolved gluons separated by an initial state parton. Such a configuration cannot occur in the physical matrix elements for either the quark initiated process or the X_6 topology of the gluonic process. This demonstrates that not only are the general properties of the physical cross section mimicked by the antenna formalism, but also the spurious behaviour of the antenna formalism is to a large degree process independent, with the specific form of the antenna used to remove any spurious behaviour dictated by the process dependent information.

The comparison between gluonic and quark initiated subtraction terms also highlights a disadvantage of the antenna subtraction method at NNLO. For processes requiring quark-gluon or gluon-gluon four-parton antennae in either the final-final or initial-final configurations the singularity structure of the antenna does not exactly match the singularity structure of the physical matrix elements. The colour structure of the physical amplitudes used to define the quark-gluon and gluon-gluon antenna functions is a trace over adjoint colour indices. This colour structure will never match the colour structure (and thus IR singularities) of a particular string of partons in a physical matrix element due to the colour correlations between partons at either end of the antenna, not present in the physical matrix elements. In the case of the final-final antennae, the problem is solved by decomposing the antenna into sub-antennae which have singularity structures appropriate to the colour ordering of the physical matrix elements. The additional colour correlations in the initial-final antennae are taken care of by allowing a single antenna to provide the subtraction for several matrix elements with permuted gluon orderings. The remaining singularities associated with unphysical configurations are removed using initial-initial antennae, such as the $F_4^0(1,i,2,k)$ and $\tilde{A}_4^0(1,i,k,2)$ previously discussed.

Although the similarities between gluonic and quark subtraction terms highlight some interesting issues, the correspondence between the two is limited. The main problem when introducing quarks is the identity changing nature of many collinear

limits. Gluonic scattering processes only contain one flavour of parton whereas scattering processes involving quarks have to accommodate gluon-gluon, quark-gluon and quark-anti-quark collinear limits. The quark-antiquark collinear limits change the type of process being considered, with each quark-anti-quark collinear configuration reducing the number of quarks in the resulting configuration by two. The antenna subtraction method is well suited to accommodate such configurations through use of the E, G and H species of antenna functions which contain the appropriate limits.

The quark-gluon collinear limits are more problematic because although they do not change the overall partonic content of the process, the identity of an initial-state parton may change in such a limit. The issue of gluon initiated antennae involving quarks was discussed in detail in sections 2.5.1 and 2.6.1. At NLO, the issue of initial-state gluons has been tackled by partitioning the quark-gluon antennae into sub-antennae via partial fractioning, as described in [36]. This method has been demonstrated by explicit calculations in chapters 3 and 4 where use was made of the gluon initiated D_3^0 sub-antennae. In this thesis an alternative method for dealing with such configurations has been presented. Instead of decomposing the antennae into sub-antennae, the IR divergent limits are removed using a particular choice of full antenna functions, some of which belong to the initial-initial configuration. This method is equivalent to the sub-antenna approach at NLO but it less straightforward so has not been used for the practical calculations presented here.

Where the new method is applicable is at NNLO for double unresolved configurations involving initial-state gluons and final-state quarks. The sub-antenna approach to this problem has not been fully developed and may require additional master integrals to compute the integrated sub-antenna. Unlike the case for the decomposition of the final-final antennae into sub-antennae, where only the integral of the full antenna was required, the quark-gluon or gluon-quark sub-antennae contained within the initial-final D_4^0 antenna factor onto physically different matrix elements so the analytic integration of the sub-antennae themselves would be required. The alternative approach using full antennae, as outlined in 2.6.1, requires no additional integrals or decompositions to the ones already documented. The problematic

configurations occur in the quark-gluon and gluon-gluon initiated channels for two-quark four-gluon scattering and implementing the method described in section 2.6.1 is an important next step in the $pp \to 2j$ calculation. Although implemented for a different purpose, the method of using an initial-initial antenna to remove spurious singularities has been used before when removing the spurious limits of the initial-final F_4^0 and D_4^0 antennae. It is encouraging that this method has been shown to work in two different calculations, the details of which may provide useful guidance when implementing the method for initial-state gluons.

By resolving the remaining issues associated with unresolved configurations involving quarks, the method of antenna subtraction at NNLO for hadronic collisions involving quarks is now at the same level of development as is the case for purely gluonic scattering. The double real, real-virtual and double virtual subtraction terms are currently under construction for the remaining partonic channels involving quarks contributing to dijet production at the LHC.

The other main aim of the research presented in this thesis is to understand the structures present in the double real, real-virtual and double virtual subtraction terms within the antenna subtraction method. At NLO the construction of the real subtraction term is straightforward and general subtraction terms have been defined for every possible colour-ordered string of partons involving initial-state or final-state partons. By considering the integrated form of these general subtraction terms and studying the form of the NLO mass factorization contributions, the concept of an integrated antenna string has been introduced. By systematically combining the mass factorization terms and the integrated antennae into an integrated antenna string free from initial-state collinear poles, the explicit IR poles of the virtual subtraction term can be cancelled against the explicit poles of the virtual contribution with ease.

The formulation of the virtual subtraction term using integrated antenna strings and tree-level matrix elements reflects Catani's one-loop factorization formula and there is a simple correspondence between the poles of the colour-ordered insertion operators and the integrated antenna strings. An interesting consequence of this correspondence is that with the structure of the calculation understood, the calcu-

lation can start with the virtual contribution rather than the more complicated real contribution. The poles of the virtual contribution are easily written in terms of integrated antenna strings. From the integrated antenna strings, the unintegrated subtraction term can be inferred and applied to the IR divergent real cross section. In addition to the integrated antenna strings containing the poles of the virtual amplitude, the IR finite identity changing integrated antenna strings can also be extracted from the form of the one-loop contribution. From the identity changing integrated antenna strings the unintegrated form of the subtraction term which removes identity changing initial-state collinear divergence from the real cross section can be inferred and implemented. It is clear that by understanding the general structure of the NLO calculation at both the real and virtual levels in terms of integrated antenna strings, the antenna subtraction method can be implemented using either the real or virtual contribution as the starting point.

At NNLO, the antenna structure of the calculation is more complicated due to the multiple unresolved limits and various colour correlations between unresolved partons. Nonetheless structures have been found which naturally extend the structures present in NLO calculations and correspond to the well known singularity structures of one- and two-loop matrix elements. The structure of the double real subtraction term, previously described in [32, 108, 125] has been reorganised so that it corresponds more closely to the structures seen in the real-virtual and double virtual subtraction terms. In this new form, it is clear where in the real-virtual or double virtual subtractions terms each block of terms in the double real is added back to after integration.

At the real-virtual level, the terms inherited from the double real after integration can in many instances be collected together with the appropriate mass factorization terms to form integrated antenna strings. Such strings are useful for removing the explicit poles of one-loop physical matrix elements, reduced matrix elements and antenna functions. Understanding the general structure of the real-virtual subtraction in terms of integrated antenna strings and other predictable structures allows, in principle, for the real-virtual subtraction term to be constructed without reference to the double real subtraction term and indeed can even inform the construction of

the double real subtraction term. The presence of spurious singularities in the double real subtraction term can alter the structure at the real-virtual level, as seen by the presence of the initial-initial A_3^0 and $\tilde{A}_3^1$ antennae in the real-virtual subtraction term in chapter 5. These terms, although not precisely fitting the general structure as laid out in section 2.6, modify the formulae in a systematic and predictable fashion.

By organising the double real and real-virtual subtraction terms as described in section 2.6 the structure of the terms passed down to the double virtual subtraction term is evident. In particular, some consideration has been given to the best way to incorporate the double virtual mass factorization contribution and combine it with the various integrated antenna functions. A formulation of the double virtual subtraction term has been presented which systematically combines the mass factorization kernels and integrated antenna functions into integrated antenna strings containing explicit poles but free from initial-state collinear poles. This is achieved by defining a double unresolved integrated antenna string , $\boldsymbol{J}_n^{(2)}$, in addition to the previously defined single unresolved integrated antenna string, $\boldsymbol{J}_n^{(1)}$. The final formulation of the double virtual subtraction term reflects the structure of Catani's two loop factorization formula.

The results and discussion of chapter 5 suggest that the double unresolved integrated antenna strings may be constructed along the same lines as the single unresolved integrated antenna string, using knowledge of the colour ordering of the two-loop matrix element and the known general structure of $\boldsymbol{J}_n^{(2)}$. If so, the antenna subtraction formalism would allow the IR poles of the double virtual contribution to be straightforwardly written in terms of integrated antenna functions which have a direct analogue as subtraction terms in the double real and real-virtual calculations. The gain from this approach is that double real corrections generally involve a large number of permutations of gluons and complicated cross-cancellations between orderings. If the overall subtraction term were predictable from the virtual contribution, less time and effort would have to be paid in the construction of the double real subtraction term.

This approach may be particularly useful when dealing with sub-leading colour

contributions to the double real cross section. For relatively large numbers of partons it becomes difficult to rewrite the sub-leading colour contributions in terms of squared matrix elements with well understood factorization properties. In these cases if the form of the double real subtraction term could be inferred from the real virtual and double virtual subtraction terms then a successful double real subtraction term may be constructed without having to reformulate the sub-leading colour matrix elements into a useful form.

Further insights into the general structure of NNLO calculations within the antenna subtraction framework will come from performing additional calculations for the remaining dijet production channels, at leading and sub-leading colour, as well as the complementary V+jet and H+jet calculations currently under construction. It is anticipated that in addition to the value of the explicit calculations presented here, the techniques and structures devised during the course of research for this thesis will accelerate the completion of the remaining calculations and provide a greater understanding of precision QCD.

Appendix A

Collinear splitting kernels

A.1 Tree-level splitting kernels

The splitting kernels present in the definition of the mass factorisation terms (2.138), (2.195) and (2.207) contain colour factors which can distribute the colour ordered splitting kernels across multiple orders in the colour decomposition. In a similar fashion to the definition of b_0 and $b_{0,F}$ as the N and N_F proportional terms in the first coefficient of the QCD β-function, the colour ordered splitting kernels can be decomposed into different colour structures. The tree-level splitting kernels may be decomposed into a number of different colour structures.

The C_F, C_A, N_F decomposition

Following a decomposition in the Casimir operators C_A, C_F as well as T_R, N_F [19],

$$
\begin{aligned}
\boldsymbol{P}_{qq}^{(0)}(x) &= C_F \, \bar{p}_{qq}^{(0)}(x), \\
\boldsymbol{P}_{qg}^{(0)}(x) &= T_R \, \bar{p}_{qg}^{(0)}(x), \\
\boldsymbol{P}_{gq}^{(0)}(x) &= C_F \, \bar{p}_{gq}^{(0)}(x), \\
\boldsymbol{P}_{gg}^{(0)}(x) &= C_A \, \bar{p}_{gg}^{(0)}(x) + N_F \, \bar{p}_{gg,F}^{(0)}(x),
\end{aligned}
\tag{A.1}
$$

In this decomposition the colour ordered splitting kernels are given by [36],

$$
\bar{p}_{qq}^{(0)}(x) = 2\mathcal{D}_0(x) - 1 - x + \frac{3}{2}\delta(1-x),
$$

$$
\bar{p}_{qg}^{(0)}(x) = 1 - 2x + 2x^2,
$$

226

$$\bar{p}_{gq}^{(0)}(x) = \frac{2}{x} - 2 + x,$$

$$\bar{p}_{gg}^{(0)}(x) = 2\mathcal{D}_0(x) + \frac{2}{x} - 4 + 2x - 2x^2 + b_0\delta(1-x),$$

$$\bar{p}_{gg,F}^{(0)}(x) = b_{0,F}\delta(1-x), \tag{A.2}$$

where the distributions $\mathcal{D}_n(x)$ are defined in terms of plus-distributions,

$$\mathcal{D}_n(x) = \left(\frac{\ln^n(1-x)}{1-x}\right)_+. \tag{A.3}$$

The mass factorisation kernels are classified using a similar notation to the splitting kernels and are decomposed into the appropriate colour structures accordingly,

$$\Gamma_{qq}^1(x) = C_F\,\bar{\Gamma}_{qq}^1(x),$$

$$\Gamma_{qg}^1(x) = T_R\,\bar{\Gamma}_{qg}^1(x),$$

$$\Gamma_{gq}^1(x) = C_F\,\bar{\Gamma}_{gq}^1(x),$$

$$\Gamma_{gg}^1(x) = C_A\,\bar{\Gamma}_{gg}^1(x) + N_F\,\bar{\Gamma}_{gg,F}^1(x), \tag{A.4}$$

where the mass factorization kernels in the $\overline{\text{MS}}$ scheme are related to the splitting kernels by [47],

$$\Gamma_{ij}^1(x) = -\frac{1}{\epsilon}P_{ij}^{(0)}(x) \tag{A.5}$$

The N, N_F decomposition

An alternative decomposition is in the colour factors N and N_F. Expanding the splitting kernels into this set of colour factors defines a new set of colour ordered splitting kernels,

$$P_{qq}^{(0)}(x) = \left(\frac{N^2-1}{N}\right)p_{qq}^{(0)}(x),$$

$$P_{qg}^{(0)}(x) = p_{qg}^{(0)}(x),$$

$$P_{gq}^{(0)}(x) = \left(\frac{N^2-1}{N}\right)p_{gq}^{(0)}(x),$$

$$P_{gg}^{(0)}(x) = N\,p_{gg}^{(0)}(x) + N_F\,p_{gg,F}^{(0)}(x). \tag{A.6}$$

Decomposing the mass factorisation kernels in the same colour factors yields,

$$\Gamma_{qq}^1(x) = \left(\frac{N^2-1}{N}\right)\Gamma_{qq}^1(x),$$

$$
\begin{aligned}
\mathbf{\Gamma}_{qg}^1(x) &= \Gamma_{qg}^1(x), \\
\mathbf{\Gamma}_{gq}^1(x) &= \left(\frac{N^2-1}{N}\right)\Gamma_{gq}^1(x), \\
\mathbf{\Gamma}_{gg}^1(x) &= N\,\Gamma_{gg}^1(x) + N_F\,\Gamma_{gg,F}^1(x).
\end{aligned}
\tag{A.7}
$$

The splitting kernels in the N, N_F expansion are related to those defined in (A.2) via the relations:

$$
\begin{aligned}
p_{qq}^{(0)}(x) &= \frac{1}{2}\bar{p}_{qq}^{(0)}(x), \\
p_{qg}^{(0)}(x) &= \frac{1}{2}\bar{p}_{qg}^{(0)}(x) \\
p_{gq}^{(0)}(x) &= \frac{1}{2}\bar{p}_{gq}^{(0)}(x) \\
p_{gg}^{(0)}(x) &= \bar{p}_{gg}^{(0)}(x) \\
p_{gg,F}^{(0)}(x) &= \bar{p}_{gg,F}^{(0)}(x)
\end{aligned}
$$

$$\tag{A.8}$$

with the mass factorisation kernels in each expansion obeying equivalent relations.

A.2 One-loop splitting kernels

At NLO the $\boldsymbol{P}_{q_iq_j}^{(1)}$ and $\boldsymbol{P}_{q_i\bar{q}_j}^{(1)}$ splitting kernels contain non-trivial flavour structure and are classified according to flavour singlet, $\boldsymbol{P}^{S(1)}$, and flavour non-singlet, $\boldsymbol{P}^{V(1)}$ contributions [19].

$$
\begin{aligned}
\boldsymbol{P}_{q_iq_j}^{(1)} &= \delta_{ij}\boldsymbol{P}_{qq}^{V(1)} + \boldsymbol{P}_{qq}^{S(1)}, \\
\boldsymbol{P}_{q_i\bar{q}_j}^{(1)} &= \delta_{ij}\boldsymbol{P}_{q\bar{q}}^{V(1)} + \boldsymbol{P}_{q\bar{q}}^{S(1)},
\end{aligned}
\tag{A.9}
$$

where $\boldsymbol{P}_{q\bar{q}}^{S(1)} = \boldsymbol{P}_{qq}^{S(1)}$. The one-loop splitting kernels contain several colour structures and can be decomposed in a similar fashion to the leading-order splitting kernels.

The C_F, C_A, N_F decomposition

$$
\begin{aligned}
\boldsymbol{P}_{qq}^{V(1)} &= C_F^2\,\bar{p}_{qq,a}^{V(1)} + C_FC_A\,\bar{p}_{qq,b}^{V(1)} + C_FN_FT_R\,\bar{p}_{qq,c}^{V(1)}, \\
\boldsymbol{P}_{q\bar{q}}^{V(1)} &= C_F\left(C_F - \frac{C_A}{2}\right)\bar{p}_{q\bar{q}}^{V(1)},
\end{aligned}
$$

$$
\begin{aligned}
\boldsymbol{P}_{qq}^{S(1)} &= C_F \; \bar{p}_{qq}^{S(1)}, \\
\boldsymbol{P}_{qg}^{(1)} &= C_F T_R \; \bar{p}_{qg,a}^{(1)} + C_A T_R \; \bar{p}_{qg,b}^{(1)}, \\
\boldsymbol{P}_{gq}^{(1)} &= C_F^2 \; \bar{p}_{gq,a}^{(1)} + C_F C_A \; \bar{p}_{gq,b}^{(1)} + C_F N_F T_R \; \bar{p}_{gq,c}^{(1)}, \\
\boldsymbol{P}_{gg}^{(1)} &= C_A^2 \; \bar{p}_{gg,a}^{(1)} + C_A N_F T_R \; \bar{p}_{gg,b}^{(1)} + C_F N_F T_R \; \bar{p}_{gg,c}^{(1)}, & \text{(A.10)}
\end{aligned}
$$

where the explicit forms of the one-loop splitting kernels are documented in [19, 128, 129].

For the purposes of the DGLAP evolution, the parton distributions are decomposed into a flavour basis of non-singlet f_n and singlet f_s combinations. The flavour asymmetry distributions are given by,

$$
f_{n,ij}^{\pm} = (f_i \pm \bar{f}_i) - (f_j \pm \bar{f}_j). \tag{A.11}
$$

The total valence distribution is given by,

$$
f_n^v = \sum_{i=1}^{N_F} (f_i - \bar{f}_i), \tag{A.12}
$$

and the singlet distribution, which mixes with the gluon distribution during DGLAP evolution, is given by,

$$
f_s = \sum_{i=1}^{N_F} (f_i + \bar{f}_i). \tag{A.13}
$$

Each distribution is respectively evolved between momentum scales using their corresponding DGALP evolution kernels, $\boldsymbol{P}_n^{\pm}$, $\boldsymbol{P}_n^v$ and $\boldsymbol{P}_s$. These kernels are related to the splitting kernels which appear in fixed order calculations in the following way,

$$
\begin{aligned}
\boldsymbol{P}_n^{\pm} &= \boldsymbol{P}_{qq}^V \pm \boldsymbol{P}_{q\bar{q}}^V, \\
\boldsymbol{P}_n^v &= \boldsymbol{P}_{qq}^V - \boldsymbol{P}_{q\bar{q}}^V + N_F(\boldsymbol{P}_{qq}^S - \boldsymbol{P}_{qq}^S), \\
\boldsymbol{P}_s &= \boldsymbol{P}_{qq}^V + \boldsymbol{P}_{q\bar{q}}^V + N_F(\boldsymbol{P}_{qq}^S + \boldsymbol{P}_{q\bar{q}}^S). & \text{(A.14)}
\end{aligned}
$$

The singlet and non-singlet splitting kernels have the perturbative expansions,

$$
\begin{aligned}
\boldsymbol{P}_{qq}^V &= \boldsymbol{P}_{qq}^{(0)} + \left(\frac{\alpha_s}{2\pi}\right) \boldsymbol{P}_{qq}^{V(1)} + \mathcal{O}(\alpha_s^2), \\
\boldsymbol{P}_{q\bar{q}}^V &= \quad 0 \quad + \left(\frac{\alpha_s}{2\pi}\right) \boldsymbol{P}_{q\bar{q}}^{V(1)} + \mathcal{O}(\alpha_s^2),
\end{aligned}
$$

$$\boldsymbol{P}_{qq}^{S} = 0 + \left(\frac{\alpha_s}{2\pi}\right)\boldsymbol{P}_{qq}^{S(1)} + \mathcal{O}(\alpha_s^2),$$

$$\boldsymbol{P}_{q\bar{q}}^{S} = 0 + \left(\frac{\alpha_s}{2\pi}\right)\boldsymbol{P}_{q\bar{q}}^{S(1)} + \mathcal{O}(\alpha_s^2). \tag{A.15}$$

As previously mentioned, at one-loop order $\boldsymbol{P}_{qq}^{S(1)} = \boldsymbol{P}_{q\bar{q}}^{S(1)}$, which simplifies the one-loop DGLAP evolution kernels,

$$\boldsymbol{P}_n^{\pm(1)} = \boldsymbol{P}_{qq}^{V(1)} \pm \boldsymbol{P}_{q\bar{q}}^{V(1)},$$

$$\boldsymbol{P}_n^{v(1)} = \boldsymbol{P}_{qq}^{V(1)} - \boldsymbol{P}_{q\bar{q}}^{V(1)},$$

$$\boldsymbol{P}_s^{(1)} = \boldsymbol{P}_{qq}^{V(1)} + \boldsymbol{P}_{q\bar{q}}^{V(1)} + 2N_F \boldsymbol{P}_{qq}^{S(1)}. \tag{A.16}$$

Finally, a set of like-flavoured and unlike-flavoured quark-quark and quark-antiquark one-loop splitting kernels can be defined,

$$\boldsymbol{P}_{qq}^{(1)} = \boldsymbol{P}_{qq}^{V(1)} + \boldsymbol{P}_{qq}^{S(1)},$$

$$\boldsymbol{P}_{q\bar{q}}^{(1)} = \boldsymbol{P}_{q\bar{q}}^{V(1)} + \boldsymbol{P}_{qq}^{S(1)},$$

$$\boldsymbol{P}_{qQ}^{(1)} = \boldsymbol{P}_{qq}^{S(1)},$$

$$\boldsymbol{P}_{q\bar{Q}}^{(1)} = \boldsymbol{P}_{qq}^{S(1)}, \tag{A.17}$$

which have the following colour decompositions,

$$\boldsymbol{P}_{qq}^{(1)} = C_F\left[C_F\,\bar{p}_{qq,a}^{(1)} + C_A\,\bar{p}_{qq,b}^{(1)} + N_F T_R\,\bar{p}_{qq,c}^{(1)} + \bar{p}_{qq,d}^{(1)}\right], \tag{A.18}$$

$$\boldsymbol{P}_{q\bar{q}}^{(1)} = C_F\left[\left(C_F - \frac{C_A}{2}\right)\bar{p}_{q\bar{q},a}^{(1)} + \bar{p}_{q\bar{q},b}^{(1)}\right],$$

$$\boldsymbol{P}_{qQ}^{(1)} = C_F\,\bar{p}_{qQ}^{(1)},$$

$$\boldsymbol{P}_{q\bar{Q}}^{(1)} = C_F\,\bar{p}_{q\bar{Q}}^{(1)}, \tag{A.19}$$

where $\bar{p}_{qq,d}^{(1)} = \bar{p}_{q\bar{q},b}^{(1)} = \bar{p}_{qQ}^{(1)} = \bar{p}_{q\bar{Q}}^{(1)} = \bar{p}_{qq}^{S(1)}$ and $\boldsymbol{P}_{qq}^{S(1)} = C_F\,\bar{p}_{qq}^{S(1)}$. It is worth noting the simple colour structure of the singlet quark-quark (and quark-anti-quark) splitting kernel, it being simply an overall colour factor with no more complicated colour structures. This simplification can be traced back to the fact that the singlet splitting kernel is zero at $\mathcal{O}(\alpha_s^0)$, so the one-loop correction is actually the leading order contribution and only carries a single overall colour factor. A similar situation occurs for the non-singlet quark-anti-quark splitting function which only contains a

single overall colour structure which can be rewritten as,

$$C_F\left(C_F - \frac{C_A}{2}\right) = -\frac{C_F}{2C_A}. \tag{A.20}$$

This "leading order" overall colour structure can again be attributed to the fact that the conventional leading order contribution is zero for the quark-anti-quark splitting kernel.

Although the one-loop splitting kernels are a key ingredient for the NNLO mass factorisation contribution, it is the mass factorisation kernel $\mathbf{\Gamma}^2_{ba}(x)$ [46, 47], which enters explicitly into the formula (2.207) for the double virtual mass factorisation terms. This quantity may be decomposed into the appropriate colour structures accordingly,

$$
\begin{aligned}
\mathbf{\Gamma}^2_{qq} &= C_F\left[C_F\ \bar{\Gamma}^2_{qq,a} + C_A\ \bar{\Gamma}^2_{qq,b} + \bar{\Gamma}^2_{qq,c} + N_F\ \bar{\Gamma}^2_{qq,d}\right], \\
\mathbf{\Gamma}^2_{q\bar{q}} &= C_F\left[\bar{\Gamma}^2_{q\bar{q},a} + \left(C_F - \frac{C_F}{C_A}\right)\ \bar{\Gamma}^2_{q\bar{q},b}\right], \\
\mathbf{\Gamma}^2_{qQ} &= C_F\ \bar{\Gamma}^2_{qQ}, \\
\mathbf{\Gamma}^2_{q\bar{Q}} &= C_F\ \Gamma^2_{q\bar{Q}}, \\
\mathbf{\Gamma}^2_{qg} &= C_F\ \bar{\Gamma}^2_{qg,a} + C_A\ \bar{\Gamma}^2_{qg,b} + N_F\ \bar{\Gamma}^2_{qg,c}, \\
\mathbf{\Gamma}^2_{gq} &= C_F\left[C_F\ \bar{\Gamma}^2_{gq,a} + C_A\bar{\Gamma}^2_{gq,b} + N_F\bar{\Gamma}^2_{gq,c}\right], \\
\mathbf{\Gamma}^2_{gg} &= C_A^2\ \bar{\Gamma}^2_{gg,a} + C_A N_F\bar{\Gamma}^2_{gg,b} + C_F N_F\bar{\Gamma}^2_{gg,c} + N_F^2\bar{\Gamma}^2_{gg,d}, \tag{A.21}
\end{aligned}
$$

with the colour ordered mass factorisation kernels given by:

$$\bar{\Gamma}^2_{qq,a} = \frac{1}{2\epsilon^2}\left[\bar{p}^{(0)}_{qq} \otimes \bar{p}^{(0)}_{qq}\right] - \frac{1}{2\epsilon}\bar{p}^{(1)}_{qq,a},$$

$$\bar{\Gamma}^2_{qq,b} = \frac{b_0}{2\epsilon^2}\ \bar{p}^{(0)}_{qq} - \frac{1}{2\epsilon}\bar{p}^{(1)}_{qq,b},$$

$$\bar{\Gamma}^2_{qq,c} = \frac{1}{4\epsilon^2}\left[\bar{p}^{(0)}_{qg} \otimes \bar{p}^{(0)}_{gq}\right] - \frac{1}{2\epsilon}\bar{p}^{(1)}_{qq,d},$$

$$\bar{\Gamma}^2_{qq,d} = \frac{b_{0,F}}{2\epsilon^2}\ \bar{p}^0_{qq} - \frac{1}{4\epsilon}\bar{p}^{(1)}_{qq,c}. \tag{A.22}$$

$$\bar{\Gamma}^2_{q\bar{q},a} = \frac{1}{4\epsilon^2}\left[\bar{p}^{(0)}_{qg} \otimes \bar{p}^{(0)}_{gq}\right] - \frac{1}{2\epsilon}\bar{p}^{(1)}_{q\bar{q},b},$$

$$\bar{\Gamma}^2_{q\bar{q},b} = -\frac{1}{2\epsilon}\bar{p}^{(1)}_{q\bar{q},a}. \tag{A.23}$$

$$\bar{\Gamma}^2_{qQ} = \frac{1}{4\epsilon^2}\ \bar{p}^{(0)}_{qg} \otimes \bar{p}^{(0)}_{gq} - \frac{1}{2\epsilon}\bar{p}^{(1)}_{qQ}.$$

$$\bar{\Gamma}^2_{q\bar{Q}} = \frac{1}{4\epsilon^2}\ \bar{p}^{(0)}_{qg} \otimes \bar{p}^{(0)}_{gq} - \frac{1}{2\epsilon}\bar{p}^{(1)}_{q\bar{Q}}.$$

$$\bar{\Gamma}^2_{qg,a} = \frac{1}{4\epsilon^2} \left[\bar{p}^{(0)}_{qq} \otimes \bar{p}^{(0)}_{qg} \right] - \frac{1}{4\epsilon} \bar{p}^{(1)}_{qg,a},$$

$$\bar{\Gamma}^2_{qg,b} = \frac{1}{4\epsilon^2} \left[\left[\bar{p}^{(0)}_{qg} \otimes \bar{p}^{(0)}_{gg} \right] + b_0 \ \bar{p}^{(0)}_{qg} \right] - \frac{1}{4\epsilon} \bar{p}^{(1)}_{qg,b},$$

$$\bar{\Gamma}^2_{qg,c} = \frac{1}{4\epsilon^2} \left[\left[\bar{p}^{(0)}_{qg} \otimes \bar{p}^{(0)}_{gg,F} \right] + b_{0,F} \ \bar{p}^{(0)}_{qg} \right]. \tag{A.24}$$

$$\bar{\Gamma}^2_{gq,a} = \frac{1}{2\epsilon^2} \left[\bar{p}^{(0)}_{gq} \otimes \bar{p}^{(0)}_{qq} \right] - \frac{1}{2\epsilon} \bar{p}^{(1)}_{gq,a},$$

$$\bar{\Gamma}^2_{gq,b} = \frac{1}{2\epsilon^2} \left[\left[\bar{p}^{(0)}_{gg} \otimes \bar{p}^{(0)}_{gq} \right] + b_0 \ \bar{p}^{(0)}_{gq} \right] - \frac{1}{2\epsilon} \bar{p}^{(1)}_{gq,b},$$

$$\bar{\Gamma}^2_{gq,c} = \frac{1}{2\epsilon^2} \left[\left[\bar{p}^{(0)}_{gg,F} \otimes \bar{p}^{(0)}_{gq} \right] + b_{0,F} \ \bar{p}^{(0)}_{gq} \right] - \frac{1}{4\epsilon} \bar{p}^{(1)}_{gq,c}. \tag{A.25}$$

$$\bar{\Gamma}^2_{gg,a} = \frac{1}{2\epsilon^2} \left[\left[\bar{p}^{(0)}_{gg} \otimes \bar{p}^{(0)}_{gg} \right] + b_0 \ \bar{p}^{(0)}_{gg} \right] - \frac{1}{2\epsilon} \bar{p}^{(1)}_{gg,a},$$

$$\bar{\Gamma}^2_{gg,b} = \frac{1}{2\epsilon^2} \left[\left[\bar{p}^{(0)}_{gg} \otimes \bar{p}^{(0)}_{gg,F} + \bar{p}^{(0)}_{gg,F} \otimes \bar{p}^{(0)}_{gg} \right] + b_0 \ \bar{p}^{(0)}_{gg,F} + b_{0,F} \ \bar{p}^{(0)}_{gg} \right] - \frac{1}{4\epsilon} \bar{p}^{(1)}_{gq,b},$$

$$\bar{\Gamma}^2_{gg,c} = \frac{1}{4\epsilon^2} \left[\bar{p}^{(0)}_{gq} \otimes \bar{p}^{(0)}_{qg} \right] - \frac{1}{2\epsilon} \bar{p}^{(1)}_{gg,c},$$

$$\bar{\Gamma}^2_{gg,d} = \frac{1}{2\epsilon^2} \left[\left[\bar{p}^{(0)}_{gg,F} \otimes \bar{p}^{(0)}_{gg,F} \right] + b_{0,F} \ \bar{p}^{(0)}_{gg,F} \right]. \tag{A.26}$$

The N, N_F decomposition

As was done for the tree level splitting kernels it is possible to decompose the one-loop splitting kernels into the N, N_F colour factors:

$$\boldsymbol{P}^{(1)}_{qq} = \left(\frac{N^2 - 1}{N} \right) \left[N \ p^{(1)}_{qq} + \tilde{p}^{(1)}_{qq} + \frac{1}{N} \ \tilde{\tilde{p}}^{(1)}_{qq} + N_F \ p^{(1)}_{qq,F} \right],$$

$$\boldsymbol{P}^{(1)}_{q\bar{q}} = \left(\frac{N^2 - 1}{N} \right) \left[p^{(1)}_{q\bar{q}} + \frac{1}{N} \ \tilde{p}^{(1)}_{q\bar{q}} \right],$$

$$\boldsymbol{P}^{(1)}_{qQ} = \left(\frac{N^2 - 1}{N} \right) p^{(1)}_{qQ},$$

$$\boldsymbol{P}^{(1)}_{q\bar{Q}} = \left(\frac{N^2 - 1}{N} \right) p^{(1)}_{q\bar{Q}},$$

$$\boldsymbol{P}^{(1)}_{qg} = N \ p^{(1)}_{qg} + \frac{1}{N} \ \tilde{p}^{(1)}_{qg},$$

$$\boldsymbol{P}^{(1)}_{gq} = \left(\frac{N^2 - 1}{N} \right) \left[N \ p^{(1)}_{gq} + \frac{1}{N} \ \tilde{p}^{(1)}_{gq} + N_F \ p^{(1)}_{gq,F} \right],$$

$$\boldsymbol{P}^{(1)}_{gg} = N^2 \ p^{(1)}_{gg} + N N_F \ p^{(1)}_{gg,F} + \frac{N_F}{N} \ \tilde{p}^{(1)}_{gg,F}, \tag{A.27}$$

The relations between the two sets of colour-ordered splitting kernels are obtained by comparing coefficients,

$$p_{qq}^{(1)} = \frac{1}{4}\bar{p}_{qq,a}^{(1)} + \frac{1}{2}\bar{p}_{qq,b}^{(1)},$$

$$\tilde{p}_{qq}^{(1)} = \frac{1}{2}\bar{p}_{qq,d}^{(1)},$$

$$\tilde{\tilde{p}}_{qq}^{(1)} = -\frac{1}{4}\bar{p}_{qq,a}^{(1)},$$

$$p_{qq,F}^{(1)} = \frac{1}{4}\bar{p}_{qq,c}^{(1)}. \tag{A.28}$$

$$p_{q\bar{q}}^{(1)} = \frac{1}{2}\bar{p}_{q\bar{q},b}^{(1)},$$

$$\tilde{p}_{q\bar{q}}^{(1)} = -\frac{1}{4}\bar{p}_{q\bar{q},a}^{(1)}. \tag{A.29}$$

$$p_{qQ}^{(1)} = \frac{1}{2}\bar{p}_{qQ}^{(1)}. \tag{A.30}$$

$$p_{q\bar{Q}}^{(1)} = \frac{1}{2}\bar{p}_{q\bar{Q}}^{(1)}. \tag{A.31}$$

$$p_{qg}^{(1)} = \frac{1}{4}\bar{p}_{qg,a}^{(1)} + \frac{1}{2}\bar{p}_{qg,b}^{(1)},$$

$$\tilde{p}_{qg}^{(1)} = -\frac{1}{2}\bar{p}_{qg,a}^{(1)}. \tag{A.32}$$

$$p_{gq}^{(1)} = \frac{1}{4}\bar{p}_{gq,a}^{(1)} + \frac{1}{2}\bar{p}_{gq,b}^{(1)},$$

$$\tilde{p}_{gq}^{(1)} = -\frac{1}{4}\bar{p}_{gq,a}^{(1)},$$

$$p_{gq,F}^{(1)} = \frac{1}{4}\bar{p}_{gq,c}^{(1)}. \tag{A.33}$$

$$p_{gg}^{(1)} = \bar{p}_{gg,a}^{(1)},$$

$$p_{gg,F}^{(1)} = \frac{1}{2}\bar{p}_{gg,b}^{(1)} + \frac{1}{4}\bar{p}_{gg,c}^{(1)},$$

$$\tilde{p}_{gg,F}^{(1)} = -\frac{1}{4}\bar{p}_{gg,c}^{(1)}. \tag{A.34}$$

Using this decomposition for the tree-level and one-loop splitting kernels, the mass factorisation kernels can be written in the form,

$$\mathbf{\Gamma}_{qq}^2 = \left(\frac{N^2-1}{N}\right)\left[N\,\Gamma_{qq}^2 + \tilde{\Gamma}_{qq}^2 + \frac{1}{N}\,\tilde{\tilde{\Gamma}}_{qq}^2 + N_F\,\Gamma_{qq,F}^2\right],$$

$$\mathbf{\Gamma}_{q\bar{q}}^2 = \left(\frac{N^2-1}{N}\right)\left[\Gamma_{q\bar{q}}^2 + \frac{1}{N}\tilde{\Gamma}_{q\bar{q}}^2\right],$$

$$\mathbf{\Gamma}_{qQ}^2 = \left(\frac{N^2-1}{N}\right)\Gamma_{qQ}^2,$$

$$\mathbf{\Gamma}_{q\bar{Q}}^2 = \left(\frac{N^2-1}{N}\right)\Gamma_{q\bar{Q}}^2,$$

$$\mathbf{\Gamma}^2_{qg} = N\,\Gamma^2_{qg} + \frac{1}{N}\tilde{\Gamma}^2_{qg} + N_F\,\Gamma^2_{qg,F},$$

$$\mathbf{\Gamma}^2_{gq} = \left(\frac{N^2-1}{N}\right)\left[N\,\Gamma^2_{gq} + \frac{1}{N}\tilde{\Gamma}^2_{gq} + N_F\,\Gamma^2_{gq,F}\right],$$

$$\mathbf{\Gamma}^2_{gg} = N^2\,\Gamma^2_{gg} + NN_F\,\Gamma^2_{gg,F} + \frac{N_F}{N}\,\tilde{\Gamma}^2_{gg,F} + N_F^2\,\Gamma^2_{gg,F^2}, \tag{A.35}$$

with the colour ordered mass factorisation kernels given by:

$$\Gamma^2_{qq} = \frac{1}{2\epsilon^2}\left[\left[p^{(0)}_{qq}\otimes p^{(0)}_{qq}\right] + b_0\,p^{(0)}_{qq}\right] - \frac{1}{2\epsilon}p^{(1)}_{qq},$$

$$\tilde{\Gamma}^2_{qq} = \frac{1}{2\epsilon^2}\left[p^{(0)}_{qg}\otimes p^{(0)}_{gq}\right] - \frac{1}{2\epsilon}\tilde{p}^{(1)}_{qq},$$

$$\tilde{\tilde{\Gamma}}^2_{qq} = -\frac{1}{2\epsilon^2}\left[p^{(0)}_{qq}\otimes p^{(0)}_{qq}\right] - \frac{1}{2\epsilon}\tilde{\tilde{p}}^{(1)}_{qq},$$

$$\Gamma^2_{qq,F} = \frac{1}{2\epsilon^2}b_{0,F}\,p^{(0)}_{qq} - \frac{1}{2\epsilon}p^{(1)}_{qq,F}. \tag{A.36}$$

$$\Gamma^2_{q\bar{q}} = \frac{1}{2\epsilon^2}\left[p^{(0)}_{qg}\otimes p^{(0)}_{gq}\right] - \frac{1}{2\epsilon}p^{(1)}_{q\bar{q}},$$

$$\tilde{\Gamma}^2_{q\bar{q}} = -\frac{1}{2\epsilon}\tilde{p}^{(1)}_{q\bar{q}}. \tag{A.37}$$

$$\Gamma^2_{qQ} = \frac{1}{2\epsilon^2}\left[p^{(0)}_{qg}\otimes p^{(0)}_{gq}\right] - \frac{1}{2\epsilon}p^{(1)}_{qQ}. \tag{A.38}$$

$$\Gamma^2_{q\bar{Q}} = \frac{1}{2\epsilon^2}\left[p^{(0)}_{qg}\otimes p^{(0)}_{gq}\right] - \frac{1}{2\epsilon}p^{(1)}_{q\bar{Q}}. \tag{A.39}$$

$$\Gamma^2_{qg} = \frac{1}{2\epsilon^2}\left[\left[p^{(0)}_{qg}\otimes p^{(0)}_{gg}\right] + \left[p^{(0)}_{qq}\otimes p^{(0)}_{qg}\right] + b_0\,p^{(0)}_{qg}\right] - \frac{1}{2\epsilon}p^{(1)}_{qg},$$

$$\tilde{\Gamma}^2_{qg} = -\frac{1}{2\epsilon^2}\left[p^{(0)}_{qq}\otimes p^{(0)}_{qg}\right] - \frac{1}{2\epsilon}\tilde{p}^{(1)}_{qg},$$

$$\Gamma^2_{qg,F} = \frac{1}{2\epsilon^2}\left[\left[p^{(0)}_{qg}\otimes p^{(0)}_{gg,F}\right] + b_{0,F}\,p^{(0)}_{qg}\right]. \tag{A.40}$$

$$\Gamma^2_{gq} = \frac{1}{2\epsilon^2}\left[\left[p^{(0)}_{gg}\otimes p^{(0)}_{gq} + p^{(0)}_{gq}\otimes p^{(0)}_{qq}\right] + b_0\,p^{(0)}_{gq}\right] - \frac{1}{2\epsilon}p^{(1)}_{gq},$$

$$\tilde{\Gamma}^2_{gq} = \frac{1}{2\epsilon^2}\left[p^{(0)}_{gq}\otimes p^{(0)}_{qq}\right] - \frac{1}{2\epsilon}\tilde{p}^{(1)}_{gq},$$

$$\Gamma^2_{gq,F} = \frac{1}{2\epsilon^2}\left[\left[p^{(0)}_{gg,F}\otimes p^{(0)}_{gq}\right] + b_{0,F}\,p^{(0)}_{gq}\right] - \frac{1}{2\epsilon}p^{(1)}_{gq,F}. \tag{A.41}$$

$$\Gamma^2_{gg} = \frac{1}{2\epsilon^2}\left[\left[p^{(0)}_{gg}\otimes p^{(0)}_{gg}\right] + b_0\,p^{(0)}_{gg}\right] - \frac{1}{2\epsilon}p^{(1)}_{gg},$$

$$\Gamma^2_{gg,F} = \frac{1}{2\epsilon^2}\left[2\left[p^{(0)}_{gg}\otimes p^{(0)}_{gg,F}\right] + \left[p^{(0)}_{gq}\otimes p^{(0)}_{qg}\right] + b_0\,p^{(0)}_{gg,F} + b_{0,F}\,p^{(0)}_{gg}\right] - \frac{1}{2\epsilon}p^{(1)}_{gg,F},$$

$$\tilde{\Gamma}^2_{gg,F} = -\frac{1}{2\epsilon^2}\left[p^{(0)}_{gq}\otimes p^{(0)}_{qg}\right] - \frac{1}{2\epsilon}\tilde{p}^{(1)}_{gg,F},$$

$$\Gamma^2_{gg,F^2} = \frac{1}{2\epsilon^2}\left[\left[p^{(0)}_{gg,F}\otimes p^{(0)}_{gg,F}\right] + b_{0,F}\,p^{(0)}_{gg,F}\right]. \tag{A.42}$$

Appendix B

Integrated antenna strings

In this chapter a number of explicit expressions for the relevant integrated antenna strings are collected for reference. In the initial-final and initial-initial configurations the following notation is employed: $\delta_1 = \delta(1 - x_1)$, $\delta_2 = \delta(1 - x_2)$.

B.1 Single unresolved integrated antenna strings

Final state strings:

$$
\begin{aligned}
\boldsymbol{J}_2^{(1)}(i_q, j_{\bar{q}}) &= \mathcal{A}_3^0(s_{ij}) \\
\boldsymbol{J}_3^{(1)}(i_q, j_g, k_{\bar{q}}) &= \frac{1}{2}\mathcal{D}_3^0(s_{ij}) + \frac{1}{2}\mathcal{D}_3^0(s_{jk}) \\
\boldsymbol{J}_n^{(1)}(a_q, i_g, j_g, \cdots, k_g, l_g, b_{\bar{q}}) &= \frac{1}{2}\mathcal{D}_3^0(s_{ai}) + \frac{1}{3}\mathcal{F}_3^0(s_{ij}) + \cdots + \frac{1}{3}\mathcal{F}_3^0(s_{kl}) + \frac{1}{2}\mathcal{D}_3^0(s_{lb}) \\
\boldsymbol{J}_n^{(1)}(i_g, j_g, \cdots, k_g, l_g) &= \frac{1}{3}\mathcal{F}_3^0(s_{ij}) + \cdots + \frac{1}{3}\mathcal{F}_3^0(s_{kl}) + \frac{1}{3}\mathcal{F}_3^0(s_{il}) \\
\boldsymbol{J}_{2,N_F}^{(1)}(i_g, j_g) &= \frac{1}{2}\mathcal{G}_3^0(s_{ij}) \\
\boldsymbol{J}_{2,N_F}^{(1)}(i_q, j_g) &= \frac{1}{2}\mathcal{E}_3^0(s_{ij}) \tag{B.1}
\end{aligned}
$$

Initial-final strings:

$$
\begin{aligned}
\boldsymbol{J}_2^{(1)}(\hat{\bar{1}}_g, i_g) &= \frac{1}{2}\mathcal{F}_{3,g}^0(s_{\bar{1}i}) - \frac{1}{2}\Gamma_{gg}^1\delta_2, \\
\boldsymbol{J}_{2,N_F}^{(1)}(\hat{\bar{1}}_g, i_g) &= \mathcal{G}_{3,g}^0(s_{\bar{1}i}), \\
\boldsymbol{J}_2^{(1)}(\hat{\bar{1}}_q, i_{\bar{q}}) &= \mathcal{A}_{3,q}^0(s_{\bar{1}i}) - \Gamma_{qq}^1\delta_2,
\end{aligned}
$$

$$\boldsymbol{J}_2^{(1)}(\hat{\bar{1}}_q, i_g) = \frac{1}{2}\mathcal{D}_{3,q}^0(s_{\bar{1}i}) - \Gamma_{qq}^1\delta_2,$$

$$\boldsymbol{J}_2^{(1)}(i_q, \hat{\bar{1}}_g) = \mathcal{D}_{3,g,gq}^0(s_{\bar{1}i}) - \frac{1}{2}\Gamma_{gg}^1\delta_2,$$

$$\boldsymbol{J}_{2,N_F}^{(1)}(\hat{\bar{1}}_q, i_g) = \frac{1}{2}\mathcal{E}_{3;q,q'\bar{q}'}^0(s_{\bar{1}i}),$$

$$\boldsymbol{J}_{2,N_F}^{(1)}(i_q, \hat{\bar{1}}_g) = -\Gamma_{gg,F}^1\delta_2,$$

$$\boldsymbol{J}_{2,g\to q}^{(1)}(\hat{\bar{1}}_q, i_{\bar{q}}) = \mathcal{A}_{3,g}^0(s_{\bar{1}i}) - \Gamma_{qg}^1\delta_2,$$

$$\boldsymbol{J}_{2,g\to q}^{(1)}(\hat{\bar{1}}_q, i_g) = \mathcal{D}_{3,g,qg}^0(s_{\bar{1}i}) - \Gamma_{qg}^1\delta_2,$$

$$\boldsymbol{J}_{2,q\to g}^{(1)}(i_q, \hat{\bar{1}}_g) = \mathcal{E}_{3;q,qq'}^0(s_{\bar{1}i}) - \Gamma_{gq}^1\delta_2,$$

$$\boldsymbol{J}_{2,q\to g}^{(1)}(i_g, \hat{\bar{1}}_g) = \mathcal{G}_{3,q}^0(s_{\bar{1}i}) - \Gamma_{gq}^1\delta_2 \tag{B.2}$$

Initial-initial strings:

$$\boldsymbol{J}_2^{(1)}(\hat{\bar{1}}_g, \hat{\bar{2}}_g) = \mathcal{F}_{3,gg}^0(s_{\bar{1}\bar{2}}) - \frac{1}{2}\Gamma_{gg}^1(x_1)\delta_2 - \frac{1}{2}\Gamma_{gg}^1(x_2)\delta_1,$$

$$\boldsymbol{J}_{2,N_F}^{(1)}(\hat{\bar{1}}_g, \hat{\bar{2}}_g) = -\Gamma_{gg,F}^1(x_1)\delta_2 - \Gamma_{gg,F}^1(x_2)\delta_1,$$

$$\boldsymbol{J}_2^{(1)}(\hat{\bar{1}}_q, \hat{\bar{2}}_{\bar{q}}) = \mathcal{A}_{3,q\bar{q}}^0(s_{\bar{1}\bar{2}}) - \Gamma_{qq}^1(x_1)\delta_2 - \Gamma_{qq}^1(x_2)\delta_1,$$

$$\boldsymbol{J}_2^{(1)}(\hat{\bar{1}}_q, \hat{\bar{2}}_g) = \mathcal{D}_{3,qg}^0(s_{\bar{1}\bar{2}}) - \Gamma_{qq}^1(x_1)\delta_2 - \frac{1}{2}\Gamma_{gg}^1(x_2)\delta_1,$$

$$\boldsymbol{J}_{2,g\to q}^{(1)}(\hat{\bar{1}}_q, \hat{\bar{2}}_{\bar{q}}) = \mathcal{A}_{3,qg}^0(s_{\bar{1}\bar{2}}) - \Gamma_{qg}^1(x_1)\delta_2,$$

$$\boldsymbol{J}_{2,g\to q}^{(1)}(\hat{\bar{1}}_q, \hat{\bar{2}}_g) = \mathcal{D}_{3,gg}^0(s_{\bar{1}\bar{2}}) - \Gamma_{qg}^1(x_1)\delta_2,$$

$$\boldsymbol{J}_{2,q\to g}^{(1)}(\hat{\bar{1}}_q, \hat{\bar{2}}_g) = \mathcal{E}_{3,qq'}^0(s_{\bar{1}\bar{2}}) - \Gamma_{gq}^1(x_2)\delta_1,$$

$$\boldsymbol{J}_{2,q\to g}^{(1)}(\hat{\bar{1}}_g, \hat{\bar{2}}_g) = \mathcal{G}_{3,gq}^0(s_{\bar{1}\bar{2}}) - \Gamma_{gq}^1(x_2)\delta_1 \tag{B.3}$$

B.2 Double unresolved integrated antenna strings

$$\boldsymbol{J}_2^{(2)}(\hat{\bar{1}}_q, \hat{\bar{2}}_{\bar{q}}) = \mathcal{A}_{4,q\bar{q}}^0(s_{\bar{1}\bar{2}}) + \mathcal{A}_{3,q\bar{q}}^1(s_{\bar{1}\bar{2}}) + \frac{b_0}{\epsilon}\mathcal{A}_{3,q\bar{q}}^0(s_{\bar{1}\bar{2}})\left(\frac{s_{\bar{1}\bar{2}}}{\mu^2}\right)^{-\epsilon}$$

$$- \frac{1}{2}\left[\mathcal{A}_{3,q\bar{q}}^0 \otimes \mathcal{A}_{3,q\bar{q}}^0\right](s_{\bar{1}\bar{2}}) - \Gamma_{qq}^2(z_1)\delta_2 - \Gamma_{qq}^2(z_2)\delta_1$$

$$+ \frac{1}{2}\left[\Gamma_{qq}^1 \otimes \Gamma_{qq}^1\right](z_1)\delta_2 + \frac{1}{2}\left[\Gamma_{qq}^1 \otimes \Gamma_{qq}^1\right](z_2)\delta_1,$$

$$\boldsymbol{J}_{2,N_F}^{(2)}(\hat{\bar{1}}_q, \hat{\bar{2}}_{\bar{q}}) = \mathcal{B}_{4,q\bar{q}}^0(s_{\bar{1}\bar{2}}) + \hat{\mathcal{A}}_{3,q\bar{q}}^1(s_{\bar{1}\bar{2}}) + \frac{b_{0,F}}{\epsilon}\,\mathcal{A}_{3,q\bar{q}}^0(s_{\bar{1}\bar{2}})\left(\frac{s_{\bar{1}\bar{2}}}{\mu^2}\right)^{-\epsilon}$$

$$+\Gamma_{qq,N_F}^2(z_1)\delta_2 + \Gamma_{qq,N_F}^2(z_2)\delta_1,$$

$$\widetilde{J}_2^{(2)}(\hat{\bar{1}}_q, \hat{\bar{2}}_{\bar{q}}) = \frac{1}{2}\widetilde{\mathcal{A}}_{4,q\bar{q}}^0(s_{\bar{1}\bar{2}}) - 2\mathcal{C}_{4,q\bar{q}}^0(s_{\bar{1}\bar{2}}) + \widetilde{\mathcal{A}}_{3,q\bar{q}}^1(s_{\bar{1}\bar{2}})$$

$$- \frac{1}{2}\big[\mathcal{A}_{3,q\bar{q}}^0 \otimes \mathcal{A}_{3,q\bar{q}}^0\big](s_{\bar{1}\bar{2}}) - \Gamma_{qq,1/N}^2(z_1)\delta_2 + \Gamma_{qq,1/N}^2(z_2)\delta_1$$

$$+ \frac{1}{2}\big[\Gamma_{qq}^1 \otimes \Gamma_{qq}^1\big](z_1)\delta_2 + \frac{1}{2}\big[\Gamma_{qq}^1 \otimes \Gamma_{qq}^1\big](z_2)\delta_1,$$

$$\boldsymbol{J}_{2,q\to g\to q}^{(2)}(\hat{\bar{1}}_q, \hat{\bar{2}}_{\bar{q}}) = \mathcal{B}_{4,q\bar{Q}}^0(s_{\bar{1}\bar{2}}) + \mathcal{B}_{4,\bar{Q}q}^0(s_{\bar{1}\bar{2}})$$

$$+ \big[\Gamma_{gq}^1 \otimes \Gamma_{qg}^1\big](z_2)\delta_1 + \big[\Gamma_{qg}^1 \otimes \Gamma_{qg}^1\big](z_2)\delta_1,$$

$$- \big[\Gamma_{gq}^1 \otimes \mathcal{A}_{3,qg}^0\big](s_{\bar{1}\bar{2}}) - \big[\Gamma_{gq}^1 \otimes \mathcal{A}_{3,gq}^0\big](s_{\bar{1}\bar{2}}),$$

$$\boldsymbol{J}_{2,g\to q}^{(2)}(\hat{\bar{1}}_q, \hat{\bar{2}}_{\bar{q}}) = \mathcal{A}_{4,qg}^{0,\text{adj}}(s_{\bar{1}\bar{2}}) + \mathcal{A}_{4,qg}^{0,\text{n.adj}}(s_{\bar{1}\bar{2}}) + \mathcal{A}_{3,qg}^1(s_{\bar{1}\bar{2}}) + \frac{b_0}{\epsilon}\mathcal{A}_{3,qg}^0(s_{\bar{1}\bar{2}})\left(\frac{s_{\bar{1}\bar{2}}}{\mu^2}\right)^{-\epsilon},$$

$$- \Gamma_{qg}^2(z_2) + \big[\Gamma_{gg}^1 \otimes \Gamma_{qg}^1\big](z_2) + \Gamma_{qq}^1(z_1)\Gamma_{qg}^1(z_2) - \big[\Gamma_{qq}^1 \otimes \Gamma_{qq}^1\big](z_2)$$

$$+ \big[\Gamma_{qq}^1 \otimes \mathcal{A}_{3,qg}^0\big](s_{\bar{1}\bar{2}}) - \big[\Gamma_{gg}^1 \otimes \mathcal{A}_{3,qg}^0\big](s_{\bar{1}\bar{2}}) - \big[\Gamma_{qg}^1 \otimes \mathcal{A}_{3,q\bar{q}}^0\big](s_{\bar{1}\bar{2}}),$$

$$\widetilde{J}_{2,g\to q}^{(2)}(\hat{\bar{1}}_q, \hat{\bar{2}}_{\bar{q}}) = \widetilde{\mathcal{A}}_{4,qg}^0(s_{\bar{1}\bar{2}}) + \widetilde{\mathcal{A}}_{3,qg}^1(s_{\bar{1}\bar{2}}) - \widetilde{\Gamma}_{qg}^2(z_2) - \big[\Gamma_{qg}^1 \otimes \Gamma_{qq}^1\big](z_2)$$

$$- \Gamma_{qq}^1(z_1)\Gamma_{qg}^1(z_2) + \big[\Gamma_{qq}^1 \otimes \mathcal{A}_{qg}^0\big](s_{\bar{1}\bar{2}}) + \big[\Gamma_{gg,F}^1 \otimes \mathcal{A}_{qg}^0\big](s_{\bar{1}\bar{2}})$$

$$+ \big[\Gamma_{qg}^1 \otimes \mathcal{A}_{q\bar{q}}^0\big](s_{\bar{1}\bar{2}}),$$

$$\boldsymbol{J}_{2,g\to q,g\to q}^{(2)}(\hat{\bar{1}}_q, \hat{\bar{2}}_{\bar{q}}) = 2\mathcal{A}_{4,gg}^0(s_{\bar{1}\bar{2}}) + \Gamma_{qg}^1(z_1)\Gamma_{qg}^1(z_2) - \big[\Gamma_{qg}^1 \otimes \mathcal{A}_{3,qg}^0(s_{\bar{1}\bar{2}}; z_2)\big](z_1)\delta_2$$

$$- \big[\Gamma_{qg}^1 \otimes \mathcal{A}_{3,gq}^0(s_{\bar{1}\bar{2}}; z_1)\big](z_2)\delta_1,$$

$$\boldsymbol{J}_{2,Q\to\bar{q}}^{(2)}(\hat{\bar{1}}_q, \hat{\bar{2}}_{\bar{q}}) = \mathcal{B}_{4,qQ}^0(s_{\bar{1}\bar{2}}) + \mathcal{B}_{4,Qq}^0(s_{\bar{1}\bar{2}}) - \Gamma_{q\bar{Q}}^2(z_2) - \big[\Gamma_{gq}^1 \otimes \Gamma_{qg}^1\big](z_2)\delta_1$$

$$+ \big[\Gamma_{gq}^1 \otimes \mathcal{A}_{3gq}^0(s_{\bar{1}\bar{2}}; z_2)\big](z_1) + \big[\Gamma_{gq}^1 \otimes \mathcal{A}_{3gq}^0(s_{\bar{1}\bar{2}}; z_1)\big](z_2),$$

$$\boldsymbol{J}_{2,q\to\bar{q}}^{(2)}(\hat{\bar{1}}_q, \hat{\bar{2}}_{\bar{q}}) = \mathcal{C}_{4,q\bar{q}}^0(s_{\bar{1}\bar{2}}) - \Gamma_{q\bar{q}}^2(z_2)$$

$$\widetilde{J}_{2,g\to q,g\to q}^{(2)}(\hat{\bar{1}}_q, \hat{\bar{2}}_{\bar{q}}) = \widetilde{\mathcal{A}}_4^0(s_{\bar{1}\bar{2}}) + \Gamma_{qg}^1(z_1)\Gamma_{qg}^1(z_2) - \big[\Gamma_{qg}^1 \otimes \mathcal{A}_{3,qg}^0(s_{\bar{1}\bar{2}}; z_2)\big](z_1)\delta_1,$$

$$- \big[\Gamma_{qg}^1 \otimes \mathcal{A}_{3,gq}^0(s_{\bar{1}\bar{2}}; z_1)\big](z_2)\delta_1,$$

$$\boldsymbol{J}_{2,g\to q,N_F}^{(2)}(\hat{\bar{1}}_q, \hat{\bar{2}}_{\bar{q}}) = \hat{\mathcal{A}}_{3,qg}^1(s_{\bar{1}\bar{2}}) + \frac{b_{0,F}}{\epsilon}\mathcal{A}_{3,qg}^0(s_{\bar{1}\bar{2}})\left(\frac{s_{\bar{1}\bar{2}}}{\mu^2}\right)^{-\epsilon}$$

$$- \Gamma_{qg,F}^2(z_2)\delta_1 + \big[\Gamma_{gg,F}^1 \otimes \Gamma_{qg}^1\big](z_2)\delta_1,$$

$$\boldsymbol{J}_2^{(2)}(\hat{\bar{1}}_g, \hat{\bar{2}}_g) = 2\mathcal{F}_{4,gg}^{0,\text{adj}}(s_{\bar{1}\bar{2}}) + \mathcal{F}_{4,gg}^{0,\text{n.adj}}(s_{\bar{1}\bar{2}}) + \mathcal{F}_{3,gg}^1(s_{\bar{1}\bar{2}}) + \frac{b_0}{\epsilon}\mathcal{F}_{3,gg}^0(s_{\bar{1}\bar{2}})\left(\frac{s_{\bar{1}\bar{2}}}{\mu^2}\right)^{-\epsilon}$$

$$- \Gamma_{gg}^2(z_1)\delta_2 - \Gamma_{gg}^2(z_2)\delta_1 - 2\big[\mathcal{F}_{3,gg}^0 \otimes \mathcal{F}_{3,gg}^0\big]$$

$$+ \frac{1}{2}\big[\Gamma_{gg}^1 \otimes \Gamma_{gg}^1\big](z_1)\delta_2 + \frac{1}{2}\big[\Gamma_{gg}^1 \otimes \Gamma_{gg}^1\big](z_2)\delta_1,$$

$$\boldsymbol{J}_{2,N_F}^{(2)}(\hat{\bar{1}}_g, \hat{\bar{2}}_g) = 2\mathcal{G}_{4,gg}^0(s_{\bar{1}\bar{2}}) + \hat{\mathcal{F}}_{3,gg}^1(s_{\bar{1}\bar{2}}) + \frac{b_{0,F}}{\epsilon}\,\mathcal{F}_{3,gg}^0(s_{\bar{1}\bar{2}})\left(\frac{s_{\bar{1}\bar{2}}}{\mu^2}\right)^{-\epsilon}$$

$$- \Gamma_{gg,F}^2(x_1)\delta_2 - \Gamma_{gg,F}^2(x_2)\delta_1 - \frac{1}{2}\big[\mathcal{F}_{3,gg}^0 \otimes \mathcal{F}_{3,gg}^0\big](s_{\bar{1}\bar{2}})$$

$$+ \quad \frac{1}{2}\left[\Gamma_{gg}^1 \otimes \Gamma_{gg,F}^1\right](z_1)\delta_2 + \frac{1}{2}\left[\Gamma_{gg}^1 \otimes \Gamma_{gg,F}^1\right](z_2)\delta_1$$

$$\widetilde{\boldsymbol{J}}_{2,N_F}^{(2)}(\hat{\bar{1}}_g, \hat{\bar{2}}_g) = \tilde{\mathcal{G}}_{4,gg}(s_{\bar{1}\bar{2}}) - \tilde{\Gamma}_{gg,F}^1(z_1) - \tilde{\Gamma}_{gg,F}^1(z_2),$$

$$\boldsymbol{J}_{2,N_F^2}^{(1)}(\hat{\bar{1}}_g, \hat{\bar{2}}_g) = -\Gamma_{gg,N_F^2}^2(z_1)\delta_2 - \Gamma_{gg,N_F^2}^2(z_2)\delta_1.$$

$$\boldsymbol{J}_{2,q\to g}^{(2)}(\hat{\bar{1}}_g, \hat{\bar{2}}_g) = \mathcal{G}_{4,qg}^{0,\mathrm{adj}}(s_{\bar{1}\bar{2}}) + \mathcal{G}_{4,qg}^{0,\mathrm{n.adj}}(s_{\bar{1}\bar{2}}) + \mathcal{G}_{3,qg}^1(s_{\bar{1}\bar{2}}) + \frac{b_0}{\epsilon}\mathcal{G}_{3,qg}^0(s_{\bar{1}\bar{2}})\left(\frac{s_{\bar{1}\bar{2}}}{\mu^2}\right)^{-\epsilon}$$

$$- \quad \Gamma_{gq}^2(z_1) + \left[\Gamma_{gq}^1 \otimes \Gamma_{gg}^1\right](z_1) + \left[\Gamma_{qq}^1 \otimes \Gamma_{gq}^1\right](z_1)$$

$$- \quad 2\left[\mathcal{F}_{gg}^0 \otimes \mathcal{F}_{gg}^0\right](s_{\bar{1}\bar{2}}) - \left[\Gamma_{gg}^1 \otimes \mathcal{G}_{gq}^0\right](s_{\bar{1}\bar{2}}) - \left[\Gamma_{qq}^1 \otimes \mathcal{G}_{gq}^0\right](s_{\bar{1}\bar{2}}),$$

$$\widetilde{\boldsymbol{J}}_{2,q\to g}^{(2)}(\hat{\bar{1}}_g, \hat{\bar{2}}_g) = \tilde{\mathcal{G}}_{4,qg}^0(s_{\bar{1}\bar{2}}) + \tilde{\mathcal{G}}_{3,qg}^1(s_{\bar{1}\bar{2}}) - \tilde{\Gamma}_{gq}^2(z_1)$$

$$- \quad \left[\Gamma_{qq}^1 \otimes \Gamma_{gq}^1\right](z_1) - \left[\Gamma_{qq}^1 \otimes \mathcal{G}_{gq}^0\right](s_{\bar{1}\bar{2}}),$$

$$\boldsymbol{J}_{2,q\to g,N_F}^{(2)}(\hat{\bar{1}}_g, \hat{\bar{2}}) = \hat{\mathcal{G}}_{3,qg}^1(s_{\bar{1}\bar{2}}) + \frac{b_{0,F}}{\epsilon}\mathcal{G}_{3,qg}^0(s_{\bar{1}\bar{2}})\left(\frac{s_{\bar{1}\bar{2}}}{\mu^2}\right)^{-\epsilon} - \Gamma_{gg,F}^2(z_1)$$

$$+ \quad \left[\Gamma_{gq}^1 \otimes \Gamma_{gg,F}^1\right](z_1),$$

$$\boldsymbol{J}_{2,q\to g,\bar{q}\to g}^{(2)}(\hat{\bar{1}}_g, \hat{\bar{2}}_g) = \mathcal{H}_{4,q\bar{q}}^0(s_{\bar{1}\bar{2}}) + \Gamma_{gq}^1(z_1)\Gamma_{gq}^1(z_2)$$

$$- \quad \left[\Gamma_{gq}^1 \otimes \mathcal{G}_{3,qg}^0\right](z_1, z_2; s_{\bar{1}\bar{2}}) - \left[\Gamma_{gq}^1 \otimes \mathcal{G}_{3,gq}^0\right](z_1, z_2; s_{\bar{1}\bar{2}}),$$

$$\boldsymbol{J}_4^{(2)}(\hat{\bar{1}}_q, i_g, j_g, \hat{\bar{2}}_{\bar{q}}) = \mathcal{D}_{4,q}^0(s_{\bar{1}i}) + \frac{1}{2}\mathcal{F}_4^0(s_{ij}) + \mathcal{D}_{4,q}^0(s_{\bar{2}j}) - \tilde{\mathcal{A}}_{4,q\bar{q}}^0(s_{\bar{1}\bar{2}})$$

$$+ \quad \mathcal{D}_{3,q}^1(s_{\bar{1},i}) + \mathcal{F}_3^1(s_{ij}) + \mathcal{D}_{3,q}^1(s_{\bar{2},j}) - \mathcal{A}_{3,q\bar{q}}^1(s_{\bar{1}\bar{2}})$$

$$+ \quad \frac{b_0}{\epsilon}\left(\frac{s_{\bar{1}i}}{\mu^2}\right)^{-\epsilon}\frac{1}{2}\mathcal{D}_3^0(s_{\bar{1}i}) + \frac{b_0}{\epsilon}\left(\frac{s_{ij}}{\mu^2}\right)^{-\epsilon}\frac{1}{3}\mathcal{F}_3^0(s_{ij})$$

$$+ \quad \frac{b_0}{\epsilon}\left(\frac{s_{\bar{2}j}}{\mu^2}\right)^{-\epsilon}\frac{1}{2}\mathcal{D}_3^0(s_{\bar{2}j}) - \frac{1}{4}\left[\mathcal{D}_{3,q}^0 \otimes \mathcal{D}_{3,q}^0\right](s_{\bar{1}i})$$

$$- \quad \frac{1}{9}\left[\mathcal{F}_3^0 \otimes \mathcal{F}_3^0\right](s_{ij}) - \frac{1}{4}\left[\mathcal{D}_{3,q}^0 \otimes \mathcal{D}_{3,q}^0\right](s_{\bar{2}j})$$

$$+ \quad \frac{1}{2}\left[\mathcal{A}_{3,q\bar{q}}^0 \otimes \mathcal{A}_{3,q\bar{q}}^0\right](s_{\bar{1}\bar{2}}) - \Gamma_{qq}^2(z_1) - \Gamma_{qq}^2(z_2)$$

$$+ \quad \frac{1}{2}\left[\Gamma_{qq}^1 \otimes \Gamma_{qq}^1\right](z_1) + \frac{1}{2}\left[\Gamma_{qq}^1 \otimes \Gamma_{qq}^1\right](z_2) \tag{B.4}$$

Bibliography

[1] Charalampos Anastasiou, Lance Dixon, Kirill Melnikov, and Frank Petriello. High-precision qcd at hadron colliders: Electroweak gauge boson rapidity distributions at next-to-next-to leading order. *Phys. Rev. D*, 69:094008, May 2004.

[2] A. Martin, W. Stirling, R. Thorne, and G. Watt. Parton distributions for the lhc. *The European Physical Journal C - Particles and Fields*, 63:189–285, 2009. 10.1140/epjc/s10052-009-1072-5.

[3] W.J. Stirling. private communication. 2008.

[4] ATLAS Collaboration. Measurement of inclusive jet and dijet production in pp collisions at $\sqrt{s}$=7 TeV using the atlas detector. *Phys. Rev. D*, 86:014022, Jul 2012.

[5] CMS Collaboration. Measurement of the inclusive jet cross section in pp collisions at $\sqrt{s} = 7$ TeV. *Phys. Rev. Lett.*, 107:132001, Sep 2011.

[6] The D0 Collaboration. Determination of the strong coupling constant from the inclusive jet cross section in $p\bar{p}$ collisions at $\sqrt{s} = 1.96$ TeV. *Phys. Rev. D*, 80:111107, Dec 2009.

[7] CMS Collboration. Observation of a new boson at a mass of 125 gev with the cms experiment at the lhc. *Physics Letters B*, 716(1):30 – 61, 2012.

[8] G.D. Rochester and C.C. Butler. Evidence for the Existence of New Unstable Elementary Particles. *Nature*, 160:855–857, 1947.

[9] M. Gell-Mann. Isotopic spin and new unstable particles. *Phys. Rev.*, 92:833–834, Nov 1953.

[10] Kazuhiko Nishijima. Charge independence theory of v particles. *Progress of Theoretical Physics*, 13(3):285–304, 1955.

[11] M. Gell-Mann. The Eightfold Way: A Theory of Strong Interaction Symmetry. Mar 1961.

[12] Y. Ne'Eman. Derivation of strong interactions from a gauge invariance. *Nucl.Phys*, 26:222–229, aug 1961.

[13] V. E. Barnes, P. L. Connolly, D. J. Crennell, B. B. Culwick, W. C. Delaney, W. B. Fowler, P. E. Hagerty, E. L. Hart, N. Horwitz, P. V. C. Hough, J. E. Jensen, J. K. Kopp, K. W. Lai, J. Leitner, J. L. Lloyd, G. W. London, T. W. Morris, Y. Oren, R. B. Palmer, A. G. Prodell, D. Radojičić, D. C. Rahm, C. R. Richardson, N. P. Samios, J. R. Sanford, R. P. Shutt, J. R. Smith, D. L. Stonehill, R. C. Strand, A. M. Thorndike, M. S. Webster, W. J. Willis, and S. S. Yamamoto. Observation of a hyperon with strangeness minus three. *Phys. Rev. Lett.*, 12:204–206, Feb 1964.

[14] M. Gell-Mann. A schematic model of baryons and mesons. *Physics Letters*, 8(3):214 – 215, 1964.

[15] G. Zweig. An SU(3) Model for Strong Interaction Symmetry and its Breaking. 1964.

[16] O. W. Greenberg. Spin and unitary-spin independence in a paraquark model of baryons and mesons. *Phys. Rev. Lett.*, 13:598–602, Nov 1964.

[17] M.Y. Han and Yoichiro Nambu. Three Triplet Model with Double SU(3) Symmetry. *Phys.Rev.*, 139:B1006–B1010, 1965.

[18] M.E. Peskin and D.V. Schroeder. *An Introduction To Quantum Field Theory*. Advanced Book Program. Westview Press, 1995.

[19] R. Keith Ellis, W. James Stirling, and B. R. Webber. *QCD and Collider Physics*, volume 8. Cambridge University Press, 1996.

[20] S. Catani and M. H. Seymour. A general algorithm for calculating jet cross sections in NLO QCD. *Nucl. Phys.*, B485:291–419, 1997.

[21] Michelangelo L. Mangano, Stephen J. Parke, and Zhan Xu. Dual Amplitudes and Multi - Gluon Processes. 1987.

[22] Michelangelo L. Mangano and Stephen J. Parke. Quark - Gluon Amplitudes in the Dual Expansion. *Nucl.Phys.*, B299:673, 1988.

[23] Michelangelo L. Mangano and Stephen J. Parke. Multi-parton amplitudes in gauge theories. *Physics Reports*, 200(6):301 – 367, 1991.

[24] John C. Collins, Davison E. Soper, and George F. Sterman. Factorization for Short Distance Hadron - Hadron Scattering. *Nucl.Phys.*, B261:104, 1985.

[25] J C Collins and Davison Eugene Soper. The theorems of perturbative qcd. Technical Report OITS-350, Oregon Univ. Inst. Theor. Sci., Eugene, OR, Mar 1987.

[26] J.C. Collins. *Renormalization: An Introduction to Renormalization, the Renormalization Group and the Operator-Product Expansion.* Cambridge Monographs on Mathematical Physics. Cambridge University Press, 1986.

[27] S. Weinberg. *The Quantum Theory of Fields.* Number v. 1. Cambridge University Press, 1996.

[28] Kenneth G. Wilson and J. Kogut. The renormalization group and the ϵ expansion. *Physics Reports*, 12(2):75 – 199, 1974.

[29] Gerard 't Hooft and M.J.G. Veltman. Regularization and Renormalization of Gauge Fields. *Nucl.Phys.*, B44:189–213, 1972.

[30] Kenneth G. Wilson. Quantum field - theory models in less than 4 dimensions. *Phys. Rev. D*, 7:2911–2926, May 1973.

[31] S. Catani. The singular behaviour of QCD amplitudes at two-loop order. *Phys. Lett.*, B427:161–171, 1998.

[32] A. Gehrmann-De Ridder, T. Gehrmann, and E. W. N. Glover. Antenna Subtraction at NNLO. *JHEP*, 09:056, 2005.

[33] Stephen J. Parke and T.R. Taylor. An Amplitude for n Gluon Scattering. *Phys.Rev.Lett.*, 56:2459, 1986.

[34] R. Keith Ellis, G. Marchesini, and B.R. Webber. Soft Radiation in Parton Parton Scattering. *Nucl.Phys.*, B286:643, 1987.

[35] Guido Altarelli and G. Parisi. Asymptotic Freedom in Parton Language. *Nucl. Phys.*, B126:298, 1977.

[36] A. Daleo, T. Gehrmann, and D. Maître. Antenna subtraction with hadronic initial states. *JHEP*, 04:016, 2007.

[37] Stefano Catani and Massimiliano Grazzini. Infrared factorization of tree level QCD amplitudes at the next-to-next-to-leading order and beyond. *Nucl.Phys.*, B570:287–325, 2000.

[38] Z. Bern, V. Del Duca, and C. R. Schmidt. The infrared behavior of one-loop gluon amplitudes at next-to-next-to-leading order. *Phys. Lett.*, B445:168–177, 1998.

[39] Z. Bern, V. Del Duca, W. B. Kilgore, and Carl R. Schmidt. The infrared behavior of one-loop QCD amplitudes at next-to-next-to-leading order. *Phys. Rev.*, D60:116001, 1999.

[40] Z. Bern, L. J. Dixon, D. C. Dunbar, and D. A. Kosower. One-Loop n-Point Gauge Theory Amplitudes, Unitarity and Collinear Limits. *Nucl. Phys.*, B425:217–260, 1994.

[41] Frits A. Berends and W.T. Giele. Multiple Soft Gluon Radiation in Parton Processes. *Nucl.Phys.*, B313:595, 1989.

[42] John M. Campbell and E.W. Nigel Glover. Double unresolved approximations to multiparton scattering amplitudes. *Nucl.Phys.*, B527:264–288, 1998.

[43] F. Bloch and A. Nordsieck. Note on the Radiation Field of the electron. *Phys.Rev.*, 52:54–59, 1937.

[44] T. Kinoshita. Mass singularities of Feynman amplitudes. *J. Math. Phys.*, 3:650–677, 1962.

[45] T. D. Lee and M. Nauenberg. Degenerate Systems and Mass Singularities. *Phys. Rev.*, 133:B1549–B1562, 1964.

[46] Charalampos Anastasiou and Kirill Melnikov. Higgs boson production at hadron colliders in NNLO QCD. *Nucl.Phys.*, B646:220–256, 2002.

[47] A. Gehrmann-De Ridder, E. W. N. Glover, and J. Pires. Real-Virtual corrections for gluon scattering at NNLO. 2011.

[48] R. Keith Ellis, Howard Georgi, Marie Machacek, H. David Politzer, and Graham G. Ross. Factorization and the Parton Model in QCD. *Phys.Lett.*, B78:281, 1978.

[49] Stefano Catani, Daniel de Florian, and German Rodrigo. Space-like (versus time-like) collinear limits in QCD: Is factorization violated? *JHEP*, 1207:026, 2012.

[50] V.N. Gribov and L.N. Lipatov. Deep inelastic e p scattering in perturbation theory. *Sov.J.Nucl.Phys.*, 15:438–450, 1972.

[51] Yuri L. Dokshitzer. Calculation of the Structure Functions for Deep Inelastic Scattering and e+ e- Annihilation by Perturbation Theory in Quantum Chromodynamics. *Sov.Phys.JETP*, 46:641–653, 1977.

[52] E.A. Kuraev, L.N. Lipatov, and Victor S. Fadin. The Pomeranchuk Singularity in Nonabelian Gauge Theories. *Sov.Phys.JETP*, 45:199–204, 1977.

[53] I.I. Balitsky and L.N. Lipatov. The Pomeranchuk Singularity in Quantum Chromodynamics. *Sov.J.Nucl.Phys.*, 28:822–829, 1978.

[54] L.V. Gribov, E.M. Levin, and M.G. Ryskin. Semihard Processes in QCD. *Phys.Rept.*, 100:1–150, 1983.

[55] Gavin P. Salam. Towards Jetography. *Eur.Phys.J.*, C67:637–686, 2010.

[56] S. Catani, B. Webber, and Yu. Dokshitzer. The K(T) clustering algorithm for jets in deep inelastic scattering. *Nucl.Phys.Proc.Suppl.*, 29A:136–143, 1992.

[57] Stephen D. Ellis and Davison E. Soper. Successive combination jet algorithm for hadron collisions. *Phys. Rev. D*, 48:3160–3166, Oct 1993.

[58] Yuri L. Dokshitzer, G.D. Leder, S. Moretti, and B.R. Webber. Better jet clustering algorithms. *JHEP*, 9708:001, 1997.

[59] M. Wobisch and T. Wengler. Hadronization corrections to jet cross-sections in deep inelastic scattering. 1998.

[60] M. Cacciari, G. P. Salam, and G. Soyez. The Anti-k(t) jet clustering algorithm. *JHEP*, 0804:063, 2008.

[61] W. Bartel et al. Experimental Studies on Multi-Jet Production in e+ e- Annihilation at PETRA Energies. *Z.Phys.*, C33:23, 1986.

[62] Matteo Cacciari, Juan Rojo, Gavin P. Salam, and Gregory Soyez. Quantifying the performance of jet definitions for kinematic reconstruction at the LHC. *JHEP*, 0812:032, 2008.

[63] George Sterman and Steven Weinberg. Jets from quantum chromodynamics. *Phys. Rev. Lett.*, 39:1436–1439, Dec 1977.

[64] M.H. Seymour. Jet shapes in hadron collisions: Higher orders, resummation and hadronization. *Nuclear Physics B*, 513(12):269 – 300, 1998.

[65] Gavin P. Salam. A Practical seedless infrared safe cone algorithm. 2007.

[66] E.W.N. Glover. Progress in nnlo calculations for scattering processes. *Nuclear Physics B - Proceedings Supplements*, 116(0):3 – 7, 2003. Proceedings of the

6th International Symposium on Radiative Corrections and the 6th Zeuthen Workshop on Elementary Particle Theory.

[67] Mrinal Dasgupta. Power corrections in QCD. *J.Phys.G*, G28:907–914, 2002.

[68] Andreas Hoecker and Vakhtang Kartvelishvili. Svd approach to data unfolding. *Nuclear Instruments and Methods in Physics Research Section A: Accelerators, Spectrometers, Detectors and Associated Equipment*, 372(3):469 – 481, 1996.

[69] CMS Collaboration. Measurement of the differential dijet production cross section in proton-proton collisions at. *Physics Letters B*, 700:187 – 206, 2011.

[70] W. T. Giele, E. W. N. Glover, and J. Yu. Determination of α_s at hadron colliders. *Phys. Rev. D*, 53:120–130, Jan 1996.

[71] B. Malaescu and P. Starovoitov. Evaluation of the strong coupling constant α_s using the atlas inclusive jet cross-section data. *The European Physical Journal C - Particles and Fields*, 72:1–14, 2012. 10.1140/epjc/s10052-012-2041-y.

[72] ATLAS Collaboration. Observation of a new particle in the search for the standard model higgs boson with the atlas detector at the lhc. *Physics Letters B*, 716(1):1 – 29, 2012.

[73] K. Fabricius, I. Schmitt, G. Kramer, and G. Schierholz. Higher Order Perturbative QCD Calculation of Jet Cross-Sections in e+ e- Annihilation. *Z.Phys.*, C11:315, 1981.

[74] W.T. Giele and E.W. Nigel Glover. Higher order corrections to jet cross-sections in e+ e- annihilation. *Phys.Rev.*, D46:1980–2010, 1992.

[75] W. T. Giele, E. W. N. Glover, and D. A. Kosower. Higher order corrections to jet cross-sections in hadron colliders. *Nucl. Phys.*, B403:633–670, 1993.

[76] A. Gehrmann-De Ridder and E.W. Nigel Glover. A Complete O (alpha alpha-s) calculation of the photon + 1 jet rate in e+ e- annihilation. *Nucl.Phys.*, B517:269–323, 1998.

[77] S. Frixione, Z. Kunszt, and A. Signer. Three jet cross-sections to next-to-leading order. *Nucl. Phys.*, B467:399–442, 1996.

[78] T. Binoth and G. Heinrich. An automatized algorithm to compute infrared divergent multi-loop integrals. *Nucl. Phys.*, B585:741–759, 2000.

[79] T. Binoth and G. Heinrich. Numerical evaluation of multi-loop integrals by sector decomposition. *Nucl. Phys.*, B680:375–388, 2004.

[80] T. Binoth and G. Heinrich. Numerical evaluation of phase space integrals by sector decomposition. *Nucl. Phys.*, B693:134–148, 2004.

[81] A.V. Smirnov, V.A. Smirnov, and M. Tentyukov. Fiesta 2: Parallelizeable multiloop numerical calculations. *Computer Physics Communications*, 182(3):790 – 803, 2011.

[82] G. Heinrich. A numerical method for NNLO calculations. *Nucl. Phys. Proc. Suppl.*, 116:368–372, 2003.

[83] C. Anastasiou, K. Melnikov, and F. Petriello. A new method for real radiation at NNLO. *Phys. Rev.*, D69:076010, 2004.

[84] G. Heinrich. The sector decomposition approach to real radiation at NNLO. *Nucl. Phys. Proc. Suppl.*, 157:43–47, 2006.

[85] G. Somogyi, Z. Trocsanyi, and V. Del Duca. A subtraction scheme for computing QCD jet cross sections at NNLO: regularization of doubly-real emissions. *JHEP*, 01:070, 2007.

[86] C. Anastasiou, F. Herzog, and A. Lazopoulos. On the factorization of overlapping singularities at NNLO. *JHEP*, 03:038, 2011.

[87] M. Czakon. Double-real radiation in hadronic top quark pair production as a proof of a certain concept. *Nucl. Phys.*, B849:250–295, 2011.

[88] M. Czakon. A novel subtraction scheme for double-real radiation at NNLO. *Phys. Lett.*, B693:259–268, 2010.

[89] Radja Boughezal, Kirill Melnikov, and Frank Petriello. A subtraction scheme for NNLO computations. *Phys.Rev.*, D85:034025, 2012.

[90] Jonathon Carter and Gudrun Heinrich. Secdec: A general program for sector decomposition. *Computer Physics Communications*, 182(7):1566 – 1581, 2011.

[91] Klaus Hepp. Proof of the Bogolyubov-Parasiuk theorem on renormalization. *Commun.Math.Phys.*, 2:301–326, 1966.

[92] R. Keith Ellis and J.C. Sexton. QCD Radiative Corrections to Parton Parton Scattering. *Nucl.Phys.*, B269:445, 1986.

[93] D. A. Kosower. Antenna factorization of gauge-theory amplitudes. *Phys. Rev.*, D57:5410–5416, 1998.

[94] Z. Bern, L. J. Dixon, and D. A. Kosower. A Two loop four gluon helicity amplitude in QCD. *JHEP*, 0001:027, 2000.

[95] C. Anastasiou, E. W. N. Glover, C. Oleari, and M. E. Tejeda-Yeomans. Two loop QCD corrections to massless identical quark scattering. *Nucl.Phys.*, B601:341–360, 2001.

[96] C. Anastasiou, E. W. N. Glover, C. Oleari, and M. E. Tejeda-Yeomans. Two-loop QCD corrections to the scattering of massless distinct quarks. *Nucl.Phys.*, B601:318–340, 2001.

[97] C. Anastasiou, E. W. N. Glover, C. Oleari, and M. E. Tejeda-Yeomans. One loop QCD corrections to quark scattering at NNLO. *Phys.Lett.*, B506:59–67, 2001.

[98] E. W. N. Glover, C. Oleari, and M. E. Tejeda-Yeomans. Two loop QCD corrections to gluon-gluon scattering. *Nucl.Phys.*, B605:467–485, 2001.

[99] C. Anastasiou, E. W. N. Glover, C. Oleari, and M. E. Tejeda-Yeomans. Two loop QCD corrections to massless quark gluon scattering. *Nucl.Phys.*, B605:486–516, 2001.

[100] E. W. N. Glover and M.E. Tejeda-Yeomans. One loop QCD corrections to gluon-gluon scattering at NNLO. *JHEP*, 0105:010, 2001.

[101] Z. Bern, A. De Freitas, and L. J. Dixon. Two loop helicity amplitudes for gluon-gluon scattering in QCD and supersymmetric Yang-Mills theory. *JHEP*, 0203:018, 2002.

[102] E. W. N. Glover and M. E. Tejeda-Yeomans. Two loop QCD helicity amplitudes for massless quark massless gauge boson scattering. *JHEP*, 0306:033, 2003.

[103] D. A. Kosower. Antenna factorization in strongly-ordered limits. *Phys. Rev.*, D71:045016, 2005.

[104] Z. Bern, A. De Freitas, and L. J. Dixon. Two loop helicity amplitudes for quark gluon scattering in QCD and gluino gluon scattering in supersymmetric Yang-Mills theory. *JHEP*, 0306:028, 2003.

[105] A. De Freitas and Z. Bern. Two-loop helicity amplitudes for quark-quark scattering in QCD and gluino-gluino scattering in supersymmetric Yang-Mills theory. *JHEP*, 0409:039, 2004.

[106] A. Gehrmann-De Ridder, T. Gehrmann, and E. W. N. Glover. Quark-Gluon Antenna Functions from Neutralino Decay. *Phys. Lett.*, B612:36–48, 2005.

[107] A. Gehrmann-De Ridder, T. Gehrmann, and E. W. N. Glover. Gluon-Gluon Antenna Functions from Higgs Boson Decay. *Phys. Lett.*, B612:49–60, 2005.

[108] A. Gehrmann-De Ridder, T. Gehrmann, E. W. N. Glover, and G. Heinrich. Infrared structure of $e^+e^- \to 3$ jets at NNLO. *JHEP*, 11:058, 2007.

[109] S. Weinzierl. NNLO corrections to 3-jet observables in electron-positron annihilation. *Phys. Rev. Lett.*, 101:162001, 2008.

[110] S. Weinzierl. The infrared structure of $e^+e^- \to 3$ jets at NNLO reloaded. *JHEP*, 07:009, 2009.

[111] A. Daleo, A Gehrmann-De Ridder, T. Gehrmann, and G. Luisoni. Antenna subtraction at NNLO with hadronic initial states: initial-final configurations. *JHEP*, 01:118, 2010.

[112] A. Gehrmann-De Ridder and M. Ritzmann. NLO Antenna Subtraction with Massive Fermions. *JHEP*, 07:041, 2009.

[113] R. Boughezal, A. Gehrmann-De Ridder, and M. Ritzmann. Antenna subtraction at NNLO with hadronic initial states: double real radiation for initial-initial configurations with two quark flavours. *JHEP*, 02:098, 2011.

[114] E. W. N. Glover and J. Pires. Antenna subtraction for gluon scattering at NNLO. *JHEP*, 06:096, 2010.

[115] T. Gehrmann and P. F. Monni. Antenna subtraction at NNLO with hadronic initial states: real-virtual initial-initial configurations. 2011.

[116] G. Abelof and A. Gehrmann-De Ridder. Antenna subtraction for the production of heavy particles at hadron colliders. *JHEP*, 04:063, 2011.

[117] W. Bernreuther, C. Bogner, and O. Dekkers. The real radiation antenna function for $S \rightarrow Q\bar{Q}q\bar{q}$ at NNLO QCD. *JHEP*, 06:032, 2011.

[118] A. Gehrmann-De Ridder, T. Gehrmann, and E. W. N. Glover. Infrared Structure of $e^+e^- \rightarrow 2$ jets at NNLO. *Nucl. Phys.*, B691:195–222, 2004.

[119] A.G. Grozin. Integration by parts: An Introduction. *Int.J.Mod.Phys.*, A26:2807–2854, 2011.

[120] A. Gehrmann-De Ridder, T. Gehrmann, and G. Heinrich. Four-particle phase space integrals in massless QCD. *Nucl. Phys.*, B682:265–288, 2004.

[121] Ruth Britto, Freddy Cachazo, and Bo Feng. Generalized unitarity and one-loop amplitudes in super-yangmills. *Nuclear Physics B*, 725(12):275 – 305, 2005.

[122] Giovanni Ossola, Costas G. Papadopoulos, and Roberto Pittau. Reducing full one-loop amplitudes to scalar integrals at the integrand level. *Nuclear Physics B*, 763(12):147 – 169, 2007.

[123] C.F. Berger, Z. Bern, L.J. Dixon, F. Febres Cordero, D. Forde, H. Ita, D.A. Kosower, and D. Maître. One-loop calculations with blackhat. *Nuclear Physics B - Proceedings Supplements*, 183(0):313 – 319, 2008. Proceedings of the 9th DESY Workshop on Elementary Particle Theory.

[124] Sebastian Becker, Christian Reuschle, and Stefan Weinzierl. Numerical nlo qcd calculations. *Journal of High Energy Physics*, 2010:1–61, 2010. 10.1007/JHEP12(2010)013.

[125] J. Pires and E. W. N. Glover. Double real radiation corrections to gluon scattering at NNLO. *Nucl. Phys. Proc. Suppl.*, 205-206:176–181, 2010.

[126] T. Gehrmann, T. Huber, and D. Maître. Two-loop quark and gluon form factors in dimensional regularisation. *Physics Letters B*, 622(34):295 – 302, 2005.

[127] R. Kleiss, W. J. Stirling, and S. D. Ellis. A new Monte Carlo treatment of multiparticle phase space at high-energies. *Comput.Phys.Commun.*, 40:359, 1986.

[128] S. Moch, J.A.M. Vermaseren, and A. Vogt. The three-loop splitting functions in qcd: the non-singlet case. *Nuclear Physics B*, 688(12):101 – 134, 2004.

[129] A. Vogt, S. Moch, and J.A.M. Vermaseren. The three-loop splitting functions in qcd: the singlet case. *Nuclear Physics B*, 691(12):129 – 181, 2004.